

July 2017

Probing the Domain Architecture and Structural Dynamics of Caspase-6 for its Specific Regulation

Kevin Buadlart Dagbay
University of Massachusetts Amherst

Follow this and additional works at: https://scholarworks.umass.edu/dissertations_2



Part of the [Biochemistry Commons](#), [Other Biochemistry](#), [Biophysics](#), and [Structural Biology Commons](#), and the [Structural Biology Commons](#)

Recommended Citation

Dagbay, Kevin Buadlart, "Probing the Domain Architecture and Structural Dynamics of Caspase-6 for its Specific Regulation" (2017). *Doctoral Dissertations*. 961.
<https://doi.org/10.7275/10008135.0> https://scholarworks.umass.edu/dissertations_2/961

This Campus-Only Access for Five (5) Years is brought to you for free and open access by the Dissertations and Theses at ScholarWorks@UMass Amherst. It has been accepted for inclusion in Doctoral Dissertations by an authorized administrator of ScholarWorks@UMass Amherst. For more information, please contact scholarworks@library.umass.edu.

**PROBING THE DOMAIN ARCHITECTURE AND STRUCTURAL DYNAMICS
OF CASPASE-6 FOR ITS SPECIFIC REGULATION**

A Dissertation Presented

by

KEVIN BUADLART DAGBAY

Submitted to the Graduate School of the
University of Massachusetts Amherst in partial fulfillment
of the requirements for the degree of

DOCTOR OF PHILOSOPHY

MAY 2017

Chemistry

© Copyright by Kevin Buadlart Dagbay 2017

All Rights Reserved

**PROBING THE DOMAIN ARCHITECTURE AND STRUCTURAL DYNAMICS
OF CASPASE-6 FOR ITS SPECIFIC REGULATION**

A Dissertation Presented

by

KEVIN BUADLART DAGBAY

Approved as to style and content by:

Jeanne A. Hardy, Chair

Lila M. Gierasch, Member

Craig T. Martin, Member

Scott C. Garman, Member

Richard W. Vachet, Department Head
Department of Chemistry

DEDICATION

For the loving memory of my Papa Nestor and Mama Noning,
for their perpetual guidance.

For my hardworking parents, Papa Frank and Mama Rose,
for their utmost concern in every part of my being.

For my little Bastee,
for constantly painting a smile on my face and joy in my heart.

For my wife Dolly,
for the lasting friendship, comfort, care, and
for providing us a place called HOME.

For those who THINK BIG and DREAM BIG
in the midst of relentless struggles...

ACKNOWLEDGMENTS

This Journey Employed A Village Of Amazing People That Fueled My Determination And Persistence To Finish My PhD. To My Research Advisor Jeanne Hardy For The Endless Support And Guidance Throughout My Journey. To Scott Garman. Lila Gierasch. Craig Martin For Being Part Of The Team That Allowed Me To Receive This Awesome PhD Degree. It Was Truly An Honor And I Will Be Forever Grateful For Your Efforts. To All The Professors And Mentors Who Shared Their Wealth Of Knowledge And Contributed To My Critical Thinking Skill. Min Chen. Matthew Holden. Vincent Rotello. Scott Auerbach. Bob Weis. Karsten Theis. Alejandro Heuck. Lymarie Thompson. Michael Knapp. Richard Vachet. Susan Roberts. Surita Bhatia. Shana Passono. Shelly Peyton. Jennifer Ross. Michelle Farkas. Stephen Eyles. To The Hardy Lab Past And Present Members. Sravanti. Eli. Witold. Kristen. Sam. Muslum. Scott. Bay. Yunlong. Maureen. Derek. DiLin. Alesia. Elizabeth. Jacob. Ishan. Yifei. Nicolas. Narasimha. For Letting Me Feel A Sense Of Belongingness And Family In This Fleeting Journey Of Graduate School Life. To My Friends And Colleagues In The Chemistry Department As Well As In The Chemical Biology Interface Training Program And Molecular And Cell Biology Program. Special Mention To Indu Santhanagopalan. Nilima Kolli. Matt MetCalf. Rubul Muot. Gulen Yesilbag. Di Huang. Derek Deming. My Classmates UMass Chemistry Batch Of 2010. Ziya Aydin. Raymond Devaughn. Sukru Elci. Bukola Fatumbi. Lola Fatumbi. Jack Fuller. Adam Gann. Timothy Gehan. Kim Hua. Ying Jiang. Joelle Labastide. En Hsin Lee. Longyu Li. Xuni Li. Devon McCarthy. Angela Miques. Khaja Muneeruddin. Gustavo Sanchez. Debra Sondak. Ryan Sullivan. Hui Wang. Xian Wang. Sung Eui Youn. Hanwei Zhao. Being Surrounded By These Amazing And Talented People Were Pretty Nuturing Personally And Professionally. To The Newman Catholic Center For The Spiritual Nourishment And For Always Reminding Me The Greatness Of God Through Songs And Praises And Readings From The Bible. To Laura And Bill For Taking Care Of Our Little Baste While We Were Immersed In The Business Of Pursuing Our Dreams. To The Amherst Pals. For The Enduring Friendship And Countless Laughters We Have Shared Along The Way. And For Being Our Home Away From Home. To Myles. JB. Kuya Amiel And Ate Juelle. To Vanessa And Joe And Big Boy Alex. To Cess And Nanay And Too Cute James. To Bernard And Aileen And Adorable Ari. To Ron And Phey And Very Smart Naya. To Risha And Lem. Kristine And Francis And Beautiful Francine And Judah. To Dennis. To Mahalia And Bay. To Rose And Witold And Endearing Oliver. To Jenny And Karen. Rae. To Tunde Gyorgy. For The Warm Friendship And Kindness. To Cristina Martin. For Embracing Us And Becoming Part Of Our Family. For Your Unwavering Friendship And For All The Endless Favors. We Are Eternally Grateful To You. To My Parents. Mama Rose And Papa Frank. For Being There From Day One. For The Constant Support And Selfless Sacrifices. To My Siblings Ate Karen And Jun. For Constantly Reminding Me To Be Thankful For Today And Be Hopeful Of Tomorrow. To Mama Elms And Bai Lolong. For Letting Me Part Of Your Awesome Family. To Archie and Ate Apple. For Being So Dependable In Everyway And For Being Our Saving Grace In Times Of Great Need. To Prime For Being So Unselfish And Our Great Wall In The Midst Of Stormy Days. To Andrae For The Constant Love And Understanding And For Being Great As You Are. To My Relatives And Friends In The Philippines For The Endless Support And Inspiration To Do My Best. To My Little Sebastian. For Being A Source Of Strength And Motivation. To My Wife Dolly. For Being On My Side Through Good And Bad Times And For Taking Care Of Us. We Love You. To God Be The Glory.

“You have brains in your head. You have feet in your shoes. You can steer yourself in any direction you choose. You're on your own, and you know what you know. And you are the guy who'll decide where to go.” – **Dr. Seuss**

ABSTRACT

PROBING THE DOMAIN ARCHITECTURE AND STRUCTURAL DYNAMICS OF CASPASE-6 FOR ITS SPECIFIC REGULATION

MAY 2017

KEVIN BULADLART DAGBAY, B.S., UNIVERSITY OF THE PHILIPPINES
MANILA

M.S., UNIVERSITY OF THE PHILIPPINES DILIMAN

Ph.D., UNIVERSITY OF MASSACHUSETTS AMHERST

Directed by: Professor Jeanne A. Hardy

Caspases are *cysteine aspartate* proteases that direct programmed cell death in multicellular organisms. Activation of caspases is tightly regulated to secure maintenance of cellular homeostasis. The aberrant regulation of caspases can act as molecular triggers for a range of diseases from cancer to neurodegeneration. The detailed exploration of caspase structure, dynamics, function, and regulation is crucial to better understand and precisely control their cellular functions. This body of work specifically provides a multi-level understanding of the unique structural dynamics and regulation of caspase-6, the function of which is implicated in Alzheimer's and Huntington's diseases. A detailed map of conformational flexibility of caspase-6 upon the five stages of proteolytic activation revealed critical regions with discrete conformations that offers a comprehensive scaffold for strategic design of therapeutics for neurodegeneration. Meanwhile, the exploration on the natural mutations in caspase-6 that have arisen from abnormally regulated tumor cells uncovered key stabilizing interaction in regulatory region that appears to be exploited across the family of caspases. In addition, the finding of ATP as a natural ligand of procaspase-6 provides another layer of regulation to the already complex caspase-6-associated signaling. Finally, the discovery of the most potent and selective inhibitor of caspase-6 to date enabled specific regulation possible by targeting a unique cysteine in the most diversified region in caspases.

TABLE OF CONTENTS

	Page
ACKNOWLEDGMENTS	v
ABSTRACT	vi
LIST OF TABLES	xii
LIST OF FIGURES	xiii
CHAPTER	
1. APOPTOTIC CASPASE STRUCTURE, FUNCTION, REGULATION, AND DISEASE IMPLICATIONS	1
1.1 Caspases in Programmed Cell Death	1
1.2 The Essential Elements of the Apoptotic Pathway	2
1.3 The Structure and Activation Mechanisms of Caspases	4
1.4 Distinguishing Features of Caspase-6	8
1.5 Regulatory Mechanisms of Caspase-6	11
1.6 Cancer-Associated Functions of Caspase-6	12
1.7 Neurodegenerative Attributes of Caspase-6	15
1.8 Targeted Regulation of Caspase-6 using Natural and Synthetic Inhibitors	17
1.9 References	20
2. CASPASE-6 UNDERGOES A DISTINCT HELIX-STRAND INTERCONVERSION UPON SUBTRATE BINDING	27
2.1 Abstract	27
2.2 Introduction	28
2.3 Results	34
2.3.1 Overall H/DX-MS Profiles of Caspase-6 and Caspase-7	34
2.3.2 Caspase-7 Adopts the Canonical Strand Conformation Before and After Substrate Binding	46
2.3.3 Caspase-6 Shows Different H/D Exchange Dynamics in the 130's Region Compared to Caspase-7	52
2.3.4 Local pK _a s of Key Amino Acid Residues Within the 130's Region Vary Between the Unliganded (Helical) and the VEID-bound (Strand) States of Caspase-6	54
2.3.5 Protonation State of Glu-135 is Key to Conformational Changes in the Caspase-6 130's Region	57
2.3.6 E135Q, a Mimic of Protonated E135, Stabilizes Caspase-6	58

2.4 Discussion	62
2.5 Materials and Methods	67
2.4.1 Generation of Caspase Variants.....	67
2.4.2 Caspase Protein Expression and Purification.....	68
2.4.3 Caspase Activity Assays.....	69
2.4.4 Hydrogen/Deuterium Exchange Mass Spectrometry.....	70
2.4.5 Circular Dichroism Spectroscopy.....	72
2.4.6 Caspase Activity versus pH	73
2.4.7 <i>In Silico</i> Model Preparation.....	73
2.4.8 Simulated Annealing Studies of Protonation Variants	75
2.6 Acknowledgments	76
2.7 References	76
3. THE MULTIPLE PROTEOLYTIC EVENTS THAT LEAD TO CASPASE-6 ACTIVATION EACH IMPACT THE CONFORMATION OF DISCRETE STRUCTURAL REGIONS.....	83
3.1 Abstract	83
3.2 Introduction.....	84
3.3 Results.....	89
3.3.1 H/DX-MS Profile of Caspase-6 Maturation State Variants.....	89
3.3.2 Intramolecular Self-Cleavage at Asp-193 Influences Local Conformation and Dynamics	94
3.3.3 Complete Removal of the Linker is Important to Attain the Fully Exposed Substrate-Binding Cavity	99
3.3.4 Substrate-binding Groove is Accessible in Cleaved Caspase-6, Independent of the Presence of the Prodomain or Linker.....	102
3.3.5 The Prodomain is Intrinsically Disordered	106
3.3 Discussion	109
3.4 Materials and Methods	122
3.4.1 Generation of Caspase Variants.....	122
3.4.2 Caspase Protein Expression and Purification.....	122
3.4.3 Caspase Activity Assays.....	123
3.4.4 Tau Protein Expression and Purification.....	124
3.4.5 Proteolysis of Tau Protein by Caspase-6 Variants	125
3.4.6 Hydrogen/Deuterium Exchange Mass Spectrometry.....	125
3.4.7 Circular Dichroism Spectroscopy.....	126
3.4.8 Intrinsic Fluorescence Spectroscopy	127
3.4.9 Caspase-6 Model Building and Disorder Prediction	127
3.5 Acknowledgments	128
3.6 References	128

4.	TUMOR-ASSOCIATED MUTATIONS IN CASPASE-6 NEGATIVELY IMPACT ITS CATALYTIC EFFICIENCY	134
4.1	Abstract	134
4.2	Introduction	135
4.3	Results and Discussion	139
4.3.1	Mutations in <i>CASP6</i> Gene Have Been Identified in Tumor Tissues	139
4.3.2	Caspase-6 Variants from Tumor Tissues Have Decreased Activity	142
4.3.3	Caspase-6 R259H Disrupts Interaction Necessary for the Proper Assembly of the Substrate-Binding Groove	148
4.4	Conclusions	152
4.5	Materials and Methods	154
4.5.1	Database Analysis of <i>CASP6</i> Gene Mutations	154
4.5.2	Generation of Caspase-6 Tumor-Associated Variants	155
4.5.3	Caspase-6 Protein Expression and Purification	155
4.5.4	Caspase-6 Activity Assays	156
4.5.5	Self-Proteolysis Assay of Caspase-6 Tumor- Associated Variants	157
4.5.6	Proteolysis of Procasapase-6 FL C163S Protein by Caspase-6 Tumor-Associated Variants	157
4.5.7	Intrinsic Fluorescence Spectroscopy	157
4.5.8	Caspase-6 Full-length Structural Model Generation.....	158
4.6	References	158
5.	PROCASPASE-6 IS INHIBITED BY NUCLEOTIDES AT THE DIMER INTERFACE	162
5.1	Introduction	162
5.2	Results	164
5.2.1	Procaspase-6 is Robustly Labeled by the ActivX ATP Acyl Phosphate Probe	164
5.2.2	Procaspase-6 Self-Processing is Inhibited by ATP	167
5.2.3	ATP Binds Procaspase-6 at Y198	168
5.2.4	Multiple Nucleotides Inhibit Procaspase-6	173
5.3	Discussion	174
5.4	Materials and Methods	178
5.4.1	Generation of Caspase Variants	178
5.4.2	Caspase Protein Expression and Purification	178
5.4.3	ATP Probe Labeling and Mass Spectrometry	180
5.4.4	Caspase-6 Activity Assays	180
5.4.5	Effect of ATP on the Activity of Cleaved and Active Caspase-6	181
5.4.6	Effect of ATP on the Proteolytic Cleavage of Procaspase-6 by Active Caspase-6	181

5.4.7 Effect of Nucleotides on the Self-Activation of Caspase-6.....	182
5.5 References	183
6. DISCOVERY OF POTENT AND SELECTIVE INHIBITORS OF CASPASE-6	187
6.1 Abstract	187
6.2 Introduction.....	188
6.3 Results and Discussion	192
6.3.1 Compound A is the Most Selective Caspase-6 Inhibitor to Date.....	192
6.3.2 Compound A Stabilizes Caspase-6	194
6.3.3 Compound A Inhibits Caspase-6 in Neuronal Cells.....	195
6.3.4 Intrinsic Chemical Reactivity Underlies Selectivity of Compound A	196
6.3.5 The Furoxan Moiety is Required for Compound A Reactivity.....	198
6.3.6 The Phenyl Ring Composition Is Important for Affinity	200
6.3.7 The Central Ring in Compound A Can Be Modified	206
6.3.8 The Bis- <i>N</i> -Oxides are Predicted to Have Good Blood- Brain Barrier Penetration	207
6.4 Summary and Conclusion	207
6.5 Materials and Methods	208
6.5.1 Sources of Compound A and its Analogs	208
6.5.2 Site-Directed Mutagenesis of Caspase-6	209
6.5.3 Caspase-3 Protein Expression and Purification	209
6.5.4 Caspase-6 Protein Expression and Purification	210
6.5.5 Caspase-7 Protein Expression and Purification	211
6.5.6 Caspase-8 Protein Expression and Purification	212
6.5.7 Caspase-9 Protein Expression and Purification	213
6.5.8 Caspase-6 Activity Assays	214
6.5.9 Caspase-6 Inhibition Assay	214
6.5.10 Caspase Selectivity Assays	215
6.5.11 Denaturing Mass Spectrometry of Caspase- 6:Compound A Complex.....	217
6.5.12 Tandem Mass Spectrometry of Caspase- 6:Compound A Complex.....	218
6.5.13 Thermal Stability by Differential Scanning Fluorimetry	218
6.5.14 Cell-Based Caspase-6 Inhibition Assay.....	219
6.5.15 Synthetic Schemes	221
6.6 References	237
7. UNIQUELY CASPASE-6: PROPOSITIONS OF THE DISTINCT STRUCTURAL ARCHITECTURES ON FUNCTION AND TARGETED REGULATION OF CASPASE-6.....	241

7.1 Proposed Functional and Regulatory Roles of the Structural Switch	244
7.2 Implications of the Local Dynamic Changes and the Disordered Prodomain	246
7.3 Consequences of the Mutagenic Pressure in Caspases-6.....	249
7.4 Caspase Dimer Interface, a Structural Hideout for Natural Ligands	251
7.5 Cys-264, a Perfect Anchor for the Specific Regulation of Caspase-6	253
7.6 References	254
8. BIBLIOGRAPHY	257

LIST OF TABLES

Table	Page
Table 2.1 Percent of Total Amide Hydrogen Exchanged with Deuterium....	54
Table 4.1 Identified Missense and Nonsense Mutations in Caspase-6 from Various Tumor Tissue Types and its Corresponding Tissue Distribution	143
Table 4.2 Kinetic Parameters of Selected Caspase-6 Tumor-Associated Variants Identified from COSMIC Database (Forbes, Bindal et al., 2011) and Other Sources (Lee, Kim et al., 2006).....	144
Table 6.1A Compound Analogs with Substitutions at the Phenyl Ring on the Triazole Moiety	201
Table 6.1B Compound Analogs with Substitutions at the Phenyl Ring on the Triazole Moiety	202
Table 6.1C Compound Analogs with Substitutions at the Phenyl Ring on the Triazole Moiety	203
Table 6.1D Compound Analogs with Substitutions at the Phenyl Ring on the Triazole Moiety	204
Table 6.1E Compound Analogs with Substitutions at the Phenyl Ring on the Triazole Moiety	205
Table 6.2 Compound Analogs with Double Bond at the Central Cyclohexane Ring.....	206

LIST OF FIGURES

Figure	Page
Figure 1.1: The Apoptotic Pathway.....	3
Figure 1.2: The Structural Organization of Caspases.....	5
Figure 1.3: Structures of Caspase-6 Maturation Variants.....	8
Figure 2.1: Caspase-6 Undergoes Helix-Strand Transition Upon Substrate Binding.....	32
Figure 2.2: H/D exchange Heat Map of the Relative Deuterium Incorporation.....	36
Figure 2.3: Relative Deuterium Incorporation of Caspase-6 Mapped onto its Corresponding Structures.....	37
Figure 2.4: Heat Maps of the Percent Difference in Deuterium Level Between Caspase-6 and Caspase-7.....	38
Figure 2.5: Heat Maps of the Percent Difference in Deuterium Level Between Caspase-6 and Caspase-7 Mapped onto its Corresponding Structures.....	39
Figure 2.6: Deuterium Uptake Plots of Caspase-7 in the Unliganded and DEVD-bound States.....	40
Figure 2.7: Deuterium Uptake Plots of Caspase-6 in the Unliganded and VEID-bound States.....	42
Figure 2.8: H/DX-MS Peptide Coverage Map for Caspase-6 and Caspase-7.....	45
Figure 2.9: Caspase-6 Shows Distinct Conformational Dynamics in its 130's Region.....	48
Figure 2.10: Representative MS Spectra of Key Peptides in Caspase-7....	50
Figure 2.11: Representative MS Spectra of Key Peptides in Caspase-6....	51
Figure 2.12: Protonation State of Glu-135 is Critical to the Dynamics of the 130's Region.....	56

Figure 2.13: E135Q Has Similar Kinetics and pH Profile as WT Caspase-6	60
Figure 2.14: The Stabilizing Effect of Constantly Protonated E135Q Variant is More Pronounced at Higher pH	61
Figure 2.15: Electrostatic Potential Map of Caspase-6	66
Figure 2.16: Model Showing Caspase-6 Undergoes a Helix-Strand Transition Upon Substrate Binding	66
Figure 3.1: Caspase-6 Maturation-State Variants	87
Figure 3.2: H/D Exchange Heat Map of the Relative Deuterium Incorporation for Caspase-6 Maturation-State Variants	92
Figure 3.3 The Percent Relative Deuterium Incorporations of Caspase- 6 Mutation Variants over the Course of the H/D Exchange Incubation Period are Mapped onto the Model Structure of Caspase-6	93
Figure 3.4: Coverage Map of the Peptic Peptides of Caspase-6 Maturation Variants Identified from H/DX-MS	94
Figure 3.5: Caspase-6 Displays Variable Conformational Flexibility Across States of its Proteolytic Activation.....	96
Figure 3.6: Map of the Electrostatic Potential of the Model Structure of Procaspase-6 Built from the Zymogen Crystal Structures	98
Figure 3.7: Intersubunit Linker Cleavage Increases Conformational Flexibility of All Substrate-Binding Loops	104
Figure 3.8: Intersubunit Linker Cleavage Leads to Increased Exposure of the Substrate-Binding Groove	105
Figure 3.9: The Prodomain is Intrinsically Disordered	108
Figure 3.10: A Schematic Model Highlighting the Changes in the Conformational Flexibility of Caspase-6 Along its Path to Proteolytic Maturation	111
Figure 3.11: Representative MS Spectra of Key Peptic Peptides Following H/D Exchange Experiments of Caspase-6 Maturation Variants	117

Figure 3.12: Additional Representative MS spectra of Key Peptic Peptides Following H/D Exchange Experiments of Caspase-6 Maturation Variants	118
Figure 3.13: Intrinsic Fluorescence Profile of Caspase-6 Maturation Variants Excited at 280 nm	119
Figure 3.14: Prediction of Disorder and Protein Binding in Caspases	119
Figure 3.15: Relative Deuterium Uptake Plots of Caspase-6 Maturation Variants Over the Course of the H/D Exchange Experiment	120
Figure 3.16: Additional Relative Deuterium Uptake Plots of Caspase-6 Maturation Variants Over the Course of the H/D Exchange Experiment	121
Figure 4.1: Tumor-Associated Mutations are Widely Distributed Across Caspase-6	137
Figure 4.2: Aberrant <i>CASP6</i> Gene Regulation Correlates with Percent Mutation in Caspase-6 in Tumor-Associated Tissue Types	141
Figure 4.3: Selected Caspase-6 Tumor-Associated Variants Showed Decreased in Proteolytic Activity	146
Figure 4.4: R259H Disrupts Interactions Necessary for Proper Assembly of the Substrate-Binding Groove.....	149
Figure 5.1: An Allosteric Site Exists at the Dimer Interface of Caspases.....	166
Figure 5.2: The ActivX ATP Acyl Phosphate Probe Binds Lys-133 in Procaspase-6.....	166
Figure 5.3: ATP Attenuates the Procaspase-6 Activity But Not Caspase-6 Activity	168
Figure 5.4: Tyr-198 of Procaspase-6 is a Putative Binding Site for ATP Acyl Phosphate Probe and ATP	170
Figure 5.5: The Crystal Structure of Procaspase-6 Bound to Compound 3	172
Figure 5.6: Caspase-6 Variants Showed Variation in Cleavage Patterns Dependent on its Activation State.	172

Figure 5.7: Structures of Small-Molecule Metabolites	174
Figure 6.1: High Throughput Screen Identified Potent and Selective Inhibitors of Caspase-6	193
Figure 6.2: Compound A Shows Exquisite Selectivity for Caspase-6	193
Figure 6.3: Compound A Binds and Stabilizes Caspase-6	194
Figure 6.4: Compound A Inhibits Caspase-6 Function in Neuronal Cells..	195
Figure 6.5: Compound A Covalently Binds to a Unique and Non-Active Site Cys-264	197
Figure 6.6: The Furozan <i>N</i> -Oxide in the Furoxan Moiety is Required for Reactivity, But the Triazole <i>N</i> -Oxide is Not Required for Function	199
Figure 6.7: The Selectivity Profile of a Representative Compound A Analog (CASP-6-III-20) Shows Potency Higher Than Compound A.....	205
Figure 7.1: Visual Summary of PhD Research Projects	241

CHAPTER 1

APOPTOTIC CASPASE STRUCTRE, FUNCTION, REGULATION, AND DISEASE IMPLICATIONS

1.1 Caspases in Programmed Cell Death

Multicellular organisms are composed of highly organized community of cells. This exquisite cellular organization affords tight regulations in both cell division and cell death necessary to maintain cellular homeostasis. Unwanted cells undergo suicide through a mechanism known as an intracellular *programmed cell death*, commonly referred to as *apoptosis* (from a Greek word meaning “falling off,” as leaves from a tree) (Kerr et al., 1972). Morphologically, apoptotic cell death is characterized by cell shrinkage, decrease in cell size, and tightly packed cytoplasm with visibly dense chromatin organization. Although apoptosis is typically associated with cell death, it has far-reaching influence on key cellular processes in organismal development, cellular differentiation, inflammation, and across diverse human diseases from cancer to neurodegeneration.

A family of highly conserved cysteine aspartate proteases, also known as *caspases*, is central to the execution of apoptosis. The momentous discovery of the first caspase in the family, caspase-1, was initially described (Black et al., 1989; Kostura et al., 1989) and further characterized by two independent research labs (Cerretti et al., 1992; Thornberry et al., 1992). This cysteine protease was originally given a name interleukin-1 β -converting enzyme (ICE) based on its ability to cleave interleukin-1 β . Around that time, an essential gene,

Ced-3, in the roundworm *Caenorhabditis elegans* was reported to have roles in programmed cell death during its development and shares greater than 24% identity with ICE (Yuan et al., 1993). This marks for the first time a cysteine protease was associated with programmed cell death. This finding inspired rapid identification and characterization of other caspases in the family. Later on, caspase-3 was identified to be the human homologue of *Ced-3* (Fernandes-Alnemri et al., 1994). Thereafter, other caspases were identified and characterized and an official nomenclature was established (Alnemri et al., 1996). There are now 12 human caspases that are broadly classified based on their function as either inflammatory (caspase-1, -4, and -5) or apoptotic. With the exception of caspase-14, which appears to be a highly specialized enzyme involved in the differentiation of corneocytes in the epidermis (Denecker et al., 2008), caspases are further classified based on their entry into the apoptotic cascades either as initiator (caspase-2, -8, -9, and -10) or executioner (-3, -6, and -7).

1.2 The Essential Elements of the Apoptotic Pathway

Apoptotic signaling (Figure 1.1) showcases the death-inducing power of caspases along with other factors that trigger their activation. Initiator caspase activation typically involves the formation of signaling complexes such as DISC (death-inducing signaling complex) (Muzio et al., 1998), the apoptosome (Cain et al., 2000), or the PIDDosome (Tinel and Tschopp, 2004) following the so-called extrinsic or intrinsic activation routes (MacKenzie and Clark, 2012). In the

extrinsic pathway, death ligands bind to death receptors to form a platform for binding of initiator caspases through its DED (death effector domain) motifs in the prodomain (Muzio et al., 1996) resulting in the oligomerization and subsequent activation of procaspases (Muzio et al., 1998; Oberst et al., 2010). In the intrinsic pathway, the exposure of the cell to various stimuli such as cytotoxic drugs, DNA damage, reactive oxygen species (ROS) triggers the activation of procaspase-9 through formation of the apoptosome, a multiprotein complex dependent on the binding of the cytochrome c, upon its release from the mitochondria, to the Apaf-1 and the CARD (caspase recruitment domain) of caspase-9 (Bao and Shi, 2007; Chu et al., 2001; Pop et al., 2006).

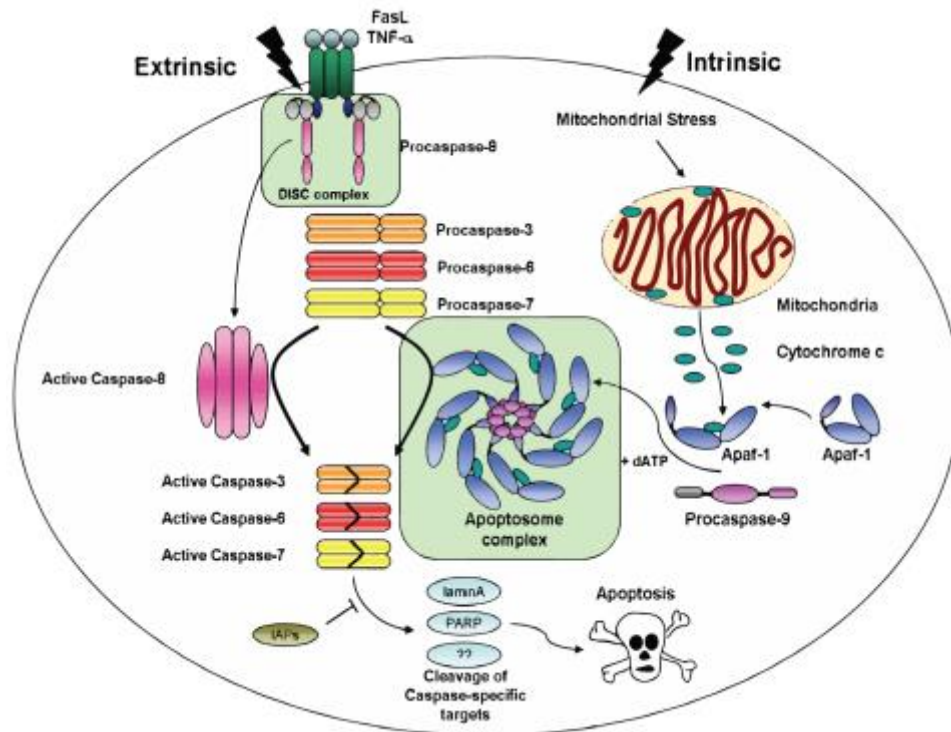


Figure 1.1 The Apoptotic Pathway

The initiation steps from both extrinsic and intrinsic apoptotic pathways are geared towards the activation of the initiator caspases that then activate the downstream executioner caspases to ultimately induce cellular death through series of proteolytic cleavage events of apoptotic targets. Clearly, the central contribution of caspases in the apoptotic pathway is a determinant of life and death of a cell, thus, underscoring the necessity to dissect every aspect of caspase structure, function, activation, and regulation. In this way, when the time comes we need to control these caspases for therapeutic reasons, we have the necessary tools to do so.

1.3 The Structure and Activation Mechanisms of Caspases

Nature has been very clever in the design of the activation pathways for these death-inducing caspases. Cells synthesize these caspases as inactive precursors, known interchangeably as *procaspases* or *zymogens*, to avoid unsolicited activation. It is only upon appropriate signal received by the cells that these caspases are activated through chain of proteolytic cleavage events. Moreover, these procaspases are organized to contain highly conserved aspartate residues that are positioned in between the prodomain and large subunit and in their intersubunit linker, which connects the large and small subunits together (Figure 1.2). Positioning these aspartate residues in these designated locations within procaspases ensures proper order of proteolytic events to occur for their appropriate activation.

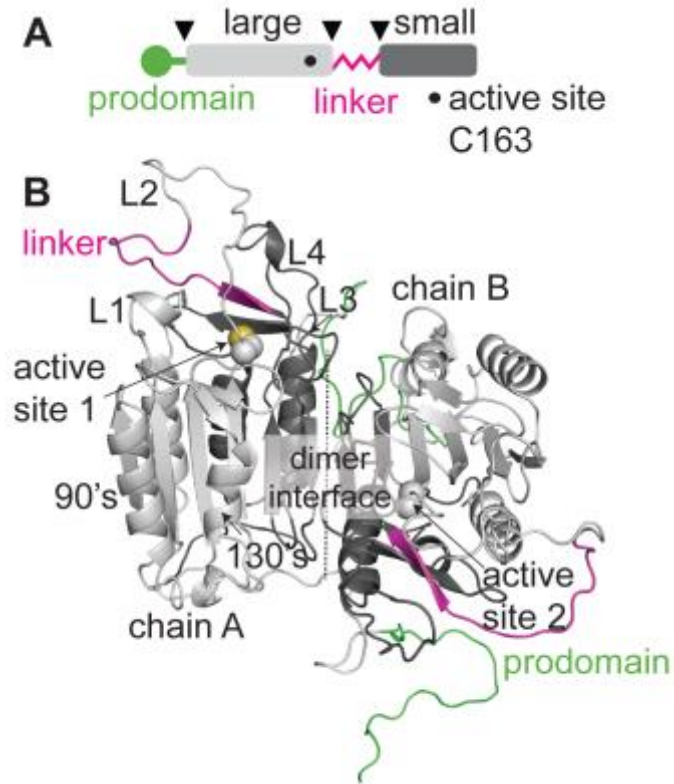


Figure 1.2 The Structural Organization of Caspase

(A) Linear cartoon of procaspase-6 illustrating the prodomain (*green*), large subunit (*light gray*), intersubunit linker (*magenta*) and small subunit (*dark gray*). The active site Cys–163 is denoted by a dot. Arrows indicate proteolytic cleavage sites. (B) Model of full-length procaspase-6 zymogen.

Initiator caspases generally exist as monomers and are subsequently activated by dimerization, which is mediated by formation of molecular platform (Bao and Shi, 2007; Chu et al., 2001; Muzio et al., 1996; Oberst et al., 2010; Pop et al., 2006)

In contrast, executioner caspases exist as dimeric inactive zymogens and are activated by limited proteolysis by initiator caspases. The proteolytic cleavage at the intersubunit linker allows conformational change that brings the two active sites of executioner caspase dimer together and forms a functional mature caspase (Pop and Salvesen, 2009; Riedl and Shi, 2004). The activated

executioner caspase can then cleave and activate other caspases creating a productive feedback loop for sustained caspase activation.

Despite variations in the mode to activation, there are unifying biochemical and structural features across the family of caspases. As enzymes, caspases engage the Cys–His catalytic dyad in their active site from each monomer of a homodimer (Figure 1.2) to cleave a peptide bond adjacent to an aspartate residue at the P1 cleavage site in select protein substrates. Moreover, the active site of caspases is composed of four mobile loops (L1, L2, L3, L4) that must be properly oriented to afford binding and efficient catalytic turnover of the target substrate. These mobile loops sample an ensemble of conformational states throughout the lifetime of the protein that enable flexibility of caspases to accommodate a spectrum of substrates and regulators.

Evidence for rearrangement in the mobile loops in caspase-6 along its path to proteolytic activation has been suggested by protein X-ray crystallography. The procaspase-6 zymogen (Cao et al., 2014; Wang et al., 2010), mature, unliganded caspase-6 (Baumgartner et al., 2009; Vaidya et al., 2011), and the substrate-bound (Muller et al., 2011; Wang et al., 2010) structures have all been solved (Figure 1.3) and will be described in the following sections to infer from the absence of key pieces of electron density that loop rearrangement in caspases are key to achieving a catalytically competent state of the enzyme. In the procaspase-6 zymogen structure, L3 is pinned down by the linker, which sits atop the active site cavity. L4 is disordered indicating a highly flexible loop that is possibly not engaged in interaction with other loops. The L2

that includes the catalytic Cys-163 is buried and stabilized across the dimer interface, a configuration far from a substrate-binding competent state. Cleavage in the intersubunit linker generates a mature and active caspase-6 wherein all loops deviate from the loop orientation of procaspase-6 zymogen. Also, with the intersubunit cleaved, L3 orients closer to L4, together with the reoriented L2, forms the catalytically active substrate-binding cavity. The conformations of the 60's and the 130's region in the mature unliganded caspase-6 are extended, which represent a noncanonical conformation of caspase-6. In particular, the observed conformation in the 130's region is not present in any other caspases. All other caspases are constitutively found in the canonical (strand) conformation, regardless of the activation state of the enzyme. Upon binding to an active site peptide-based inhibitor, L2 engages with L2' of the other half of the dimer and the rest of the loops are oriented to form the active site poised to bind and cleave substrates. The structural details of the activation of caspase-6 provide the platform to ascertain how mechanistically a caspase can be specifically targeted. Several inhibitors designed to target the mature caspase-6 have been shown to revert to its zymogen-like conformation particularly L2 being buried deep in the dimer interface cavity and thus suggests that the mobility of these loops is critical for the proper assembly of the substrate-binding groove for efficient binding and catalysis of substrates. Despite the abundance of crystal structures of the various forms of caspases, the information on the conformational dynamics of regions not visible in the crystal structures possibly due to their high flexibility are still missing specially the regions of the prodomain, linker, and in

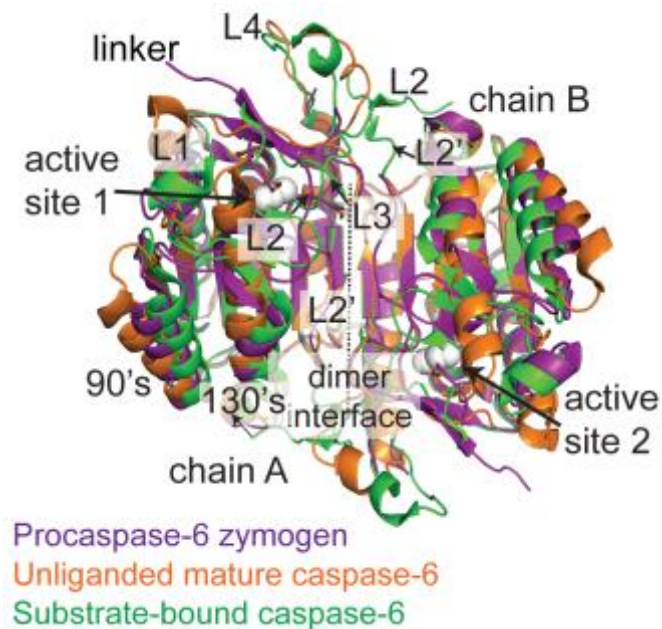


Figure 1.3 Structures of Caspase-6 Maturation Variants

The structures of procaspase-6 zymogen (PBD code 3NR2), the mature unliganded (PBD code 2WDP), and the substrate-bound (PDB code 3OD5) caspase-6.

some parts of L2 and L4. Thus, to provide a complete picture of the underlying mechanism of caspase activation, the missing information on the conformational dynamics in these disordered regions must be satisfied. This dissertation is geared to address this information gap with emphasis on the impact of the prodomain and linker on the conformational dynamics of caspase-6 along its route to proteolytic activation.

1.4 Distinguishing Features of Caspase-6

The discovery of unique and exploitable features in a caspase is an impeccable contribution towards efforts on targeted regulation of caspases. The

fact that caspases, in addition to having the same overall protein fold, share the same active site chemistry making targeted regulation of caspases very challenging. Structural studies have uncovered several key features in caspase-6 that are distinguishing from the rest of the member of the caspase family. Mature, unliganded caspase-6 displays an extended helical conformation in its 60's and 130's regions (Baumgartner et al., 2009; Vaidya et al., 2011) as well as having a longer L2, atypical for caspases. When locked in the extended helical conformation, mature caspase-6 is incompetent to bind substrates. This inability to bind and catalyze substrate turnover can be attributed to the Cys–His catalytic dyad, whose reactive centers should be within 1.8 to 3.5 Å (Štrajbl et al., 2000), are pushed way from each other by 9 Å (Vaidya et al., 2011) while a longer L2 was shown to regulate the autoactivation process of a procaspase-6 zymogen (Wang et al., 2010). In addition, sequence alignment analysis revealed that the regions of lowest amino acid conservation are in the regions of the prodomain and L4 across all caspases. Thus, despite some unique structural features of unknown functions, these points to an opportunity for strategic design of targeted regulation of caspases through enhanced understanding of these regions.

Biochemical and cellular studies of caspases have been important in underscoring unique functions and regulatory mechanisms of caspases. Particularly, the cellular studies in caspase-6 that revealed a unique self-activation mechanism (Klaiman et al., 2009), which could possibly be associated with caspase-6 being only weakly apoptotic, with its major roles outside the apoptotic pathways. The mechanism of self-activation of procaspase-6 was

further elucidated using structural studies through protein X-ray crystallography (Wang et al., 2010). Caspase-6 has been shown to often be activated by caspase-3, which is not typical for an executioner caspase that are usually activated by initiator caspases. Caspase-6 assumes roles that overlap to the roles of other caspases including as an inflammatory caspase being activated by caspase-1 (Guo et al., 2006) and as an initiator caspase directly cleaving caspase-8 (Cowling and Downward, 2002). In addition, although caspase-6 shares 41% and 37% sequence identity with executioner caspase-3 and caspase-7, respectively, its substrate specificity differs from that of executioners and matches closely to that of the initiator caspases (Julien et al., 2016; Thornberry et al., 1997). Lastly, IAPs (inhibitor of apoptosis proteins), known inhibitors of caspase-3 and caspase-7, which binds in the active site, cannot bind and inhibit caspase-6 (Suzuki et al., 2001). This suggests the possible existence of a unique conformational ensemble of caspase-6 in cellular conditions. Together, these data on the unique structural, biochemical, and cellular functions of caspase-6 suggest the potential for targeted regulation in caspase-6 that are open to exploration. This dissertation stages the exploitation of a unique cysteine in the most diversified loop (L4) in caspases, which has enabled targeted regulation of caspase-6.

1.5 Regulatory Mechanisms of Caspase-6

Several regulatory mechanisms have been demonstrated in caspase-6, which emphasizes the importance of its functions in the various cellular processes. One of the regulatory mechanisms in caspase-6 is through its prodomain. The prodomain in caspase-6 is not as clearly associated with particular cellular functions as in other caspases where the prodomain has been shown to participate, for example, in protein-protein interactions, which impact protein folding (Feeney and Clark, 2005) and proteasomal degradation (Choi et al., 2009). Recently, the prodomain has been found to inhibit the self-activation of procaspase-6 in HEK293T cells (Klaiman et al., 2009) and *in vitro* at low protein concentrations (Cao et al., 2014). In addition, zinc binding to caspase-6 has been reported to inhibit the enzyme activity of caspase-6. The regulatory mechanism was further explored using crystallography and found that zinc allosterically binds to caspase-6 in a region with low amino acid sequence conservation and thus is proposed to be an exosite unique to caspase-6 (Velazquez-Delgado and Hardy, 2012b).

One of the most highly interrogated mechanisms of enzyme regulation is through posttranslational modification and caspase-6 is not an exception. It has been shown that caspase-6 is phosphorylated at Ser-257 *in vivo* and *in vitro* (Suzuki et al., 2004). As a phosphomimetic to interrogate the mechanism of inhibition, the S257D substitution was introduced into mature caspase-6 and its crystal structure was solved, revealing the inhibitory action of phosphorylation, which stems from a steric clash that causes misalignment of substrate binding

groove resulting to a substrate-binding incompetent conformation (Velazquez-Delgado and Hardy, 2012a). Meanwhile, this same position was interrogated and a phosphomimetic S257E was introduced into the procaspase-6 zymogen and was found, in addition to the steric hindrance regulatory mechanism, to affect the self-activation of procaspase-6 by “locking” the enzyme in the TEVD-bound inhibited state (Cao et al., 2012). Quite recently, palmitoylation of caspase-6 by palmitoyl acyltransferase HIP4 was found to exert inhibitory mechanism to caspase-6 (Skotte et al., 2016). Predominant palmitoylation was found to be at the unique Cys–264 within L4 of caspase-6, which results in steric blockage of the substrate-binding groove as well as possibly through inhibition of caspase-6 dimerization.

Taken together, the fact that caspase-6 is tightly regulated at several levels indicate the sensitivity of the cellular homeostatic machineries to the presence of caspase-6. To add to this already complex regulatory mechanism of caspase-6, this dissertation explores cellular nucleotides as regulatory natural ligands specific for procaspase-6 zymogen form, of which cellular consequences remain to be uncovered.

1.6 Cancer-Associated Functions of Caspase-6

One of the hallmarks of cancer is the failure of apoptosis (Hanahan and Weinberg, 2011). Caspase-6 is broadly classified as one of the executioner caspases in the apoptotic cascade; however, the association of caspase-6 in cancer has been largely unexplored. Recent MS-based proteomics approach

revealed several unique caspase-6 substrates (Julien et al., 2016) that were identified to be tumor-associated based on its inclusion in the census of human cancer genes (Futreal et al., 2004). Notable substrates, among many others, include the subcellular tumor antigen p53, TP53 and the breast cancer type 1 susceptibility protein, BRCA1. Thus, the association of caspase-6 with these known tumor-associated substrates suggests the potential involvement of caspase-6 in the development of cancer.

In addition, a study on inflammation-induced tumorigenesis in a mouse model of colon cancer was shown to be independent of caspase-6.(Foveau et al., 2014). Mice overexpressing caspase-6 showed changes in the colonic tumor multiplicity, burden or distribution to be like that of the caspase-6 deficient mouse model of colon cancer. Thus, suggesting that caspase-6 is unlikely to contribute to colitis-associated tumors. However, in a separate study, it was shown that survivin-3B promotes chemoresistance and immune system surveillance escape by inhibiting caspase-8 and -6 in cancer cells (Vegran and Boidot, 2013). Survivin-3B increases the resistance of neoplastic cells to chemotherapeutics by inhibiting caspase-6 and caspase-8 activation (Vegran and Boidot, 2013). Moreover, survivin-3B overexpression also mediated resistance to cancer chemotherapy, in this case, through interactions with procaspase-6. Also, survivin-3B binding to procaspase-6 inhibited its activation despite mitochondrial depolarization and caspase-3 activation. Thus, suggesting the potential role of caspase-6 inhibition in promoting chemoresistance in cancer cells.

It has also been shown that select routes of chemotherapeutic intervention

depend on caspase-6 for cancer apoptotic cell death. One example where apoptotic execution was found to be solely dependent on caspase-6 rather than caspase-3 or caspase-7 in cancer apoptosis is aloe emodin (AE), a natural anthraquinone, is reported to have anti-proliferative activity in various cancer cell lines and induces apoptosis specifically through the activation of caspase-6 (Suboj et al., 2012). Thus, caspase-6-dependent apoptosis in these cancer cell lines indicates the unexplored impact of caspase-6 functions in cancer prevention.

Uncontrolled cell growth and reduced susceptibility to apoptosis are other hallmarks of cancer, and caspase inhibition can reduce the tendency of cells to undergo apoptosis, thus promoting tumorigenesis (Hanahan and Weinberg, 2011). Likewise, the development of inhibitory somatic mutations could potentially diminish cancer cell apoptosis. The Catalogue of Somatic Mutations in Cancer (COSMIC) database (Forbes et al., 2011), a comprehensive resource of occurring somatic mutations in human cancer, identified several *CASP6* gene somatic mutations. In addition, a mutational analysis study (Lee et al., 2006) found several missense and nonsense mutations in *CASP6* gene in gastric and colorectal tumor tissues. The identified tumor mutations have no reports on the functional characterization of the proteins resulting from mutant *CASP6* gene. This dissertation attempts to determine the effect of these mutations in caspase-6 function as a step to contribute to uncovering the roles of caspase-6 in cancer.

1.7 Neurodegenerative Attributes of Caspase-6

Unlike other executioner caspases, which require processing by initiator caspases for activation (Chai et al., 2001), caspase-6 can undergo self-cleavage and activation (Klaiman et al., 2009; Wang et al., 2010). Although self-cleavage does not lead to apoptosis, caspase-6 self-cleavage may account for some nonapoptotic roles of caspase-6 including axonal pruning in development (Harrington et al., 2010; Nikolaev et al., 2009; Schoenmann et al., 2010; Simon et al., 2012) and in the context of neurodegeneration. Caspase-6 cleaves a compelling set of neuronal substrates including microtubule-associated protein Tau (Horowitz et al., 2004). In that study, caspase-6 cleaved tau at Asp-13 in the *N*-terminal region implicates caspase-6 in the neurofibrillary tangle formation as well as in the evolution and progression of Alzheimer's disease (AD).

Caspase-6 also cleaves the AD-associated substrates amyloid precursor protein (APP) and presenilin I (PSENI) and II (PSENII) (Albrecht et al., 2009). In the Albrecht et al. (2009) study, caspase-6 activity was observed in APP Swedish and PSENI hippocampus and correlated with increased levels of beta amyloid peptide levels in these samples. The study suggested that the presence of caspase-6 activity in the AD APP, PSENI, and PSENII mutants implicates caspase-6 in the pathophysiology of AD.

In addition, caspase-6 also cleaves the Huntington's disease (HD)-associated polyglutamine-expanded and native huntingtin (htt) protein (Graham et al., 2010; Graham et al., 2006). Those prior studies showed that caspase-6 activity is observed before the onset of motor abnormalities in humans and in

murine models of HD and further showed that caspase-6 levels were directly proportional with CAG size and inversely correlated with age of onset. Moreover, in the YAC mice expressing caspase-6 resistant (C6R) mutant htt, where Asp-586 caspase-6 cleavage site in htt was mutated, showed decreases in both caspase-6 activity and apoptotic cell death. These data suggest that C6R mhtt is neuroprotective by influencing neuronal and excitotoxic pathways in HD. In a recent report, the genetic knockout of caspase-6 in the YAC128 mouse model of HD showed a decrease in mhtt-586 fragment that resulted in a partial rescue of body weight and reversal of depression-like phenotype, thus implicates caspase-6 as a key contributor to some features of HD (Wong et al., 2015).

Finally, caspase-6 cleaves Parkinson disease protein 7 (PARK7), also known as protein deglycase DJ-1 (Giaime et al., 2010). In that study, cleavage of DJ-1 by caspase-6 fully accounts for the p-53-dependent cell death and suggested to be neuroprotective. An early-onset PD-associated mutation in caspase-6 cleavage (D149A) in DJ-1 showed resistance to caspase-6 proteolysis and diminished its neuroprotective phenotype in PD.

Caspase-6 has now been embraced as a promising molecular target for neurodegenerative treatments because cleavage of these neuronal substrates plays key roles in the pathophysiological outcome in Alzheimer's (Albrecht et al., 2007; Galvan et al., 2002; Galvan et al., 2006; Gervais et al., 1999; Guo et al., 2004; Klaiman et al., 2008; LeBlanc, 2013; Lu et al., 2000; Nguyen et al., 2008; Saganich et al., 2006; Zhao et al., 2003), Huntington's (Aharony et al., 2015; Graham et al., 2010; Graham et al., 2006; Hermel et al., 2004; Milnerwood et al.,

2010; Riechers et al., 2016; Warby et al., 2008; Wong et al., 2015), and Parkinson's diseases (Giaime et al., 2010). Thus, understanding of caspase-6 structure and its relation to function is central to achieving targeted caspase-6 regulation in neurodegeneration.

1.8 Targeted Regulation of Caspase-6 using Natural and Synthetic Inhibitors

Because of the association of caspase-6 with neurodegeneration, the need to search for specific inhibitors of caspase-6 invokes a heightened interest. Unfortunately, caspases have overlapping substrate specificities (McStay et al., 2008), thus inhibitors directed at the active site will not be selective for only one caspase. This was demonstrated by the promiscuity of several competitive peptide-based inhibitor including ED11 (Wong et al., 2015), z-VEID-fmk (Eichhold et al., 1997) and aza-peptide epoxide and Michael acceptors class of inhibitors (Ekici et al., 2006; James et al., 2004) and the peptide-based inhibitor that was designed based on the caspase-6 cleavage site in the transcription factor AP-2 alpha (Nyormoi et al., 2003). The same promiscuity of caspase-6 active-site directed small molecule inhibitors was also observed including methylene blue (Pakavathkumar et al., 2015), the class of pancaspase irreversible inhibitors identified through substrate-based fragment approach (Leyva et al., 2010) and several other series of sulfonamide Isatin Michael acceptors (Chu et al., 2009). Taken together, due to the similarity of the binding interfaces and chemistry of caspases in their active sites, the aim of targeted

caspase-6 regulation using active site directed inhibitors is nearly impossible.

Several attempts to synthesize uncompetitive small molecule inhibitors have also been reported. A seemingly potent (11 nM) and selective (10-fold) caspase-6-specific inhibitors were uncompetitive inhibitors (Heise et al., 2012). Its inability to inhibiting cleavage of lamin A by caspase-6 *in vitro*, led the authors to realize that this inhibitor only works with fluorogenic substrate but not with other fluorogenic substrate nor any native substrates. Thus, this class of inhibitors has no potential whatsoever as a drug lead. This finding underscores the need for new classes of caspase-6 inhibitors.

So far, any attempts to inhibit caspase-6 exploiting the active site have not been successful, thus allosteric inhibition to enable capase-6 specific inhibition is promising. An example of an allosteric peptide inhibitor is Pep419 (Stanger et al., 2012), a low micromolar inhibitor that binds and promotes procaspase-6 zymogen tetramerization, thus preventing proteolytic activation of procaspase-6. Pep419 was identified through phage display. It has been shown to be selective for caspase-6 in neuronal cells but exhibited poor cell penetration properties, as it required electroporation for delivery to neuronal cells. This suggests a clear limitation for applications in cellular studies and as a future therapeutic lead. Lastly, an allosteric small molecular inhibitor from a fragment-merging strategy identified nanomolar-affinity ligands that bind in the dimer interface and stabilize procaspase-6 and prevent it from activation. These compounds have been shown to lock L2 in the inactive conformation, thus preventing its rearrangement as part of the loop assembly to form the substrate-binding competent active site

cavity (Murray et al., 2014). However, these compounds have unknown selectivity profile, thus making it less promising to become therapeutic leads. Moreover, active caspase-6 accumulates before the onset of AD symptoms (Albrecht et al., 2007), thus stabilizing procaspase-6 zymogen conformation may be less impactful in the treatment of AD.

Finally, the only known caspase-6-specific natural inhibitor is the alternatively spliced isoform of caspase-6 known as procaspase-6b (Lee et al., 2010). This natural inhibitor binds procaspase-6 and inhibits its proteolytic activation *in vitro* and *in vivo*. However, although the procaspase-6b active site Cys-163 is intact, it shows no activity nor it can inhibit already activated caspase-6. The potential of this natural inhibitor as a scaffold for the design of a peptide-based caspase-6-specific inhibitors is encouraging. The fact that it shows cell-based activity against procaspase-6 proteolytic activation suggests favorable binding characteristics that can potentially be exploited for therapeutic purposes.

In summary, caspases impact a spectrum of diseases from cancer to neurodegeneration. Thus, understanding their structure, dynamics, function, activation, and regulation is critical to providing means to control its cellular functions for therapeutic purposes. The findings of caspase-6 to be highly associated in neurodegeneration and cancer provide the necessary inspiration to search for strategies to specifically target its activity and its associated debilitating functions. In this dissertation, we use multi-level approach to probe the domain architecture and structural dynamics of caspase-6 for its targeted regulation.

1.9 References

- Aharony, I., D. E. Ehrnhoefer, A. Shruster, X. Qiu, S. Franciosi, M. R. Hayden, and D. Offen. 2015. A Huntingtin-based peptide inhibitor of caspase-6 provides protection from mutant Huntingtin-induced motor and behavioral deficits. *Hum Mol Genet*, 24:2604-14.
- Albrecht, S., N. Bogdanovic, B. Ghetti, B. Winblad, and A. C. LeBlanc. 2009. Caspase-6 activation in familial Alzheimer disease brains carrying amyloid precursor protein or presenilin I or presenilin II mutations. *J Neuropathol Exp Neurol*, 68:1282-93.
- Albrecht, S., M. Bourdeau, D. Bennett, E. J. Mufson, M. Bhattacharjee, and A. C. LeBlanc. 2007. Activation of caspase-6 in aging and mild cognitive impairment. *Am J Pathol*, 170:1200-9.
- Alnemri, E. S., D. J. Livingston, D. W. Nicholson, G. Salvesen, N. A. Thornberry, W. W. Wong, and J. Yuan. 1996. Human ICE/CED-3 protease nomenclature. *Cell*, 87:171.
- Bao, Q., and Y. Shi. 2007. Apoptosome: a platform for the activation of initiator caspases. *Cell Death and Differentiation*, 14:56-65.
- Baumgartner, R., G. Meder, C. Briand, A. Decock, A. D'Arcy, U. Hassiepen, R. Morse, and M. Ratus. 2009. The crystal structure of caspase-6, a selective effector of axonal degeneration. *Biochem J*, 423:429-39.
- Black, R. A., S. R. Kronheim, and P. R. Sleath. 1989. Activation of interleukin-1 beta by a co-induced protease. *FEBS Letters*, 247:386-90.
- Cain, K., S. B. Bratton, C. Langlais, G. Walker, D. G. Brown, X. M. Sun, and G. M. Cohen. 2000. Apaf-1 oligomerizes into biologically active approximately 700-kDa and inactive approximately 1.4-MDa apoptosome complexes. *Journal of Biological Chemistry*, 275:6067-70.
- Cao, Q., X. J. Wang, L. F. Li, and X. D. Su. 2014. The regulatory mechanism of the caspase 6 pro-domain revealed by crystal structure and biochemical assays. *Acta Crystallogr D Biol Crystallogr*, 70:58-67.
- Cao, Q., X. J. Wang, C. W. Liu, D. F. Liu, L. F. Li, Y. Q. Gao, and X. D. Su. 2012. Inhibitory mechanism of caspase-6 phosphorylation revealed by crystal structures, molecular dynamics simulations, and biochemical assays. *J Biol Chem*, 287:15371-9.
- Cerretti, D. P., C. J. Kozlosky, B. Mosley, N. Nelson, K. Van Ness, T. A. Greenstreet, C. J. March, S. R. Kronheim, T. Druck, L. A. Cannizzaro, and et al. 1992. Molecular cloning of the interleukin-1 beta converting enzyme. *Science*, 256:97-100.
- Chai, J., Q. Wu, E. Shiozaki, S. M. Srinivasula, E. S. Alnemri, and Y. Shi. 2001. Crystal structure of a procaspase-7 zymogen: mechanisms of activation and substrate binding. *Cell*, 107:399-407.
- Choi, Y. E., M. Butterworth, S. Malladi, C. S. Duckett, G. M. Cohen, and S. B. Bratton. 2009. The E3 ubiquitin ligase cIAP1 binds and ubiquitinates caspase-3 and -7 via unique mechanisms at distinct steps in their processing. *Journal of Biological Chemistry*, 284:12772-82.

- Chu, W., J. Rothfuss, Y. Chu, D. Zhou, and R. H. Mach. 2009. Synthesis and in vitro evaluation of sulfonamide isatin Michael acceptors as small molecule inhibitors of caspase-6. *J Med Chem*, 52:2188-91.
- Chu, Z. L., F. Pio, Z. Xie, K. Welsh, M. Krajewska, S. Krajewski, A. Godzik, and J. C. Reed. 2001. A novel enhancer of the Apaf1 apoptosome involved in cytochrome c-dependent caspase activation and apoptosis. *Journal of Biological Chemistry*, 276:9239-45.
- Cowling, V., and J. Downward. 2002. Caspase-6 is the direct activator of caspase-8 in the cytochrome c-induced apoptosis pathway- absolute requirement for removal of caspase-6 prodomain. *Cell Death and Differentiation*, 9:1046-1056.
- Denecker, G., P. Ovaere, P. Vandenabeele, and W. Declercq. 2008. Caspase-14 reveals its secrets. *Journal of Cell Biology*, 180:451-8.
- Eichhold, T. H., E. B. Hookfin, Y. O. Taiwo, B. De, and K. R. Wehmeyer. 1997. Isolation and quantification of fluoroacetate in rat tissues, following dosing of Z-Phe-Ala-CH₂-F, a peptidyl fluoromethyl ketone protease inhibitor. *Journal of Pharmaceutical and Biomedical Analysis*, 16:459-467.
- Ekici, O. D., Z. Z. Li, A. J. Campbell, K. E. James, J. L. Asgjan, J. Mikolajczyk, G. S. Salvesen, R. Ganesan, S. Jelakovic, M. G. Grutter, and J. C. Powers. 2006. Design, synthesis, and evaluation of aza-peptide Michael acceptors as selective and potent inhibitors of caspases-2, -3, -6, -7, -8, -9, and -10. *J Med Chem*, 49:5728-49.
- Feeney, B., and A. C. Clark. 2005. Reassembly of active caspase-3 is facilitated by the propeptide. *J Biol Chem*, 280:39772-85.
- Fernandes-Alnemri, T., G. Litwack, and E. S. Alnemri. 1994. CPP32, a novel human apoptotic protein with homology to *Caenorhabditis elegans* cell death protein Ced-3 and mammalian interleukin-1 beta-converting enzyme. *Journal of Biological Chemistry*, 269:30761-4.
- Forbes, S. A., N. Bindal, S. Bamford, C. Cole, C. Y. Kok, D. Beare, M. Jia, R. Shepherd, K. Leung, A. Menzies, J. W. Teague, P. J. Campbell, M. R. Stratton, and P. A. Futreal. 2011. COSMIC: mining complete cancer genomes in the Catalogue of Somatic Mutations in Cancer. *Nucleic Acids Res*, 39:D945-50.
- Foveau, B., L. Van Der Kraak, N. Beauchemin, S. Albrecht, and A. C. LeBlanc. 2014. Inflammation-induced tumorigenesis in mouse colon is caspase-6 independent. *PLoS One*, 9:e114270.
- Futreal, P. A., L. Coin, M. Marshall, T. Down, T. Hubbard, R. Wooster, N. Rahman, and M. R. Stratton. 2004. A census of human cancer genes. *Nat Rev Cancer*, 4:177-183.
- Galvan, V., S. Chen, D. Lu, A. Logvinova, P. Goldsmith, E. H. Koo, and D. E. Bredesen. 2002. Caspase cleavage of members of the amyloid precursor family of proteins. *J Neurochem*, 82:283-94.

- Galvan, V., O. F. Gorostiza, S. Banwait, M. Ataie, A. V. Logvinova, S. Sitaraman, E. Carlson, S. A. Sagi, N. Chevallier, K. Jin, D. A. Greenberg, and D. E. Bredesen. 2006. Reversal of Alzheimer's-like pathology and behavior in human APP transgenic mice by mutation of Asp664. *Proc Natl Acad Sci U S A*, 103:7130-5.
- Gervais, F. G., D. Xu, G. S. Robertson, J. P. Vaillancourt, Y. Zhu, J. Huang, A. LeBlanc, D. Smith, M. Rigby, M. S. Shearman, E. E. Clarke, H. Zheng, L. H. T. Van Der Ploeg, S. C. Ruffolo, N. A. Thornberry, S. Xanthoudakis, R. J. Zamboni, S. Roy, and D. W. Nicholson. 1999. Involvement of Caspases in Proteolytic Cleavage of Alzheimer's Amyloid- β Precursor Protein and Amyloidogenic A β Peptide Formation. *Cell*, 97:395-406.
- Giaime, E., C. Sunyach, C. Druon, S. Scarzello, G. Robert, S. Grosso, P. Auburger, M. S. Goldberg, J. Shen, P. Heutink, J. Pouyssegur, G. Pages, F. Checler, and C. Alves da Costa. 2010. Loss of function of DJ-1 triggered by Parkinson's disease-associated mutation is due to proteolytic resistance to caspase-6. *Cell Death Differ*, 17:158-69.
- Graham, R. K., Y. Deng, J. Carroll, K. Vaid, C. Cowan, M. A. Pouladi, M. Metzler, N. Bissada, L. Wang, R. L. Faull, M. Gray, X. W. Yang, L. A. Raymond, and M. R. Hayden. 2010. Cleavage at the 586 amino acid caspase-6 site in mutant huntingtin influences caspase-6 activation in vivo. *J Neurosci*, 30:15019-29.
- Graham, R. K., Y. Deng, E. J. Slow, B. Haigh, N. Bissada, G. Lu, J. Pearson, J. Shehadeh, L. Bertram, Z. Murphy, S. C. Warby, C. N. Doty, S. Roy, C. L. Wellington, B. R. Leavitt, L. A. Raymond, D. W. Nicholson, and M. R. Hayden. 2006. Cleavage at the caspase-6 site is required for neuronal dysfunction and degeneration due to mutant huntingtin. *Cell*, 125:1179-91.
- Guo, H., S. Albrecht, M. Bourdeau, T. Petzke, C. Bergeron, and A. C. LeBlanc. 2004. Active caspase-6 and caspase-6-cleaved tau in neuropil threads, neuritic plaques, and neurofibrillary tangles of Alzheimer's disease. *Am J Pathol*, 165:523-31.
- Guo, H., D. Petrin, Y. Zhang, C. Bergeron, C. G. Goodyer, and A. C. LeBlanc. 2006. Caspase-1 activation of caspase-6 in human apoptotic neurons. *Cell Death Differ*, 13:285-92.
- Hanahan, D., and R. A. Weinberg. 2011. Hallmarks of cancer: the next generation. *Cell*, 144:646-74.
- Harrington, E. P., C. Zhao, S. P. Fancy, S. Kaing, R. J. Franklin, and D. H. Rowitch. 2010. Oligodendrocyte PTEN is required for myelin and axonal integrity, not remyelination. *Annals of Neurology*, 68:703-16.
- Heise, C. E., J. Murray, K. E. Augustyn, B. Bravo, P. Chugha, F. Cohen, A. M. Giannetti, P. Gibbons, R. N. Hannoush, B. R. Hearn, P. Jaishankar, C. Q. Ly, K. Shah, K. Stanger, M. Steffek, Y. Tang, X. Zhao, J. W. Lewcock, A. R. Renslo, J. Flygare, and M. R. Arkin. 2012. Mechanistic and structural understanding of uncompetitive inhibitors of caspase-6. *PLoS One*, 7:e50864.

- Hermel, E., J. Gafni, S. S. Propp, B. R. Leavitt, C. L. Wellington, J. E. Young, A. S. Hackam, A. V. Logvinova, A. L. Peel, S. F. Chen, V. Hook, R. Singaraja, S. Krajewski, P. C. Goldsmith, H. M. Ellerby, M. R. Hayden, D. E. Bredesen, and L. M. Ellerby. 2004. Specific caspase interactions and amplification are involved in selective neuronal vulnerability in Huntington's disease. *Cell Death and Differentiation*, 11:424-438.
- Horowitz, P. M., K. R. Patterson, A. L. Guillozet-Bongaarts, M. R. Reynolds, C. A. Carroll, S. T. Weintraub, D. A. Bennett, V. L. Cryns, R. W. Berry, and L. I. Binder. 2004. Early N-terminal changes and caspase-6 cleavage of tau in Alzheimer's disease. *J Neurosci*, 24:7895-902.
- James, K. E., J. L. Asgian, Z. Z. Li, O. D. Ekici, J. R. Rubin, J. Mikolajczyk, G. S. Salvesen, and J. C. Powers. 2004. Design, synthesis, and evaluation of aza-peptide epoxides as selective and potent inhibitors of caspases-1, -3, -6, and -8. *J Med Chem*, 47:1553-74.
- Julien, O., M. Zhuang, A. P. Wiita, A. J. O'Donoghue, G. M. Knudsen, C. S. Craik, and J. A. Wells. 2016. Quantitative MS-based enzymology of caspases reveals distinct protein substrate specificities, hierarchies, and cellular roles. *Proceedings of the National Academy of Sciences of the United States of America*, 113:E2001-10.
- Kerr, J. F., A. H. Wyllie, and A. R. Currie. 1972. Apoptosis: a basic biological phenomenon with wide-ranging implications in tissue kinetics. *British Journal of Cancer*, 26:239-57.
- Klaiman, G., N. Champagne, and A. C. LeBlanc. 2009. Self-activation of Caspase-6 in vitro and in vivo: Caspase-6 activation does not induce cell death in HEK293T cells. *Biochim Biophys Acta*, 1793:592-601.
- Klaiman, G., T. L. Petzke, J. Hammond, and A. C. Leblanc. 2008. Targets of caspase-6 activity in human neurons and Alzheimer disease. *Mol Cell Proteomics*, 7:1541-55.
- Kostura, M. J., M. J. Tocci, G. Limjuco, J. Chin, P. Cameron, A. G. Hillman, N. A. Chartrain, and J. A. Schmidt. 1989. Identification of a monocyte specific pre-interleukin 1 beta convertase activity. *Proceedings of the National Academy of Sciences of the United States of America*, 86:5227-31.
- LeBlanc, A. C. 2013. Caspase-6 as a novel early target in the treatment of Alzheimer's disease. *Eur J Neurosci*, 37:2005-18.
- Lee, A. W., N. Champagne, X. Wang, X. D. Su, C. Goodyer, and A. C. Leblanc. 2010. Alternatively spliced caspase-6B isoform inhibits the activation of caspase-6A. *J Biol Chem*, 285:31974-84.
- Lee, J. W., M. R. Kim, Y. H. Soung, S. W. Nam, S. H. Kim, J. Y. Lee, N. J. Yoo, and S. H. Lee. 2006. Mutational analysis of the CASP6 gene in colorectal and gastric carcinomas. *APMIS*, 114:646-50.
- Leyva, M. J., F. Degiacomo, L. S. Kaltenbach, J. Holcomb, N. Zhang, J. Gafni, H. Park, D. C. Lo, G. S. Salvesen, L. M. Ellerby, and J. A. Ellman. 2010. Identification and evaluation of small molecule pan-caspase inhibitors in Huntington's disease models. *Chem Biol*, 17:1189-200.

- Lu, D. C., S. Rabizadeh, S. Chandra, R. F. Shayya, L. M. Ellerby, X. Ye, G. S. Salvesen, E. H. Koo, and D. E. Bredesen. 2000. A second cytotoxic proteolytic peptide derived from amyloid β -protein precursor. *Nature Medicine*, 6:397-404.
- MacKenzie, S. H., and A. C. Clark. 2012. Death by caspase dimerization. *Advances in Experimental Medicine and Biology*, 747:55-73.
- McStay, G. P., G. S. Salvesen, and D. R. Green. 2008. Overlapping cleavage motif selectivity of caspases: implications for analysis of apoptotic pathways. *Cell Death Differ*, 15:322-31.
- Milnerwood, A. J., C. M. Gladding, M. A. Pouladi, A. M. Kaufman, R. M. Hines, J. D. Boyd, R. W. Ko, O. C. Vasuta, R. K. Graham, M. R. Hayden, T. H. Murphy, and L. A. Raymond. 2010. Early increase in extrasynaptic NMDA receptor signaling and expression contributes to phenotype onset in Huntington's disease mice. *Neuron*, 65:178-90.
- Muller, I., M. B. Lamers, A. J. Ritchie, C. Dominguez, I. Munoz-Sanjuan, and A. Kiselyov. 2011. Structure of human caspase-6 in complex with Z-VAD-FMK: New peptide binding mode observed for the non-canonical caspase conformation. *Bioorg Med Chem Lett*, 21:5244-7.
- Murray, J., A. M. Giannetti, M. Steffek, P. Gibbons, B. R. Hearn, F. Cohen, C. Tam, C. Pozniak, B. Bravo, J. Lewcock, P. Jaishankar, C. Q. Ly, X. Zhao, Y. Tang, P. Chugha, M. R. Arkin, J. Flygare, and A. R. Renslo. 2014. Tailoring small molecules for an allosteric site on procaspase-6. *ChemMedChem*, 9:73-7, 2.
- Muzio, M., A. M. Chinnaiyan, F. C. Kischkel, K. O'Rourke, A. Shevchenko, J. Ni, C. Scaffidi, J. D. Bretz, M. Zhang, R. Gentz, M. Mann, P. H. Krammer, M. E. Peter, and V. M. Dixit. 1996. FLICE, a novel FADD-homologous ICE/CED-3-like protease, is recruited to the CD95 (Fas/APO-1) death-inducing signaling complex. *Cell*, 85:817-27.
- Muzio, M., B. R. Stockwell, H. R. Stennicke, G. S. Salvesen, and V. M. Dixit. 1998. An induced proximity model for caspase-8 activation. *Journal of Biological Chemistry*, 273:2926-30.
- Nguyen, T. V., V. Galvan, W. Huang, S. Banwait, H. Tang, J. Zhang, and D. E. Bredesen. 2008. Signal transduction in Alzheimer disease: p21-activated kinase signaling requires C-terminal cleavage of APP at Asp664. *J Neurochem*, 104:1065-80.
- Nikolaev, A., T. McLaughlin, D. D. O'Leary, and M. Tessier-Lavigne. 2009. APP binds DR6 to trigger axon pruning and neuron death via distinct caspases. *Nature*, 457:981-9.
- Nyormoi, O., Z. Wang, and M. Bar-Eli. 2003. Sequence-based discovery of a synthetic peptide inhibitor of caspase 6. *Apoptosis*, 8:371-6.
- Oberst, A., C. Pop, A. G. Tremblay, V. Blais, J. B. Denault, G. S. Salvesen, and D. R. Green. 2010. Inducible dimerization and inducible cleavage reveal a requirement for both processes in caspase-8 activation. *Journal of Biological Chemistry*, 285:16632-42.

- Pakavathkumar, P., G. Sharma, V. Kaushal, B. Foveau, and A. C. LeBlanc. 2015. Methylene Blue Inhibits Caspases by Oxidation of the Catalytic Cysteine. *Sci Rep*, 5:13730.
- Pop, C., and G. S. Salvesen. 2009. Human caspases: activation, specificity, and regulation. *Journal of Biological Chemistry*, 284:21777-81.
- Pop, C., J. Timmer, S. Sperandio, and G. S. Salvesen. 2006. The apoptosome activates caspase-9 by dimerization. *Molecular Cell*, 22:269-75.
- Riechers, S. P., S. Butland, Y. Deng, N. Skotte, D. E. Ehrnhoefer, J. Russ, J. Laine, M. Laroche, M. A. Pouladi, E. E. Wanker, M. R. Hayden, and R. K. Graham. 2016. Interactome network analysis identifies multiple caspase-6 interactors involved in the pathogenesis of HD. *Hum Mol Genet*, 25:1600-18.
- Riedl, S. J., and Y. Shi. 2004. Molecular mechanisms of caspase regulation during apoptosis. *Nat Rev Mol Cell Biol*, 5:897-907.
- Saganich, M. J., B. E. Schroeder, V. Galvan, D. E. Bredesen, E. H. Koo, and S. F. Heinemann. 2006. Deficits in synaptic transmission and learning in amyloid precursor protein (APP) transgenic mice require C-terminal cleavage of APP. *J Neurosci*, 26:13428-36.
- Schoenmann, Z., E. Assa-Kunik, S. Tiomny, A. Minis, L. Haklai-Topper, E. Arama, and A. Yaron. 2010. Axonal degeneration is regulated by the apoptotic machinery or a NAD⁺-sensitive pathway in insects and mammals. *Journal of Neuroscience*, 30:6375-86.
- Simon, D. J., R. M. Weimer, T. McLaughlin, D. Kallop, K. Stanger, J. Yang, D. D. O'Leary, R. N. Hannoush, and M. Tessier-Lavigne. 2012. A caspase cascade regulating developmental axon degeneration. *Journal of Neuroscience*, 32:17540-53.
- Skotte, N. H., S. S. Sanders, R. R. Singaraja, D. E. Ehrnhoefer, K. Vaid, X. Qiu, S. Kannan, C. Verma, and M. R. Hayden. 2016. Palmitoylation of caspase-6 by HIP14 regulates its activation. *Cell Death and Differentiation*.
- Stanger, K., M. Steffek, L. Zhou, C. D. Poznaniak, C. Quan, Y. Franke, J. Tom, C. Tam, J. M. Elliott, J. W. Lewcock, Y. Zhang, J. Murray, and R. N. Hannoush. 2012. Allosteric peptides bind a caspase zymogen and mediate caspase tetramerization. *Nat Chem Biol*, 8:655-60.
- Štrajbl, M., J. Florián, and A. Warshel. 2000. Ab initio/LD studies of chemical reactions in solution: Reference free-energy surfaces for acylation reactions occurring in serine and cysteine proteases. *International Journal of Quantum Chemistry*, 77:44-53.
- Suboj, P., S. Babykutty, P. Srinivas, and S. Gopala. 2012. Aloe emodin induces G2/M cell cycle arrest and apoptosis via activation of caspase-6 in human colon cancer cells. *Pharmacology*, 89:91-8.
- Suzuki, A., G. Kusakai, A. Kishimoto, Y. Shimojo, S. Miyamoto, T. Ogura, A. Ochiai, and H. Esumi. 2004. Regulation of caspase-6 and FLIP by the AMPK family member ARK5. *Oncogene*, 23:7067-75.

- Suzuki, Y., Y. Nakabayashi, K. Nakata, J. C. Reed, and R. Takahashi. 2001. X-linked inhibitor of apoptosis protein (XIAP) inhibits caspase-3 and -7 in distinct modes. *Journal of Biological Chemistry*, 276:27058-63.
- Thornberry, N. A., H. G. Bull, J. R. Calaycay, K. T. Chapman, A. D. Howard, M. J. Kostura, D. K. Miller, S. M. Molineaux, J. R. Weidner, J. Aunins, and et al. 1992. A novel heterodimeric cysteine protease is required for interleukin-1 beta processing in monocytes. *Nature*, 356:768-74.
- Thornberry, N. A., T. A. Rano, E. P. Peterson, D. M. Rasper, T. Timkey, M. Garcia-Calvo, V. M. Houtzager, P. A. Nordstrom, S. Roy, J. P. Vaillancourt, K. T. Chapman, and D. W. Nicholson. 1997. A combinatorial approach defines specificities of members of the caspase family and granzyme B. Functional relationships established for key mediators of apoptosis. *J Biol Chem*, 272:17907-11.
- Tinel, A., and J. Tschopp. 2004. The PIDDosome, a protein complex implicated in activation of caspase-2 in response to genotoxic stress. *Science*, 304:843-6.
- Vaidya, S., E. M. Velazquez-Delgado, G. Abbruzzese, and J. A. Hardy. 2011. Substrate-induced conformational changes occur in all cleaved forms of caspase-6. *J Mol Biol*, 406:75-91.
- Vegran, F., and R. Boidot. 2013. Survivin-3B promotes chemoresistance and immune escape by inhibiting caspase-8 and -6 in cancer cells. *Oncoimmunology*, 2:e26328.
- Velazquez-Delgado, E. M., and J. A. Hardy. 2012a. Phosphorylation regulates assembly of the caspase-6 substrate-binding groove. *Structure*, 20:742-51.
- . 2012b. Zinc-mediated allosteric inhibition of caspase-6. *J Biol Chem*, 287:36000-11.
- Wang, X. J., Q. Cao, X. Liu, K. T. Wang, W. Mi, Y. Zhang, L. F. Li, A. C. LeBlanc, and X. D. Su. 2010. Crystal structures of human caspase 6 reveal a new mechanism for intramolecular cleavage self-activation. *EMBO Rep*, 11:841-7.
- Warby, S. C., C. N. Doty, R. K. Graham, J. B. Carroll, Y. Z. Yang, R. R. Singaraja, C. M. Overall, and M. R. Hayden. 2008. Activated caspase-6 and caspase-6-cleaved fragments of huntingtin specifically colocalize in the nucleus. *Hum Mol Genet*, 17:2390-404.
- Wong, B. K., D. E. Ehrnhoefer, R. K. Graham, D. D. Martin, S. Ladha, V. Uribe, L. M. Stanek, S. Franciosi, X. Qiu, Y. Deng, V. Kovalik, W. Zhang, M. A. Pouladi, L. S. Shihabuddin, and M. R. Hayden. 2015. Partial rescue of some features of Huntington Disease in the genetic absence of caspase-6 in YAC128 mice. *Neurobiol Dis*, 76:24-36.
- Yuan, J., S. Shaham, S. Ledoux, H. M. Ellis, and H. R. Horvitz. 1993. The *C. elegans* cell death gene *ced-3* encodes a protein similar to mammalian interleukin-1 beta-converting enzyme. *Cell*, 75:641-52.
- Zhao, M., J. Su, E. Head, and C. W. Cotman. 2003. Accumulation of caspase cleaved amyloid precursor protein represents an early neurodegenerative event in aging and in Alzheimer's disease. *Neurobiol Dis*, 14:391-403.

CHAPTER 2

CASPASE-6 UNDERGOES A DISTINCT HELIX-STRAND INTERCONVERSION UPON SUBSTRATE BINDING

This chapter was published as: Dagbay, K. B., N. Bolik-Coulon, S. N. Savinov, and J. A. Hardy. 2017. Caspase-6 Undergoes a Distinct Helix-Strand Interconversion Upon Substrate Binding. *Journal of Biological Chemistry*, 292:4885-4897. K.B.D. initiated and performed all experimental aspects of the study, performed the extensive final analysis of H/DX-MS data, prepared all final figures and was the principal author for the manuscript. N.B.C. worked with K.B.D. to prepare the samples for H/DX-MS and perform H/DX analysis, and performed initial analysis of H/DX-MS peptides and wrote an early draft of the manuscript. S.S. built and analyzed molecular models of caspase-6, performed molecular dynamics simulation, and helped prepare the manuscript. J.A.H conceptualized the project, secured funding, directed the research project, wrote parts of the manuscript and edited the manuscript.

2.1 Abstract

Caspases are cysteine aspartate proteases that are major players in key cellular processes, including apoptosis and inflammation. Specifically, caspase-6 has also been implicated in playing a unique and critical role in neurodegeneration; however structural similarities between caspase-6 and other caspases have hampered precise targeting of caspase-6. All caspases can exist in a canonical conformation, in which the substrate binds atop a beta-strand platform in the 130's region. This caspase-6 region can also adopt a helical conformation that has not been seen in any other caspases. Understanding the dynamics and interconversion between the helical and strand conformations in caspase-6 is critical to fully assess its function and regulation. Here, hydrogen/deuterium exchange mass spectrometry indicated that caspase-6 is inherently and dramatically more conformationally dynamic than closely related caspase-7. In contrast to caspase-7, which rests constitutively in the strand

conformation before and after substrate binding, the hydrogen/deuterium exchange data in the L2' and 130's regions suggested that prior to substrate binding, caspase-6 exists in a dynamic equilibrium between the helix and strand conformations. Caspase-6 transitions exclusively to the canonical strand conformation only upon substrate binding. Glu-135, which showed a noticeably different calculated pK_as in the helix and strand conformations, appears to play a key role in the interconversion between the helix and strand conformations. Because caspase-6 has roles in several neurodegenerative diseases, exploiting the unique structural features and conformational changes identified here may provide new avenues for regulating specific caspase-6 functions for therapeutic purposes.

2.2 Introduction

Caspases are cysteine proteases that recognize aspartate-containing substrates, and are major players in key cellular processes, including apoptosis and inflammation. Caspase active sites contain a Cys–His dyad required for cleavage of peptide bonds adjacent to aspartate residues in select protein substrates. There are two main classes of caspases, initiator and executioner caspases, classified based on their cellular function and domain organization. Initiator caspases (caspase-2, -8, and -9) function upstream in the apoptotic pathway and activate the downstream executioner caspases (caspase-3, -6, and -7) by proteolytic cleavage at an intersubunit linker between large and small subunits. Executioner caspases then cleave a select group of protein targets to promote apoptosis. Initiator caspases generally exist as monomers and are

subsequently activated by dimerization mediated by formation of molecular platform, e.g. apoptosome (Boatright et al., 2003). In contrast, executioner caspases exist as dimeric inactive zymogens and upon activation by limited proteolysis become functional dimers (Pop and Salvesen, 2009). Significantly, classification of caspase-6 as an executioner has not been unequivocal. Caspase-6 is weakly apoptotic, although overexpression of caspase-6 in mammalian cells does result in apoptosis (Suzuki et al., 2004). As an executioner, caspase-6 has been identified as the only caspase that cleaves the nuclear lamellar protein, lamin A/C during apoptosis (Orth et al., 1996; Srinivasula et al., 1996; Takahashi et al., 1996). Caspase-6 has been shown to cleave caspase-8 (Cowling and Downward, 2002) and be activated by caspase-3 (Srinivasula et al., 1998) and caspase-1 (Guo et al., 2006), suggesting that caspase-6 assumes simultaneous roles as an executioner, initiator, and inflammatory caspase.

Unlike other executioner caspases, which necessitate processing by initiator caspases for activation (Chai et al., 2001), caspase-6 is capable of self-cleavage and activation (Klaiman et al., 2009; Wang et al., 2010). Although self-cleavage does not lead to apoptosis, this caspase-6 self-cleavage may account for some nonapoptotic roles of caspase-6 including axonal pruning in development (Harrington et al., 2010; Nikolaev et al., 2009; Schoenmann et al., 2010; Simon et al., 2012) and in adult brains (Park et al., 2010) as well as in B cell activation and differentiation (Watanabe et al., 2008). In the context of neurodegeneration, caspase-6 cleaves a compelling set of neuronal substrates

including microtubule-associated protein tau (Horowitz et al., 2004), amyloid precursor protein (Albrecht et al., 2009), presenilin I and II (Albrecht et al., 2009), polyglutamine-expanded and native huntingtin protein (Graham et al., 2006), and Parkinson disease protein 7 (PARK7), also known as protein deglycase DJ-1 (Giame et al., 2010). Caspase-6 is considered a promising molecular target for neurodegeneration treatments because cleavage of these neuronal substrates plays key roles in the pathophysiological outcome in Alzheimer's (Albrecht et al., 2007; Galvan et al., 2002; Galvan et al., 2006; Gervais et al., 1999; Guo et al., 2004; Klaiman et al., 2008; LeBlanc, 2013; Lu et al., 2000; Nguyen et al., 2008; Saganich et al., 2006; Zhao et al., 2003), Huntington's (Aharony et al., 2015; Graham et al., 2010; Graham et al., 2006; Hermel et al., 2004; Milnerwood et al., 2010; Riechers et al., 2016; Warby et al., 2008; Wong et al., 2015), and Parkinson's diseases (Giame et al., 2010). Thus, a full understanding of caspase-6 structure and its relation to function is central to achieving caspase-6-specific regulation in neurodegeneration.

Perhaps the most unique feature of caspase-6 is that it is the only caspase that can adopt two very different structural conformations. These two conformations stem from structural changes in the 130's region, which generates the platform upon which substrate binds (Figure 2.1). Structures of the procaspase-6 zymogen, in which the intersubunit linker occupies and orients the active site loops (Cao et al., 2014; Wang et al., 2010), and mature caspase-6 bound to a substrate-like inhibitor (Liu et al., 2011; Muller et al., 2011a; Wang et al., 2010) are similar to other caspases and show the canonical strand

conformation. These structures underscore the observation that caspase-6 is fully capable of adopting the canonical caspase active site conformation. The mature unliganded caspase-6 is also capable of adopting a distinctive and noncanonical conformation, with extended helices in the 60's region (residues 57-70) and 130's region (residues 125-142) (Baumgartner et al., 2009; Vaidya et al., 2011). These conformational changes are also accompanied by a 21° outward rotation of the 90's helix (Figure 2.1). This helical conformation of unliganded caspase-6 is not seen in crystal structures of other caspases. In fact, the helical form is disallowed in all other caspases by the presence of helix-breaking residues in this region (Vaidya and Hardy, 2011; Vaidya et al., 2011). In caspase-6, when the 130's region is in the extended helical conformation, the Cys-His catalytic dyad, whose reactive centers must be within 1.8 to 3.5 angstroms of one another to achieve catalysis (Štrajbl et al., 2001), are pushed away from each other by 9Å. In addition, the top of the 130's helix prevents substrate binding. As a consequence, caspase-6 is catalytically inactive when locked in this conformation. In order for caspase-6 to accommodate a substrate in the active site, a conformational rearrangement has to occur in the 60's, 90's, and 130's helices and loops 1 to 4. This transition is thought to occur through a low stability/high energy intermediate strand-containing state in the 130's region (Vaidya and Hardy, 2011). Unliganded caspase-6 has also been crystallized in the canonical strand conformation with a more properly

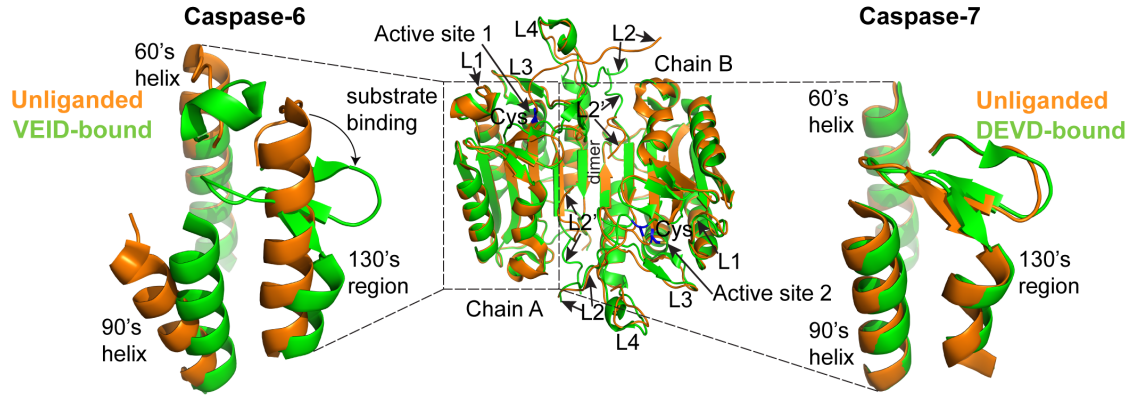


Figure 2.1 Caspase-6 Undergoes Helix-Strand Transition Upon Substrate Binding

The overall fold of canonical caspases before and after substrate binding is represented by the superimposition of the unliganded (*orange*, PDB code 1K86) and the peptide-based substrate mimic DEVD-bound (*green*, PDB code 1F1J) structures of caspase-7 (*middle*). Highlighted regions are the active-site cysteine (*blue*), the dimer interface, and the substrate binding loops 1 to 4 (L1, L2, L3, L4). Caspase-7, like all other caspases, adopts a canonical strand conformation in its 130's region in both the unliganded state (*orange*, PDB code 1K86) and the peptide-based substrate mimic DEVD-bound (*green*, PDB code 1F1J) states (*right*). In contrast, caspase-6 can adopt a noncanonical extended helical conformation in its 130's region in the unliganded state (*orange*, PDB code 2WDP) but recovers the canonical strand conformation upon binding to a peptide-based substrate mimic VEID-aldehyde (*green*, PDB code 3OD5) (*left*).

positioned Cys–His dyad (separated only by 3.6Å) capable of binding substrate (Muller et al., 2011b). This structure of the mature unliganded form of caspase-6 is similar to all other caspases. Thus, it is clear that caspase-6 is capable of adopting both helical and strand conformation of the 130's region in the absence of substrate. These structures underscore the remaining question: what is the physiologically relevant structural ensemble for unliganded caspase-6? The goal of this work is to understand the relative populations of the helical and strand conformations of mature caspase-6 prior to substrate binding.

The crystal structures of caspase-6 are static molecular snapshots. A complimentary study to depict temporal dynamic changes is needed to define the

conformational ensemble of caspase-6 prior to substrate binding. Hydrogen/deuterium exchange mass spectrometry (H/DX-MS) is a powerful technique to study protein conformation and dynamics (for review (Pirrone et al., 2015)) and has been applied to several systems including protein/ligand complexes (Landgraf et al.), chaperones (Kirschke et al., 2014), amyloid fibrils (Hodkinson et al., 2012), viral proteins (Snijder et al., 2014), antibody-drug conjugates (Pan et al., 2014), and even peripheral (Burke et al., 2012) and transmembrane (Mehmood et al., 2012) proteins. H/DX-MS reports the extent of hydrogen bonding and relative solvent exposure of the backbone amide hydrogens, and is well suited for extrapolating different protein conformations (Wales and Engen, 2006).

In this study, H/DX-MS combined with molecular dynamics (MD) simulations, was used to probe the distinct conformational dynamics in caspase-6 relative to caspase-7 upon peptide-based substrate binding. Caspase-7 serves as an ideal control, possessing the same overall fold, but maintaining constitutively the strand-form before and after substrate binding. Our results show that caspase-6 displays a unique backbone dynamics in the 130's region compared to caspase-7, consistent with the helix-strand interconversion upon substrate binding. Moreover, the protonation of Glu-135 in this region was found to be an important contributor to the stability of the helical state of unliganded caspase-6. Exploiting these unique structural features may provide new avenues for regulating specific caspase-6 functions.

2.3 Results

2.3.1 Overall H/DX-MS Profiles of Caspase-6 and Caspase-7

To explore the differences in the backbone dynamics and conformational flexibility of caspases, caspase-6 and caspase-7 were profiled using H/DX-MS in the mature unliganded and bound to a substrate-like inhibitor states. The substrate-bound states were achieved by binding inhibitors built from the tetrapeptide recognition substrates, VEID-aldehyde for caspase-6 and DEVD-aldehyde for caspase-7. The H/D exchange rate of the backbone amide hydrogen with deuterium in the solvent is interpreted as reporting the local fluctuations of the conformational states of proteins (Englander and Kallenbach, 1983). Thus, fast rates of H/D exchange indicate higher solvent accessibility and flexibility of associated protein region, whereas those regions that show slow rates of H/D exchange are characterized as being buried and rigid (Wales and Engen, 2006). Peptide heat maps show the extent of the relative deuterium uptake of the peptic peptides of caspase-6 and caspase-7 in both the unliganded and inhibitor-bound forms after being subjected to between 10 seconds and 2 hours of H/D exchange (Figure 2.2). The corresponding relative deuterium uptake profiles were mapped onto the crystal structures of caspase-6 (PDB code 2WDP) and caspase-7 (PDB code 1K86) (Figure 2.3). The percent difference in the relative deuterium uptake of the unliganded and inhibitor-bound states of caspase-6 and caspase-7 were also mapped onto the linear amino acid sequences (Figure 2.4) and onto the corresponding crystal structures (Figure 2.5). All deuterium uptake plots for both unliganded and bound states of

caspase-7 and caspase-6 were also prepared (Figure 2.6 and Figure 2.7). Overall, peptides covering 91% and 93% of the linear sequences of caspase-6 and caspase-7, respectively, were observed (Figure 2.8). Approximately 70% of the backbone amide hydrogens in both caspase-6 and caspase-7 underwent less than 30% H/D exchange within 10 seconds, suggesting well-folded and dynamically stable proteins overall. In contrast, the other 30% of the backbone amide hydrogens were rapidly deuterated. These rapidly deuterated regions are predominantly observed in the highly flexible regions, including the loop bundles (L2, L2', L3, L4), which form the substrate-binding groove of caspases (Fig. 1). The reproducibility of the H/DX-MS experiment was extremely high across the majority of the sequence, and even small differences in the susceptibility to H/D exchange between the unliganded and liganded states of caspases could be accurately quantified, facilitating identification of regions in which H/D exchange was altered in the presence of a peptide-based substrate-mimic (Figure 2.6 and Figure 2.7).

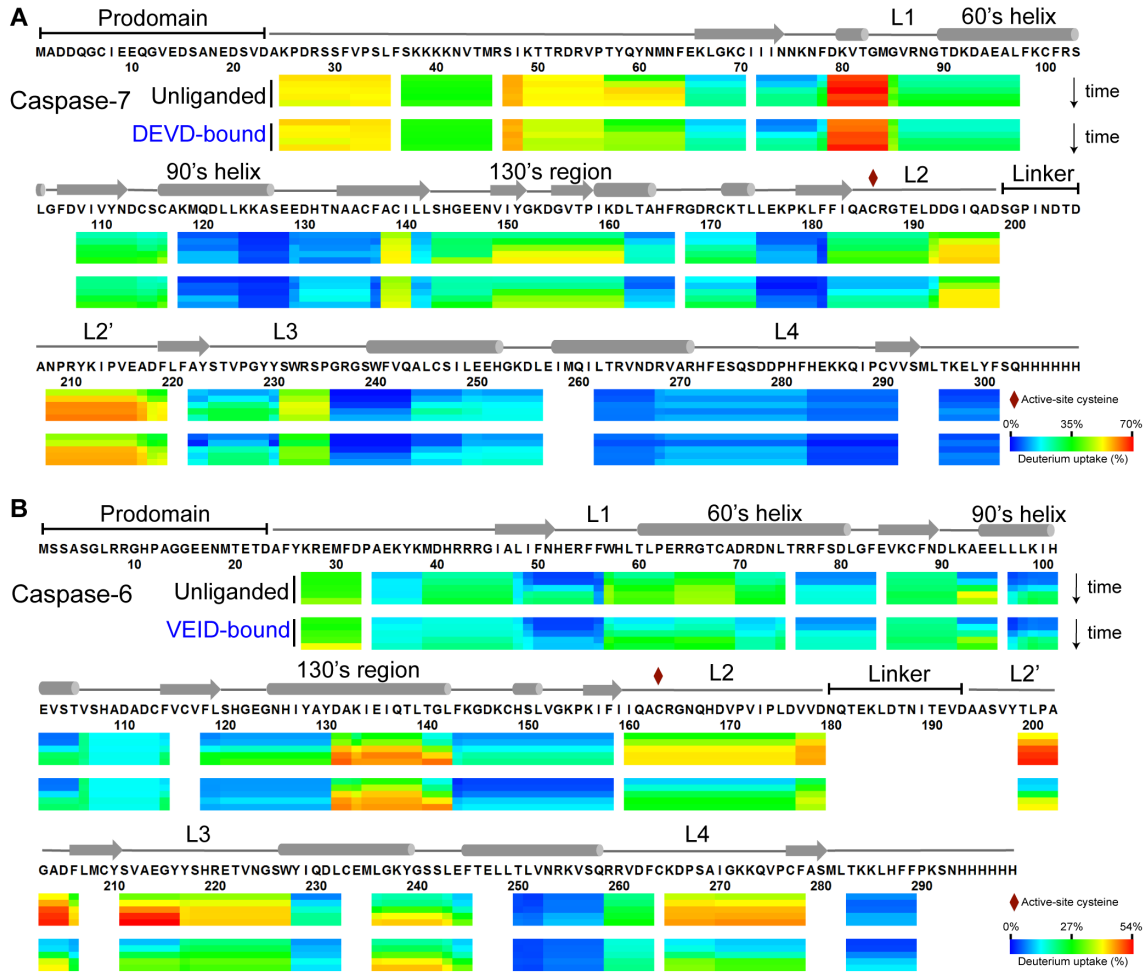


Figure 2.2 H/D Exchange Heat Map of the Relative Deuterium Incorporation

For each peptic peptide of the unliganded and the peptide-based substrate mimic-bound states of caspase-7 (A) and caspase-6 (B), the percent relative deuterium level for each H/D exchange incubation time (*minutes*: 0.17, 1, 10, 60, and 120) is mapped onto its corresponding linear sequence. The percent relative deuterium incorporation is calculated by dividing the observed deuterium uptake by the theoretical maximum deuterium uptake for each peptide. The H/DX MS experiments followed 64 peptides common to both unliganded and DEVD-bound caspase-7 that covers 93% of the linear sequence. Likewise, H/DX MS experiments followed 70 peptides common to both unliganded and VEID-bound caspase-6 that covers 91% of the linear sequence. Peptic peptides with no H/D exchange data at any given incubation time are colored *white*. All caspase-6 and caspase-7 variants used in the H/DX-MS experiments were cleaved and active forms lacking both the prodomain (residues 1-23 in both caspase-6 and caspase-7) and linker (residues 180-193 in caspase-6; residues 199-206 in caspase-7). The secondary structural elements are also shown on top of the caspase-6 and caspase-7 sequences. The percent relative deuterium level of each peptic peptide represents the average values of duplicate experiments performed on two separate days.

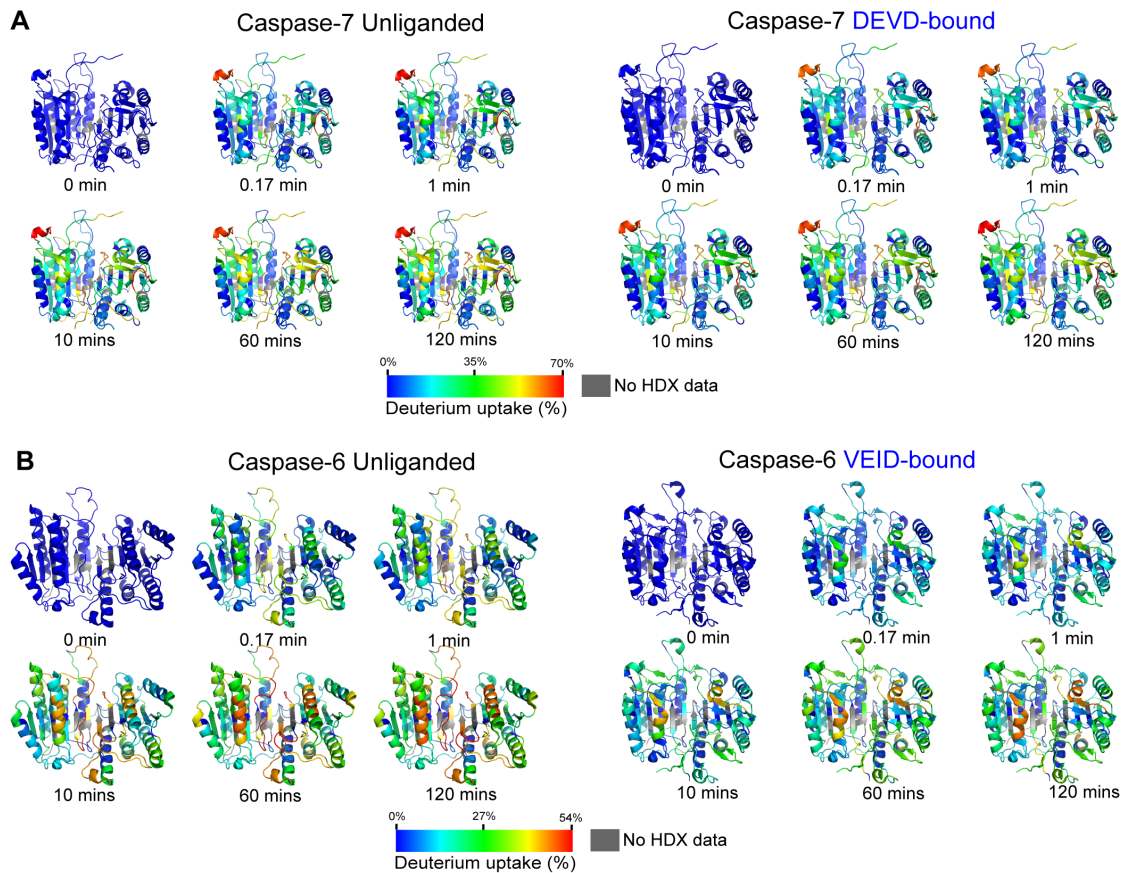


Figure 2.3 Relative Deuterium Incorporation of Caspase-6 and Caspase-7 Mapped onto its Corresponding Structures

The percent relative deuterium incorporation of caspase-7 (A) and caspase-6 (B) before and after binding to peptide-based substrate mimic as a function of H/D exchange incubation period are shown mapped onto its corresponding crystal structures. The percent relative deuterium incorporation is calculated by dividing the observed deuterium uptake by the theoretical maximum deuterium uptake for each peptide. Caspase-7 percent deuterium uptake is mapped onto its unliganded (PBD code 1K86) and DEVD-bound (PBD code 1F1J) crystal structures. Caspase-6 percent deuterium uptake is mapped onto its unliganded (PBD code 2WDP) and DEVD-bound (PBD code 3OD5) crystal structures. Regions of the protein without H/D exchange data are shown in gray.

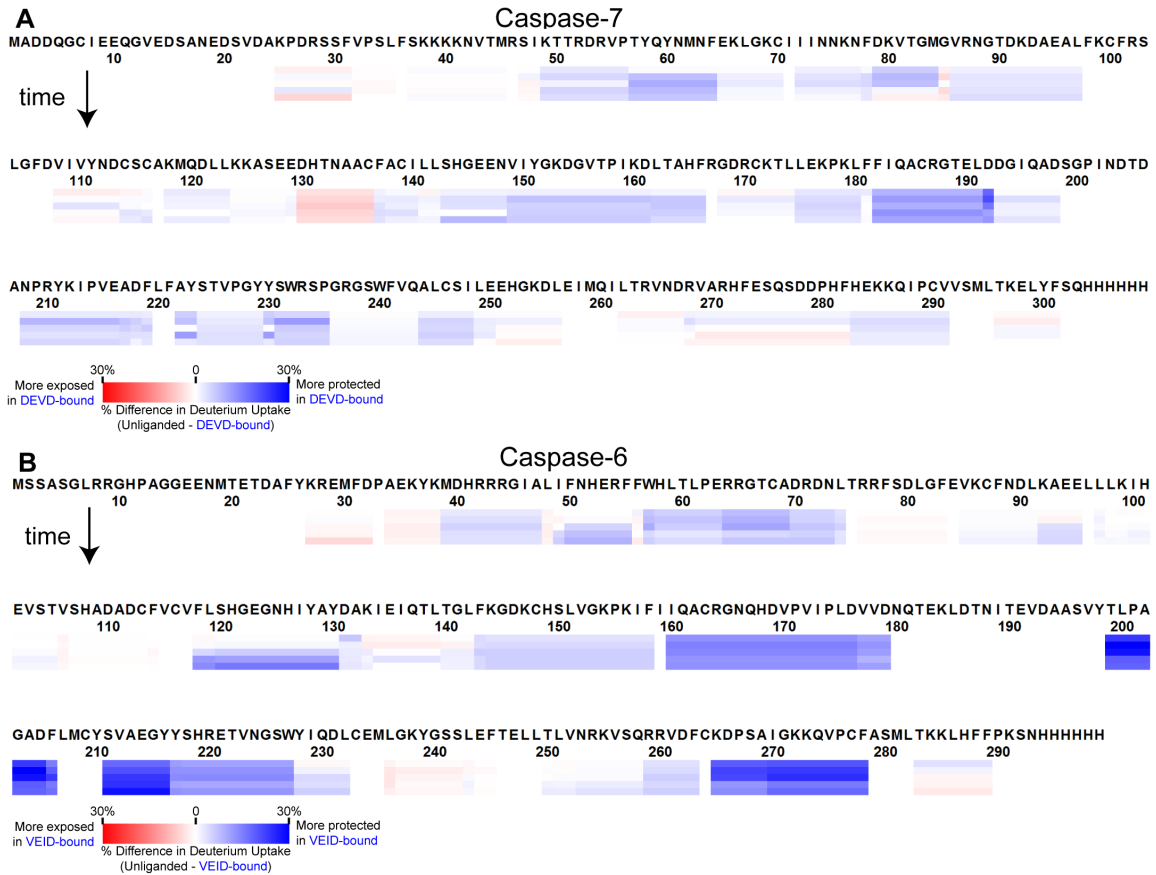


Figure 2.4 Heat Maps of the Percent Difference in Deuterium Level Between Caspase-6 and Caspase-7

Heat maps of the percent difference in the deuterium uptake level between the unliganded and the peptide-based substrate mimic-bound states of caspase-7 (A) and caspase-6 (B) are shown mapped onto its corresponding linear sequence. The H/D exchange incubation period (*minutes*: 0.17, 1, 10, 60, and 120) are shown from *top* to *bottom*. The percent relative deuterium incorporation is calculated by dividing the observed deuterium uptake by the theoretical maximum deuterium uptake for each peptide. *Red* regions undergo more H/D exchange (less protected, more flexible) in the unliganded state compared to the peptide-based substrate-bound state. *Blue* regions undergo less H/D exchange (more protected, less flexible) in the unliganded state compared to the peptide-based substrate-bound state. Peptic peptides with no H/D exchange data are colored *white*.

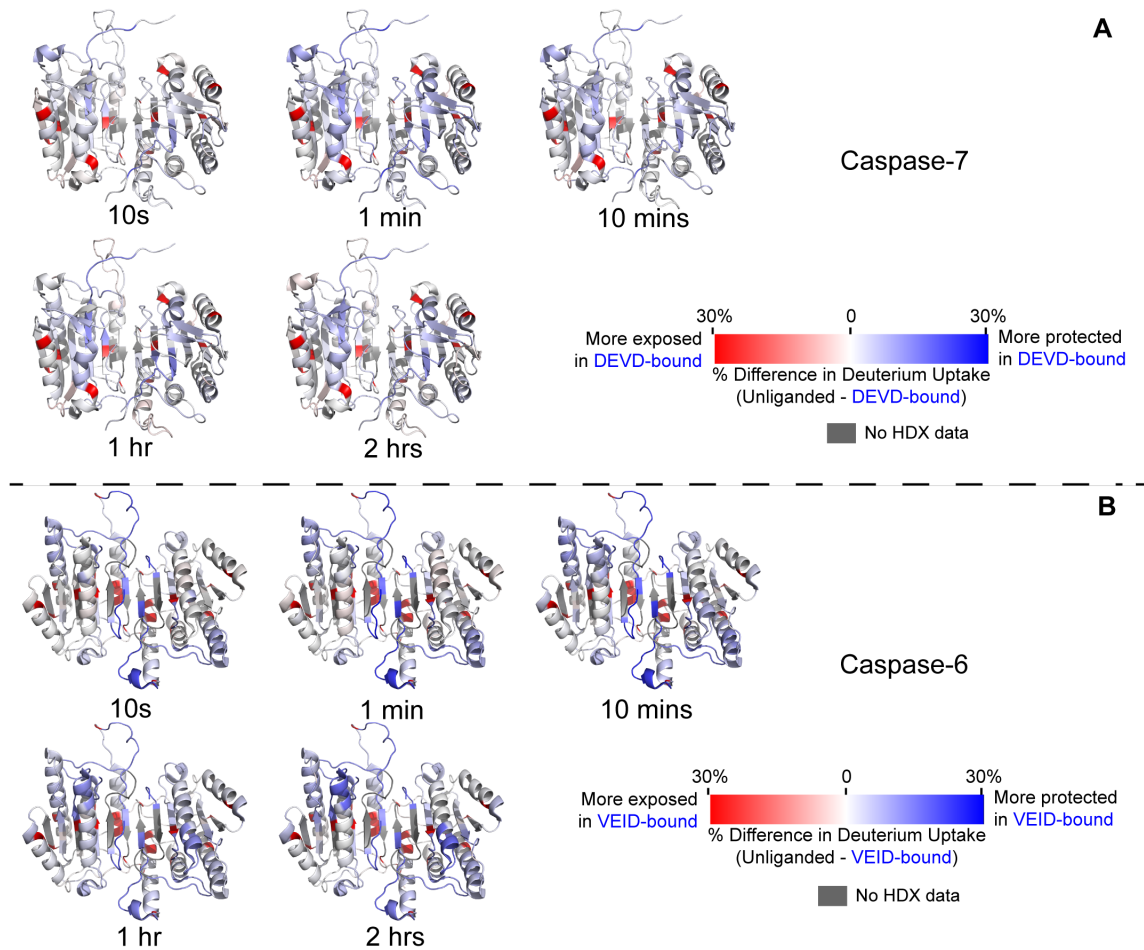


Figure 2.5 Heat Maps of the Percent Difference in Deuterium Level Between Caspase-6 and Caspase-7 Mapped onto its Corresponding Structures

Heat maps of the percent difference in the deuterium uptake level between the unliganded and the peptide-based substrate mimic-bound states of caspase-7 (A) and caspase-6 (B) are shown mapped onto its corresponding crystal structures (PBD code 1K86 for caspase-7; PBD code 2WDP for caspase-7). Regions of the protein without H/D exchange data are shown in *gray*.

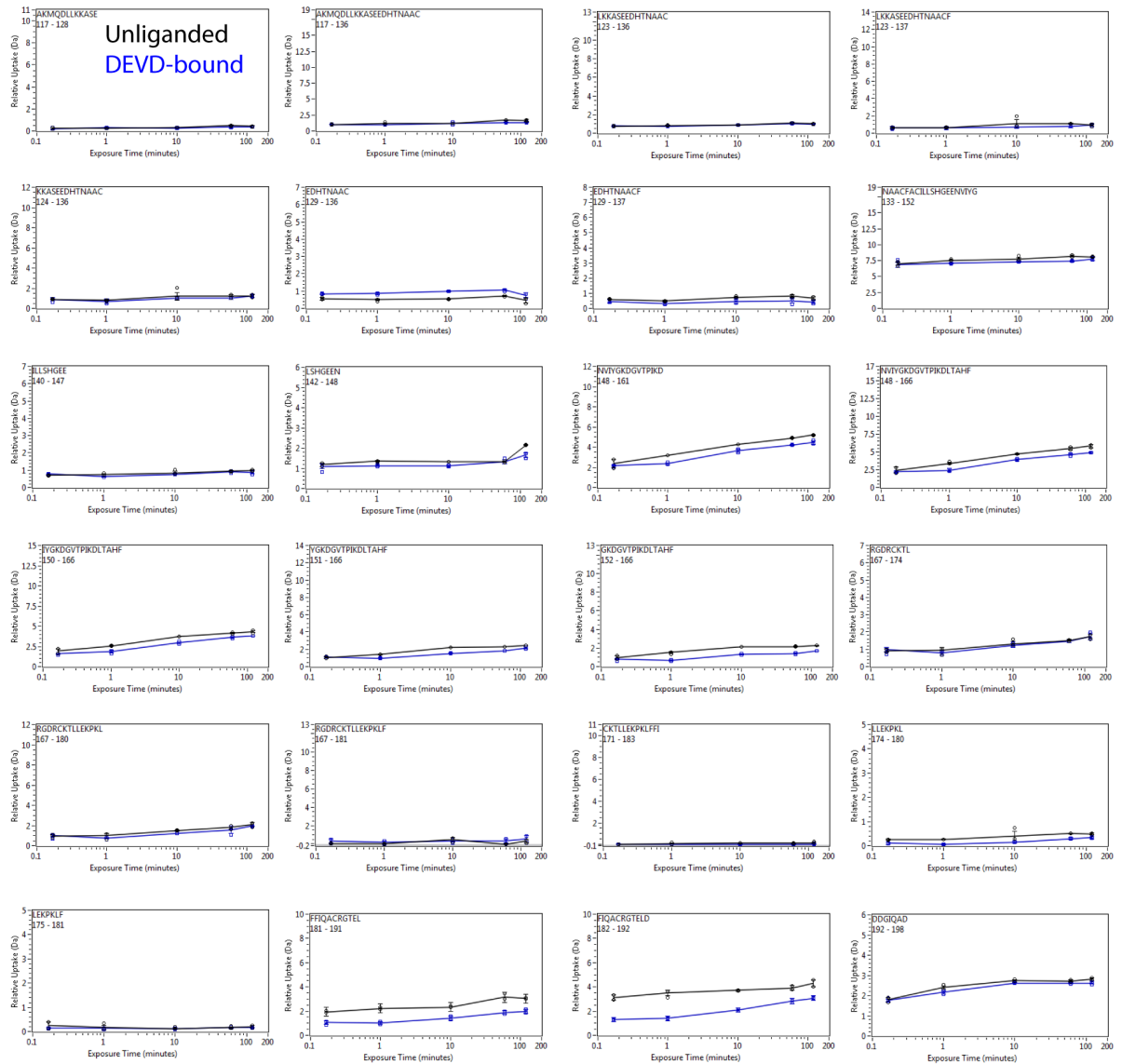


Figure 2.6 Deuterium Uptake Plots of Caspase-7 in the Unliganded and DEVD-bound States

Relative deuterium uptake plots comparing the unliganded (*black line*) and the DEVD-bound (*blue line*) states of caspase-7 as a function of H/D exchange incubation period. The amino acid sequence and number are shown for each peptic peptide of caspase-7. The standard deviations of two independent H/DX-MS experiments performed in two separate days are indicated.

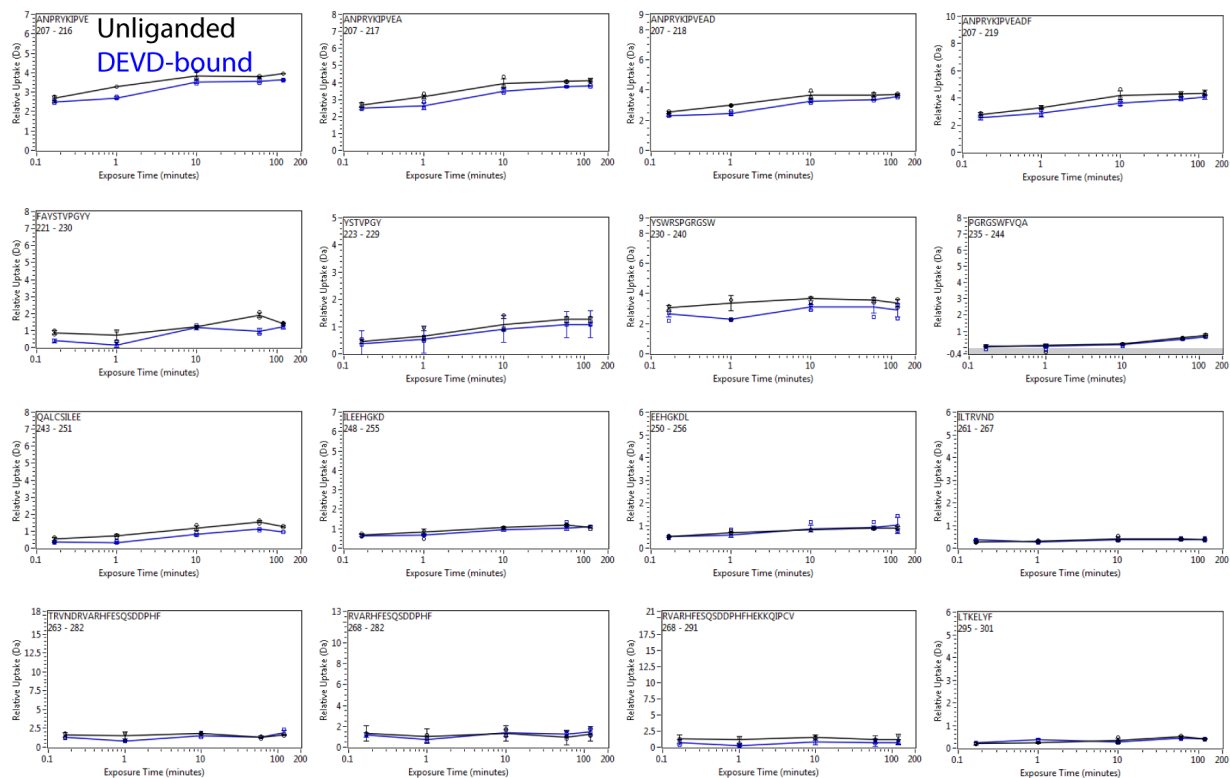


Figure 2.6 Deuterium Uptake Plots of Caspase-7 in the Unliganded and DEVD-bound States (continue...)

Relative deuterium uptake plots comparing the unliganded (*black line*) and the DEVD-bound (*blue line*) states of caspase-7 as a function of H/D exchange incubation period. The amino acid sequence and number are shown for each peptic peptide of caspase-7. The standard deviations of two independent H/DX-MS experiments performed in two separate days are indicated.

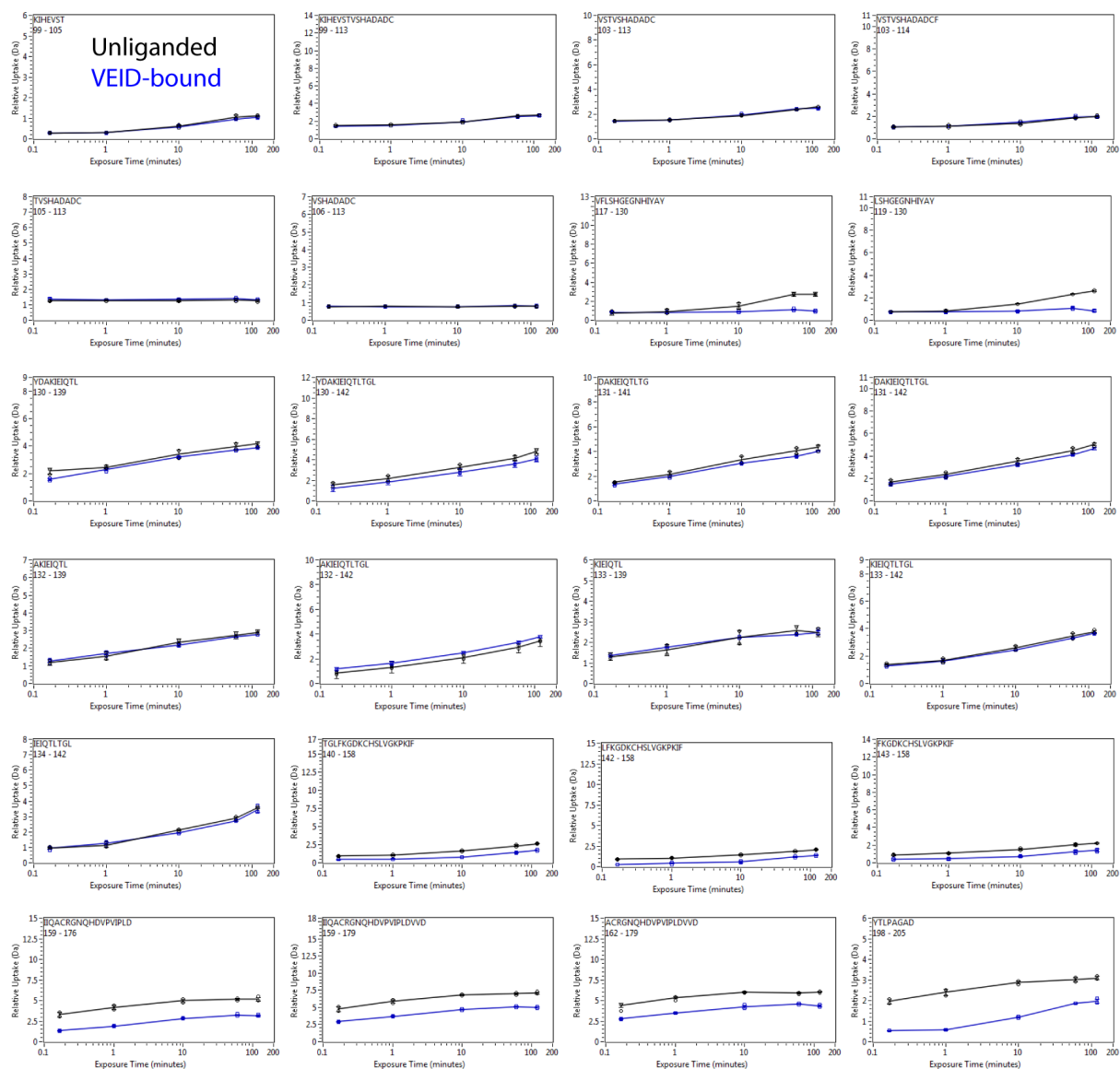


Figure 2.7 Deuterium Uptake Plots of Caspase-6 in the Unliganded and VEID-bound States

Relative deuterium uptake plots comparing the unliganded (black line) and the VEID-bound (blue line) states of caspase-6 as a function of H/D exchange incubation period. The amino acid sequence and number are shown for each peptic peptide of caspase-6. The standard deviations of two independent H/DX-MS experiments performed in two separate days are indicated.

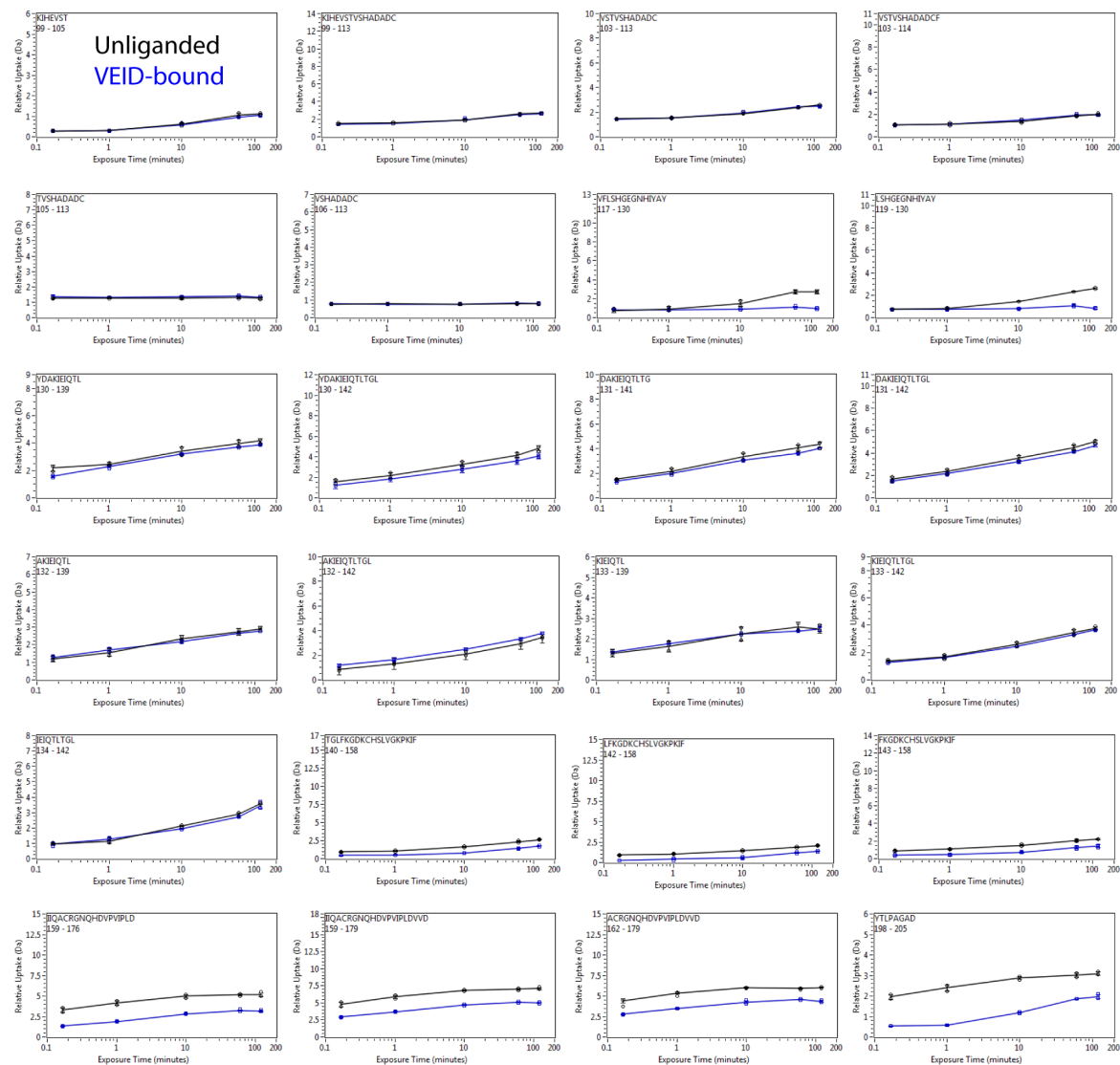


Figure 2.7 Deuterium Uptake Plots of Caspase-6 in the Unliganded and VEID-bound States (continue...)

Relative deuterium uptake plots comparing the unliganded (black line) and the VEID-bound (blue line) states of caspase-6 as a function of H/D exchange incubation period. The amino acid sequence and number are shown for each peptic peptide of caspase-6. The standard deviations of two independent H/DX-MS experiments performed in two separate days are indicated.

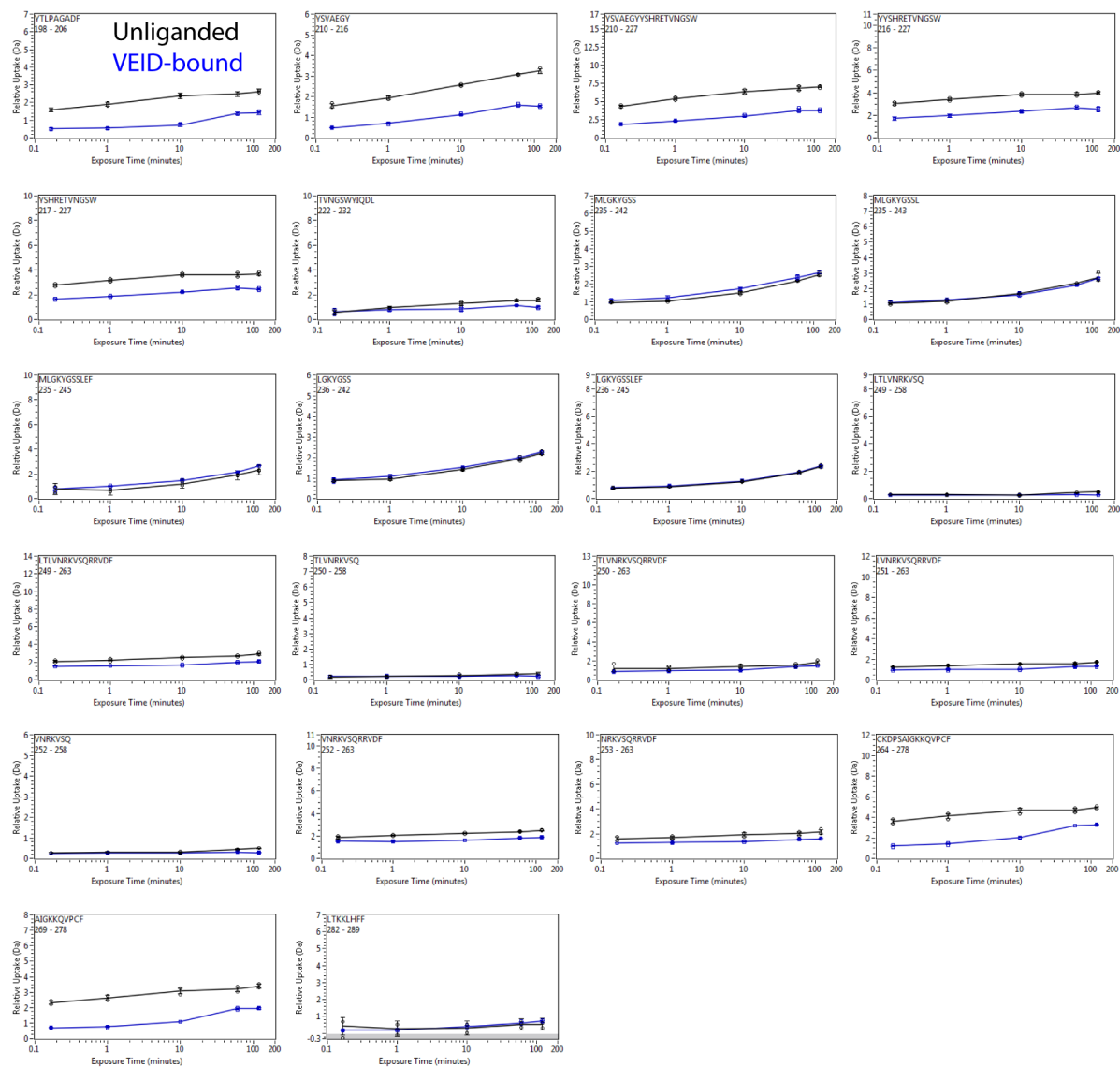


Figure 2.7 Deuterium Uptake Plots of Caspase-6 in the Unliganded and VEID-bound States (continue...)

Relative deuterium uptake plots comparing the unliganded (black line) and the VEID-bound (blue line) states of caspase-6 as a function of H/D exchange incubation period. The amino acid sequence and number are shown for each peptic peptide of caspase-6. The standard deviations of two independent H/DX-MS experiments performed in two separate days are indicated.

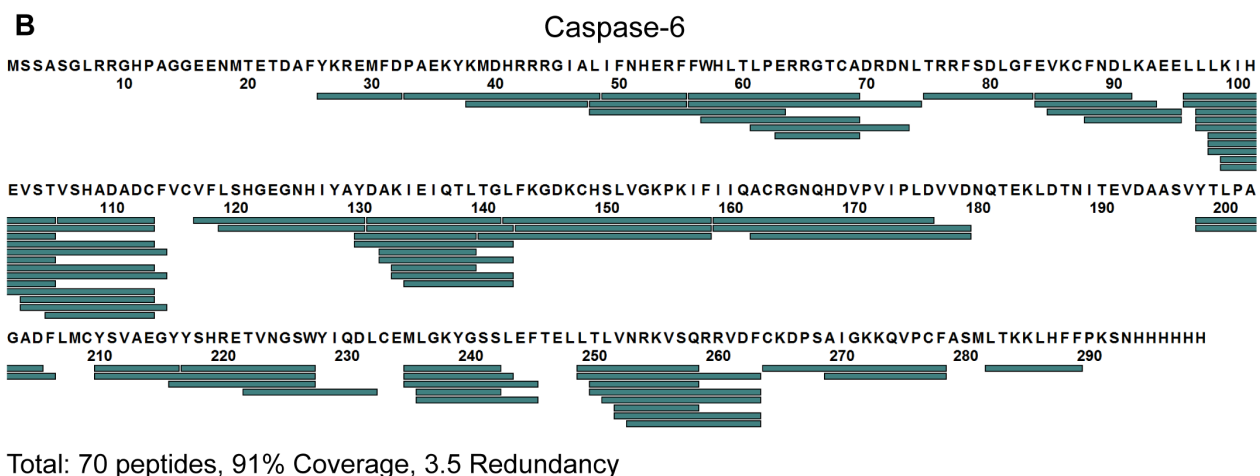
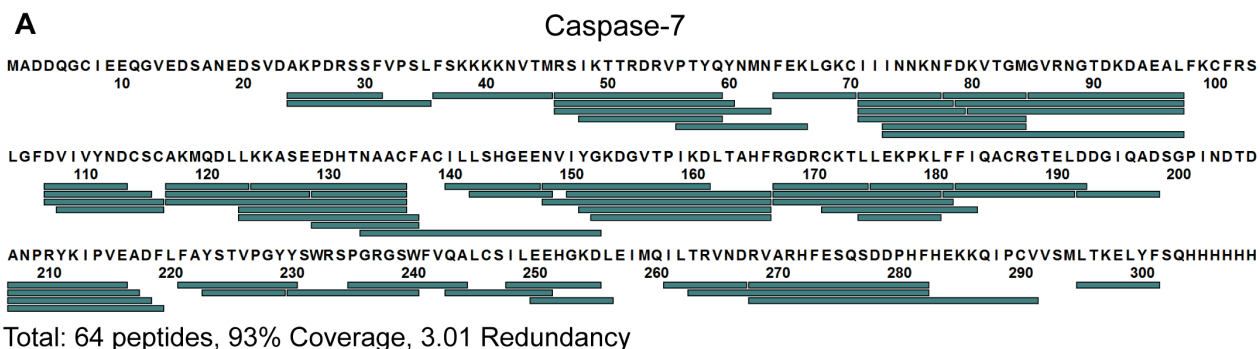


Figure 2.8 H/DX-MS Peptide Coverage Map for Caspase-6 and Caspase-7
 Coverage Map of the peptic peptides identified from H/DX-MS experiments for caspase-7 (A) and caspase-6 (B) in both unliganded and peptide-based substrate mimic-bound states. In both caspase-6 and caspase-7, the protein constructs used were designed to exclude the prodomain and linker, which represents the fully cleaved and active form of the enzyme.

2.3.2 Caspase-7 Adopts the Canonical Strand Conformation Before and After Substrate Binding

Caspase-7 serves as an ideal control for observing conformational changes and dynamics in a canonical caspase before and after binding of a substrate-like inhibitor. All crystal structures of caspase-7 to date show the canonical (130's strand) structure before and after binding of a substrate-like peptide-based inhibitor, DEVD (Figure 2.1). During H/DX-MS on caspase-7, only slight changes in the overall H/D exchange occurred upon binding of a substrate-like inhibitor (DEVD) (Fig. 2.2–A). The percent relative deuterium incorporation is calculated by dividing the observed deuterium uptake by the theoretical maximum deuterium uptake for each peptide. As expected, the most significant differences in the deuterium uptake in the unliganded versus the DEVD-bound states mapped onto peptides from within the active site loop 2 (L2, peptides 181-191 and 182-192). There were no significant changes in the deuterium uptake between the unliganded and the DEVD-bound states in the 60's and 90's helices of caspase-7, which were covered by peptides 85-97 and 117-136, respectively (Figure 2.9A, C, and D). The 130's is the region that undergoes a helix-strand interconversion in caspase-6. The 130's region comprises residues 125-142 for caspase-6 and 148-165 for caspase-7. In caspase-7, the corresponding 130's region was covered by five peptides: 148-161, 148-166, 150-166, 151-166, and 152-166. In particular, peptide 150-166 within the 130's region of caspase-7 (Figure 3A, C, and Figure 2.10) showed changes in deuterium incorporation that are observable from the earliest time point and persisted throughout the

deuterium labeling time with almost the same difference between the unliganded and the DEVD-bound states. The shape of this deuterium incorporation curve indicates (Morgan and Engen, 2009) that one rapidly exchanging amide hydrogen at Ile-150 and one at other residue between 152-166 are deuterated prior to the earliest time point of the H/D exchange experiment (Figure 2.9C). Nevertheless, these data showed only very slight difference (2-6%) in the deuterium uptake in the unliganded versus the DEVD-bound state (Figure 2.4A) suggesting that the 130's region of caspase-7 is partially protected and moderately dynamic but that binding of DEVD does not impact the overall structure. The minor changes in conformational dynamics in the 60's and 130's regions with virtually no changes in the 90's helix of caspase-7 in the unliganded versus the DEVD-bound states are consistent with the reported invariantly canonical strand structures of caspase-7 (Chai et al., 2001; Wei et al., 2000) (Figure 2.1). Importantly, this demonstrates that the magnitude of change in the theoretical maximum deuterium uptake expected to occur directly from substrate-like inhibitor binding to a caspase active site should be on the range of 2-6%, if not accompanied by changes in protein conformational states or their dynamics.

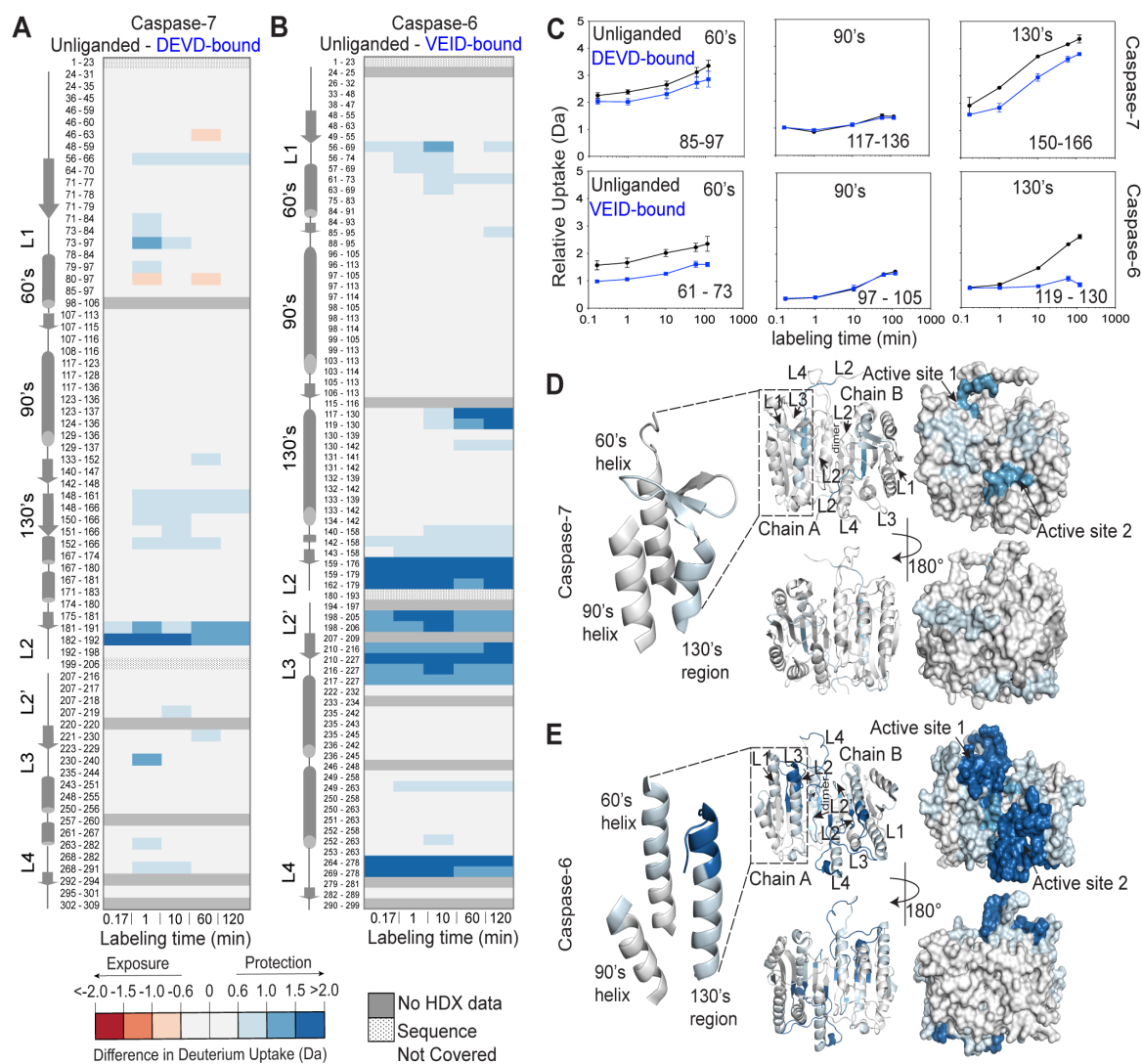


Figure 2.9 Caspase-6 Shows Distinct Conformational Dynamics in its 130's Region

Difference in deuterium uptake (Da) of the corresponding peptic peptides in the unliganded and the peptide-based substrate mimic-bound states of caspase-7 (A) and caspase-6 (B) at the indicated time points of exposure to deuterium in solution. The residue numbers for each peptic peptide are listed with corresponding secondary structural elements. For these data, a deuterium uptake difference greater than 0.6 Da is considered significant at 98% confidence interval. The intensity of the *blue* color represents the peptides that undergo significant decrease in H/D exchange (less solvent exposed, less flexible) upon peptide-based substrate mimic binding. The intensity of the *red* color represents

the peptides that undergo significant increase in H/D exchange (more solvent exposed, more flexible) upon peptide-based substrate mimic binding. (C) Representative deuterium incorporation plots for peptic peptides covering the 60's, 90's, and the 130's region of caspase-7 (*upper panel*) and caspase-6 (*lower panel*) in both unliganded (*black lines*) and peptide-based substrate mimic-bound (*blue lines*) states. The representative MS spectra of the highlighted peptic peptides are shown in Figure 2.10 and Figure 2.11. Error bars represent the standard deviation (SD) of duplicate H/DX-MS measurements done on two separate days. The residue numbering is listed for the homologous regions in caspase-7 and caspase-6, which have different numbering for the structurally homologous regions due to differences in the lengths of their respective subunits. (D) Difference in deuterium uptake between the unliganded and the DEVD-bound states of caspase-7 after 2-hr incubation mapped onto the structure of caspase-7 (PDB code 1K86) shown in both ribbon and surface representations. (E) Difference in deuterium uptake between the unliganded and the VEID-bound states of caspase-6 after 2-hr incubation mapped onto the structure of caspase-6 (PDB code 2WDP) shown in both ribbon and surface representations.

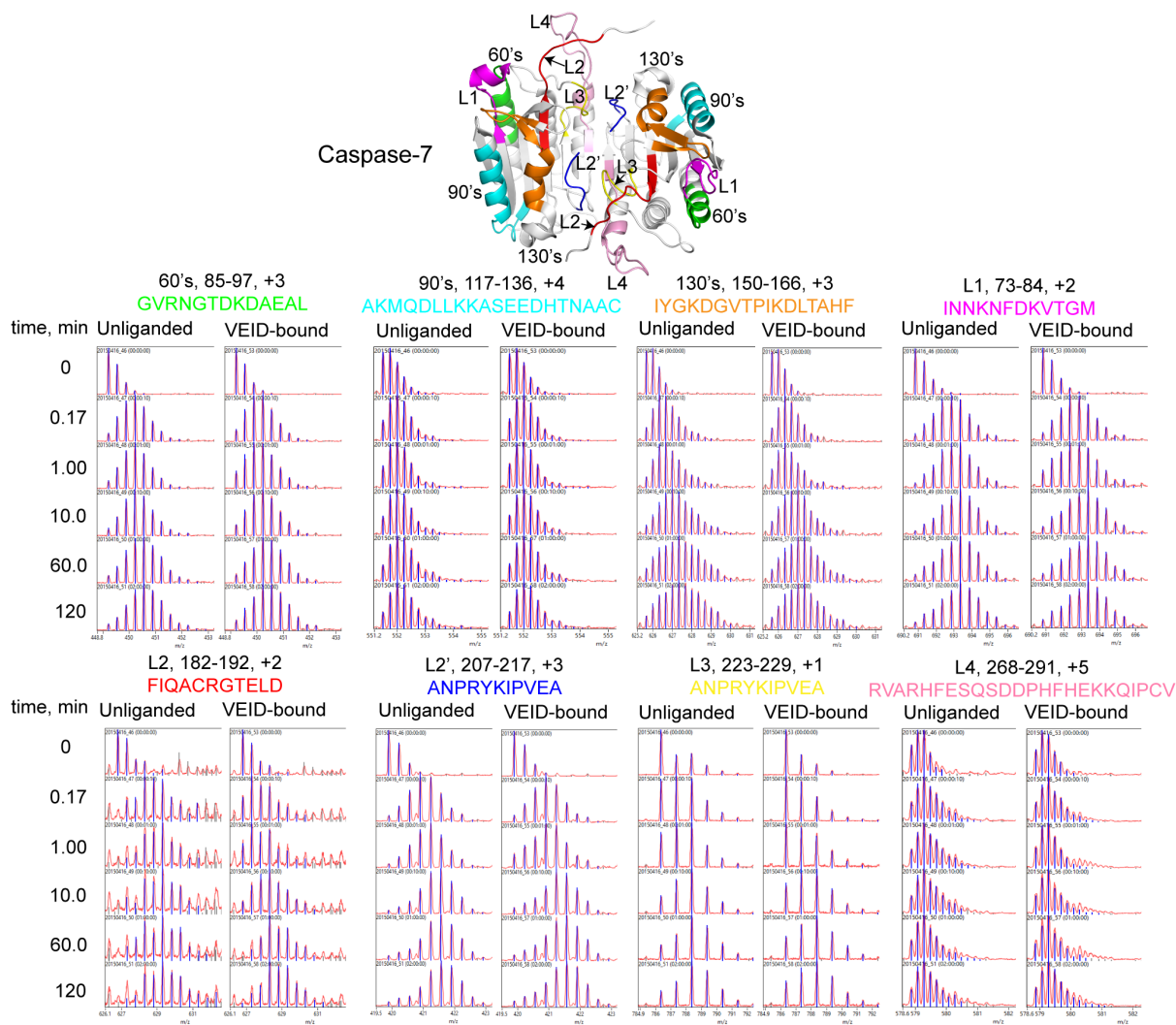


Figure 2.10 Representative MS Spectra of Key Peptides in Caspase-7

Representative MS spectra of the peptic peptides following H/D exchange experiments of the unliganded and peptide-based substrate mimic-bound states of caspase-7. The relative location of the highlighted regions (60's, green; 90's, cyan; 130's, orange; L1, magenta; L2, red; L3, yellow; L4, pink) and its representative peptic peptides are shown mapped onto the corresponding crystal structure of caspase-7 (PDB code 1K86). The amino acid sequence, the charge state and the residue number covered by the representative peptic peptide are also indicated.

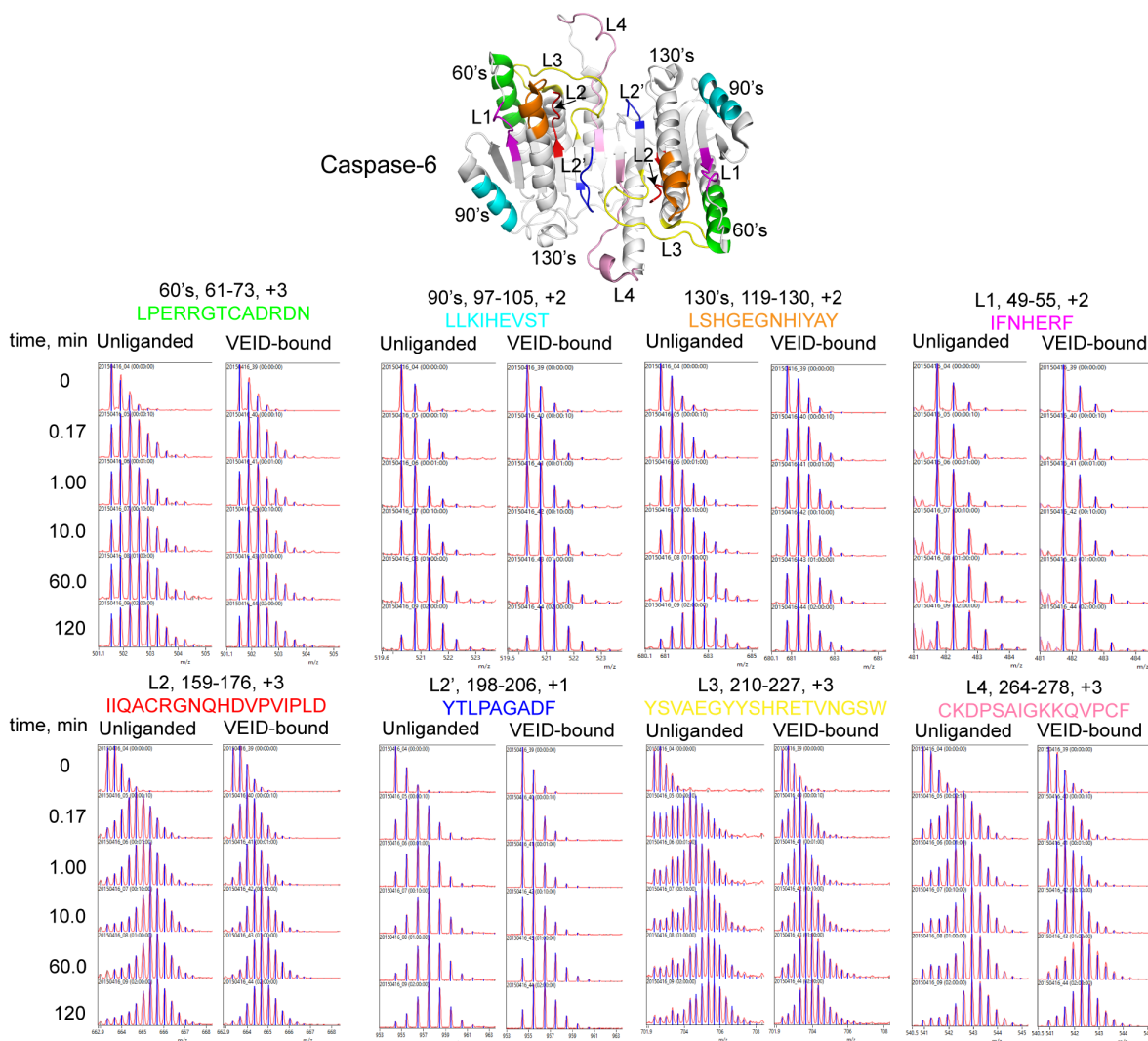


Figure 2.11 Representative MS Spectra of Key Peptides in Caspase-6
 Representative MS spectra of the peptic peptides following H/D exchange experiments of the unliganded and peptide-based substrate mimic-bound states of caspase-6. The relative location of the highlighted regions (60's, green; 90's, cyan; 130's, orange; L1, magenta; L2, red; L3, yellow; L4, pink) and its representative peptic peptides are shown mapped onto the corresponding crystal structure of caspase-6 (PDB code 2WDP). The amino acid sequence, the charge state and the residue number covered by the representative peptic peptide are also indicated.

2.3.3 Caspase-6 Shows Different H/D Exchange Dynamics in the 130's Region Compared to Caspase-7

In terms of conformational flexibility, caspase-6 might be expected to differ from all other caspases. Caspase-6 has been observed to exist in both the canonical strand and helical conformations in the 130's region (Figure 2.1) suggesting that interchange between two conformations could be involved in its function. We anticipated that H/DX-MS would allow identification of regions of caspase-6 that undergo significant conformational interchange, particularly in the native state, and are therefore more highly susceptible to H/D exchange. H/DX-MS on caspase-6 in the unliganded state or bound to an inhibitor built from the cognate caspase-6 tetrapeptide substrate (VEID-aldehyde) revealed dramatic changes in the deuterium uptake levels in several regions of the protein (Figure 2.9–B and –E). H/D exchange in the substrate-binding loops (L2, L2', L3, and L4), which are engaged in accommodating the tetrapeptide in the active site, significantly decreased by 12 to 30% upon VEID binding (Figure 3B and Figure 2.4–B). In particular, the L2' region of caspase-6 is the most exchangeable region of the protein before VEID binding, but becomes much less susceptible to exchange after binding. This is in contrast to caspase-7. In the canonical conformation of both caspase-6 and -7, L2' is engaged in interactions with L2. In caspase-7, L2' does not show nearly the magnitude in changes in H/D exchange that L2' shows in caspase-6. In the helical form of caspase-6, L2' is not engaged in any stabilizing interactions (Figure 2.11). Thus, H/D exchange is consistent

with the model of L2' being exposed in caspase-6 prior to VEID binding, as is observed in the helical conformation.

In addition to significant changes in L2', H/D exchange in the 130's region (peptide 119-130) significantly decreased 12-16% upon VEID binding (Figure 2.9B and C; Figure 2.4B), which suggests that this region also becomes substantially more ordered when substrate binds. The deuterium uptake profile of caspase-6 peptide 119-130 (Figure 2.9C) showed that in the absence of VEID binding, there is a significant protection at earlier H/D exchange time points but uptakes deuterium as a function of time. The shape of this deuterium uptake curve indicates (Morgan and Engen, 2009) that this region of unliganded caspase-6 visits the H/D exchange-competent state much more frequently than after VEID-binding. This suggests that upon substrate binding, this region becomes less dynamic. VEID- or DEVD-bound caspase-6 (Hill et al., 2016; Wang et al., 2010) is in the same canonical conformation as DEVD-bound casp-7 (Wei et al., 2000). The dispersed and significant differences in H/D exchange that are observed for caspase-6 (Figure 2.9B and E; Figure 2.4B) indicate that there are conformational differences that cannot be explained just by the protection from substrate binding changes. If unliganded caspase-6 rested in the canonical strand conformation, we would expect to see changes in the H/D exchange for unliganded vs. peptide-based substrate mimic-bound similar to those for caspase-7 (Figure 2.9). If caspase-6 rested exclusively in the helical form, we would also expect to see relatively small changes in deuterium uptake because residues in a stable helix should be resistant to H/D exchange. Only during the

transient unfolding of either the strand or helix conformations during interconversion of the 130's region, would we expect increased susceptibility to H/D exchange. Moreover, the total percentage of H/D exchange was the same between caspase-6 and caspase-7 (Table 2.1), making it possible to conclude that observed local differences in H/D exchange behavior reflects bona fide conformational differences between caspase-6 and -7. The much more significant changes in susceptibility to H/D exchange that we observed for caspase-6 in both the L2' and the 130's regions are consistent with the model that in the unliganded form caspase-6 is in a dynamic ensemble with states intermediate between the helical and strand conformations.

Table 2.1 Percent of Total Amide Hydrogen Exchanged with Deuterium

	unliganded	ligand-bound
caspase-6	22.4%	18.0%
caspase-7	23.3%	21.6%

The number of amide hydrogen exchanged in 2 hours, relative to the total number of exchangeable amide hydrogen in each peptide and corrected for % of sequence coverage achieved in each analysis is listed.

2.3.4 Local pK_as of Key Amino Acid Residues Within the 130's Region Vary Between the Unliganded (Helical) and the VEID-bound (Strand) States of Caspase-6

The H/D exchange data suggest that caspase-6 exists in a dynamic equilibrium that transitions between the helical and canonical strand conformations, but the molecular basis of this interconversion was not defined. Inspection of the 130's region in both unliganded and VEID-bound states of caspase-6 revealed an altered set of interactions among key residues in this

region (Figure 2.12A). In particular, residues His-52, Glu-63, Glu-135, and Glu-221 have distinct molecular contacts in the unliganded (helical) compared to the VEID-bound (strand) conformations. For example, His-52 makes H-bonding contacts with Asp-90, Tyr-128, and Glu-135 in the helical state but loses these contacts upon its transition to strand state upon substrate binding. The change in the microenvironment of these residues is reflected in the changes in their calculated microenvironment pK_a s between the helical and strand conformations (Figure 2.12B). The difference in the pK_a s ranges from 0.9 to 6.6 pH units and generally transitions from a basic to a more acidic microenvironment following helix-strand interconversion. In fact, the helical structures of caspase-6 were all trapped during low-pH crystallization (Baumgartner et al., 2009; Vaidya et al., 2011) whereas the strand conformation of unliganded caspase-6 was trapped during neutral pH crystallization (Muller et al., 2011b). The H/D exchange reported here was performed at neutral pH, but strongly suggests that caspase-6 is constantly undergoing an interconversion between the helical and strand states even at neutral pH. On the basis of the local pK_a changes between the two-state conformations of caspase-6, we proposed that the protonation of key residues within the 130's region would impact the dynamics of this region.

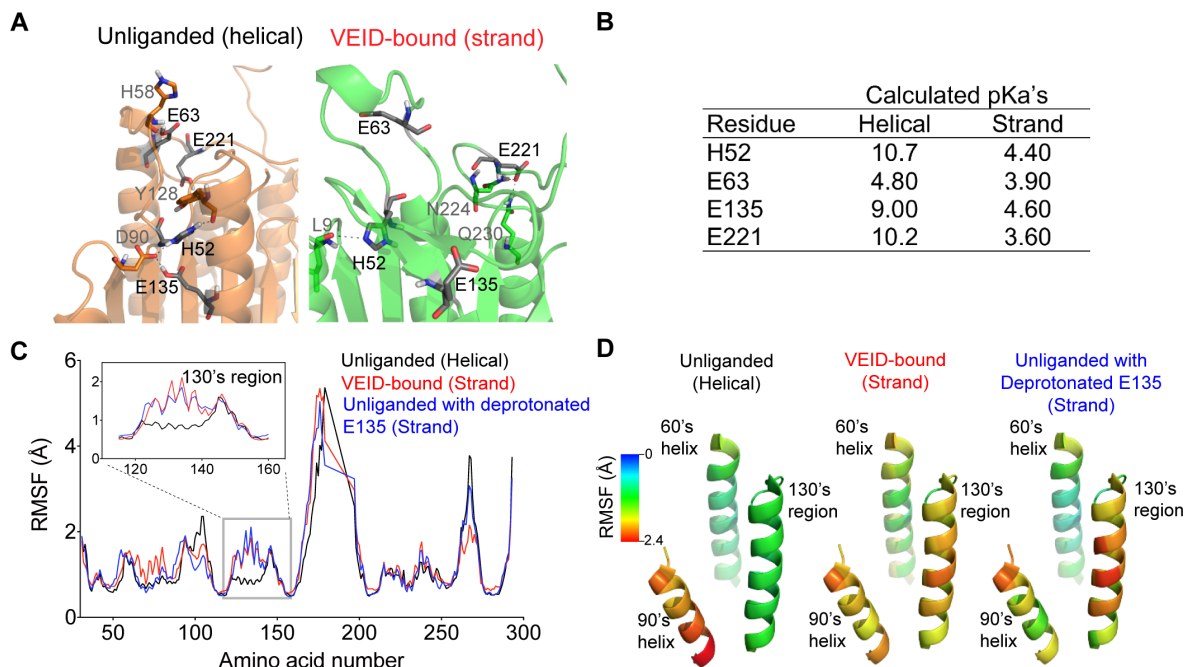


Figure 2.12 Protonation State of Glu-135 is Critical to the Dynamics of the 130's Region

(A) The unliganded (*orange*) and VEID-bound (*green*) states of caspase-6 present different local charge states of four identified residues in close proximity and within the 130's region, which are deprotonated upon substrate binding (shown in *black*). (B) Calculated local pKa's of the four amino acid residues that undergo differential protonation states between the unliganded (helical) and the VEID-bound (strand) states of caspase-6. (C) Plot of root-mean-square fluctuation (RMSF, Å) against the backbone atoms of each amino acid in caspase-6. A 1.2 ns-long simulated annealing-based MD simulation was performed in all caspase-6 protonation variants. The unliganded helical protonation variant represents the control ensemble of the triply protonated state (HisH-52, GluH-135, GluH-221) of caspase-6. The VEID-bound (strand) protonation variant represents the control ensemble of the triply deprotonated state (His-52, Glu-135, Glu-221) of caspase-6. The unliganded with deprotonated E135 represents the protonation variant of caspase-6 with deprotonated Glu-135 but remains protonated at the other two residues (HisH-52 and GluH-221). Residue-by-residue fluctuations are shown for caspase-6 in the unliganded (helical) state (*black*), VEID-bound (strand) state (*red*), and the unliganded caspase-6 with deprotonated Glu-135 (*blue*). The RMSF profile of unliganded caspase-6 with deprotonated Glu-135 behaves similarly to VEID-bound (strand) state in the 130's region (*inset view*). (D) Variation of the RMSF (Å) along key regions of caspase-6 mapped onto the structure of unliganded caspase-6 (PDB code 2WDP) highlighting only the 60's, 90's and 130's regions.

2.3.5 Protonation State of Glu-135 is Key to Conformational Changes in the Caspase-6 130's Region

We performed 1.2 ns-long simulated annealing-based molecular dynamics simulations on the unliganded (PDB code 2WDP) and VEID-bound (PDB code 3OD5) caspase-6 to determine the key factors that contribute to the helix-strand transition. In these studies, protonation states of His-52, Glu-135, and Glu-221 were varied from fully protonated (optimal for the unliganded structure) to fully deprotonated (optimal for the VEID-bound structure). A simulation plot of the annealing studies (Figure 2.12C) shows pronounced difference in the root-mean-square fluctuation (RMSF) profile between the control ensembles of the triply protonated and triply deprotonated states, particularly in the amino acid residues within the 130's region (*inset view*). Altering the protonation states of His-52 and Glu-221 did not result in significant changes in the RMSF profile compared to the control ensembles of caspase-6. Significantly, the protonation state of a single residue, Glu-135, appeared to control the conformational dynamics of the 130's region, with Glu-135 and Glu^H-135 reproducing to a large extent the RMSF profiles of triply deprotonated and triply protonated states, respectively. This observation suggests that the protonation state of Glu-135 is critical to the transition between the unliganded helical and the canonical strand conformations of caspase-6. Mapping the displacement observed during the molecular dynamics simulations onto the structure of caspase-6 underscores the propensity of the 130's helix to undergo a structural transition (Figure 2.12D). This transition could be significantly facilitated by the deprotonation of a single residue, Glu-135,

in the helical state. On the other hand, when caspase-6 in the canonical strand conformation with deprotonated Glu-135 transitions to the helical state, the dramatic change in the microenvironment should strongly favor protonation, which would be easier to achieve at a lower pH. Once protonated, the helical conformation is stabilized. Thus, the protonation state of Glu-135 is likely one of the major contributing factors in stabilizing the helical form of caspase-6.

2.3.6 E135Q, a Mimic of Protonated E135, Stabilizes Caspase-6

Because protonation of Glu-135 appears to be a critical factor for stabilizing the helical state of caspase-6, we generated a variant, E135Q, which maintains the size of Glu, but mimics the protonated (*Glu^H*) state. The kinetic parameters of E135Q are similar to wild type (WT), suggesting that the E135Q substitution does not negatively impact caspase-6 in processing of a peptide-based substrate, VEID-AMC (Fig. 2.13–A). We expected that the E135Q mutation would have a more significant impact on basal caspase-6 function, if there were as large energy barrier to the interconversion between the helical and strand states. The activity profile of E135Q as a function of pH is also similar to that of WT caspase-6, suggesting that increasing the helical fraction does not prevent conversion to the strand form in the presence of substrate (Fig. 2.13–B) suggesting a low energy barrier between the two conformational states in the presence of substrate. WT and E135Q did not show significant differences in their CD spectra suggesting that the secondary structures are similar in the unliganded conformation (Figure 2.14A). In contrast, E135Q showed a pH-

dependent thermal stability profile distinct from that of WT caspase-6 (Fig. 2.14B and E), consistent with the calculated fraction of Glu-135 protonated in the helical state (Figure 2.14C). E135Q is more stable than WT caspase-6, particularly at pH 7.5 and 8.5 (Figure 2.14E). Although this is a small stabilization, it is of the same magnitude as the stability increase when WT caspase-6 binds an active-site ligand (Vaidya et al., 2011), suggesting that stabilization is relevant. At a lower pH, helical WT caspase-6 should be predominantly protonated at the E135 position (Figure 2.14C) and H-bonding interactions with neighboring residues Arg-54 and Glu-131 will be favored (Figure 2.14D). Meanwhile, at a higher pH, deprotonation of Glu-135 is expected to occur and a stronger negative charge of the side chain carboxylate group of Glu-135 will be enhanced, leading to electrostatic interactions as the dominant interaction with neighboring Arg-54 and His-52 in the vicinity. In addition, just 3.8 Å above Glu-135 sits the negatively charged Glu-131 residue, which will likely also be deprotonated at a higher pH promoting electrostatic repulsion that should destabilize the helical structure in the 130's region. Conversely, the Glu^H-135-mimicking E135Q will likely engage in H-bonding with neighboring residues Arg-54 and Glu-131 and avoid the helix destabilizing electrostatic repulsion. At a more basic pH, the stabilizing effect of the E135Q is more pronounced due to the deprotonation of Glu-135 in the helical state and the sustained H-bonding interaction with Arg-54 and Glu-131 that results in higher stability of the E135Q compared to caspase-6 WT. In summary, using E135Q as a surrogate for Glu^H-135 suggests that protonation of this residue leads to overall stabilization of caspase-6. This further suggests that a

significant fraction of caspase-6 exists in the helical state, since deprotonation, which should favor conversion to the strand conformation leads to a destabilization relative to the E135Q variant.

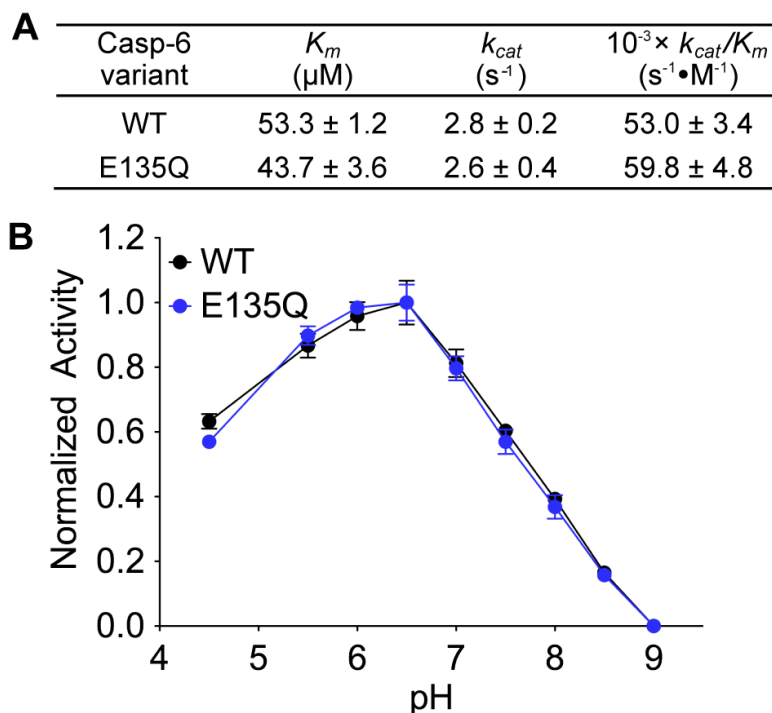


Figure 2.13 E135Q Has Similar Kinetics and pH Profile as WT Caspase-6

(A) The Michaelis-Menten kinetic parameters of caspase-6 WT and the “constantly protonated” variant, E135Q. The values are reported as mean \pm SEM of three independent trials performed on three separate days. (B) The activity of caspase-6 WT (*black line*) and E135Q (*blue line*) variants as a function of pH. For normalization, the highest and the lowest relative fluorescence response for each data set was set to 100% and 0%, respectively and reported as fractions. Error bars represent the standard deviation (SD) of duplicate measurements on two separate days. All caspase-6 activity assays used fluorescence-based measurements following cleavage of a peptide-based substrate mimic VEID-AMC by caspase-6.

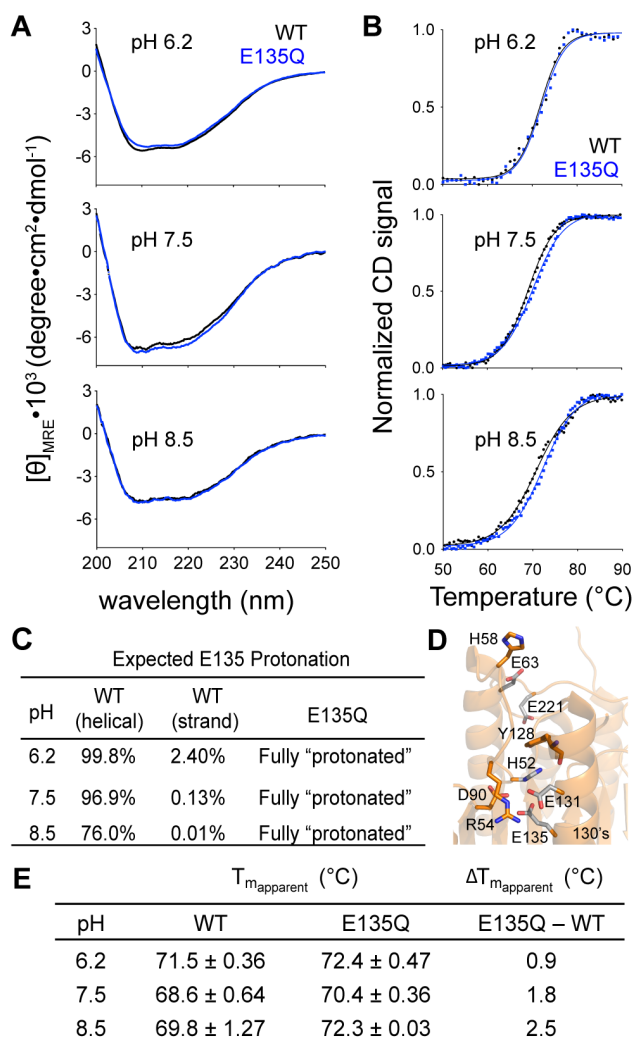


Figure 2.14 The Stabilizing Effect of Constantly Protonated E135Q Variant is More Pronounced at Higher pH

(A) The CD spectra of caspase-6 WT (*black line*) and the E135Q (*blue line*) variant measured at different pHs. (B) CD thermal denaturation profiles of caspase-6 WT (*black dotted line*) and E135Q (*blue dotted line*) at the indicated pHs. Normalization of the CD signal was achieved by setting the highest and the lowest values for each data set as 100% and 0%, respectively. The thermal denaturation data were then fitted to the Boltzmann sigmoidal equation (*black solid line* in WT and *blue solid line* in E135Q) where the midpoint of the curve was determined to be the apparent T_m . (C) The expected percent protonation of Glu-135 at different pH was determined based on the calculated pK_a s in Figure 2.12B following the Henderson-Hasselbalch equation. (D) Interactions between Glu-135 and adjacent residues that impact the helix-strand interconversion. (E) The individual apparent T_m s and the differences in the apparent T_m values of caspase-6 WT and E135Q at different pH are tabulated. The apparent T_m values are reported as mean \pm SD of duplicate measurements on two independently prepared samples performed on two different days.

2.4 Discussion

This study reveals that caspase-6 has local backbone dynamics in L2' and in the 130's region consistent with the helix-strand interconversion. These data showing a helix-strand interconversion are in contrast to previous work on the unliganded caspase-6 determined at the physiological pH 7.4, which showed a canonical strand structure in the 130's region of unliganded caspase-6. The authors concluded that the earlier two helical structures of unliganded caspase-6 assumed a pH-inactivated form as it was crystallized at pH 4.5 (Muller et al., 2011b). If that was true, and in solution caspase-6 existed exclusively in the canonical strand conformation, the H/D exchange for caspase-6 should mirror caspase-7. The fact that the H/D exchange for caspase-6 with and without a substrate-mimic is so strikingly different from that of caspase-7 with and without a substrate-mimic strongly supports the helix-strand interconversion model as governing caspase-6 structure and dynamics prior to substrate binding.

All caspases have mobile loops critical for substrate binding and catalysis. Caspase-6 is different because it has additional mobile regions. Two distinct conformational states have been identified in the 130's region by crystallography, and H/DX-MS has identified a unique interconversion likely between those two states. Although caspase-6 is the only caspase known to adopt the helical conformation and can interconvert to the canonical form upon substrate binding, this type of secondary structural shift is not confined to caspases but has also been observed in other protein systems. Helix-strand interconversion is exploited in nature to allow GTP hydrolysis by EF-Tu (Abel et al., 1996; Polekhina et al.,

1996), susceptibility to conformational diseases (Pan et al., 1993), and membrane association (Liao et al., 2013; Shepard et al., 1998; Yassine et al., 2009). For example, the influenza A M2 protein, a proton channel that facilitates viral assembly and budding, is found to interconvert between alpha-helical and beta-sheet conformations dependent on the membrane composition (Liao et al., 2013). The binding of M2 protein to 1,2-dimyristoyl-sn-glycero-3-phosphocholine (DMPC) promotes the beta-sheet conformation while its binding to cholesterol-rich membrane enriched the alpha-helical conformation. Thus, the biological role of the secondary structure switch in caspase-6 is intriguing. One could imagine such a change in structure to play roles in other yet unidentified functions such as substrate recognition and specificity, cellular signaling and transport, or even binding of natural regulators in the cell.

Our work suggests that the helix-strand interconversion is dependent on the microenvironment pK_a s of a specific residue in the 130's region and, correspondingly, on the pH. Protonation–conformation coupling is important for the function of several protein systems including the nitric oxide carrier heme protein, Nitrophorin 4 (Di Russo et al., 2012), β -lactoglobulin (Qin et al., 1998) and the *E. coli* multidrug efflux transporter AcrB (Murakami et al., 2006). Specific titratable amino acids in a region influence the conformation and function of the protein. These amino acids are expected to have different protonation states in the helical and strand conformations resulting from two sets of distinct pK_a values. In caspase-6, the Glu-135 within the 130's region displays two distinct microenvironment pK_a values, which are 4.4 pH units apart between the helical

and the strand conformations. In our simulations, the change in the protonation state of the Glu-135 impacts the relative stability of the helical state of caspase-6. The relevance of this finding may be explained in the context of the pH of the environment that caspase-6 experiences. The pH may dictate the preference of one conformation of caspase-6 than the other. It has been suggested that pH fluctuation happens in the cellular context where oxidative stress results in cytosolic acidification that can ultimately lead to neurodegeneration (for review (Majdi et al., 2016)). Oxidative stress, a trigger for apoptosis, induced by addition of hydrogen peroxide in HEK 293/Tau cells, increases active caspase-6 and caspase-3 activity (Zhao et al., 2014). An increase in caspase-6 activity has been also documented in global brain ischemia (Ding et al., 2012) and acute ischemic stroke (Akpan et al., 2011) where slight intracellular acidification has been observed to acidify slightly to pH 6.43 (Nedergaard et al., 1991). Although the precise role of the two-state conformations of caspase-6 is still not known, pH changes in the context of neurodegeneration could conformationally enrich caspase-6 in either helical or strand conformations. The pH-induced conformational change may explain the propensity of caspase-6 to recognize different substrates at various cellular processes including apoptosis and neurodegeneration. Future studies on determining the substrate preference of caspase-6 in the context of varying intracellular pH condition may shed light into the importance of the unique two-state conformation of the protein.

In addition to having strikingly different secondary structures, the helical and the strand states of caspase-6 have different electrostatic surface potentials

(supplemental Figure 2.15). Interestingly, the caspase-6 helical conformation exposes an aromatic-rich hydrophobic patch at the top of the 130's helix (Figure 2.16). Hydrophobic patches are often involved in substrate recognition (Schulman et al., 1998). The differences in electrostatics and hydrophobic exposure might be expected to influence substrate recognition and function. Critical inspection of the helical and the strand structures of caspase-6 revealed that the top of the 130's helix as well as the surrounding residues within loop 1 are flopped with exposed hydrophobic patch that contains Phe-55, Phe-56, Trp-57 and Tyr-128. One might imagine that this cluster of aromatic residues could potentially function as an exosite for initial substrate recruitment by helical caspase-6. Accommodation of the substrate near the active site might then facilitate transition of helical caspase-6 to the substrate-binding competent strand state for efficient catalysis. Upon the eventual release of the substrate, caspase-6 may then return to continuous helix-strand interconversion. This potential role of the hydrophobic patch on caspase-6 is at present unexplored and untapped. Future studies dissecting potential exosites for cellular and neuronal substrates of caspase-6, e.g. tau and huntingtin proteins, could shed light on protein-protein interactions that might fruitfully be exploited for novel therapeutics in the future.

Caspase-6 has been predicted to be the only caspase capable of undergoing a helix-strand interconversion (Vaidya and Hardy, 2011; Vaidya et al., 2011), however this assertion has been debated (Muller et al., 2011b). Our H/D exchange data convincingly confirm that the structural dynamics of caspase-6 are fundamentally different than that of other caspases, which are always in the

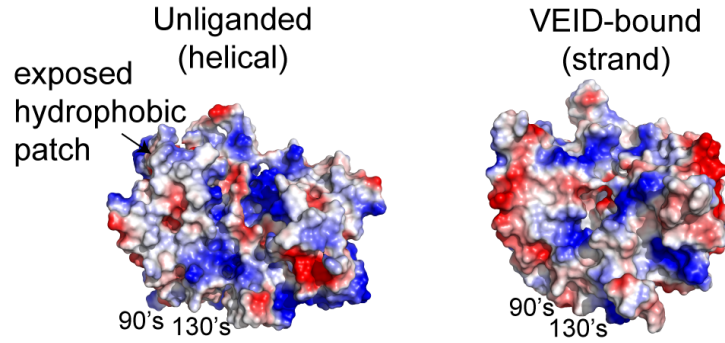


Figure 2.15 Electrostatic Potential Map of Caspase-6

Map of the electrostatic potential of caspase-6 in the unliganded (*left*, PDB code 2WDP) and the VEID-bound (*right*, PDB code 3OD5) states are shown (*red*, acidic regions; *blue*, basic regions; *white*, hydrophobic/neutral regions). The vacuum electrostatic potential maps were generated using Pymol (Schrödinger) and the arrow indicates electrostatic potential map around the hydrophobic patch.

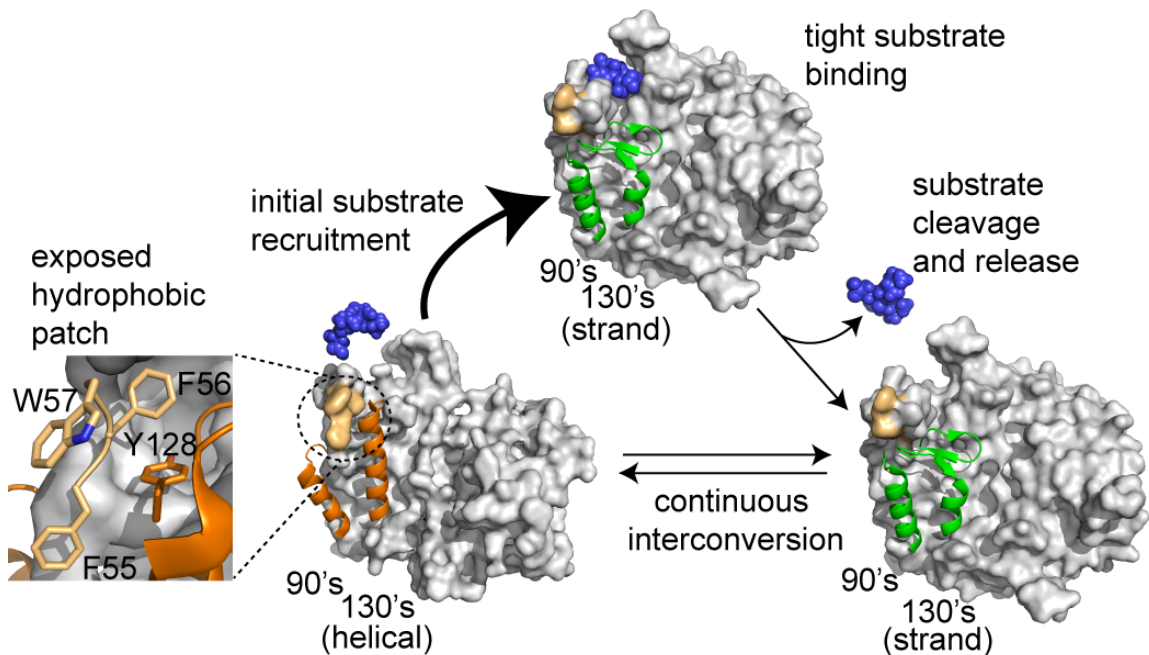


Figure 2.16 A Model Showing Caspase-6 Undergoes a Helix-Strand Transition Upon Substrate Binding

Prior to substrate binding, caspase-6 favors the noncanonical (helical) conformation and transition to canonical strand conformation upon substrate binding. This transition may be facilitated by the presence of a dynamic hydrophobic patch (*light orange, inset view*) that may also function as an exosite for substrate binding. After substrate cleavage and release, caspase-6 exists in a dynamic equilibrium between the helical and strand states.

canonical strand conformation. These data further support strongly a model where unliganded caspase-6 interconverts between the helical and strand conformations. Studies on caspase-6 structure and dynamics are particularly relevant as caspase-6 is implicated in several neurodegenerative disorders including Alzheimer's and Huntington's diseases. Thus, if trapping the helical conformation is indeed inactivating, then stabilizing the helical conformation may be a promising mode of achieving caspase-6-specific inhibition. On the other hand, cleavage of the neuronal substrate DJ-1 (Giame et al., 2010) appears to be protective against neurodegeneration in Parkinson's disease. If the exposed hydrophobic patch does serve as a substrate-recruiting exosite (Figure 2.16), promoting the caspase-6 helical conformation might increase interaction with substrates like DJ-1, for which cleavage is neuroprotective.

2.5 Materials and Methods

2.5.1 Generation of Caspase Variants

The wild-type (WT) caspase-6 used in this study was a constitutive two-chain (CT) form of caspase-6 derived from the synthetic, *E. coli* codon-optimized (His)₆ C-terminally tagged caspase-6 gene (Celtek Bioscience) that was ligated into the NdeI/BamHI sites of pET11a vector (Vaidya et al., 2011). The wild-type caspase-7 used was a constitutively two-chain corrected (CTC) version in pET23b that is designed to independently express the large and small subunits of caspase-7 with (His)₆ tag at the C-terminus (Witkowski and Hardy, 2011). In

both caspase-6 and caspase-7, the protein constructs were designed to exclude the prodomain (residues 1-23 in both caspase-6 and caspase-7) and linker (residues 180-193 in caspase-6; residues 199-206 in caspase-7). Phusion® site-directed mutagenesis (Thermo Scientific™) was used to introduce the E135Q mutation in the caspase-6 CT construct.

2.5.2 Caspase Protein Expression and Purification

The caspase-6 and caspase-7 constructs were transformed into the BL21(DE3) T7 express strain of *E. coli* (NEB). Overnight seed cultures were initially grown in 2×YT media supplemented with 0.1 mg/mL ampicillin (Sigma) at 37 °C. Dense cultures were then diluted 1000-fold with 2×YT containing 0.1 mg/mL ampicillin and shaken at 37 °C until OD₆₀₀ reached 0.6. Protein expression was induced by the addition of 1 mM IPTG, and shaken at 20 °C for 18 hours. Cells were centrifuged at 4,700 x g for 10 min at 4 °C and stored at -20 °C until use. Freeze-thawed cells were lysed using a microfluidizer (Microfluidics, Inc.) in lysis buffer (50 mM Tris, pH 8.5, 300 mM NaCl, 5% glycerol, 50 mM imidazole) and centrifuged at 30,600 x g for 1 hour at 4 °C. The supernatant was loaded into a 5-mL HiTrap nickel-affinity column (GE Healthcare) and washed with lysis buffer until the absorbance returned to baseline. The protein was eluted with elution buffer (50 mM Tris, pH 8.5, 300 mM NaCl, 5% glycerol, 250 mM imidazole) and diluted 5-fold with buffer A (20 mM Tris, pH 8.5, 2 mM DTT) to reduce the salt concentration. This protein sample was then loaded into a 5-mL HiTrap Q HP column (GE Healthcare). The column was developed with a linear

NaCl gradient and the protein was eluted in 20 mM Tris, pH 8.5, 200 mM NaCl, 2 mM DTT. This eluted protein was stored at -80 °C until use. The purified caspases were analyzed by SDS-PAGE to confirm identity and purity.

2.5.3 Caspase Activity Assays

To measure caspase activity, 100 nM purified caspase was assayed over 7 min at 37 °C in casp-6 activity assay buffer (100 mM HEPES, 120 mM NaCl, 0.1% CHAPS, 10% sucrose, 5 mM DTT) or in caspase-7 activity assay buffer (100 mM HEPES pH 7.5, 5 mM CaCl₂, 10% PEG 400, 0.1% CHAPS, 5 mM DTT). For substrate titration, a range of 0-500 μM fluorogenic substrate VEID-AMC [N-acetyl-Val-Glu-Ile-Asp-(7-amino-4-methyl-coumarin), Enzo Life Sciences Inc.] was used for caspase-6 and a range of 0-200 μM fluorogenic substrate DEVD-AMC [N-acetyl-Asp-Glu-Val-Asp-7-amino-4-methylcoumarin, Enzo Life Sciences Inc.] was used for caspase-7. Fluorescence kinetic measurements ($\lambda_{ex}/\lambda_{em}$: 365nm/495nm) were performed in three independent trials on three different days in 100-μL reactions in a 96-well format using a microplate reader (SpectraMax M5, Molecular Devices). Initial velocities versus substrate concentration were fit to a rectangular hyperbola using GraphPad Prism (GraphPad Software, San Diego, USA) to determine the kinetic parameters K_m and k_{cat} . Enzyme concentrations were determined by active-site titration with the quantitative covalent inhibitor VEID-CHO (N-Acetyl-Val-Glu-Ile-Asp-aldehyde; Enzo Life Sciences Inc.) for caspase-6 or DEVD-CHO (N-Acetyl-Asp-Glu-Val-Asp-aldehyde; Enzo Life Sciences Inc.) for caspase-7. Protein was added to

inhibitor solvated in DMSO in 96-wells V-bottom plates at room temperature for 1.5 hours in caspase activity assay buffer. Aliquots (90 μ L) were transferred in duplicate to black-well plates and assayed with 50-fold molar excess of substrate. The protein concentration was determined to be the lowest concentration at which full inhibition was observed and was thus used to calculate k_{cat} .

2.5.4 Hydrogen/Deuterium Exchange Mass Spectrometry

H/D exchange experiments were performed using an initial stock of 15 μ M caspase-6 or caspase-7 in 20 mM Tris pH 8.5, 200 mM NaCl and 2 mM DTT in H₂O. For samples without substrate-like inhibitor, 1 μ L of DMSO was added to a final volume of 200 μ L; and for substrate-like inhibitor-bound protein samples, 1 μ L of 30 μ M peptide substrate-like inhibitor was added (VEID-CHO for caspase-6; DEVD-CHO for caspase-7) to a final volume of 200 μ L. The protein samples were incubated at room temperature for 1 hour and then introduced into the nanoACQUITY system equipped with H/D exchange technology for UPLC separation (Wales et al., 2008) (Waters Corp., Milford, MA), which performed all subsequent manipulations for the H/D exchange. H/D exchange was initiated by dilution of each sample 15-fold with D₂O exchange buffer (10 mM phosphate pD 7.5, 200 mM NaCl) and the mixture was incubated at predetermined H/D exchange time points (*mins*: 0.17, 1, 10, 60, 120) at 25 °C. At the indicated H/D exchange time point, an aliquot from the exchange reaction was removed and deuterium labeling was quenched by adding equal volume of quench buffer (100

mM phosphate pH 2.5, 200 mM NaCl) at 3 °C. For the non-deuterated samples, the same procedure was performed in H₂O buffers. Quenched samples were introduced into a 5 µm BEH 2.1 x 30 mm Enzymate™ immobilized pepsin column (Waters Corp., Milford, MA) at 100 µL/min in 0.1% formic acid at 10 °C then incubated for 4.5 min to allow on-column digestion. Peptide fragments were collected at 0 °C on a C18 VanGuard trap column (1.7 µm x 30 mm) (Waters Corp., Milford, MA) for desalting with 0.1% formic acid in H₂O and were then separated using 1.8 µm HSS T3 C18 2.1 x 30 mm nanoACQUITY UPLC® column (Waters Corp., Milford, MA) for 10-min gradient from 0.1% formic acid to acetonitrile (7 min: 5-35%, 1 min: 35-85%, 2 min hold: 85% acetonitrile) at 40 µL/min at 0 °C. Fragments were subsequently mass-analyzed using Synapt G2Si ESI-Q-ToF mass spectrometer (Waters Corp., Milford, MA). In between sample injections, a wash step was performed to minimize peptide carry-over. Accurate mass and collision-induced dissociation in data-independent acquisition mode (MS^E) (Geromanos et al., 2009) and ProteinLynx Global Server (PLGS) 3.0 software (Waters Corp., Milford, MA) were used to determine the peptic peptides in the undeuterated protein samples analyzed on the same UPLC-ESI-Q-ToF system used for H/DX-MS experiments. Peptic peptides generated from PLGS were imported into DynamX 3.0 (Waters Corp., Milford, MA) with peptide quality thresholds of MS¹ signal intensity ≥5000, maximum sequence length of 25 amino acids, maximum mass error of 1 ppm, and minimum products per amino acid of ≥0.3. Automated results were manually inspected to ensure the corresponding m/z and isotopic distributions at various charge states were properly assigned to

the appropriate peptic peptide. DynamX 3.0 was then used to generate the relative deuterium incorporation plot and H/DX heat map for each peptic peptide. The relative deuterium incorporation of each peptide was determined by subtracting the weight-averaged centroid mass of the isotopic distribution of undeuterated control sample from that of the weight-averaged centroid mass of the isotopic distribution of deuterium-labeled samples at each labeling time point. All comparisons were performed under identical experimental conditions, thus negating the need for back exchange correction in the determination of the deuterium incorporation. Thus, H/D exchange levels are reported as relative (Wales and Engen, 2006). The fractional relative deuterium uptake was calculated by dividing the relative deuterium uptake of each peptic peptide by its theoretical maximum uptake. All H/DX-MS experiments were performed in duplicate on two separate days and a 98% confidence limit for the uncertainty of the mean relative deuterium uptake of ± 0.6 Da was calculated as described (Houde et al., 2011). Differences in deuterium uptake between two states that exceed 0.6 Da were considered significant.

2.5.5 Circular Dichroism Spectroscopy

Thermal stability of caspase-6 variants at various pHs was monitored by loss of circular dichroism signal at 222 nm over a range of 20-90 °C. CD spectra (250-190 nm) were measured on a J-1500 CD spectrometer (Jasco) with Peltier temperature controller. An appropriate buffer for effective buffering capacity was used at a particular pH (20 mM MES pH 6.2, 120 mM NaCl; 20 mM phosphate

buffer pH 7.5, 120 mM NaCl; or 20 mM Tris pH 8.5, 120 mM NaCl). Sample proteins were buffer exchanged three times into each appropriate buffer using an Amicon Ultra-0.5 mL centrifugal filter (MWCO 10K) (Millipore) and the protein concentration (5 μ M) was determined by absorbance at 280 nm (Nanodrop 2000C spectrophotometer). All data were collected at least in duplicate on different days. The melting curves were plotted using GraphPad Prism (GraphPad software) and fitted to a Boltzmann-Sigmoidal plot to determine the apparent melting temperature, $T_{m, \text{apparent}}$.

2.5.6 Caspase Activity versus pH

The activity of caspase-6 variants were assessed as a function of pH using 20 nM protein and 60 μ M of VEID-AMC as a substrate in appropriate buffer at various pH (4.5-9.0). The common components for all buffer at different pHs contained 120 mM NaCl, 0.1% CHAPS, 10% sucrose, 5% glycerol and 5 mM DTT. The following buffers were used at 100 mM concentration with its corresponding pH range: acetate (pH 4.5-5.0), MES (pH 5.5-6.5), HEPES (pH 7.0-7.5), and Tris base (pH 8.0-9.0). Fluorescence kinetic measurements ($\lambda_{\text{ex}}/\lambda_{\text{em}}$: 365nm/495nm) were performed in duplicate in 100- μ L reactions in a 96-well format using a SpectraMax M5 microplate reader (Molecular Devices).

2.5.7 *In Silico* Model Preparation

The initial model for the mature dimeric human Caspase-6 was generated by producing an all-atom structure of the truncated enzyme by using the

coordinates of C (residues 31–165 & 201–293) and D (residues 31–165 & 199–293) chains in the ligand-free structure (PDB code: 2WDP) and Maestro's Protein Preparation Wizard (Schrödinger, LLC). Next, the C-terminus of the cleaved intersubunit linker in each protomer was rebuilt by i) grafting the residues 166–175 from procaspase-6 structure (PDB code: 4N5D, chain A) using the Prime's Protein Splicing tool (version 3.8, Schrödinger, LLC), and ii) attaching the pentapeptide terminus (residues 175–179) in its extended conformation to the resulting chimeric structures. The N-terminal residues of the linker (194–201), missing in the 2WDP chains was reconstructed using the coordinates from a Zn(II)-bound caspase-6 structure (PDB code: 4FXO). The resulting chimeric dimer was subjected to a protonation state assignment algorithm (Epik, Schrödinger, LLC) and restrained minimization (force field: OPLS3) sequence within Maestro's Protein Preparation Wizard. The model was further refined via a simulated annealing sequence within Desmond (version 4.0, D. E. Shaw Research & Schrödinger, LLC). Thus, an NVT ensemble was built with neutralized (by 8 Cl⁻ ions) system and further Na⁺ and Cl⁻ ions to simulate 150 mM concentration in an explicit SPC solvent model (16,783 water molecules), using an orthorhombic simulation box (10Å buffer) with periodic boundary conditions. The ensemble was then subjected to the following 7-stage schedule: i) incubation at 10K for 30 ps, ii) heating to 100K for 70ps, iii) heating to 300K for 100ps, iv) heating to 400K for 100ps, v) incubation at 400K for 200ps, vi) cool down to 300K for 500ps, vii) incubation at 300K for 200ps. The structure from the

final frame of the 1.2-ns simulation was re-minimized (Prime, OPLS3) and selected as the starting point for all subsequent simulations.

2.5.8 Simulated Annealing Studies of Protonation Variants

Protonation states of the residues in the two forms of caspase-6 were obtained using Epik algorithm (Schrödinger, LLC) and the all-atom models derived from unliganded (PDB code 2WDP) and VEID-bound (PDB code 3OD5) forms. Using the refined model obtained above, several protonation state variants at Glu and His residues (His H -protonated His; Glu H -protonated Glu) were produced: i) '2WDP-like' or the triply protonated helical caspase-6 variant (His H -52, Glu H -135, and Glu H -221), ii) '3OD5-like' or the triply deprotonated strand caspase-6 variant (His-52, Glu-135, and Glu-221), iii) 'His-52' (His-52, Glu H -135, and Glu H -221), iv) 'Glu-135' (His H -52, Glu-135, and Glu H -221) and v) 'Glu-221' (His H -52, Glu H -135, and Glu-221). The resulting models were neutralized with the corresponding number of Cl⁻ ions and treated as described above to produce starting NVT ensembles for simulated annealing experiments. The 1.2-ns-long 7-stage schedule was re-applied on the protonation variants, and the root-mean-square fluctuation (RMSF) analysis was performed using the Simulation Event Analysis tool within Desmond.

2.6 Acknowledgments

This work was supported by the National Institutes of Health (GM080532). We thank Stephen J. Eyles, director of the UMass Institute of Applied Life Sciences Mass Spectrometry core facility for abundant assistance with H/D exchange mass spectrometry data collection and processing.

2.7 References

- Abel, K., M. D. Yoder, R. Hilgenfeld, and F. Jurnak. 1996. An alpha to beta conformational switch in EF-Tu. *Structure*, 4:1153-9.
- Aharony, I., D. E. Ehrnhoefer, A. Shruster, X. Qiu, S. Franciosi, M. R. Hayden, and D. Offen. 2015. A Huntingtin-based peptide inhibitor of caspase-6 provides protection from mutant Huntingtin-induced motor and behavioral deficits. *Hum Mol Genet*, 24:2604-14.
- Akpan, N., E. Serrano-Saiz, B. E. Zacharia, M. L. Otten, A. F. Ducruet, S. J. Snipas, W. Liu, J. Velloza, G. Cohen, S. A. Sosunov, W. H. Frey, 2nd, G. S. Salvesen, E. S. Connolly, Jr., and C. M. Troy. 2011. Intranasal delivery of caspase-9 inhibitor reduces caspase-6-dependent axon/neuron loss and improves neurological function after stroke. *J Neurosci*, 31:8894-904.
- Albrecht, S., N. Bogdanovic, B. Ghetti, B. Winblad, and A. C. LeBlanc. 2009. Caspase-6 activation in familial alzheimer disease brains carrying amyloid precursor protein or presenilin i or presenilin II mutations. *J Neuropathol Exp Neurol*, 68:1282-93.
- Albrecht, S., M. Bourdeau, D. Bennett, E. J. Mufson, M. Bhattacharjee, and A. C. LeBlanc. 2007. Activation of caspase-6 in aging and mild cognitive impairment. *Am J Pathol*, 170:1200-9.
- Baumgartner, R., G. Meder, C. Briand, A. Decock, A. D'Arcy, U. Hassiepen, R. Morse, and M. Ratus. 2009. The crystal structure of caspase-6, a selective effector of axonal degeneration. *Biochem J*, 423:429-39.
- Boatright, K. M., M. Ratus, F. L. Scott, S. Sperandio, H. Shin, I. M. Pedersen, J. E. Ricci, W. A. Edris, D. P. Sutherlin, D. R. Green, and G. S. Salvesen. 2003. A unified model for apical caspase activation. *Molecular Cell*, 11:529-41.
- Burke, J. E., O. Perisic, G. R. Masson, O. Vadas, and R. L. Williams. 2012. Oncogenic mutations mimic and enhance dynamic events in the natural activation of phosphoinositide 3-kinase p110alpha (PIK3CA). *Proceedings of the National Academy of Sciences of the United States of America*, 109:15259-64.
- Cao, Q., X. J. Wang, L. F. Li, and X. D. Su. 2014. The regulatory mechanism of the caspase 6 pro-domain revealed by crystal structure and biochemical assays. *Acta Crystallogr D Biol Crystallogr*, 70:58-67.

- Chai, J., Q. Wu, E. Shiozaki, S. M. Srinivasula, E. S. Alnemri, and Y. Shi. 2001. Crystal structure of a procaspase-7 zymogen: mechanisms of activation and substrate binding. *Cell*, 107:399-407.
- Cowling, V., and J. Downward. 2002. Caspase-6 is the direct activator of caspase-8 in the cytochrome c-induced apoptosis pathway- absolute requirement for removal of caspase-6 prodomain. *Cell Death and Differentiation*, 9:1046-1056.
- Di Russo, N. V., D. A. Estrin, M. A. Marti, and A. E. Roitberg. 2012. pH-Dependent conformational changes in proteins and their effect on experimental pK(a)s: the case of Nitrophenol 4. *PLoS Comput Biol*, 8:e1002761.
- Ding, Z. M., B. Wu, W. Q. Zhang, X. J. Lu, Y. C. Lin, Y. J. Geng, and Y. F. Miao. 2012. Neuroprotective effects of ischemic preconditioning and postconditioning on global brain ischemia in rats through the same effect on inhibition of apoptosis. *Int J Mol Sci*, 13:6089-101.
- Englander, S. W., and N. R. Kallenbach. 1983. Hydrogen exchange and structural dynamics of proteins and nucleic acids. *Q Rev Biophys*, 16:521-655.
- Galvan, V., S. Chen, D. Lu, A. Logvinova, P. Goldsmith, E. H. Koo, and D. E. Bredesen. 2002. Caspase cleavage of members of the amyloid precursor family of proteins. *J Neurochem*, 82:283-94.
- Galvan, V., O. F. Gorostiza, S. Banwait, M. Ataie, A. V. Logvinova, S. Sitaraman, E. Carlson, S. A. Sagi, N. Chevallier, K. Jin, D. A. Greenberg, and D. E. Bredesen. 2006. Reversal of Alzheimer's-like pathology and behavior in human APP transgenic mice by mutation of Asp664. *Proc Natl Acad Sci U S A*, 103:7130-5.
- Geromanos, S. J., J. P. Vissers, J. C. Silva, C. A. Dorschel, G. Z. Li, M. V. Gorenstein, R. H. Bateman, and J. I. Langridge. 2009. The detection, correlation, and comparison of peptide precursor and product ions from data independent LC-MS with data dependant LC-MS/MS. *Proteomics*, 9:1683-95.
- Gervais, F. G., D. Xu, G. S. Robertson, J. P. Vaillancourt, Y. Zhu, J. Huang, A. LeBlanc, D. Smith, M. Rigby, M. S. Shearman, E. E. Clarke, H. Zheng, L. H. T. Van Der Ploeg, S. C. Ruffolo, N. A. Thornberry, S. Xanthoudakis, R. J. Zamboni, S. Roy, and D. W. Nicholson. 1999. Involvement of Caspases in Proteolytic Cleavage of Alzheimer's Amyloid- β Precursor Protein and Amyloidogenic A β Peptide Formation. *Cell*, 97:395-406.
- Giaime, E., C. Sunyach, C. Druon, S. Scarzello, G. Robert, S. Grosso, P. Auburger, M. S. Goldberg, J. Shen, P. Heutink, J. Pouyssegur, G. Pages, F. Checler, and C. Alves da Costa. 2010. Loss of function of DJ-1 triggered by Parkinson's disease-associated mutation is due to proteolytic resistance to caspase-6. *Cell Death Differ*, 17:158-69.
- Graham, R. K., Y. Deng, J. Carroll, K. Vaid, C. Cowan, M. A. Pouladi, M. Metzler, N. Bissada, L. Wang, R. L. Faull, M. Gray, X. W. Yang, L. A. Raymond, and M. R. Hayden. 2010. Cleavage at the 586 amino acid caspase-6 site in mutant huntingtin influences caspase-6 activation in vivo. *J Neurosci*, 30:15019-29.

- Graham, R. K., Y. Deng, E. J. Slow, B. Haigh, N. Bissada, G. Lu, J. Pearson, J. Shehadeh, L. Bertram, Z. Murphy, S. C. Warby, C. N. Doty, S. Roy, C. L. Wellington, B. R. Leavitt, L. A. Raymond, D. W. Nicholson, and M. R. Hayden. 2006. Cleavage at the caspase-6 site is required for neuronal dysfunction and degeneration due to mutant huntingtin. *Cell*, 125:1179-91.
- Guo, H., S. Albrecht, M. Bourdeau, T. Petzke, C. Bergeron, and A. C. LeBlanc. 2004. Active caspase-6 and caspase-6-cleaved tau in neuropil threads, neuritic plaques, and neurofibrillary tangles of Alzheimer's disease. *Am J Pathol*, 165:523-31.
- Guo, H., D. Petrin, Y. Zhang, C. Bergeron, C. G. Goodyer, and A. C. LeBlanc. 2006. Caspase-1 activation of caspase-6 in human apoptotic neurons. *Cell Death Differ*, 13:285-92.
- Harrington, E. P., C. Zhao, S. P. Fancy, S. Kaing, R. J. Franklin, and D. H. Rowitch. 2010. Oligodendrocyte PTEN is required for myelin and axonal integrity, not remyelination. *Annals of Neurology*, 68:703-16.
- Hermel, E., J. Gafni, S. S. Propp, B. R. Leavitt, C. L. Wellington, J. E. Young, A. S. Hackam, A. V. Logvinova, A. L. Peel, S. F. Chen, V. Hook, R. Singaraja, S. Krajewski, P. C. Goldsmith, H. M. Ellerby, M. R. Hayden, D. E. Bredesen, and L. M. Ellerby. 2004. Specific caspase interactions and amplification are involved in selective neuronal vulnerability in Huntington's disease. *Cell Death and Differentiation*, 11:424-438.
- Hill, M. E., D. J. MacPherson, P. Wu, O. Julien, J. A. Wells, and J. A. Hardy. 2016. Reprogramming Caspase-7 Specificity by Regio-Specific Mutations and Selection Provides Alternate Solutions for Substrate Recognition. *ACS Chem Biol*, 11:1603-12.
- Hodkinson, J. P., S. E. Radford, and A. E. Ashcroft. 2012. The role of conformational flexibility in beta2-microglobulin amyloid fibril formation at neutral pH. *Rapid Communications in Mass Spectrometry*, 26:1783-92.
- Horowitz, P. M., K. R. Patterson, A. L. Guillozet-Bongaarts, M. R. Reynolds, C. A. Carroll, S. T. Weintraub, D. A. Bennett, V. L. Cryns, R. W. Berry, and L. I. Binder. 2004. Early N-terminal changes and caspase-6 cleavage of tau in Alzheimer's disease. *J Neurosci*, 24:7895-902.
- Houde, D., S. A. Berkowitz, and J. R. Engen. 2011. The utility of hydrogen/deuterium exchange mass spectrometry in biopharmaceutical comparability studies. *J Pharm Sci*, 100:2071-86.
- Kirschke, E., D. Goswami, D. Southworth, P. R. Griffin, and D. A. Agard. 2014. Glucocorticoid receptor function regulated by coordinated action of the Hsp90 and Hsp70 chaperone cycles. *Cell*, 157:1685-97.
- Klaiman, G., N. Champagne, and A. C. LeBlanc. 2009. Self-activation of Caspase-6 in vitro and in vivo: Caspase-6 activation does not induce cell death in HEK293T cells. *Biochim Biophys Acta*, 1793:592-601.
- Klaiman, G., T. L. Petzke, J. Hammond, and A. C. LeBlanc. 2008. Targets of caspase-6 activity in human neurons and Alzheimer disease. *Mol Cell Proteomics*, 7:1541-55.

- Landgraf, Rachele R., D. Goswami, F. Rajamohan, Melissa S. Harris, M. F. Calabrese, Lise R. Hoth, R. Magyar, Bruce D. Pascal, Michael J. Chalmers, Scott A. Busby, R. G. Kurumbail, and Patrick R. Griffin. Activation of AMP-Activated Protein Kinase Revealed by Hydrogen/Deuterium Exchange Mass Spectrometry. *Structure*, 21:1942-1953.
- LeBlanc, A. C. 2013. Caspase-6 as a novel early target in the treatment of Alzheimer's disease. *Eur J Neurosci*, 37:2005-18.
- Liao, S. Y., K. J. Fritzsching, and M. Hong. 2013. Conformational analysis of the full-length M2 protein of the influenza A virus using solid-state NMR. *Protein Science*, 22:1623-38.
- Liu, X., H. Zhang, X. J. Wang, L. F. Li, and X. D. Su. 2011. Get phases from arsenic anomalous scattering: de novo SAD phasing of two protein structures crystallized in cacodylate buffer. *PLoS One*, 6:e24227.
- Lu, D. C., S. Rabizadeh, S. Chandra, R. F. Shayya, L. M. Ellerby, X. Ye, G. S. Salvesen, E. H. Koo, and D. E. Bredesen. 2000. A second cytotoxic proteolytic peptide derived from amyloid β -protein precursor. *Nature Medicine*, 6:397-404.
- Majidi, A., J. Mahmoudi, S. Sadigh-Eteghad, S. E. Golzari, B. Sabermarouf, and S. Reyhani-Rad. 2016. Permissive role of cytosolic pH acidification in neurodegeneration: A closer look at its causes and consequences. *Journal of Neuroscience Research*, 94:879-87.
- Mehmood, S., C. Domene, E. Forest, and J. M. Jault. 2012. Dynamics of a bacterial multidrug ABC transporter in the inward- and outward-facing conformations. *Proceedings of the National Academy of Sciences of the United States of America*, 109:10832-6.
- Milnerwood, A. J., C. M. Gladding, M. A. Pouladi, A. M. Kaufman, R. M. Hines, J. D. Boyd, R. W. Ko, O. C. Vasuta, R. K. Graham, M. R. Hayden, T. H. Murphy, and L. A. Raymond. 2010. Early increase in extrasynaptic NMDA receptor signaling and expression contributes to phenotype onset in Huntington's disease mice. *Neuron*, 65:178-90.
- Morgan, C. R., and J. R. Engen. 2009. Investigating solution-phase protein structure and dynamics by hydrogen exchange mass spectrometry. *Curr Protoc Protein Sci*, Chapter 17:Unit 17 6 1-17.
- Muller, I., M. B. Lamers, A. J. Ritchie, C. Dominguez, I. Munoz-Sanjuan, and A. Kiselyov. 2011a. Structure of human caspase-6 in complex with Z-VAD-FMK: New peptide binding mode observed for the non-canonical caspase conformation. *Bioorg Med Chem Lett*, 21:5244-7.
- Muller, I., M. B. Lamers, A. J. Ritchie, H. Park, C. Dominguez, I. Munoz-Sanjuan, M. Maillard, and A. Kiselyov. 2011b. A new apo-caspase-6 crystal form reveals the active conformation of the apoenzyme. *Journal of Molecular Biology*, 410:307-15.
- Murakami, S., R. Nakashima, E. Yamashita, T. Matsumoto, and A. Yamaguchi. 2006. Crystal structures of a multidrug transporter reveal a functionally rotating mechanism. *Nature*, 443:173-9.

- Nedergaard, M., R. P. Kraig, J. Tanabe, and W. A. Pulsinelli. 1991. Dynamics of interstitial and intracellular pH in evolving brain infarct. *American Journal of Physiology*, 260:R581-8.
- Nguyen, T. V., V. Galvan, W. Huang, S. Banwait, H. Tang, J. Zhang, and D. E. Bredesen. 2008. Signal transduction in Alzheimer disease: p21-activated kinase signaling requires C-terminal cleavage of APP at Asp664. *J Neurochem*, 104:1065-80.
- Nikolaev, A., T. McLaughlin, D. D. O'Leary, and M. Tessier-Lavigne. 2009. APP binds DR6 to trigger axon pruning and neuron death via distinct caspases. *Nature*, 457:981-9.
- Orth, K., A. M. Chinnaiyan, M. Garg, C. J. Froelich, and V. M. Dixit. 1996. The CED-3/ICE-like protease Mch2 is activated during apoptosis and cleaves the death substrate lamin A. *J Biol Chem*, 271:16443-6.
- Pan, K. M., M. Baldwin, J. Nguyen, M. Gasset, A. Serban, D. Groth, I. Mehlhorn, Z. Huang, R. J. Fletterick, F. E. Cohen, and et al. 1993. Conversion of alpha-helices into beta-sheets features in the formation of the scrapie prion proteins. *Proceedings of the National Academy of Sciences of the United States of America*, 90:10962-6.
- Pan, L. Y., O. Salas-Solano, and J. F. Valliere-Douglass. 2014. Conformation and dynamics of interchain cysteine-linked antibody-drug conjugates as revealed by hydrogen/deuterium exchange mass spectrometry. *Analytical Chemistry*, 86:2657-64.
- Park, K. J., C. A. Grosso, I. Aubert, D. R. Kaplan, and F. D. Miller. 2010. p75NTR-dependent, myelin-mediated axonal degeneration regulates neural connectivity in the adult brain. *Nature Neuroscience*, 13:559-66.
- Pirrone, G. F., R. E. Iacob, and J. R. Engen. 2015. Applications of hydrogen/deuterium exchange MS from 2012 to 2014. *Anal Chem*, 87:99-118.
- Polekhina, G., S. Thirup, M. Kjeldgaard, P. Nissen, C. Lippmann, and J. Nyborg. 1996. Helix unwinding in the effector region of elongation factor EF-Tu-GDP. *Structure*, 4:1141-51.
- Pop, C., and G. S. Salvesen. 2009. Human caspases: activation, specificity, and regulation. *Journal of Biological Chemistry*, 284:21777-81.
- Qin, B. Y., M. C. Bewley, L. K. Creamer, H. M. Baker, E. N. Baker, and G. B. Jameson. 1998. Structural basis of the Tanford transition of bovine beta-lactoglobulin. *Biochemistry*, 37:14014-23.
- Riechers, S. P., S. Butland, Y. Deng, N. Skotte, D. E. Ehrnhoefer, J. Russ, J. Laine, M. Laroche, M. A. Pouladi, E. E. Wanker, M. R. Hayden, and R. K. Graham. 2016. Interactome network analysis identifies multiple caspase-6 interactors involved in the pathogenesis of HD. *Hum Mol Genet*, 25:1600-18.
- Saganich, M. J., B. E. Schroeder, V. Galvan, D. E. Bredesen, E. H. Koo, and S. F. Heinemann. 2006. Deficits in synaptic transmission and learning in amyloid precursor protein (APP) transgenic mice require C-terminal cleavage of APP. *J Neurosci*, 26:13428-36.

- Schoenmann, Z., E. Assa-Kunik, S. Tiomny, A. Minis, L. Haklai-Topper, E. Arama, and A. Yaron. 2010. Axonal degeneration is regulated by the apoptotic machinery or a NAD⁺-sensitive pathway in insects and mammals. *Journal of Neuroscience*, 30:6375-86.
- Schulman, B. A., D. L. Lindstrom, and E. Harlow. 1998. Substrate recruitment to cyclin-dependent kinase 2 by a multipurpose docking site on cyclin A. *Proceedings of the National Academy of Sciences of the United States of America*, 95:10453-8.
- Shepard, L. A., A. P. Heuck, B. D. Hamman, J. Rossjohn, M. W. Parker, K. R. Ryan, A. E. Johnson, and R. K. Tweten. 1998. Identification of a membrane-spanning domain of the thiol-activated pore-forming toxin *Clostridium perfringens* perfringolysin O: an alpha-helical to beta-sheet transition identified by fluorescence spectroscopy. *Biochemistry*, 37:14563-74.
- Simon, D. J., R. M. Weimer, T. McLaughlin, D. Kallop, K. Stanger, J. Yang, D. D. O'Leary, R. N. Hannoush, and M. Tessier-Lavigne. 2012. A caspase cascade regulating developmental axon degeneration. *Journal of Neuroscience*, 32:17540-53.
- Snijder, J., M. Benevento, C. L. Moyer, V. Reddy, G. R. Nemerow, and A. J. Heck. 2014. The cleaved N-terminus of pVI binds peripentonal hexons in mature adenovirus. *Journal of Molecular Biology*, 426:1971-9.
- Srinivasula, S. M., M. Ahmad, M. MacFarlanes, Z. Luo, Z. HUang, T. Fernandes-Alnemri, and E. S. Alnemri. 1998. Generation of Constitutively Active Recombinant Caspases-3 and -6 by Rearrangement of Their Subunits. *The Journal of Biological Chemistry*, 273:10107-10111.
- Srinivasula, S. M., T. Fernandes-Alnemri, J. Zangrilli, N. Robertson, R. C. Armstrong, L. Wang, J. A. Trapani, K. J. Tomaselli, G. Litwack, and E. S. Alnemri. 1996. The Ced-3:Interleukin 1b Converting Enzyme-like Homolog Mch6 and the Lamin-cleaving Enzyme Mch2a Are Substrates for the Apoptotic Mediator CPP32. *The Journal of Biological Chemistry*, 271:27099-27106.
- Štrajbl, M., J. Florián, and A. Warshel. 2001. Ab Initio Evaluation of the Free Energy Surfaces for the General Base/Acid Catalyzed Thiolytic of Formamide and the Hydrolysis of Methyl Thioformate: A Reference Solution Reaction for Studies of Cysteine Proteases. *The Journal of Physical Chemistry B*, 105:4471-4484.
- Suzuki, A., G. Kusakai, A. Kishimoto, Y. Shimojo, S. Miyamoto, T. Ogura, A. Ochiai, and H. Esumi. 2004. Regulation of caspase-6 and FLIP by the AMPK family member ARK5. *Oncogene*, 23:7067-75.
- Takahashi, A., E. S. Alnemri, Y. A. Lazebnik, T. Fernandes-Alnemri, G. Litwack, R. D. Moir, R. D. Goldman, G. G. Poirier, S. H. Kaufmann, and W. C. Earnshaw. 1996. Cleavage of lamin A by Mch2 alpha but not CPP32: multiple interleukin 1 beta-converting enzyme-related proteases with distinct substrate recognition properties are active in apoptosis. *Proc Natl Acad Sci U S A*, 93:8395-400.

- Vaidya, S., and J. A. Hardy. 2011. Caspase-6 latent state stability relies on helical propensity. *Biochemistry*, 50:3282-7.
- Vaidya, S., E. M. Velazquez-Delgado, G. Abbruzzese, and J. A. Hardy. 2011. Substrate-induced conformational changes occur in all cleaved forms of caspase-6. *J Mol Biol*, 406:75-91.
- Wales, T. E., and J. R. Engen. 2006. Hydrogen exchange mass spectrometry for the analysis of protein dynamics. *Mass Spectrometry Reviews*, 25:158-70.
- Wales, T. E., K. E. Fadgen, G. C. Gerhardt, and J. R. Engen. 2008. High-speed and high-resolution UPLC separation at zero degrees Celsius. *Anal Chem*, 80:6815-20.
- Wang, X. J., Q. Cao, X. Liu, K. T. Wang, W. Mi, Y. Zhang, L. F. Li, A. C. LeBlanc, and X. D. Su. 2010. Crystal structures of human caspase 6 reveal a new mechanism for intramolecular cleavage self-activation. *EMBO Rep*, 11:841-7.
- Warby, S. C., C. N. Doty, R. K. Graham, J. B. Carroll, Y. Z. Yang, R. R. Singaraja, C. M. Overall, and M. R. Hayden. 2008. Activated caspase-6 and caspase-6-cleaved fragments of huntingtin specifically colocalize in the nucleus. *Hum Mol Genet*, 17:2390-404.
- Watanabe, C., G. L. Shu, T. S. Zheng, R. A. Flavell, and E. A. Clark. 2008. Caspase 6 regulates B cell activation and differentiation into plasma cells. *J Immunol*, 181:6810-9.
- Wei, Y., T. Fox, S. P. Chambers, J. Sintchak, J. T. Coll, J. M. Golec, L. Swenson, K. P. Wilson, and P. S. Charifson. 2000. The structures of caspases-1, -3, -7 and -8 reveal the basis for substrate and inhibitor selectivity. *Chemistry and Biology*, 7:423-32.
- Witkowski, W. A., and J. A. Hardy. 2011. A designed redox-controlled caspase. *Protein Sci*, 20:1421-31.
- Wong, B. K., D. E. Ehrnhoefer, R. K. Graham, D. D. Martin, S. Ladha, V. Uribe, L. M. Stanek, S. Franciosi, X. Qiu, Y. Deng, V. Kovalik, W. Zhang, M. A. Pouladi, L. S. Shihabuddin, and M. R. Hayden. 2015. Partial rescue of some features of Huntington Disease in the genetic absence of caspase-6 in YAC128 mice. *Neurobiol Dis*, 76:24-36.
- Yassine, W., N. Taib, S. Federman, A. Milochau, S. Castano, W. Sbi, C. Manigand, M. Laguerre, B. Desbat, R. Oda, and J. Lang. 2009. Reversible transition between alpha-helix and beta-sheet conformation of a transmembrane domain. *Biochimica et Biophysica Acta*, 1788:1722-30.
- Zhao, H., W. Zhao, K. Lok, Z. Wang, and M. Yin. 2014. A synergic role of caspase-6 and caspase-3 in Tau truncation at D421 induced by H₂O₂. *Cell Mol Neurobiol*, 34:369-78.
- Zhao, M., J. Su, E. Head, and C. W. Cotman. 2003. Accumulation of caspase cleaved amyloid precursor protein represents an early neurodegenerative event in aging and in Alzheimer's disease. *Neurobiol Dis*, 14:391-40.

CHAPTER 3

THE MULTIPLE PROTEOLYTIC EVENTS THAT LEAD TO CASPASE-6 ACTIVATION EACH IMPACT THE CONFORMATION OF DISCRETE STRUCTURAL REGIONS

This chapter is being prepared for submission as: Dagbay, K. B. and J. A. Hardy. 2017. *The Multiple Proteolytic Events that Lead to Caspase-6 Activation Each Impact the Conformation of Discrete Structural Regions*.

3.1 Abstract

Caspase-6 is critical to the neurodegenerative pathways of Alzheimer's, Huntington's and Parkinson's disease and has been identified as a potential molecular target for treatment of neurodegeneration. Thus, understanding the fine structural details underlying the mechanism of caspase-6 activation is important to precisely control its function. In this work, hydrogen/deuterium exchange mass spectrometry (H/DX-MS) was used to map the local changes in the conformational flexibility of procaspase-6 as it undergoes the series of cleavage events that ultimately lead to the fully active, substrate-bound state. Intramolecular self-cleavage at Asp-193 evoked higher solvent exposure in the regions of the substrate binding loops L1, L3, L4 and in the 130's, the intersubunit linker region, and the 26-32 region, as well as stabilization of loop 2. Further removal of the linker allowed caspase-6 to gain more flexibility in the 130's region and in the L2 region converting caspase-6 into a competent substrate-binding state. The prodomain region is found to be intrinsically disordered independent of the activation step of caspase-6; however, its complete removal resulted in the protection of the adjacent 26-32 region, suggesting that this region may play a regulatory role. The molecular details of

caspase-6 dynamics in solution provide a comprehensive scaffold for strategic design of therapeutic approaches for neurodegenerative disorders.

3.2 Introduction

Caspases are a family of cysteine-aspartate proteases that are central players in apoptosis and inflammation. Caspases are expressed as dimeric yet inactive zymogens (procaspases) and activated via proteolytic cleavage at conserved aspartate residues to generate the large and small subunits. Based on their cellular function and domain organization, caspases are classified as initiator (caspase-2, -8, and -9) or executioner (caspase-3, -6, and -7). In the canonical caspase activation route, initiator caspases activate executioner caspases through proteolytic processing which promotes apoptosis in cells.

Caspase-6 is unique among caspases for its role in neurological disorders including Alzheimer's (Albrecht et al., 2007; Guo et al., 2004; LeBlanc, 2013), Huntington's (Aharony et al., 2015; Graham et al., 2010; Graham et al., 2006; Wong et al., 2015) , and Parkinson's (Giaime et al., 2010) diseases. Neuronal proteins that are known substrates of caspases-6 include microtubule-associated protein Tau (Horowitz et al., 2004), amyloid precursor protein (Albrecht et al., 2009), presenilin I and II (Albrecht et al., 2009), polyglutamine-expanded and native huntingtin protein (Graham et al., 2006) and Parkinson disease protein 7 (PARK7), also known as protein deglycase DJ-1 (Giaime et al., 2010). Cleavage of these neuronal substrates by caspase-6 is recognized to impact the

physiological outcomes in these neurological disorders. Thus, making caspase-6 an attractive molecular target for treatment of neurodegeneration.

Although it is categorized as an executioner caspase, caspase-6 sometimes plays roles as an initiator or even as an inflammatory caspase, making its classification complex. Even though caspase-6 is a weak executioner of apoptosis, its overexpression in mammalian cells results in apoptosis (Suzuki et al., 2004) where it is the only known caspase to cleave the nuclear lamellar protein, lamin A/C (Orth et al., 1996; Srinivasula et al., 1996; Takahashi et al., 1996). As an initiator, caspase-6 activates caspase-8 (Cowling and Downward, 2002). Caspase-6 is also associated with the inflammatory pathway by being activated by caspase-1 (Guo et al., 2006). Moreover, a noncanonical route for activation has been reported in caspase-6. Caspase-6 is often activated by caspase-3 rather than by initiator caspases (Simon et al., 2012; Slee et al., 1999); however, it can also be activated in the absence of caspase-3 (Allsopp et al., 2000; Doostzadeh-Cizeron et al., 2000; LeBlanc et al., 1999) and is reported to self-activate *in vitro* and *in vivo* (Klaiman et al., 2009; Wang et al., 2010b).

Caspase-6 cleavage sites are located at the prodomain (Asp-23) and at both sides of the intersubunit linker (Asp-179 and Asp-193) (Figure 3.1). The intersubunit linker joins the large and the small subunits of procaspase-6 with the active site Cys-163 located within the large subunit. The active site cavity of caspase-6 is composed of four flexible loops (L1, L2, L3, L4) that undergo structural rearrangement to accommodate the substrate in the substrate binding pockets (S1, S2, S3, S4). Current evidence of caspase-6 activation pathway

(Figure 3.1B) proposed that the initial intramolecular self-cleavage at Asp-193 in the intersubunit linker is required for procaspase-6 self-activation (Klaiman et al., 2009; Wang et al., 2010b), whereas caspase-3 activates caspase-6 by cleavage at Asp-179. Subsequent proteolytic cleavage by caspase-3, caspase-1, or by caspase-6 itself (intermolecularly) at Asp-23 in the prodomain and at Asp-179 in the intersubunit linker (Guo et al., 2006; Klaiman et al., 2009; Srinivasula et al., 1998; Wang et al., 2010b) leads to full maturation of caspase-6. All substrate-binding loops are then available to accommodate the substrate in the substrate-binding groove to enable proteolysis.

The prodomain is the most distinctive region of caspases in terms of its sequence conservation (Clark, 2016; Vaidya et al., 2011), and is therefore perhaps the most promising region for achieving selective regulation. As a result, the function of the prodomain varies among caspases. The prodomain of initiator caspases comprise caspase recruitment domain (CARD) or death effector domains (DED), which are typically longer than executioner caspase prodomains. The long prodomain facilitates recruitment to the activating scaffold, which is important for initiator caspase activation (Muzio et al., 1998; Qin et al., 1999). In executioner caspases, the short prodomain has a variety of functions. In caspase-3, it facilitates folding by acting as a chaperone (Feeney and Clark, 2005), suppresses zymogen activation *in vivo* (Meergans et al., 2000) and binds Hsp27 for inhibition of its proteolytic activation (Voss et al., 2007). In caspase-7, the prodomain-adjacent region acts as an exosite for substrate recognition

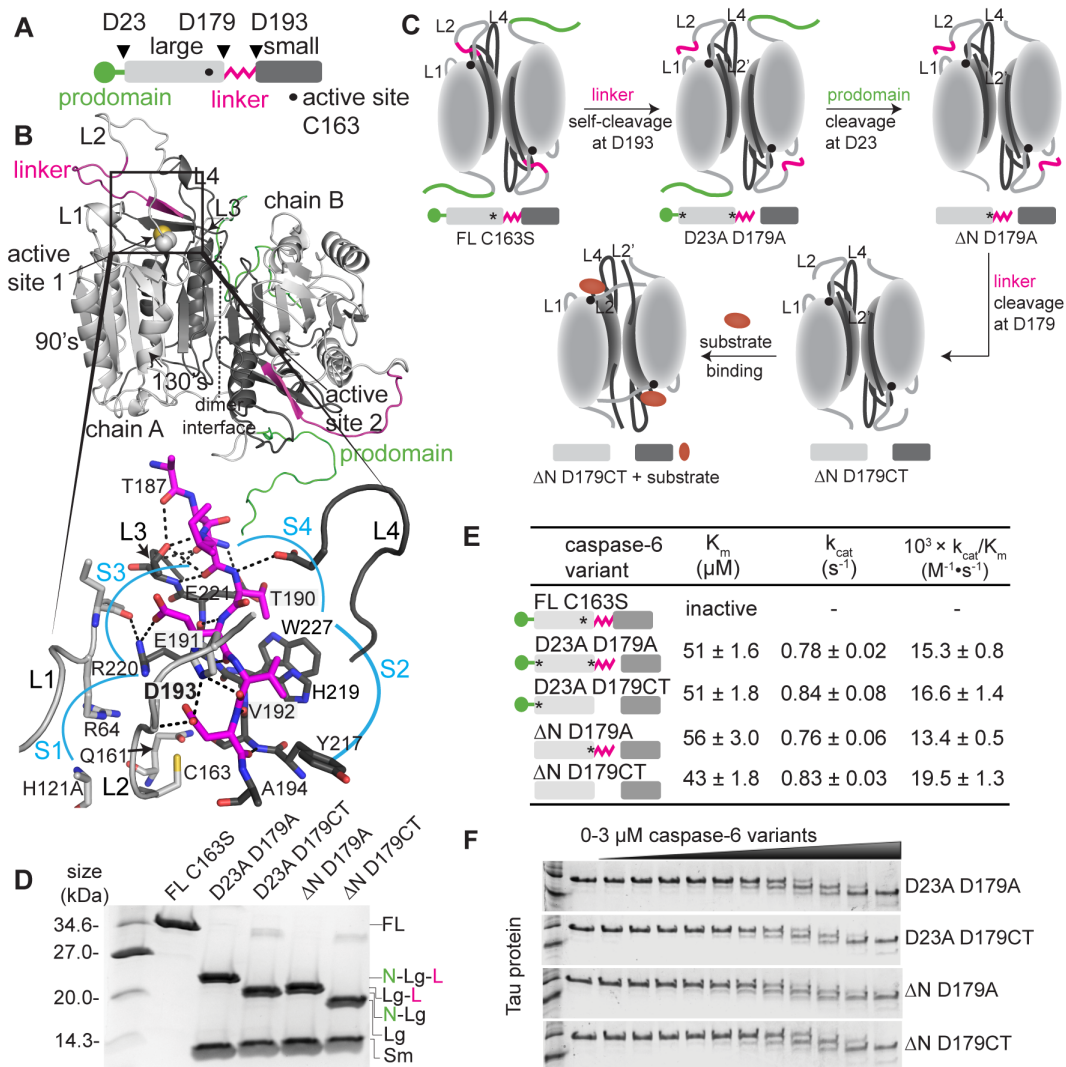


Figure 3.1. Caspase-6 Maturation State Variants

(A) Linear cartoon of procaspase-6 illustrating the prodomain (green), large subunit (light gray), intersubunit linker (magenta) and small subunit (dark gray). The active site C163 is denoted by a dot. Triangles indicate proteolytic cleavage sites. (B) Model of full-length procaspase-6 zymogen colored as in (A) was generated based on zymogen structures 4IYR and 3NR2 with missing regions modeled *de novo*. The inset view shows details of binding interactions of the intersubunit linker residues (magenta) binding into the S1–S4 subsites. (C) Cartoon of expected conformational changes in caspase-6 constructs representing various points along the zymogen maturation (cleavage) pathway colored as in (A) with substrate as an ellipsoid (red). FL indicates full-length uncleaved procaspase-6 zymogen. The C163S catalytic site substitution renders caspase-6 inactive and incapable of self-activation. ΔN indicates removal of the *N*-terminal prodomain (1–23). D23A substitution renders caspase-6 uncleavable after the prodomain. D179A prevents cleavage of the intersubunit linker. D179CT constructs have a stop codon inserted after residue 179 to allow expression of a

constitutively two-chain caspase-6, mimicking native cleavage at D179. (D) Maturation-state caspase-6 variants purified from overexpression in *E. coli*. (E) Catalytic properties of caspase-6 maturation state variants. (F) Cleavage of Tau-383 protein (3 μ M) is not impacted by the maturation state of caspase-6, tested at increasing concentrations (0–3 μ M).

(Boucher et al., 2012) and protects a nuclear localization signal (Yaoita, 2002). In caspase-6, the prodomain inhibits its self-activation *in vivo* but not *in vitro* (Klaiman et al., 2009) and silences all modes of zymogen activation *in vivo* (Cowling and Downward, 2002). Taken together, these findings clearly demonstrate that the prodomain is an integral part of caspase function and regulation.

In spite of its importance, in caspases, structural and functional details of the prodomain as well as the intersubunit linker are inadequately understood because the electron density in these regions has been missing in all caspase crystal structures to date. In particular, these regions in procaspase-6 (Cao et al., 2014) or in cleaved caspase-6 (Vaidya et al., 2011) have never been visualized. In addition to the properties of the prodomain and intersubunit linker being ethereal, the impact of the prodomain and linker on the conformational flexibility and dynamics in other regions of caspase-6 also remains elusive. Thus, probing the fine details of the influence of cleavage state and the presence or absence of the prodomain and linker on the individual conformational flexibility in all regions caspase-6 is expected to provide a complete picture detailing the underlying mechanism of caspase-6 proteolytic activation. Furthermore, insight into the functional and structural consequences of caspase-6 activation is likely to add to our understanding of other caspases as well.

Since the prodomain and the intact linker have eluded crystallization and our NMR structure determination has also not been successful, solution phase techniques, including the use of hydrogen/deuterium exchange mass spectrometry (H/DX-MS), are anticipated to be valuable to study the structural behavior over the entirety of the caspase-6 structure. H/DX-MS has emerged as a powerful tool to study changes in protein structure and dynamics resulting from protein-protein or protein-ligand interaction in solution (Chalmers et al., 2006; Englander, 2006; Konermann et al., 2011). Previously in the realm of caspases, H/DX-MS has been used to probe the unique helix-strand interconversion in caspase-6 (Dagbay et al., 2017) and the conformational changes associated with the activation of Pak2 following caspase-3 cleavage and autophosphorylation (Hsu et al., 2008). Nevertheless, a detailed understanding of the dynamic changes of a caspase as it progresses through the stages of proteolytic activation has not been undertaken. In this work, we report the use of H/DX-MS to trace the discrete conformational flexibility profile along the proteolytic activation of procaspase-6 as it matures upon initial intramolecular self-cleavage and subsequent intermolecular cleavage of the prodomain and intersubunit linker.

3.3 Results

3.3.1 H/DX-MS Profile of Caspase-6 Maturation State Variants

To map the changes in the conformational dynamics accompanied by caspase-6 proteolytic activation, a panel of caspase-6 variants that represents

each maturation state of caspase-6 (Figure 3.1 B and C) were prepared. The full-length (FL) procaspase-6 C163S, the catalytic-site inactivated variant represents the zymogen form of procaspase-6. Caspase-6 D23A D179A represents the form of caspase-6 following initial activation by intramolecular self-cleavage at Asp-193. This variant maintains the prodomain, but is self-cleaved at Asp-193 in the intersubunit linker. Caspase-6 D23A D179CT has the prodomain intact but lacks the entire intersubunit linker (residues 180–193). Caspase-6 Δ N D179CT represents the fully cleaved, mature form of caspase-6, lacking both the prodomain and intersubunit linker. All caspase-6 variants used in this study (except FL caspase-6 C163S) were active for cleaving both *tetrapeptide* substrate VEID-AMC (Figure 3.1D) and protein substrate Tau protein (Figure 3.1E).

H/DX-MS of the panel of caspase-6 maturation state variants was performed using identical protocol previously reported (Dagbay et al., 2017). Following incubation of proteins in deuterium for between 10s and 2h to allow H/D exchange on intact caspase-6, samples were subjected to on-column pepsin digestion followed by mass spectrometry for peptide mass analysis. A heat map of the relative differential deuteration profiles of regions in caspase-6 over the course of H/D exchange incubation time are depicted for each of the maturation state variants, from self-activation to full maturation and eventual binding to a substrate (Figure 3.2). The corresponding relative deuterium uptake profiles were also mapped onto a model of full-length procaspase-6 zymogen (Figure 3.3), where the crystal structures of the zymogen (PDB codes 4IYR and 3NR2)

were used as templates and the missing residues were modeled using Chimera/Modeller (Pettersen et al., 2004; Webb and Sali, 2014). The use of this hybrid model structure, which has complete sequence coverage of caspase-6, ensures all observed peptides could be represented during visualization of the results of the H/DX-MS. As anticipated, the ordered and buried regions in the core of caspase-6 had lower H/D exchange level than flexible or exposed regions of caspase-6. These most highly exchangeable regions comprised mainly the substrate binding loops, the intersubunit linker, and the prodomain. Notably, the H/D exchange at the proteolytic cleavage sites (TETD²³, DVVD¹⁷⁹, and TEVD¹⁹³) are among the highest in caspase-6, including in the zymogen form, suggesting that the higher conformational flexibility of this region is required for greater access to proteolytic cleavage by caspase-6 and other proteases. Approximately 75% of the backbone amide hydrogens underwent less than 30% of H/D exchange within 10 s, suggesting that caspase-6 is a properly folded and dynamically stable protein overall. The peptic peptide coverage ranges from 90.8–92.1% across the linear amino acid sequences of the caspase-6 maturation variants with an average redundancy of 2.46 (Figure 3.4). Together, these results suggest that all caspase-6 variants used were amenable to H/DX-MS experiments, which enable precise detection of the diverse conformational flexibility of caspase-6 upon proteolytic activation.

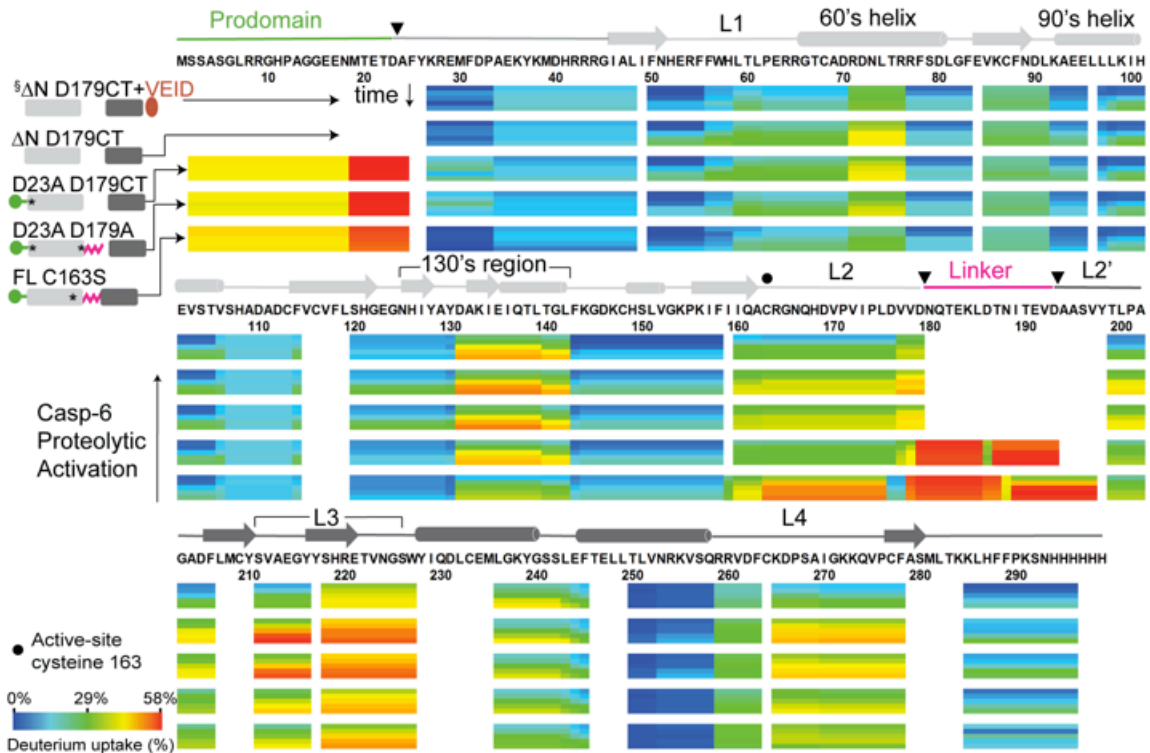


Figure 3.2. H/D Exchange Heat Map of the Relative Deuterium Incorporation for Caspase-6 Maturation-State Variants

For each peptic peptide from the caspase-6 maturation-state variants, the percent relative deuterium level for each H/D exchange incubation time (*minutes*: 0.17, 1, 10, 60, and 120) is mapped onto the corresponding linear sequence of caspase-6. The percent relative deuterium incorporation is calculated by dividing the observed deuterium uptake by the theoretical maximum deuterium uptake for each peptide. The H/DX MS experiments followed all observed peptides and covers 90.8–92.1% of the combined linear sequences. Peptic peptides with no H/D exchange data at a given incubation time or regions absent in various constructs are colored *white*. Secondary structural elements are depicted above the primary sequence. The percent relative deuterium level of each peptic peptide represents the average values of duplicate experiments performed on two separate days. $^3\text{H}/\text{DX}$ -MS data set have been reported in (Dagbay et al., 2017). See also Figure 3.3 for the percent deuterium uptake mapped onto the structure,

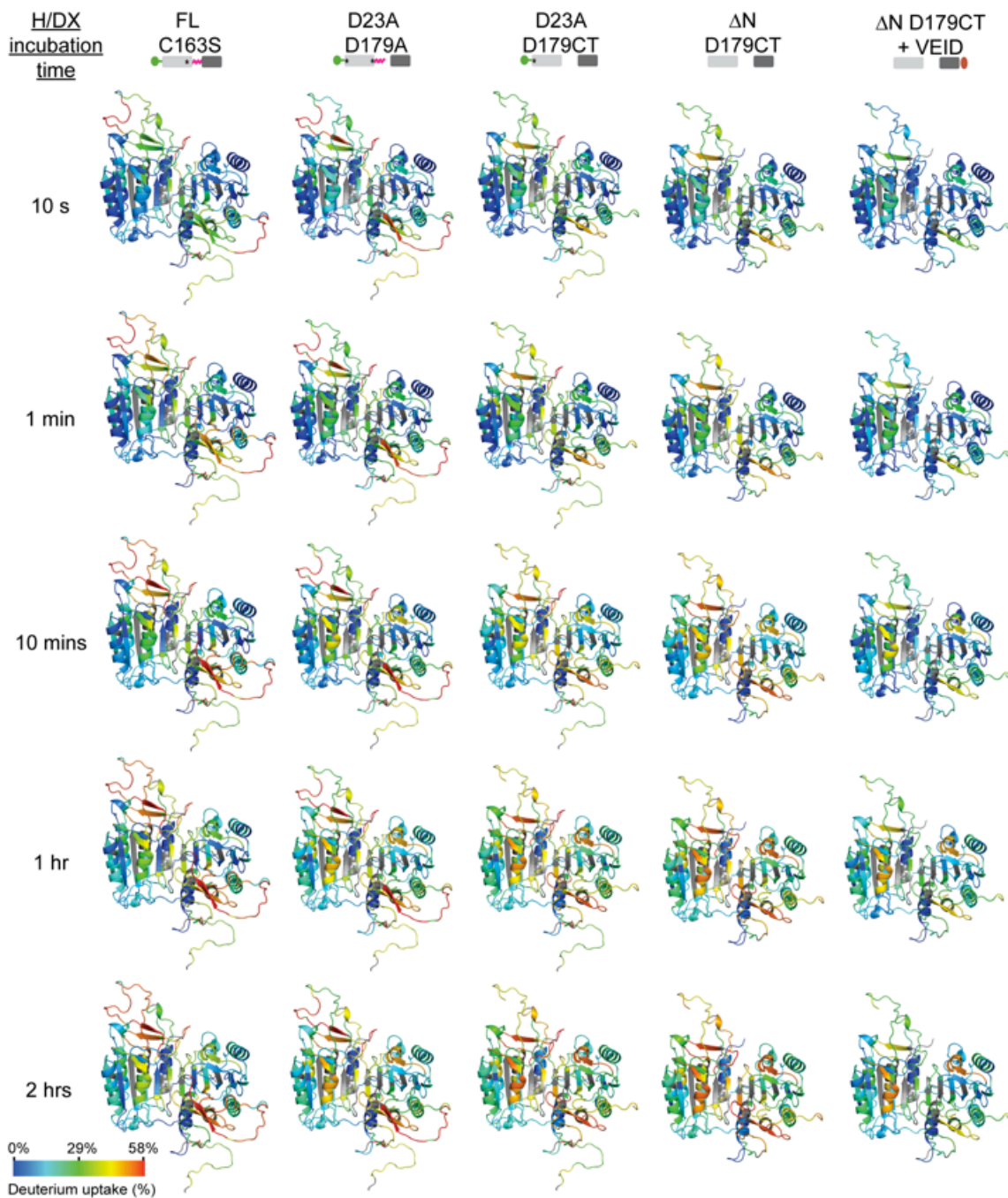


Figure 3.3. The Percent Relative Deuterium Incorporations of Caspase-6 Mutation Variants over the Course of the H/D Exchange Incubation Period are Mapped onto the Model Structure of Caspase-6

The percent relative deuterium incorporation is calculated by dividing the observed deuterium uptake by the theoretical maximum deuterium uptake for each peptide. The intensities of the *red* and *blue* colors indicate increase and decrease in H/D exchange, respectively. The regions of the protein for which not H/D exchange data are available are shown in *gray*.

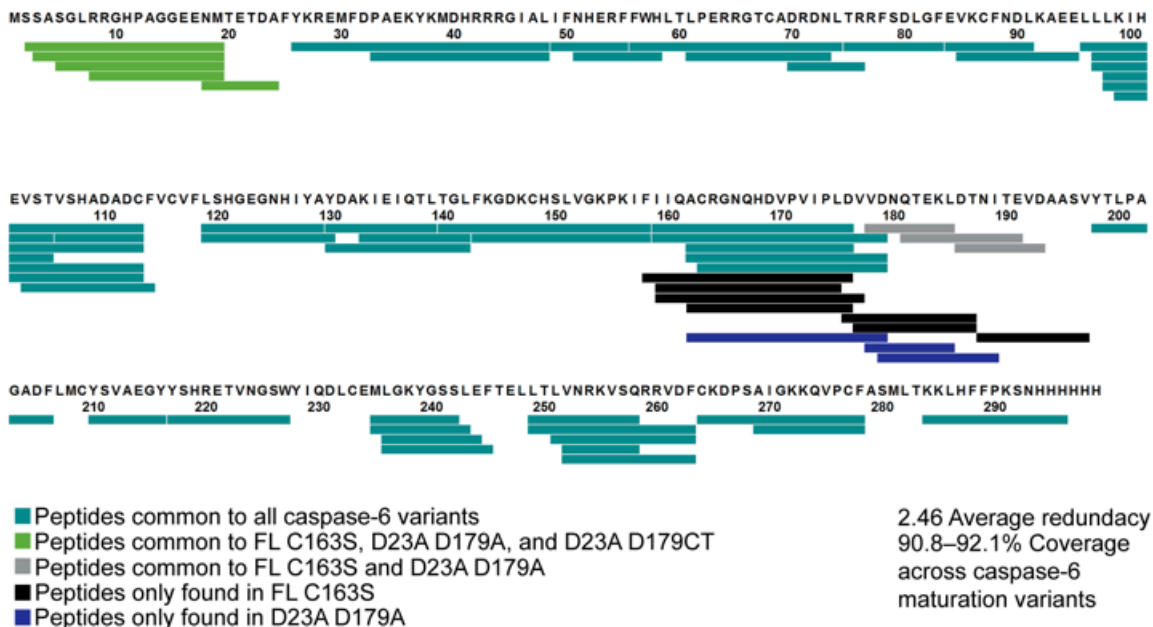


Figure 3.4. Coverage Map of the Peptic Peptides of Caspase-6 Maturation Variants Identified from H/DX-MS.

The *teal* color represents the set of peptic peptides found in all caspase-6 maturation variants covering the core regions of caspase-6. Peptic peptides highlighted in *green* were found in FL C163S, D23A D179A, and D23A D179CT covering the prodomain region. Peptic peptides highlighted in *gray* represent the linker region found only in FL C163S and D23A D179A. Peptic Peptides highlighted in *black* and *blue* colors were found in FL C163S and D23A D179A, respectively. Peptic peptides exclusively found in one or more caspase-6 maturation variants were the result from the variation in the caspase-6 constructs, including the presence of the prodomain or linker and mutations in the active-site cysteine and proteolytic cleavage sites of caspase-6. The peptic peptide coverage ranges from 90.8–92.1% across the linear amino acid sequences of the caspase-6 maturation variants with an average redundancy of 2.46.

3.3.2 Intramolecular Self-Cleavage at Asp-193 Influences Local Conformation and Dynamics

In the crystal structure of the procaspase-6 zymogen (Figure 3.1B), the active site pocket is occupied with the ¹⁹⁰TEVDA¹⁹⁴—region of the intersubunit linker—which forms an antiparallel β -sheet with ²¹⁷YSHRE²²¹ residues in the L3

through six main-chain hydrogen bonds (Wang et al., 2010b). Consequently, the scissile peptide bond between the Asp-193 and Ala-194 sits atop the active site Cys-163, which is primed for hydrolysis by intramolecular self-cleavage, a unique self-activation mechanism of caspase-6 (Klaiman et al., 2009; Wang et al., 2010b) that has not been directly observed in any other caspases, likely due to the fact that caspase-6 had a longer intersubunit linker than most other caspases. The H/D exchange of peptide 186–193, which derives from the $^{190}\text{TEVDA}^{194}$ region, significantly increased upon self-cleavage at Asp-193 (Figure 3.5A, and I). This increase in H/D exchanges suggests that the $^{190}\text{TEVDA}^{194}$ site is more exposed in the Asp-193-cleaved form (D23A D179A) compared with the zymogen (FL C163S).

Our data show that initial cleavage at Asp-193 impacts the overall conformational flexibility of caspase-6 substrate binding loops (L1, L2, L4), the regions of the 130's, and 26–32 (Figure 3.5A). In the crystal structure of procaspase-6 zymogen, the side chains of $^{190}\text{TEVDA}^{194}$ occupy the substrate binding pockets S1 to S4 (Figure 3.1A). It is therefore not surprising to observe higher H/D exchange in the L1 region (peptide 56–74) where Arg-64 is engaged as part of the S1 pocket for substrate binding. Likewise, the part of 130's region (peptide 130–142) that sits below the activity site cavity also has higher H/D exchange in the Asp-193-cleaved form compared with the zymogen. The increase in the

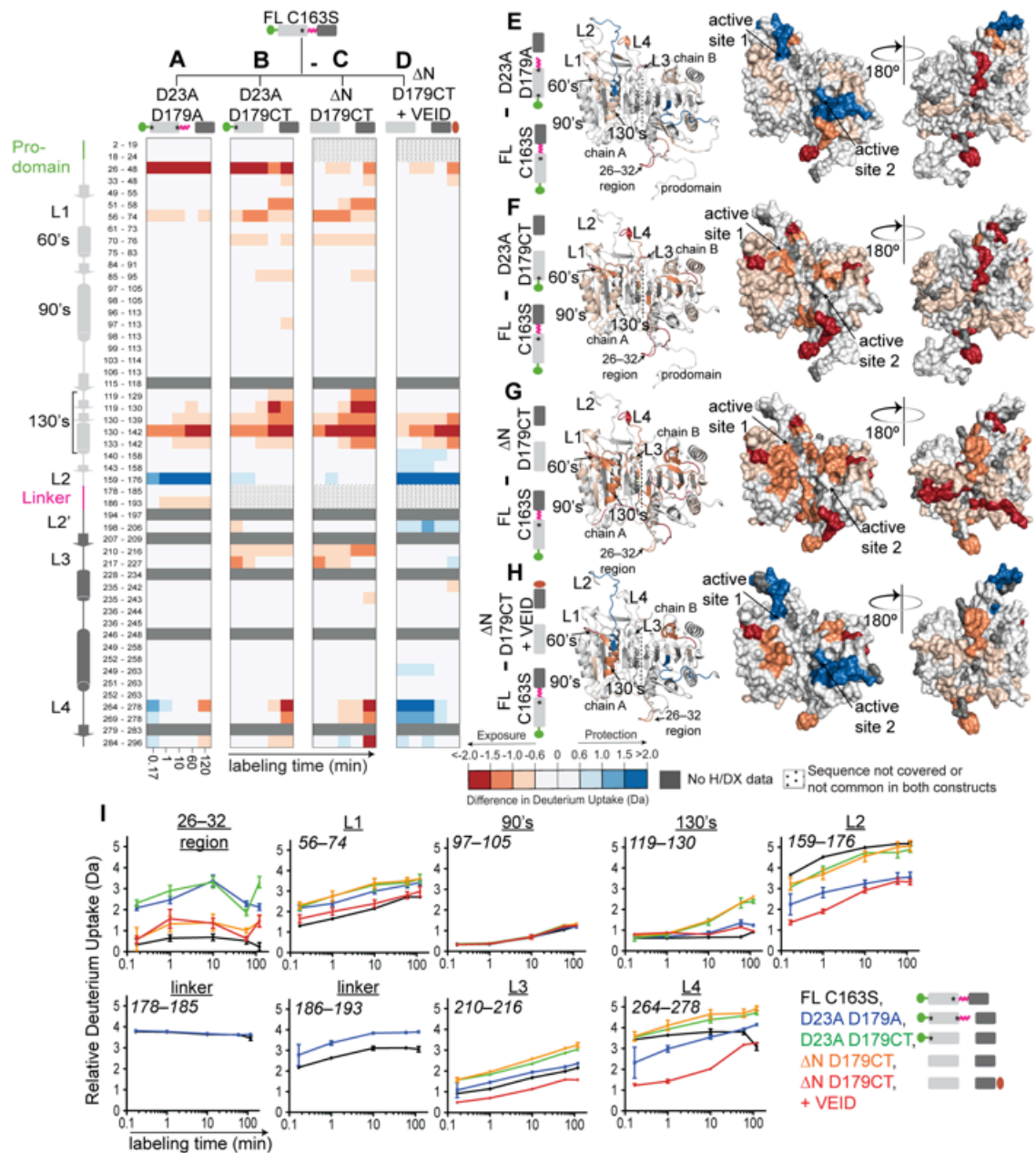


Figure 3.5. Caspase-6 Displays Variable Conformational Flexibility Across States of its Proteolytic Activation.

Differences in deuterium uptake (Da) of the corresponding peptic peptides identified in caspase-6 maturation variants [(A) *D23A D179A*, (B) *D23A D179CT*, (C) ΔN *D179CT*, and (D) ΔN *D179CT* + *VEID*] comparison to the zymogen (FL C163S) at the indicated time points of exposure to deuterated solvent. The residue numbers for each peptic peptide are listed with the corresponding secondary structural elements. These statistically significant differences in the H/D exchange between the caspase-6 maturation variants [(E) *D23A D179A*, (F) *D23A D179CT*, (G) ΔN *D179CT*, and (H) ΔN *D179CT* + *VEID*] and the zymogen (FL C163S) after 2 h incubation were mapped onto the model structure of

caspase-6 shown in both ribbon and surface representations. For these data, a deuterium uptake difference greater than 0.6 Da is considered significant at the 98% confidence interval. The intensities of the *blue* and *red* colors indicate peptides that undergo either a statistically significant decrease (less exchangeable/flexible, blue) or increase (more exchangeable/flexible, red), respectively, during H/D exchange along the path of caspase-6 proteolytic activation. (I) Representative deuterium incorporation plots of key peptic peptides identified in caspase-6 maturation variants covering the regions of 26–32, 90's, 130's, the linker and the substrate-binding loops L1 to L4. The representative MS spectra of the highlighted peptic peptides are shown in supplemental Fig. S3. *Error*, S.D. of duplicate H/DX-MS measurements done on two separate days (see Figures 3.12 and 3.13 for the deuterium uptake plots of all peptides identified).

H/D exchange levels in the L1 and 130's region suggests that these regions are relatively protected in the zymogen state and are being more exposed after initial cleavage at Asp-193 due to an overall increase in the mobility of this region.

L2 in caspase-6 is relatively long compared to L2 in caspase-3 and caspase-7. Substitution of residues in L2 of caspase-6 with L2 residues from caspase-3 and caspase-7 as well as truncation of at least three amino acid residues (170–173) from the *N*-terminus of L2 prevented self-activation of procaspase-6 (Wang et al., 2010b), suggesting that a long L2 is required for binding the sequence $^{190}\text{TEVDA}^{194}$ of the intersubunit linker into the substrate binding groove. This suggests a critical role of L2 in regulating the intramolecular self-cleavage at Asp-193. In terms of conformational dynamics, the L2 region (peptide 159–176) was found to have a significant decrease in H/D exchange upon cleavage at Asp-193 (Figure 3.5A and I). Interestingly, in the crystal structure of the procaspase-6 zymogen, part of L4 (residues 261–271) is flexible and not engaged in binding with $^{190}\text{TEVDA}^{194}$. This same region of L4 is covered

by peptide 264–278 where the H/D exchange profile was slightly perturbed (protected at early time points but exposed after 2 h) upon Asp-193 cleavage. The L4 and the L2—which are located on the same face of the protein—were the only regions of caspase-6 that experienced significant protection upon Asp-193 cleavage. The L2 peptide 159–176 and the L4 peptide 264–278 show charge complementarity: part of L2 is negatively charged and part of L4 is positively charged (Fig S3). The result that both L2 and L4 regions

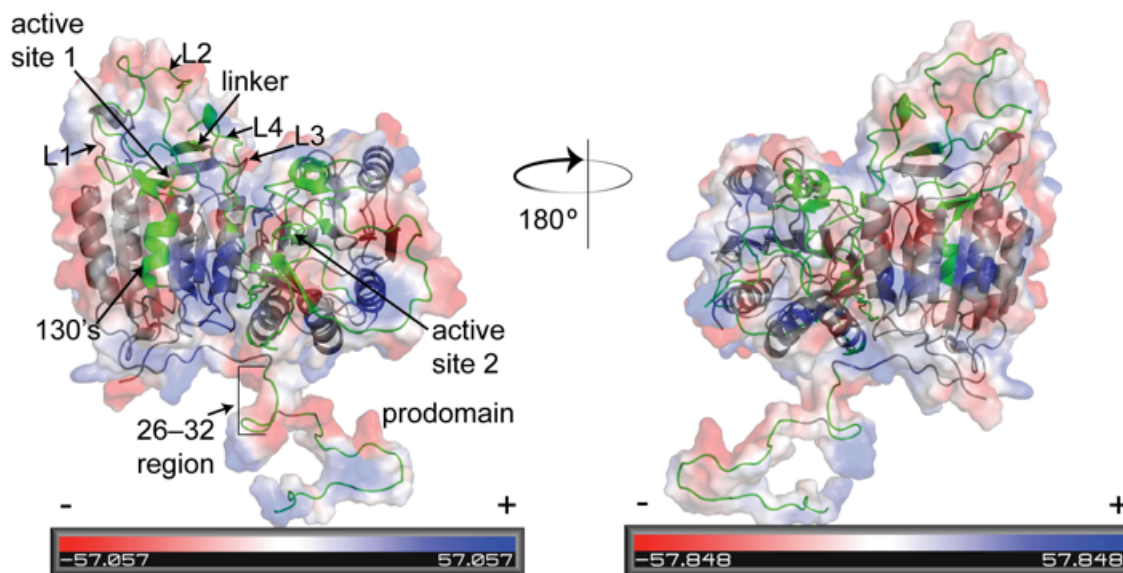


Figure 3.6. Map of the Electrostatic Potential of the Model Structure of Procaspase-6 Built from the Zymogen Crystal Structures (PDB code 4iyf and PDB code 3NR2)

The missing residues of each PDB template structures were built by *de novo* modeling using Chimera/Modeller platform. The electrostatic potential map (*red*, acidic regions; *blue*, basic regions; *white*, hydrophobic/neutral regions) was generated using PyMOL Molecular Graphics System (Schrödinger, LLC). Highlighted are key regions of in caspase-6 that undergoes statically significant changes in the H/D exchange along caspase-6 proteolytic activation.

experienced protection from H/D exchange and exhibits charged complementarity to each other suggests that L2 and L4 are interacting after self-activation of caspase-6 at Asp-193, potentially initiating loop reorganization for proper substrate binding.

Finally, it is interesting that self-activation at Asp-193 resulted in a statistically significant increase in H/D exchange of the 26–32 region after subtractive analysis of overlapping peptides 26–48 and 33–48 (Figure 3.5A, E and I). This suggests that the 26–32 region is relatively protected in the zymogen and is exposed after initial self-cleavage at Asp-193. This region immediately follows the prodomain in sequence. Intriguingly, the 26–32 region is situated in the same loop as one of the residues (K36) in the allosteric and regulatory site for zinc binding in caspase-6 (Velazquez-Delgado and Hardy, 2012) and the identified exosite in caspase-7 (³⁸KKKK⁴¹) that promotes efficient cleavage of poly(ADP ribose) polymerase 1 substrate (Boucher et al., 2012). These data collectively suggest that the initial intramolecular cleavage at Asp-193 impacts the overall flexibility of caspase-6 in the context of the proper assembly of structural elements that enables caspase-6 activation and regulation.

3.3.3 Complete Removal of the Linker is Important to Attain the Fully Exposed Substrate-Binding Cavity

The linker region contains two proteolytic cleavage sites within the regulatory L2 in caspase-6. In the zymogen structure of procaspase-6, part of this region (residues 186–193) is ordered and accommodated in the substrate-

binding groove and the rest of the linker residues are disordered (Wang et al., 2010b). After initial intramolecular self-cleavage at Asp-193 (D23A D179A), caspase-6 can exist in a state where the linker is still attached to the large subunit with the intact $^{176}\text{DVVD}^{179}$ site. This Asp-179 is not a good substrate for intramolecular cleavage by caspase-6 because the ISL is not long enough to position Asp-179 for self cleavage (Wang et al., 2010b). However, Asp-179 is the first site to be intermolecularly cleaved by caspase-3 (Srinivasula et al., 1998; Wang et al., 2010b) and other caspases intermolecularly. A crystal structure of cleaved caspase-6 with intact linker was solved but the electron density of the entire linker region (180–193) was missing. Thus, the structural behavior of the linker and its impact on the dynamics during caspase-6 activation are still unexplored. In this H/DX-MS study, 100% of the linker region was covered by peptides 178–185 and 186–193 (Figure 3.5A, B, and I). The significant increase in the H/D exchange of the C-terminal part of the linker region (186–193) between the zymogen and the Asp-cleaved form suggests that prior to cleavage at Asp-193 in the zymogen form, the region of the 186–193 is bound to the substrate binding groove—consistent with the crystal structure of procaspase-6 zymogen. However, the exchange profile of the 178–185 region between the zymogen and Asp-cleaved form was unaffected, suggesting that this region, a contiguous part of L2, has the same conformational flexibility in both the zymogen and Asp-193 cleaved form. The shape of the curve for deuterium incorporation over the time course of H/D exchange often reveals interesting structural features for particular regions of the protein, and provides meaningful

interpretation of the H/D exchange data as has been described elsewhere (Morgan and Engen, 2009). The H/D exchange profile of peptide 178–185 in both the zymogen and the Asp-193-cleaved form showed a nearly maximal uptake of deuterium even at the earliest time point (10s) and remained at that same high level throughout the H/D exchange experiment (Figure 3.5I). This deuterium uptake profile suggests that the 178-185 region has high solvent exposure and the absence of H-bond interactions, as is characteristic for unstructured regions. Conversely, peptide 185–193 exchange parameters suggest a partially protected, moderately dynamic region. Peptide 185–193 showed a one-deuterium difference between the zymogen and Asp-193 self-cleaved forms at the earliest time point (10s), suggesting that this region is more exposed after Asp-193 cleavage. This one-deuterium difference persisted throughout the H/D exchange time course (Figure 3.5I). In the crystal structure of the zymogen, the $^{190}\text{TEVDA}^{194}$ cleavage site is folded as a β -strand, which rests in the substrate-binding groove and is expected to be highly protected from H/D exchange. The fact that the 185-193 peptide in the Asp-193 cleaved form of caspase-6 shows less protection than in the zymogen suggests that only prior to zymogen activation does the intersubunit linker remains stably bound to the active site.

Further along the activation pathway of caspase-6, the complete removal of the intersubunit linker occurs when Asp-179 is cleaved (D23A D179CT or Δ ND179CT). Removal of the linker resulted to a global H/D exchange profile that is significantly altered compared with the zymogen (Figure 3.5B, C, F, G). Removal of the intersubunit linker resulted in a significant exposure—relative to

the zymogen—of the regions in the substrate binding loops: L1 (peptide 56–74), L2 (peptide 159–176), L3 (peptides 210–216 and 217–227) and L4 (peptides 264–278 and 269–278) and the 130's region (peptides 119–130, 130–142, and 133–142). Moreover, the differences in the H/D exchange between cleaved forms of caspase-6 in the absence or presence of the linker showed a similar trend where removal of the linker resulted in a statistically significant increase in the H/D exchange in the substrate binding loops and the top of the 130's region (Figure 3.7A and B). Collectively, these data suggest that the removal of the linker renders the substrate-binding groove fully exposed and competent to bind substrate.

Once the substrate-binding groove is exposed, substrate can bind to the fully cleaved, mature caspase-6 (Δ ND179CT + VEID). The H/D exchange profiles of the loop bundles (L1–L4) and the top of the 130's region (peptide 119–130) were significantly decreased relative to the zymogen upon substrate binding (Figure 3.5D, H and I). This suggests that these regions undergo significant structural reorganization and protection upon engaging substrate, resulting to a lower conformational flexibility of these regions.

3.3.4 Substrate-binding Groove is Accessible in Cleaved Caspase-6, Independent of the Presence of the Prodomain or Linker

The H/DX data show that the overall accessibility of the substrate-binding groove increases even further as caspase-6 matures into its substrate-binding competent state. To further explore this observation, we sought a complementary

technique to interrogate the conformation of the substrate-binding groove before and after substrate binding. Caspase-6 has only two tryptophan residues, which are found in L1 (Trp-57) and L3 (Trp-227) (Figure 3.8A). Trp-57 is completely exposed in crystal structures of both the zymogen and mature forms of caspase-6. However, in the zymogen, Trp-227 sits immediately adjacent to the substrate-binding groove as part of the S4 specificity pocket within L3 (Figure 3.1B), which forms an antiparallel β -strand with the linker in the zymogen state. Intrinsic tryptophan fluorescence is influenced by the polarity of the environment, where shifts in the emission maxima towards longer wavelengths (red shift) indicate higher solvent exposure. All maturation variants of caspase-6—from its zymogen to self-cleavage at Asp-193 and subsequent removal of the prodomain and linker—were subjected to intrinsic fluorescence measurements (Figure 3.8B and Fig S5). Notably, all caspase-6 cleavage variants clustered in two classes of emission spectra where all linker-cleaved (singly cleaved or complete removal of the linker) forms of caspase-6 showed a 9nm red shift towards a more solvent exposed state relative to the zymogen, irrespective of the presence of the prodomain (Figure 3.8B). This suggests that initial Asp-193 cleavage in the linker leads to the relative exposure of the bound intersubunit linker. Thus, Asp-193 cleavage activates caspase-6 by generating an open and more dynamic, substrate-binding competent active site.

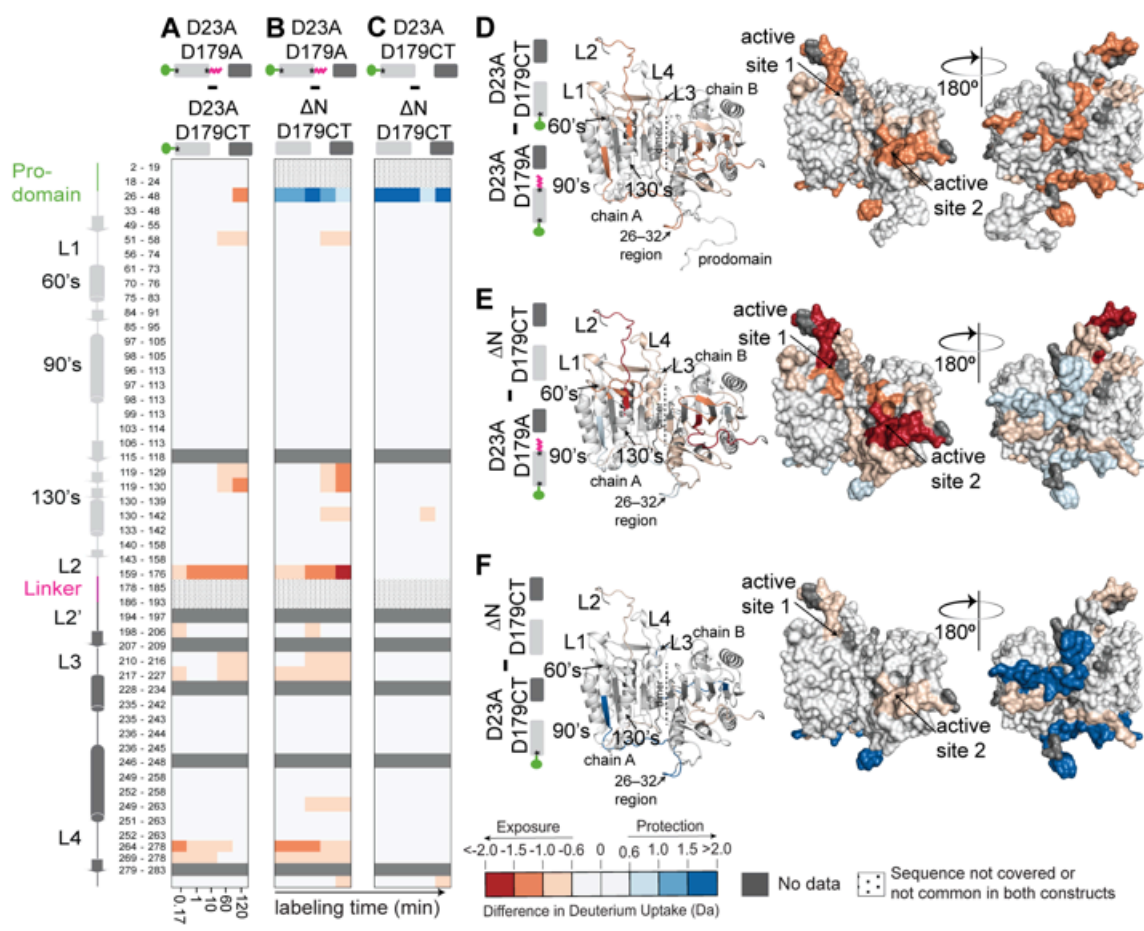


Figure 3.7 Intersubunit Linker Cleavage Increases Conformational Flexibility of All Substrate-Binding Loops

Comparative differences in the H/D exchange profiles among cleaved caspase-6 maturation variants [(A) *D23A D179A* versus *D23A D179CT*, (B) *D23A D179A* versus ΔN *D179CT*, and (C) *D23A D179CT* versus ΔN *D179CT*] at the indicated time points of exposure to deuterated solvent. These statistically significant differences in the H/D exchange among cleaved caspase-6 maturation variants [(E) *D23A D179A* versus *D23A D179CT*, (F) *D23A D179A* versus ΔN *D179CT*, and (G) *D23A D179CT* versus ΔN *D179CT*] after 2 h incubation were mapped onto the model structure of caspase-6 shown in both ribbon and surface representations. For these data, a deuterium uptake difference greater than 0.6 Da is considered significant at the 98% confidence interval. The intensities of the *blue* and *red* colors represent the peptides that undergo either a statistically significant decrease (less exchangeable/flexible, blue) or increase (more exchangeable/flexible, red), respectively, in the H/D exchange along the path of caspase-6 proteolytic activation.

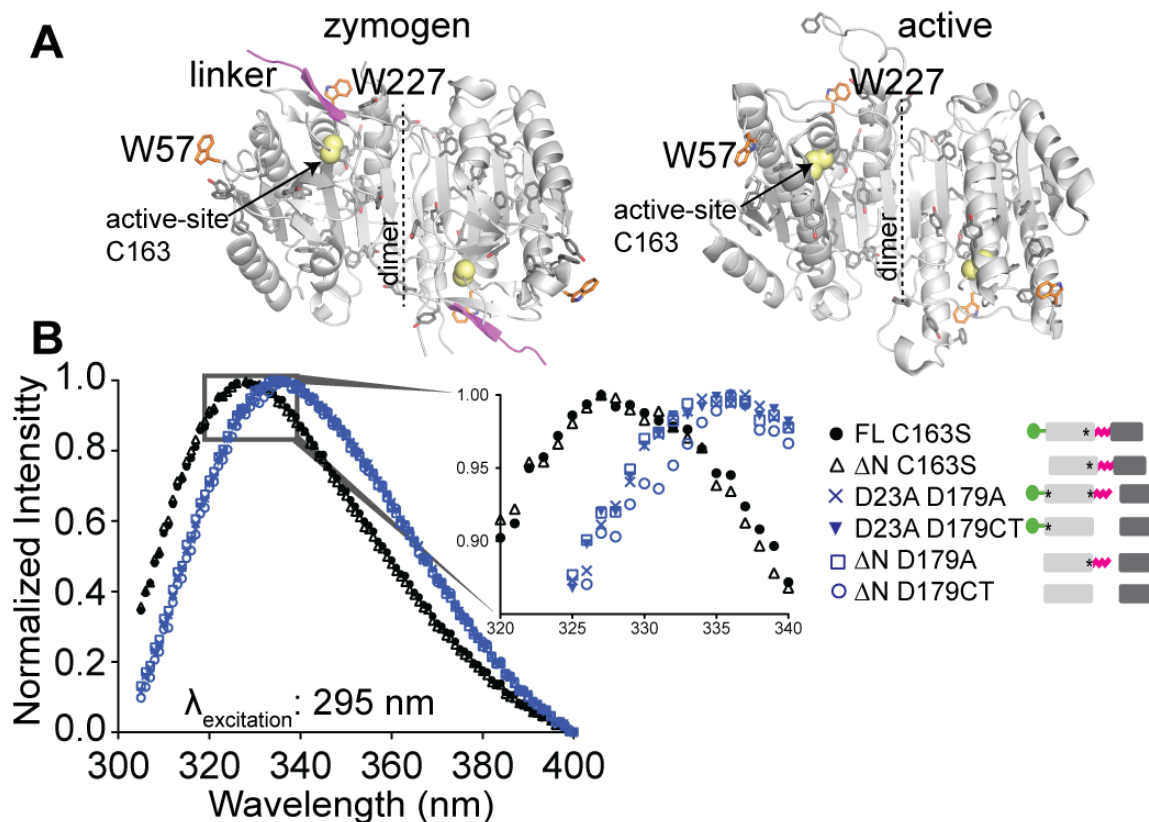


Figure 3.8 Intersubunit Linker Cleavage Leads to Increased Exposure of the Substrate-Binding Groove

(A) Comparison of the crystal structures of procaspase-6 zymogen (PDB code 3NR2) (*left*) and mature, unliganded caspase-6 (PDB 2WDP) (*right*) highlighting the only two tryptophan residues, Trp-57 and Trp-227, as well as the relative location of the intersubunit linker (*magenta*) and the active-site Cys-163. (B) The intrinsic tryptophan fluorescence profiles of caspase-6 mutation variants. Fluorescence emission scan of 305–400 nm were collected after excitation at 295 nm of 3- μM proteins in 10 mM phosphate buffer, pH 7.5, 120 mM NaCl and 2 mM DTT. Data presented here are a representative from three independent experiments (see Figure 3.13 for the λ_{ex} 280nm).

3.3.5 The Prodomain is Intrinsically Disordered

An attempt to solve the crystal structure of procaspase-6 zymogen with intact prodomain has been reported (Cao et al., 2014) but no electron density for the prodomain was visible, suggesting that the prodomain may be a mobile region. Although both biological (Klaiman et al., 2009) and biochemical studies (Cao et al., 2014; Cowling and Downward, 2002) revealed that the prodomain impacts caspase-6 function, the existing structural data on the prodomain are extremely limited. In this work, the structural properties of the prodomain were explored using H/DX-MS, as well as its impact on the dynamics of caspase-6 during proteolytic activation. The electrostatic potential map of the 23-amino acid prodomain of caspase-6 showed an obvious charged-polarized region (Figure 3.9A). The N- and C- termini are packed with positively and negatively charged residues, respectively. H/DX-MS studies covered 22 of the 23 amino acids of the prodomain represented by five overlapping peptic peptides (2-19, 3-19, 5-19, 8-19 and 18-24) (Figure 3.2, Figure 3, Figure 3.7, Figure 3.15, and Figure 3.16). The H/D exchange profile of the prodomain region showed no statistically significant changes between the zymogen and the cleaved forms of caspase-6 irrespective of the presence or absence of the linker (Figure 3A, 3B, and 6B). Likewise, the H/D exchange profile of the prodomain region showed no statistically significant changes between cleaved forms of caspase-6 with or without the linker (Figure 3.7A and 6B). The H/D exchange profiles of peptides in both the zymogen and cleaved forms of caspase-6 with intact prodomain (Figure 3.9B) showed nearly maximal uptake of deuterium by the earliest time point,

which persisted at that same level over the course of the H/D exchange experiment. The corresponding MS spectra of prodomain peptides in all forms of caspase-6 with intact prodomain of caspase-6 with intact prodomain showed a well-defined isotopic distribution (Figure 3.9C). Collectively, these data suggest that independent of the activation state of caspase-6, the prodomain is highly solvent exposed, consistent with this region being unstructured or intrinsically disordered. Subtractive analysis of the H/D exchange profiles of the cleaved caspase-6 variants (with intact prodomain but with or without the linker) and the fully cleaved, mature caspase-6 (Figure 3.7B and C) revealed statistically significant decrease in the deuterium uptake at positions 26–32 after cleavage at Asp-23. This suggests that the removal of the prodomain results in protection of the 26–32 region from H/D exchange in solution. Similar to the prodomain, the 26–32 region is polarized in terms of its electrostatic potential (Figure 3.6). The negatively charged C-terminal end of the prodomain is likely to repel the negatively charged N-terminal portion of the 26–32 region. Once the prodomain is removed, the 26–32 region folds upon itself as evidenced by the decrease in the H/D exchange upon removal of the prodomain in the absence of any significant changes in the H/D exchange to the rest of the region of caspase-6 (Figure 3.7C). The full sequence of caspase-6 was analyzed for protein disorder using DISOPRED (Webb and Sali, 2014) (Figure 3.9D). Regions of the prodomain and the linker were predicted to be in highly disordered state and further categorized these regions as being involved in protein binding. In addition, CD spectra of caspase-6 with or without the prodomain (Figure 3.9E) showed no

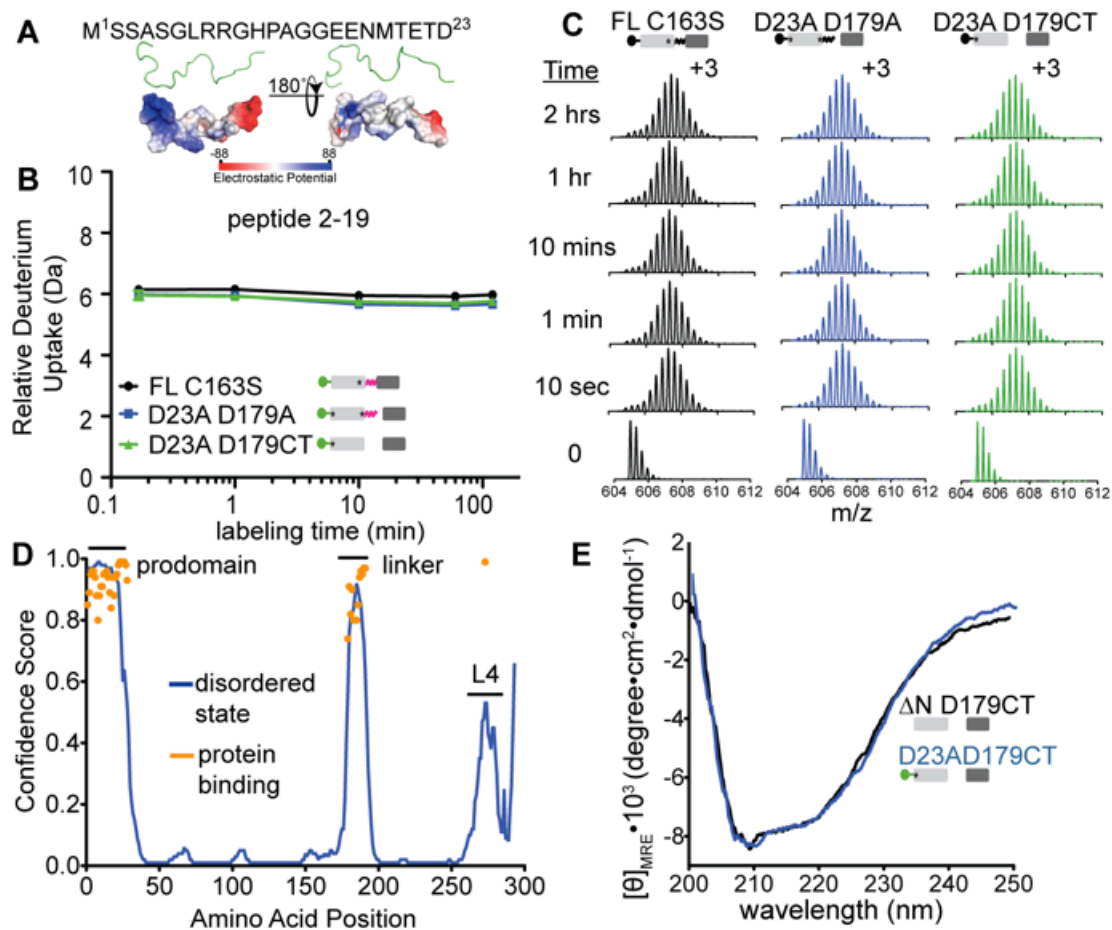


Figure 3.9. The Prodomain is Intrinsically Disordered

(A) An electrostatic potential map of the procaspase-6 prodomain with its corresponding amino acid sequence. The *blue* and *red* regions represent the relative localization of the positive and negative potentials, respectively. (B) The deuterium uptake profile of a representative peptic peptide (2–19) in the prodomain identified in the prodomain-containing caspase-6 maturation variants. *Error*, S.D. of duplicate H/DX-MS measurements done on two separate days. (C) The corresponding MS spectra of peptide 2–19 presented in (B). (D) Prediction of the disordered (*blue*) and protein binding (*orange*) regions of caspase-6 using DISOPRED server. (E) CD spectra of cleaved caspase-6 with (D23A D179CT) and without (ΔN D179CT) the prodomain.

dramatic changes in the secondary structures of caspase-6, consistent with the prodomain being in a disordered state. In addition, the intrinsic tryptophan fluorescence profile of both procaspase-6 zymogen and cleaved forms with or without the prodomain (Figure 3.8B) were superimposable, suggesting that the prodomain does not impact the Trp-227 environment near the active site. Altogether, the H/DX-MS and the biophysical measurements imply that the prodomain is an unstructured region of caspase-6, which does not form any stable contacts with neither the active site nor the caspase-6 core at any point during the course of caspase-6 proteolytic maturation.

3.4 Discussion

The H/DX reported here has allowed us to follow the diverse conformational changes that occur in caspase-6 as it progresses through the zymogen maturation pathway (Figure 3.10). These data are the first to provide insight on the prodomain and intersubunit linker of caspase-6 as these regions have been absent in all crystal structures of the enzyme. The initial intramolecular cleavage of the zymogen at Asp-193 in the linker resulted in changes in the conformational dynamics of the substrate binding loops L1 to L4, the 130's and the 26–32 regions. Moreover, the cleavage at Asp-193 also allowed region of L2 to engage with L4. Further along the proteolytic activation pathway, removal of the linker increases the conformational flexibility of all substrate binding loops, and the 130's region. Upon substrate binding, all substrate-binding loops are engaged to accommodate the substrate, including

the top of the 130's region. Importantly, the prodomain is found to be intrinsically disordered independent of the activation state of caspase-6, i.e. zymogen or Asp-193 self-cleaved form. However, the prodomain impacts the conformational flexibility of the 26–32 region dependent on the proteolytic activation state of caspase-6.

The changes in the dynamics of caspase-6 reported here reflect with previously reported changes in the thermal stability profile of maturation variants of caspase-6 (Vaidya et al., 2011). The zymogen was found to be the least stable form of caspase-6 with at least 8°C lower in the apparent melting temperature compared to its cleaved forms. The Asp-193 self-cleaved form (with intact prodomain and linker) is the most stable form of caspase-6 while the fully cleaved and mature form has intermediate stability between the zymogen and the Asp-193 self-cleaved caspase-6. The dramatic gain in the apparent thermal stability of the zymogen after the initial intramolecular self-cleavage at Asp-193 could likely be accounted as the outcome of the changes in the conformational dynamics of caspase-6. In particular, we observed a stabilizing interaction of L2 and L4 promoted by the presence of the prodomain and Asp-193-cleaved linker. Previous work on a proteome-wide thermal stability studies across various cell types from *E. coli* to mammalian cells showed a direct association between protein stability and intracellular abundance and an inverse relationship between protein stability and aggregation (Leuenberger et al., 2017). Thus, the gain of stability as a consequence of altered conformational dynamics during proteolytic

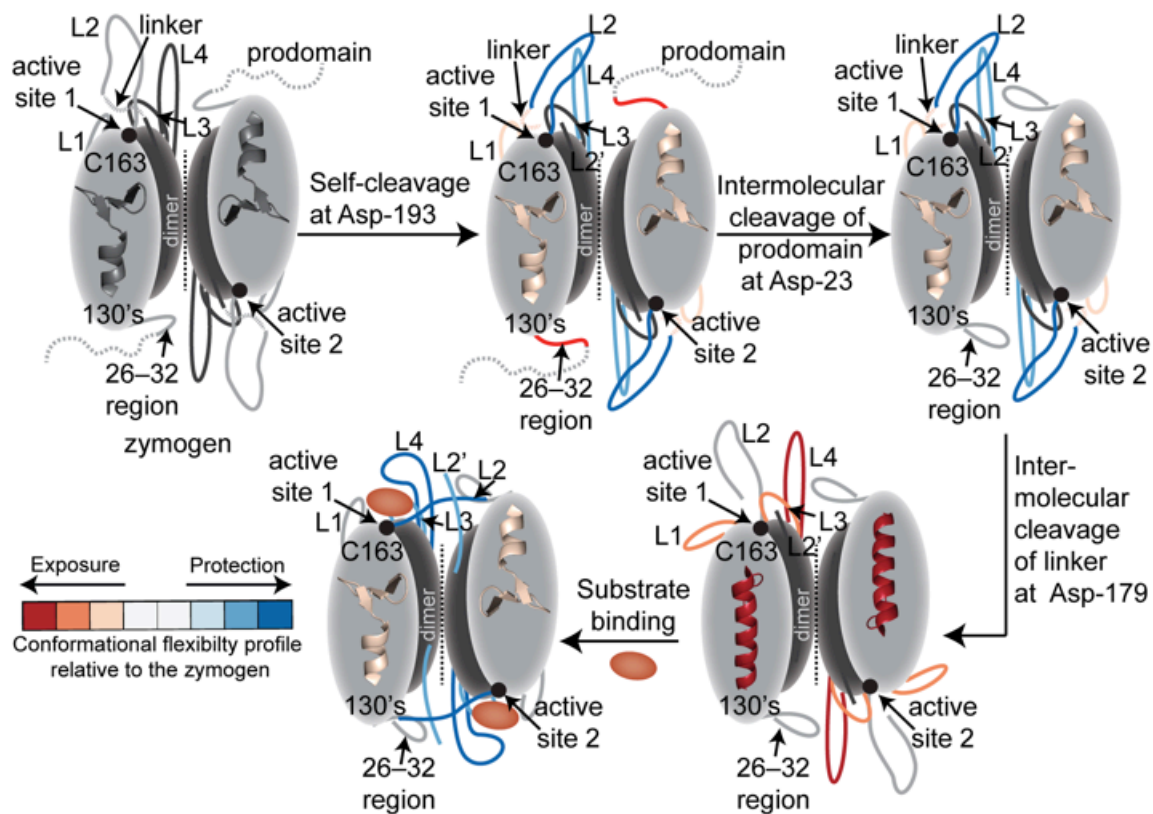


Figure 3.10. A Schematic Model Highlighting the Changes in the Conformational Flexibility of Caspase-6 Along its Path to Proteolytic Maturation

Initial intramolecular self-cleavage of the procaspase-6 zymogen at Asp-193 in the intersubunit linker results to significant exposure of the linker, the 130's, the 26–32 region, and the substrate binding loop 1 (L1) whereas L2 and L4 are engaged in a stabilizing interaction. The subsequent intermolecular cleavage of the prodomain at Asp-23 results in the protection of the 26–32 region. The complete removal of the linker upon intermolecular cleavage at the Asp-179 site results to more exposure of regions in the 130's and all the substrate binding loops 1 to 4. And upon substrate binding (*red* ellipsoid), the 130's and the substrate-binding loops 1 to 4 become protected to engage the substrate in the active site cavity. The intensities of the *red* and *blue* colors represent the exposure or protection, respectively, relative to the conformational flexibility of the procaspase-6 zymogen.

activation in caspase-6 may be relevant to the lifetime of the protein in the cell and its interaction with the proteasome for degradation. Crystal structures of the mature unliganded caspase-6 showed that prior to substrate binding, the 130's region can exist in either the canonical (strand) (Muller et al., 2011) or noncanonical (helical) (Baumgartner et al., 2009; Vaidya et al., 2011) conformations. Mature caspase-6 exists exclusively in the canonical (strand) conformation in all substrate-bound structures—a unique structural feature not observed in any other caspases. We have recently reported H/DX-MS coupled with molecular dynamics simulations which shows that the 130's region of the mature unliganded caspase-6 is in constant interconversion between the helical and strand conformations prior to substrate binding and converts completely to the strand conformation after substrate binding (Dagbay et al., 2017). H/DX-MS results presented here show that the presence of the linker affects slow H/D exchange in the 130's region in caspase-6 (Figure 3I). At long time points, the H/D exchange profile of the Asp-193 cleaved caspase-6 with intact linker was similar to the canonical (strand) caspase-6 forms: the zymogen and substrate-bound caspase-6; however, it is distinct from the H/D exchange profile of the mature unliganded caspase-6 irrespective of the presence of the prodomain. Thus, these data suggest that the presence of the linker promotes a higher fractional residence in the canonical (strand) conformation of caspase-6. This dynamic conformational state of caspase-6 may represent one of the conformational ensembles that enable fine-tuning of pathways in the cell leading to caspase-6 activation.

Although the biological consequences of the dynamic nature of the 130's region are still unknown, there have been previous cell-based studies that reported the relative activity of the maturation state variants of caspase-6. Each maturation state variant showed unique *in vivo* activity in HEK293T cells (Klaiman et al., 2009) suggesting that each cleavage state of caspase-6 may play unique functional roles in cells. These differences in cellular activity are certainly related to the dynamics changes observed in this study. In addition, the caspase-6 intersubunit linker is long relative to the other executioners, caspase-3 and -7, and is the only linker computationally classified to contain a protein binding motif (Figure 3.9D and Figure 14). This insinuates the linker as potentially playing a role in substrate selection and specificity as well as in the several protein-protein interactions in which caspase-6 has been identified to participate (Jung et al., 2014; Riechers et al., 2016).

In this work, we present several lines of evidence that the prodomain in caspase-6 is intrinsically disordered in all activation states. In addition, the crystal structure of procaspase-6 zymogen with an intact prodomain showed no visible electron density for the prodomain region (Cao et al., 2014). In this work, the prodomain of caspase-6 was computationally predicted to be both disordered and a protein-binding region. Consistent with these observations, H/DX-MS covered the region of the prodomain with H/D exchange profile suggested that the prodomain is an unstructured or intrinsically disordered region. In general, disordered regions of proteins are often involved in molecular recognition (for a review see (Mittag et al., 2010)). It is thought that several metastable

conformations of proteins with disordered binding sites enable recognition of molecular targets with remarkable specificity and low affinity. Intriguingly, the presence of the prodomain in cleaved caspase-6 is dispensable for caspase-6 activity *in vitro* against peptide substrates, but has been reported to impact caspase-6 activity intracellularly (Klaiman et al., 2009). This may indicate that the prodomain binds proteins, potentially substrates or regulatory partners. The caspase-6 prodomain has also been implicated in limiting self-activation through intermolecular cleavage at Asp-193 at low protein concentrations *in vitro* (Cao et al., 2014). Despite growing evidence of the roles of the prodomain in regulating caspase-6 activity, its biological role remains poorly understood, however our characterization as an intrinsically disordered protein might provide the insight needed to further the elucidation of prodomain roles.

The prodomains of caspase-3 and -7 are also predicted to be intrinsically disordered (Figure 14) and the prodomains of several caspases have been reported to participate in protein-protein interactions (Boucher et al., 2012; Choi et al., 2009; Voss et al., 2007; Yaoita, 2002), impacting enzyme activity and apoptotic signal transduction, as well as mediating binding to molecular chaperones, cellular localization and substrate selection. Caspase prodomains also appear to be “hot spots” for regulatory post-translational modifications (Eron et al., 2017; Martin et al., 2008; Nutt et al., 2005) modulating enzyme activity and binding to initiator caspases resulting in decreased apoptosis, as well as impacting proteasomal degradation. The prodomain also mediates folding of procaspase-3 (Feeney and Clark, 2005). The prodomain is one of the least

conserved regions of the caspase family (Clark, 2016; Vaidya et al., 2011) so it is possible or even likely that each prodomain plays unique roles that have yet to be fully uncovered.

The exchangeability of the 26–32 region, which is immediately adjacent to the prodomain, changes in unforeseen ways as caspase-6 progresses along the proteolytic activation pathway. Initial self-cleavage at Asp-193 of the zymogen results in increased exposure of the 26–32 region, suggesting that an interaction of the 26-32 region, which is present in the zymogen, is lost upon initial cleavage. However, once caspase-6 fully matures by proteolytic cleavage of the prodomain and linker, the 26–32 region exhibits a less flexible conformation similar to the zymogen state. This finding may be relevant to fine-tuning caspase-6 activity that stems from diverse conformational flexibility profile of caspase-6 along its pathway to full maturation. Notably, the 26–32 region is located in close proximity to Lys-36, one of the ligands in the allosteric site for zinc binding identified in caspase-6 (Velazquez-Delgado and Hardy, 2012). Moreover, this region is also positioned in the same loop as two regulatory sites in caspase-7. PAK2 mediated phosphorylation of Ser-30 in this region prevents caspase-7 activation by caspase-9 (Eron et al., 2017)The ³⁸KKKK site within the caspase-7 N-terminal domain is an exosite used for substrate selection and is the only identified exosite in any caspase. The differential conformational flexibility of the 26–32 region could potentially expose or protect key regulatory sites in caspases. For example, the differential exposure or protection of the 26–32 region in various activation states may explain differential substrate recruitment that has been

observed intracellularly (Klaiman et al., 2009). While it is exciting to observe enzymatic differences in the cellular context, we recognize that insights into the molecular mechanisms can only be accomplished by *in vitro* investigation such as those included in this work.

In summary, H/DX-MS revealed the distinct conformational dynamics in critical regions of the caspase-6 structure, including regions like the prodomain and intersubunit linker, which have not been observable by any other techniques. At each stage along the proteolytic activation pathway, changes in distinct regions of caspase-6 have been observed. These changes are confined in all substrate-binding loops, the 130's and 26–32 region. We anticipate that many of these changes would also be relevant in the activation pathways of other caspases. In addition, we have observed that the prodomain is intrinsically disordered. The structural dynamic changes provided in this study afforded new insights into the underlying molecular mechanism of caspase-6 activation and regulation. Caspase-6 is implicated in neurological disorders including Alzheimer's, Huntington's and Parkinson's diseases. The structural features and conformational changes described here may inspire new approaches for manipulating caspase-6 in the context of neurodegeneration.

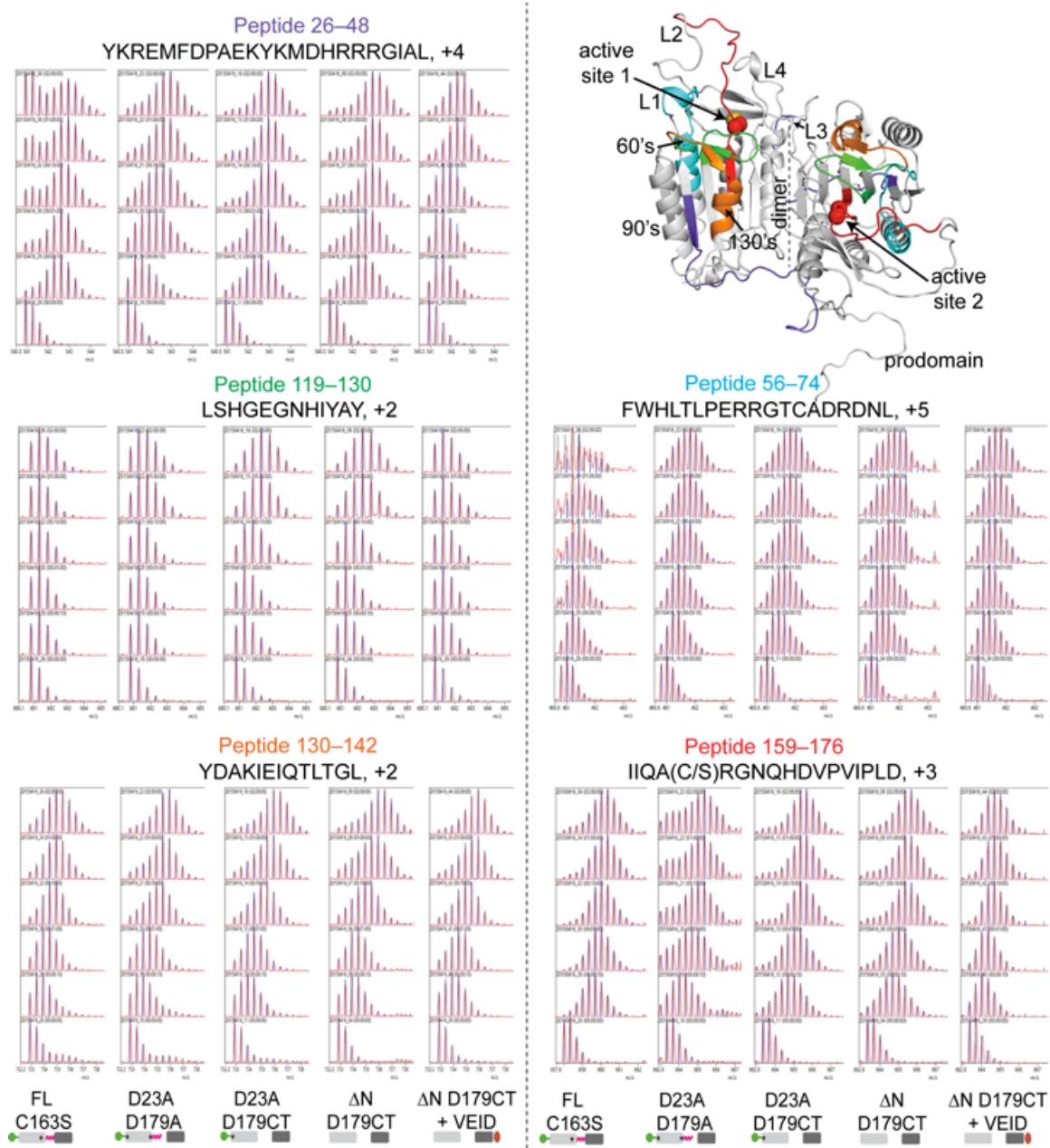


Figure 3.11. Representative MS Spectra of Key Peptic Peptides Following H/D Exchange Experiments of Caspase-6 Maturation Variants

The relative location of the highlighted peptic peptides for the following regions are mapped onto the hybrid model of procaspase-6: peptide including the 26–32 region, *purple blue*; top of 130's region, *green*; 130's region, *orange*; part of L1, *cyan*; L2, *red*. The amino acid sequence, the MS charge state distribution and the residue numbers covered by the representative peptic peptide are also indicated. (B) The relative location and charge state distribution of peptides from additional highlighted regions: L3, *yellow*; L4, *light pink*; N-terminal part of linker, *blue*; C-terminal part of linker, *magenta*).

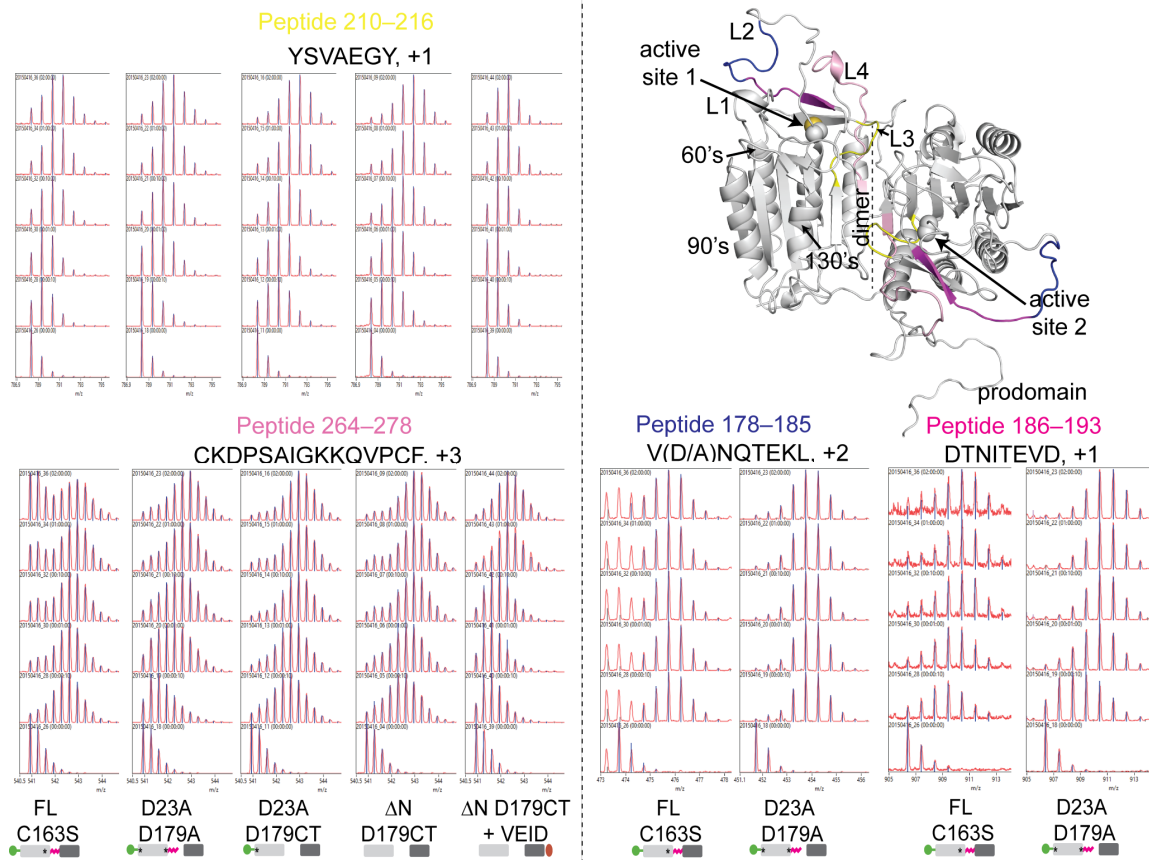


Figure 3.12. Additional Representative MS spectra of Key Peptic Peptides Following H/D Exchange Experiments of Caspase-6 Maturation Variants

The relative location of the highlighted peptic peptides for the following regions are mapped onto the hybrid model of procaspase-6: peptide including the 26–32 region, *purple blue*; top of 130's region, *green*; 130's region, *orange*; part of L1, *cyan*; L2, *red*. The amino acid sequence, the MS charge state distribution and the residue numbers covered by the representative peptic peptide are also indicated. (B) The relative location and charge state distribution of peptides from additional highlighted regions: L3, *yellow*; L4, *light pink*; N-terminal part of linker, *blue*; C-terminal part of linker, *magenta*).

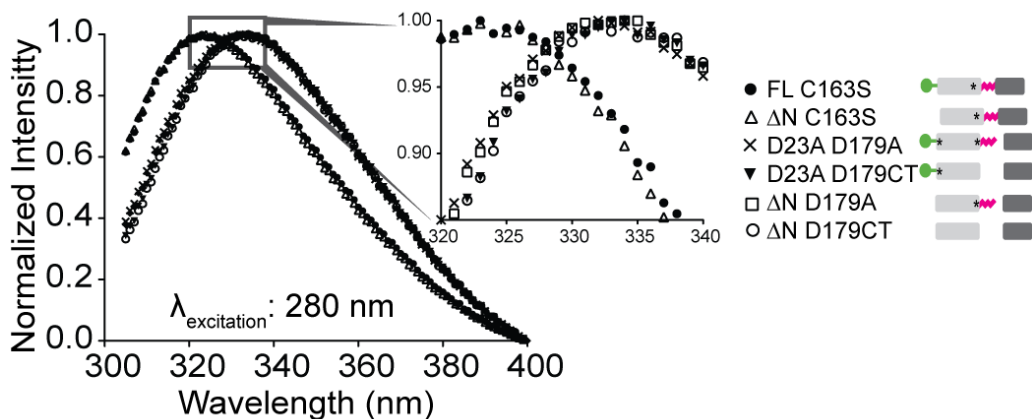


Figure 3.13 Intrinsic Fluorescence Profile of Caspase-6 Maturation Variants Excited at 280 nm

Fluorescence emission scan from 305–400 nm were collected after excitation at 280 nm of proteins (3 μ M) in 10 mM phosphate buffer, pH 7.5, 120 mM NaCl and 2 mM DTT. Data presented here are representative of three independent experiments.

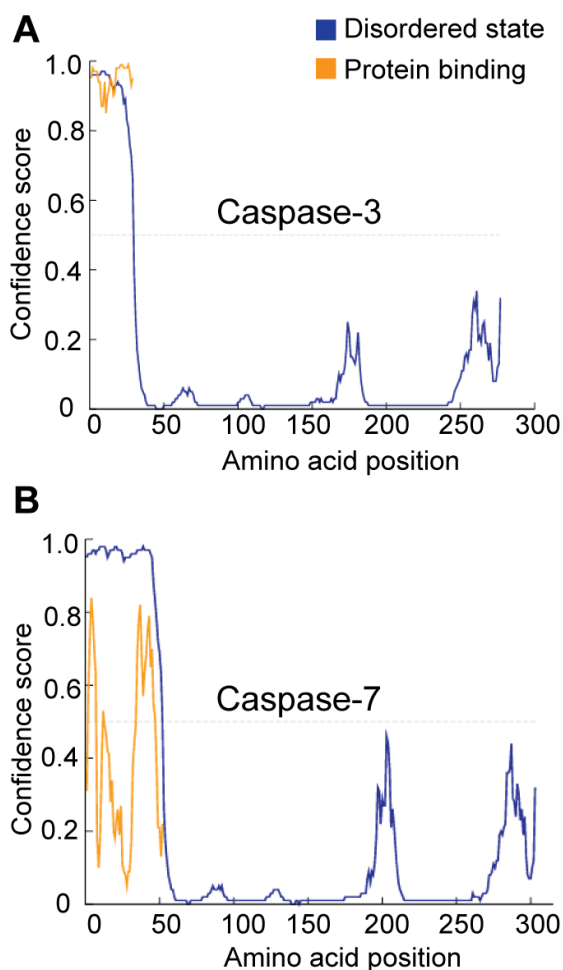


Figure 3.14 Prediction of Disorder and Protein Binding in Caspases

Amino sequence of caspases-3 (A) and caspase-7 (B) were submitted to the DISOPRED server for the prediction of regions of the protein that are disordered (*blue* line) as well as possible motifs for protein binding (*orange* lines).

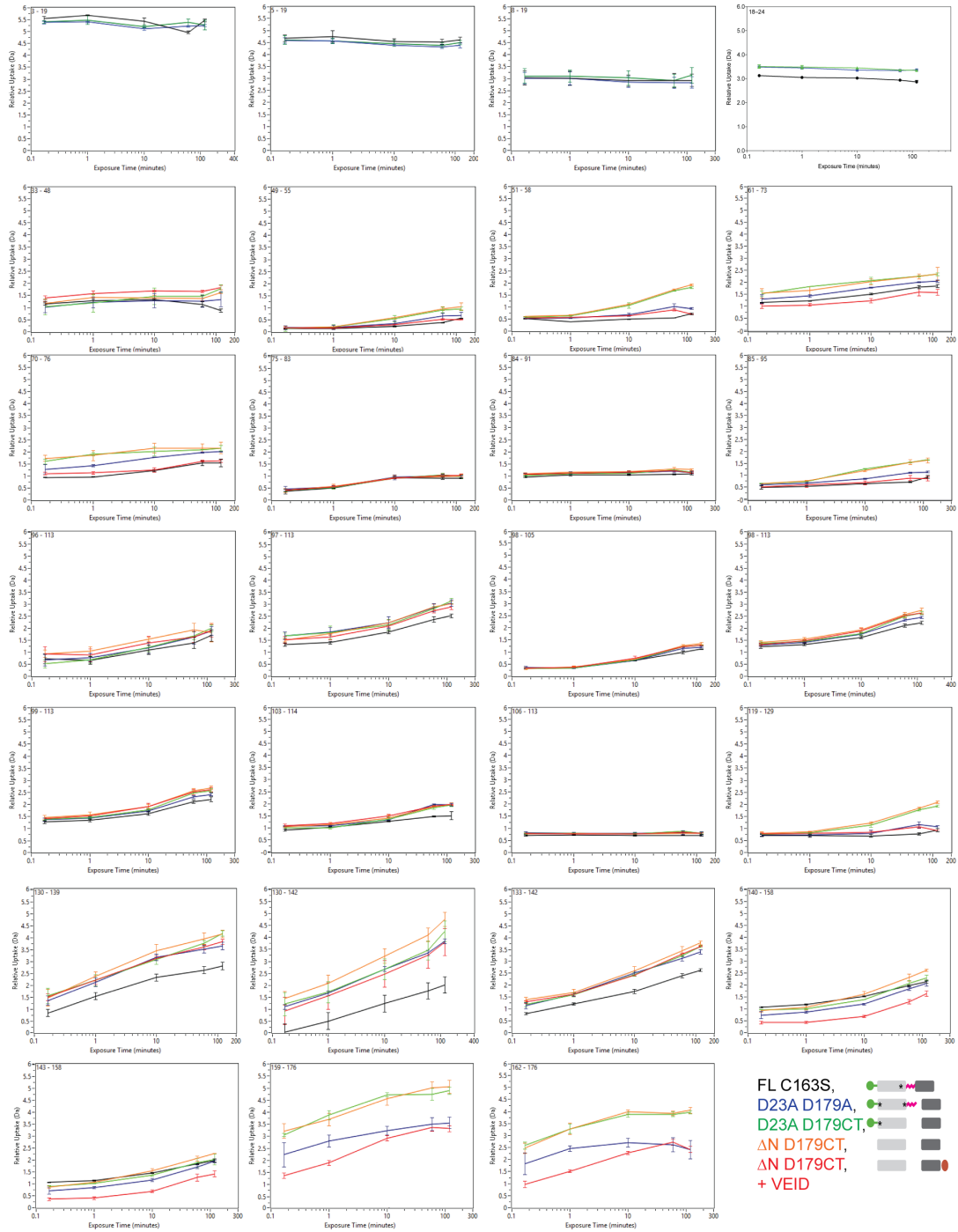


Figure 3.15. Relative Deuterium Uptake Plots of Caspase-6 Maturation Variants Over the Course of the H/D Exchange Experiment

The different colors represent the deuterium uptake profile of caspase-6 mutation variants FL C163S (*black*), D23A D179A (*blue*), D23A D179CT (*green*), Δ N D179CT (*orange*), and Δ N D179CT + VEID (*red*). The covered residues for each peptic peptide of caspase-6 mutation variants are indicated. *Error bars*, S.D. of duplicate H/DX-MS measurements done on two separate days.

continue...

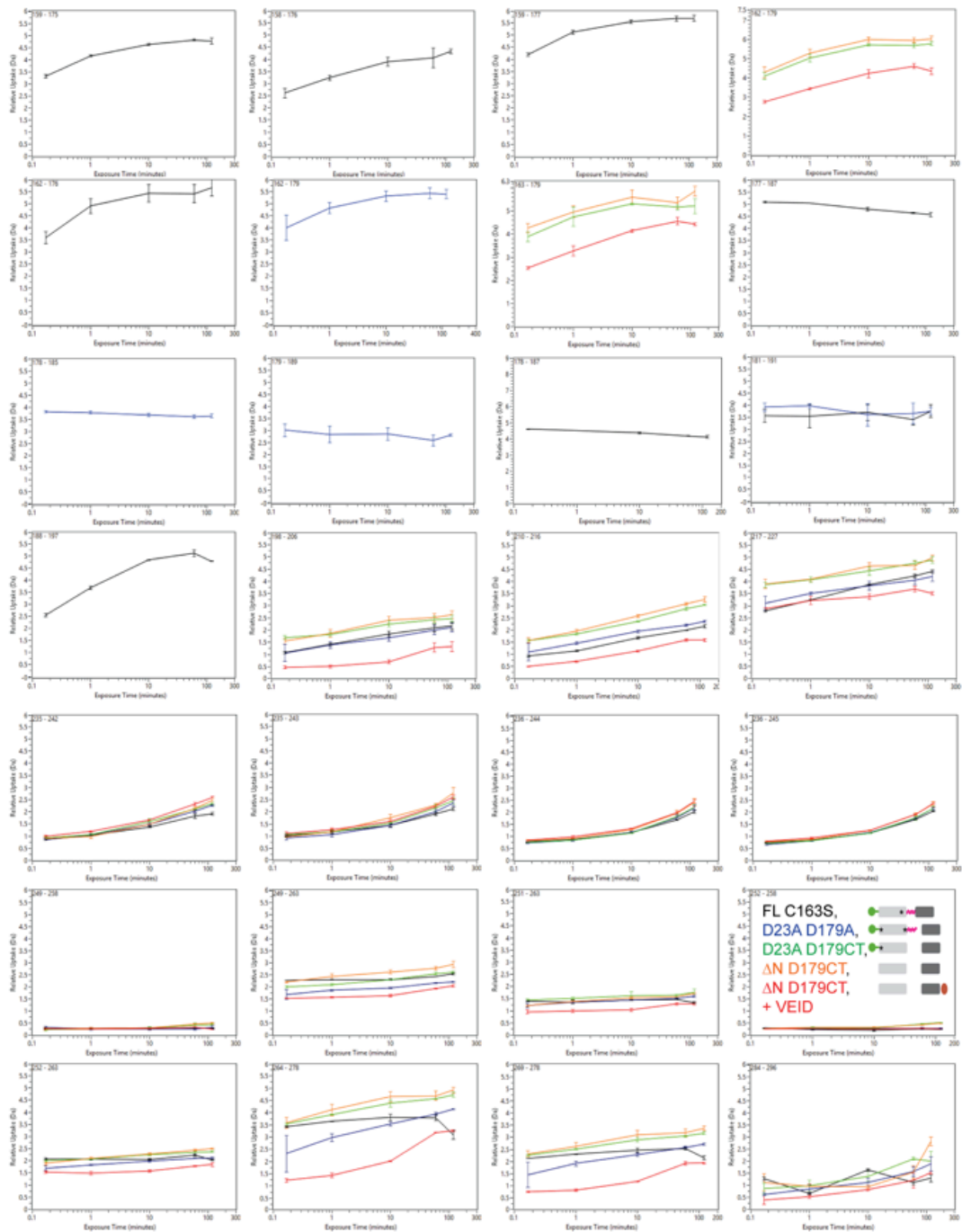


Figure 3.16. Additional Relative Deuterium Uptake Plots of Caspase-6 Maturation Variants Over the Course of the H/D Exchange Experiment

The different colors represent the deuterium uptake profile of caspase-6 mutation variants FL C163S (*black*), D23A D179A (*blue*), D23A D179CT (*green*), ΔN D179CT (*orange*), and ΔN D179CT + VEID (*red*). The covered residues for each peptic peptide of caspase-6 mutation variants are indicated. *Error bars*, S.D. of duplicate H/DX-MS measurements done on two separate days.

3.5 Materials and Methods

3.5.1 Generation of Caspase Variants

The caspase-6 variants FL C163S, D23A D179A, D23A D179CT, Δ N D179A, and Δ N D179CT were derived from the synthetic, *E. coli* codon-optimized (His)₆ C-terminally tagged caspase-6 gene (Celtek Bioscience) that were ligated into the NdeI/BamHI sites of pET11a vector (Vaidya et al., 2011). The Δ N C163S with C-terminal (His)₆-tag was generated using FL C136S as template through Phusion® site-directed mutagenesis (Thermo Scientific™).

3.5.2 Caspase Protein Expression and Purification

Caspase-6 constructs were transformed into the BL21(DE3) T7 express strain of *E. coli* (New England Biolabs). Overnight seed cultures were initially grown in 2 \times YT medium supplemented with 0.1 mg/ml ampicillin (Sigma) at 37 °C. Dense cultures were then diluted 1,000-fold with 2xYT containing 0.1 mg/ml ampicillin and shaken at 37 °C until A₆₀₀ reached 0.6. Protein expression was induced by the addition of 1mM isopropyl 1-thio- β -D-galactopyranoside and cultures were shaken at 20 °C for 18 h. Cells were centrifuged at 4,700 x g for 10 min at 4 °C and stored at -20 °C until use. Freeze-thawed cells were lysed using a microfluidizer (Microfluidics, Inc.) in lysis buffer (50 mM Tris, pH 8.5, 300 mM NaCl, 5% glycerol, 50 mM imidazole) and centrifuged at 30,600 x g for 1 h at 4 °C. The supernatant was loaded into a 5-ml HiTrap nickel affinity column (GE Healthcare) and washed with lysis buffer until the absorbance returned to

baseline. The protein was eluted with elution buffer (50 mM Tris, pH 8.5, 300 mM NaCl, 5% glycerol, 250 mM imidazole) and diluted 5-fold with buffer A (20 mM Tris, pH 8.5, 2 mM DTT) to reduce the salt concentration. This protein sample was then loaded into a 5-ml HiTrap Q HP column (GE Healthcare). The column was developed with a linear NaCl gradient, and the protein was eluted in 20mM Tris, pH 8.5, 200mM NaCl, 2mM DTT. This eluted protein was stored at $-80\text{ }^{\circ}\text{C}$ until use. The purified caspases were analyzed by SDS-PAGE to confirm identity and purity.

3.5.3 Caspase Activity Assays

To measure caspase activity, 100 nM purified caspase was assayed over 7 min at $37\text{ }^{\circ}\text{C}$ in caspase-6 activity assay buffer (100 mM HEPES, 120 mM NaCl, 0.1% CHAPS, 10% sucrose, 5 mM DTT). For substrate titration, a range of 0-500 μM fluorogenic substrate VEID-AMC [*N*-acetyl-Val-Glu-Ile-Asp-(7-amino-4-methyl-coumarin), Enzo Life Sciences Inc.] was used. Fluorescence kinetic measurements ($\lambda_{\text{ex}}/\lambda_{\text{em}}$: 365nm/495nm) were performed in three independent trials on three different days in 100- μL reactions in a 96-well format using a microplate reader (SpectraMax M5, Molecular Devices). Initial velocities versus substrate concentration were fit to a rectangular hyperbola using GraphPad Prism (GraphPad Software, San Diego, USA) to determine the kinetic parameters K_M and k_{cat} . Enzyme concentrations were determined by active-site titration with the quantitative covalent inhibitor VEID-CHO (*N*-Acetyl-Val-Glu-Ile-Asp-aldehyde; Enzo Life Sciences Inc.). Caspase-6 was added to inhibitor

solvated in DMSO in 96-wells V-bottom plates at room temperature for 1.5 hours in caspase activity assay buffer. Aliquots (90 μ L) were transferred in duplicate to black-well plates and assayed with 50-fold molar excess of substrate. The protein concentration was determined to be the lowest concentration at which full inhibition was observed and was thus used to calculate k_{cat} .

3.5.4 Tau Protein Expression and Purification

The human Tau-383 (0N4R) variant in pMXB10 vector (a generous gift from Bing Zhou) was expressed in BL21(DE3) T7 express *E. coli* strain (New England Biolabs) and purified using chitin beads (New England Biolabs) as described (Venter et al., 2011; Wang et al., 2010a). Briefly, Tau-BL21(DE3) T7 *E. coli* cells were grown in 2x YT media until A_{600} reached 0.6. Cells were harvested, lysed and centrifuged at 30,600 xg for 1 h at 4 °C. Supernatant was loaded into the column composed of chitin beads and washed with binding buffer (20 mM Tris, pH 8.5, 500 mM NaCl, 1 mM EDTA, 0.1% Tween-20) until absorbance reached baseline levels. The column was flushed with 3-column volumes of binding buffer with 50 mM DTT and incubated for 16 h at 4°C. After incubation, the protein was eluted with binding buffer. The eluted protein was loaded into HiLoad 26/600 Superdex 200 Column and eluted using 200 mM HEPES, pH 7.5, 150 mM NaCl. The purified protein was analyzed by SDS-PAGE to confirm identity and purity.

3.5.5 Proteolysis of Tau Protein by Caspase-6 Variants

Human Tau protein (3 μM) was incubated with varying concentrations of active caspase-6 activation state variants (0–3 μM , 2-fold dilution) in caspase-6 assay buffer (100 mM HEPES pH 7.5, 10% sucrose, 0.1% CHAPS, 120 mM NaCl, and 5 mM DTT) at 37 °C for 6 h. SDS loading buffer was added to the samples and boiled for 10 mins prior to analysis by 16% SDS-PAGE. The gels were imaged using ChemiDoc™ MP imaging system (Bio-Rad).

3.5.6 Hydrogen/Deuterium Exchange Mass Spectrometry

H/D exchange experiments on caspase-6 were performed as described previously (Dagbay et al., 2017). Briefly, an initial stock of 15- μM proteins in 20 mM Tris pH 8.5, 200 mM NaCl and 2 mM DTT in H₂O was prepared. The protein samples were then introduced into the nanoACQUITY system equipped with H/D exchange technology for UPLC separation (Wales et al., 2008) (Waters Corp., Milford, MA), which performed all subsequent manipulations for the H/D exchange. Accurate mass and collision-induced dissociation in data-independent acquisition mode (MS^E) (Geromanos et al., 2009) and ProteinLynx Global Server (PLGS) 3.0 software (Waters Corp., Milford, MA) were used to determine the peptic peptides in the undeuterated protein samples analyzed on the same UPLC-ESI-Q-ToF system used for H/DX-MS experiments. Data from peptic peptides generated from PLGS were imported into DynamX 3.0 (Waters Corp., Milford, MA) with peptide quality thresholds of MS¹ signal intensity ≥ 5000 , maximum sequence length of 25 amino acids, maximum mass error of 1 ppm,

and minimum products per amino acid of ≥ 0.3 . Automated results were manually inspected to ensure the corresponding m/z and isotopic distributions at various charge states were properly assigned to the appropriate peptic peptide. DynamX 3.0 was then used to generate the relative deuterium incorporation plot and H/DX heat map for each peptic peptide. The relative deuterium incorporation of each peptide was determined by subtracting the weight-averaged centroid mass of the isotopic distribution of undeuterated control sample from that of the weight-averaged centroid mass of the isotopic distribution of deuterium-labeled samples at each labeling time point. All comparisons were performed under identical experimental conditions, negating the need for back exchange correction in the determination of the deuterium incorporation. Thus, H/D exchange levels are reported as relative (Wales and Engen, 2006). The fractional relative deuterium uptake was calculated by dividing the relative deuterium uptake of each peptic peptide by its theoretical maximum uptake. All H/DX-MS experiments were performed in duplicate on two separate days and a 98% confidence limit for the uncertainty of the mean relative deuterium uptake of ± 0.6 Da was calculated as described (Houde et al., 2011). Differences in deuterium uptake between two states that exceed 0.6 Da were considered significant.

3.5.7 Circular Dichroism Spectroscopy

Caspase-6 activation state variants (8 μM) were concentrated and diluted three times in 10 mM phosphate buffer, pH 7.5 with 120 mM NaCl and in an Amicon Ultra-0.5 mL centrifugal filter (MWCO 10K) (Millipore). Following buffer

exchange, caspase-6 concentrations were determined by 280-nm absorbance. CD spectra (250-190 nm) were measured on a J-1500 CD spectrometer (Jasco) with Peltier temperature controller. All data were collected at triplicate on different days.

3.5.8 Intrinsic Fluorescence Spectroscopy

Caspase-6 activation state variants (3 μ M) in 20 mM phosphate buffer, pH 7.5, 120 mM NaCl, and 2 mM DTT were prepared. Fluorescence emission scans (305–400 nm) were collected after excitation at 280 nm or 295 nm using J-1500 spectrometer (Jasco) equipped with fluorescence emission monochromator (FMO-522) and detector (FDT-538). Signal was acquired by setting the emission detector at high-tension voltage value of 700 V, the data integration time (D.I.T) to 1 s and data pitch to 1 nm. The bandwidth used for excitation and emission was 2 nm and 10 nm, respectively.

3.5.9 Caspase-6 Model Building and Disorder Prediction

The full-length caspase-6 zymogen model (residues 1–293) was built from crystal structures of caspase-6 zymogen. In this model, chain A was derived from PDB code 4iyf (chain A); chain B of this model was derived from PDB code 3NR2 (chain A) as templates. The missing residues ([1–30, 174–186, and 292–293] in PDB code 4iyf (chain A); [1–30, 167–186, 261–271, and 292–293] in PDB code 3NR2 (chain A)) were built by *de novo* modeling using Chimera/Modeller platforms (Pettersen et al., 2004; Webb and Sali, 2014). All illustrations with

molecular visualization were generated using the PyMOL Molecular Graphics System (Schrödinger, LLC). Amino acid sequences of caspase-3, -6, and -7 were submitted to the DISOPRED (Ward et al., 2004) server for the prediction of protein disorder.

3.6 Acknowledgments

This work was supported by the National Institutes of Health (GM080532). We thank Stephen J. Eyles, director of the UMass Institute of Applied Life Sciences Mass Spectrometry core facility for abundant assistance with H/D exchange mass spectrometry data collection and processing.

3.7 References

- Aharony, I., D. E. Ehrnhoefer, A. Shruster, X. Qiu, S. Franciosi, M. R. Hayden, and D. Offen. 2015. A Huntingtin-based peptide inhibitor of caspase-6 provides protection from mutant Huntingtin-induced motor and behavioral deficits. *Hum Mol Genet*, 24:2604-14.
- Albrecht, S., N. Bogdanovic, B. Ghetti, B. Winblad, and A. C. LeBlanc. 2009. Caspase-6 activation in familial alzheimer disease brains carrying amyloid precursor protein or presenilin i or presenilin II mutations. *J Neuropathol Exp Neurol*, 68:1282-93.
- Albrecht, S., M. Bourdeau, D. Bennett, E. J. Mufson, M. Bhattacharjee, and A. C. LeBlanc. 2007. Activation of caspase-6 in aging and mild cognitive impairment. *Am J Pathol*, 170:1200-9.
- Allsopp, T. E., J. McLuckie, L. E. Kerr, M. Macleod, J. Sharkey, and J. S. Kelly. 2000. Caspase 6 activity initiates caspase 3 activation in cerebellar granule cell apoptosis. *Cell Death Differ*, 7:984-93.
- Baumgartner, R., G. Meder, C. Briand, A. Decock, A. D'Arcy, U. Hassiepen, R. Morse, and M. Renatus. 2009. The crystal structure of caspase-6, a selective effector of axonal degeneration. *Biochem J*, 423:429-39.
- Boucher, D., V. Blais, and J. B. Denault. 2012. Caspase-7 uses an exosite to promote poly(ADP ribose) polymerase 1 proteolysis. *Proc Natl Acad Sci U S A*, 109:5669-74.

- Cao, Q., X. J. Wang, L. F. Li, and X. D. Su. 2014. The regulatory mechanism of the caspase 6 pro-domain revealed by crystal structure and biochemical assays. *Acta Crystallogr D Biol Crystallogr*, 70:58-67.
- Chalmers, M. J., S. A. Busby, B. D. Pascal, Y. He, C. L. Hendrickson, A. G. Marshall, and P. R. Griffin. 2006. Probing protein ligand interactions by automated hydrogen/deuterium exchange mass spectrometry. *Analytical Chemistry*, 78:1005-14.
- Choi, Y. E., M. Butterworth, S. Malladi, C. S. Duckett, G. M. Cohen, and S. B. Bratton. 2009. The E3 ubiquitin ligase cIAP1 binds and ubiquitinates caspase-3 and -7 via unique mechanisms at distinct steps in their processing. *Journal of Biological Chemistry*, 284:12772-82.
- Clark, A. C. 2016. Caspase Allosterity and Conformational Selection. *Chem Rev*.
- Cowling, V., and J. Downward. 2002. Caspase-6 is the direct activator of caspase-8 in the cytochrome c-induced apoptosis pathway- absolute requirement for removal of caspase-6 prodomain. *Cell Death and Differentiation*, 9:1046-1056.
- Dagbay, K. B., N. Bolik-Coulon, S. N. Savinov, and J. A. Hardy. 2017. Caspase-6 Undergoes a Distinct Helix-Strand Interconversion Upon Substrate Binding. *Journal of Biological Chemistry*.
- Doostzadeh-Cizeron, J., S. Yin, and D. W. Goodrich. 2000. Apoptosis induced by the nuclear death domain protein p84N5 is associated with caspase-6 and NF-kappa B activation. *J Biol Chem*, 275:25336-41.
- Englander, S. W. 2006. Hydrogen exchange and mass spectrometry: A historical perspective. *Journal of the American Society for Mass Spectrometry*, 17:1481-9.
- Eron, S. J., K. Raghupathi, and J. A. Hardy. 2017. Dual Site Phosphorylation of Caspase-7 by PAK2 Blocks Apoptotic Activity by Two Distinct Mechanisms. *Structure*, 25:27-39.
- Feeney, B., and A. C. Clark. 2005. Reassembly of active caspase-3 is facilitated by the propeptide. *J Biol Chem*, 280:39772-85.
- Geromanos, S. J., J. P. Vissers, J. C. Silva, C. A. Dorschel, G. Z. Li, M. V. Gorenstein, R. H. Bateman, and J. I. Langridge. 2009. The detection, correlation, and comparison of peptide precursor and product ions from data independent LC-MS with data dependant LC-MS/MS. *Proteomics*, 9:1683-95.
- Giaime, E., C. Sunyach, C. Druon, S. Scarzello, G. Robert, S. Grosso, P. Auberger, M. S. Goldberg, J. Shen, P. Heutink, J. Pouyssegur, G. Pages, F. Checler, and C. Alves da Costa. 2010. Loss of function of DJ-1 triggered by Parkinson's disease-associated mutation is due to proteolytic resistance to caspase-6. *Cell Death Differ*, 17:158-69.
- Graham, R. K., Y. Deng, J. Carroll, K. Vaid, C. Cowan, M. A. Pouladi, M. Metzler, N. Bissada, L. Wang, R. L. Faull, M. Gray, X. W. Yang, L. A. Raymond, and M. R. Hayden. 2010. Cleavage at the 586 amino acid caspase-6 site in mutant huntingtin influences caspase-6 activation in vivo. *J Neurosci*, 30:15019-29.

- Graham, R. K., Y. Deng, E. J. Slow, B. Haigh, N. Bissada, G. Lu, J. Pearson, J. Shehadeh, L. Bertram, Z. Murphy, S. C. Warby, C. N. Doty, S. Roy, C. L. Wellington, B. R. Leavitt, L. A. Raymond, D. W. Nicholson, and M. R. Hayden. 2006. Cleavage at the caspase-6 site is required for neuronal dysfunction and degeneration due to mutant huntingtin. *Cell*, 125:1179-91.
- Guo, H., S. Albrecht, M. Bourdeau, T. Petzke, C. Bergeron, and A. C. LeBlanc. 2004. Active caspase-6 and caspase-6-cleaved tau in neuropil threads, neuritic plaques, and neurofibrillary tangles of Alzheimer's disease. *Am J Pathol*, 165:523-31.
- Guo, H., D. Petrin, Y. Zhang, C. Bergeron, C. G. Goodyer, and A. C. LeBlanc. 2006. Caspase-1 activation of caspase-6 in human apoptotic neurons. *Cell Death Differ*, 13:285-92.
- Horowitz, P. M., K. R. Patterson, A. L. Guillozet-Bongaarts, M. R. Reynolds, C. A. Carroll, S. T. Weintraub, D. A. Bennett, V. L. Cryns, R. W. Berry, and L. I. Binder. 2004. Early N-terminal changes and caspase-6 cleavage of tau in Alzheimer's disease. *J Neurosci*, 24:7895-902.
- Houde, D., S. A. Berkowitz, and J. R. Engen. 2011. The utility of hydrogen/deuterium exchange mass spectrometry in biopharmaceutical comparability studies. *J Pharm Sci*, 100:2071-86.
- Hsu, Y. H., D. A. Johnson, and J. A. Traugh. 2008. Analysis of conformational changes during activation of protein kinase Pak2 by amide hydrogen/deuterium exchange. *J Biol Chem*, 283:36397-405.
- Jung, J. Y., S. R. Lee, S. Kim, S. W. Chi, K. H. Bae, B. C. Park, J. H. Kim, and S. G. Park. 2014. Identification of novel binding partners for caspase-6 using a proteomic approach. *J Microbiol Biotechnol*, 24:714-8.
- Klaiman, G., N. Champagne, and A. C. LeBlanc. 2009. Self-activation of Caspase-6 in vitro and in vivo: Caspase-6 activation does not induce cell death in HEK293T cells. *Biochim Biophys Acta*, 1793:592-601.
- Konermann, L., J. Pan, and Y. H. Liu. 2011. Hydrogen exchange mass spectrometry for studying protein structure and dynamics. *Chem Soc Rev*, 40:1224-34.
- LeBlanc, A., H. Liu, C. Goodyer, C. Bergeron, and J. Hammond. 1999. Caspase-6 role in apoptosis of human neurons, amyloidogenesis, and Alzheimer's disease. *J Biol Chem*, 274:23426-36.
- LeBlanc, A. C. 2013. Caspase-6 as a novel early target in the treatment of Alzheimer's disease. *Eur J Neurosci*, 37:2005-18.
- Leuenberger, P., S. Gansch, A. Kahraman, V. Cappelletti, P. J. Boersema, C. von Mering, M. Claassen, and P. Picotti. 2017. Cell-wide analysis of protein thermal unfolding reveals determinants of thermostability. *Science*, 355.
- Martin, M. C., L. A. Allan, E. J. Mancini, and P. R. Clarke. 2008. The docking interaction of caspase-9 with ERK2 provides a mechanism for the selective inhibitory phosphorylation of caspase-9 at threonine 125. *Journal of Biological Chemistry*, 283:3854-65.

- Meergans, T., A. K. Hildebrandt, D. Horak, C. Haenisch, and A. Wendel. 2000. The short prodomain influences caspase-3 activation in HeLa cells. *Biochem J*, 349:135-40.
- Mittag, T., L. E. Kay, and J. D. Forman-Kay. 2010. Protein dynamics and conformational disorder in molecular recognition. *Journal of Molecular Recognition*, 23:105-16.
- Morgan, C. R., and J. R. Engen. 2009. Investigating solution-phase protein structure and dynamics by hydrogen exchange mass spectrometry. *Curr Protoc Protein Sci*, Chapter 17:Unit 17 6 1-17.
- Muller, I., M. B. Lamers, A. J. Ritchie, H. Park, C. Dominguez, I. Munoz-Sanjuan, M. Maillard, and A. Kiselyov. 2011. A new apo-caspase-6 crystal form reveals the active conformation of the apoenzyme. *Journal of Molecular Biology*, 410:307-15.
- Muzio, M., B. R. Stockwell, H. R. Stennicke, G. S. Salvesen, and V. M. Dixit. 1998. An induced proximity model for caspase-8 activation. *Journal of Biological Chemistry*, 273:2926-30.
- Nutt, L. K., S. S. Margolis, M. Jensen, C. E. Herman, W. G. Dunphy, J. C. Rathmell, and S. Kornbluth. 2005. Metabolic regulation of oocyte cell death through the CaMKII-mediated phosphorylation of caspase-2. *Cell*, 123:89-103.
- Orth, K., A. M. Chinnaiyan, M. Garg, C. J. Froelich, and V. M. Dixit. 1996. The CED-3/ICE-like protease Mch2 is activated during apoptosis and cleaves the death substrate lamin A. *J Biol Chem*, 271:16443-6.
- Pettersen, E. F., T. D. Goddard, C. C. Huang, G. S. Couch, D. M. Greenblatt, E. C. Meng, and T. E. Ferrin. 2004. UCSF Chimera--a visualization system for exploratory research and analysis. *J Comput Chem*, 25:1605-12.
- Qin, H., S. M. Srinivasula, G. Wu, T. Fernandes-Alnemri, E. S. Alnemri, and Y. Shi. 1999. Structural basis of procaspase-9 recruitment by the apoptotic protease-activating factor 1. *Nature*, 399:549-557.
- Riechers, S. P., S. Butland, Y. Deng, N. Skotte, D. E. Ehrnhoefer, J. Russ, J. Laine, M. Laroche, M. A. Pouladi, E. E. Wanker, M. R. Hayden, and R. K. Graham. 2016. Interactome network analysis identifies multiple caspase-6 interactors involved in the pathogenesis of HD. *Hum Mol Genet*, 25:1600-18.
- Simon, D. J., R. M. Weimer, T. McLaughlin, D. Kallop, K. Stanger, J. Yang, D. D. O'Leary, R. N. Hannoush, and M. Tessier-Lavigne. 2012. A caspase cascade regulating developmental axon degeneration. *Journal of Neuroscience*, 32:17540-53.
- Slee, E. A., M. T. Harte, R. M. Kluck, B. B. Wolf, C. A. Casiano, D. D. Newmeyer, H. G. Wang, J. C. Reed, D. W. Nicholson, E. S. Alnemri, D. R. Green, and S. J. Martin. 1999. Ordering the cytochrome c-initiated caspase cascade: hierarchical activation of caspases-2, -3, -6, -7, -8, and -10 in a caspase-9-dependent manner. *J Cell Biol*, 144:281-92.

- Srinivasula, S. M., M. Ahmad, M. MacFarlanes, Z. Luo, Z. HUang, T. Fernandes-Alnemri, and E. S. Alnemri. 1998. Generation of Constitutively Active Recombinant Caspases-3 and -6 by Rearrangement of Their Subunits. *The Journal of Biological Chemistry*, 273:10107-10111.
- Srinivasula, S. M., T. Fernandes-Alnemri, J. Zangrilli, N. Robertson, R. C. Armstrong, L. Wang, J. A. Trapani, K. J. Tomaselli, G. Litwack, and E. S. Alnemri. 1996. The Ced-3:Interleukin 1 β Converting Enzyme-like Homolog Mch6 and the Lamin-cleaving Enzyme Mch2 α Are Substrates for the Apoptotic Mediator CPP32. *The Journal of Biological Chemistry*, 271:27099-27106.
- Suzuki, A., G. Kusakai, A. Kishimoto, Y. Shimojo, S. Miyamoto, T. Ogura, A. Ochiai, and H. Esumi. 2004. Regulation of caspase-6 and FLIP by the AMPK family member ARK5. *Oncogene*, 23:7067-75.
- Takahashi, A., E. S. Alnemri, Y. A. Lazebnik, T. Fernandes-Alnemri, G. Litwack, R. D. Moir, R. D. Goldman, G. G. Poirier, S. H. Kaufmann, and W. C. Earnshaw. 1996. Cleavage of lamin A by Mch2 α but not CPP32: multiple interleukin 1 β -converting enzyme-related proteases with distinct substrate recognition properties are active in apoptosis. *Proc Natl Acad Sci U S A*, 93:8395-400.
- Vaidya, S., E. M. Velazquez-Delgado, G. Abbruzzese, and J. A. Hardy. 2011. Substrate-induced conformational changes occur in all cleaved forms of caspase-6. *J Mol Biol*, 406:75-91.
- Velazquez-Delgado, E. M., and J. A. Hardy. 2012. Zinc-mediated allosteric inhibition of caspase-6. *J Biol Chem*, 287:36000-11.
- Venter, P. A., A. Dirksen, D. Thomas, M. Manchester, P. E. Dawson, and A. Schneemann. 2011. Multivalent display of proteins on viral nanoparticles using molecular recognition and chemical ligation strategies. *Biomacromolecules*, 12:2293-301.
- Voss, O. H., S. Batra, S. J. Kolattukudy, M. E. Gonzalez-Mejia, J. B. Smith, and A. I. Doseff. 2007. Binding of caspase-3 prodomain to heat shock protein 27 regulates monocyte apoptosis by inhibiting caspase-3 proteolytic activation. *J Biol Chem*, 282:25088-99.
- Wales, T. E., and J. R. Engen. 2006. Hydrogen exchange mass spectrometry for the analysis of protein dynamics. *Mass Spectrometry Reviews*, 25:158-70.
- Wales, T. E., K. E. Fadgen, G. C. Gerhardt, and J. R. Engen. 2008. High-speed and high-resolution UPLC separation at zero degrees Celsius. *Anal Chem*, 80:6815-20.
- Wang, L., J. H. Kang, K. H. Kim, and E. K. Lee. 2010a. Expression of intein-tagged fusion protein and its applications in downstream processing. *Journal of Chemical Technology and Biotechnology*, 85:11-18.
- Wang, X. J., Q. Cao, X. Liu, K. T. Wang, W. Mi, Y. Zhang, L. F. Li, A. C. LeBlanc, and X. D. Su. 2010b. Crystal structures of human caspase 6 reveal a new mechanism for intramolecular cleavage self-activation. *EMBO Rep*, 11:841-7.

- Ward, J. J., L. J. McGuffin, K. Bryson, B. F. Buxton, and D. T. Jones. 2004. The DISOPRED server for the prediction of protein disorder. *Bioinformatics*, 20:2138-9.
- Webb, B., and A. Sali. 2014. Protein structure modeling with MODELLER. *Methods in Molecular Biology*, 1137:1-15.
- Wong, B. K., D. E. Ehrnhoefer, R. K. Graham, D. D. Martin, S. Ladha, V. Uribe, L. M. Stanek, S. Franciosi, X. Qiu, Y. Deng, V. Kovalik, W. Zhang, M. A. Pouladi, L. S. Shihabuddin, and M. R. Hayden. 2015. Partial rescue of some features of Huntington Disease in the genetic absence of caspase-6 in YAC128 mice. *Neurobiol Dis*, 76:24-36.
- Yaoita, Y. 2002. Inhibition of nuclear transport of caspase-7 by its prodomain. *Biochem Biophys Res Commun*, 291:79-84.

CHAPTER 4

TUMOR-ASSOCIATED MUTATIONS IN CASPASE-6 NEGATIVELY IMPACT ITS CATALYTIC EFFICIENCY

This chapter is being prepared for submission as: Dagbay, K. B., Barrett, and J. A. Hardy. 2017. *The Tumor-Associated Mutations in Caspase-6 Negatively Impact Catalytic Efficiency*.

4.1 Abstract

Unregulated, particularly suppressed programmed cell death is one of the distinguishing features of many cancer cells. The cysteine protease caspase-6, one of the executioners of apoptotic cell death, plays a crucial role in regulation of apoptosis. Several *CASP6* gene somatic mutations in tumor tissues have been reported. This work explores the effect of *CASP6* tumor-associated mutations on the catalytic efficiency and structure of caspase-6. In general, these mutations showed decreased overall catalytic turnover. Mutations within 8-Å of the substrate-binding pocket of caspase-6 were found to be the most catalytically deactivating. In particular, the R259H substitution was found to be the most inactivating among caspase-6 tumor-associated variants. This substitution disrupts the cation- π stacking interaction between Arg-259 and Trp-227, which is indispensable for proper assembly of substrate-binding loops in caspase-6. Sequence conservation analysis at the homologous position across the caspase family suggests a role of this cation- π stacking in the catalytic function of caspases generally. These data suggest that caspase-6 deactivating mutations contribute to the multifactorial carcinogenic transformation.

4.2 Introduction

Caspases are a family of cysteine-aspartic proteases that are critical to mediating programmed cell death and maintaining homeostasis within the cell. Caspases are synthesized as inactive procaspase zymogens consisting of a connected prodomain, large subunit, intersubunit linker region, and small subunit (Figure. 4.1A). Depending on their functions within the apoptotic cascade, caspases are classified as initiators (caspase-2, -8, -9) or executioners (caspase-3, -6, -7) (Pop and Salvesen, 2009; Yan and Shi, 2005). When the cell receives a death signal, either from cellular stress (intrinsic pathway) or an extracellular death ligand (extrinsic pathway), initiator caspases are recruited to the apoptosome (caspase-9) or DISC complex (caspase-8) to begin the signal cascade (Fuentes-Prior and Salvesen, 2004). The constitutively dimeric executioner caspases are activated when cleaved at the intersubunit linker by the initiator caspases. Active executioner caspases proteolytically cleave substrates, which are both structural and repair proteins, at critical aspartic acid residues, which can activate or deactivate the substrates. Both the extrinsic and intrinsic apoptotic pathways eventually lead to the destruction of the cell (Earnshaw et al., 1999; Grutter, 2000; Inoue et al., 2009; McIlwain et al., 2013).

Caspase-6 is expressed as an inactive zymogen that is activated by proteolytic processing at a conserved aspartate residue in the intersubunit linker (Asp-193) between the large and small subunits (Srinivasula et al., 1996). Caspase-6 is further processed in the prodomain (Asp-23) and for removal of the linker (Asp-179). Caspase-6 is often activated by caspase-3 rather than by

initiator caspases (Slee et al., 1999) and has been shown to undergo self-activation both *in vitro* and *in vivo* (Klaiman et al., 2009; Wang et al., 2010). Caspase-6 is less apoptotic than either caspase-3 and -7, which are directly processed by initiators caspase-8 and -9 (Boatright and Salvesen, 2003). However, the overexpression of caspase-6 alone has been shown to promote cell death (Suzuki et al., 2004). Structurally, caspase-6 has the closest homology with caspase-3 and caspase-7, but has a preference for cleaving VEID motifs rather than the DEVD consensus sequence favored by caspase-3 and -7 (Talanian et al., 1997). Furthermore, caspase-6 has a distinct set of substrates compared to other caspases, such as lamin A/C (Ruchaud et al., 2002). An extensive analysis of caspase-2 and caspase-6 native substrates using MS-based proteomics revealed 204 unique caspase-6 substrates (Julien et al., 2016). Many caspase-6 specific substrates that were identified are known to be tumor-associated based on its inclusion in the census of human cancer genes (Futreal et al., 2004). Representative cancer-associated caspase-6 substrates include the double-strand-break repair protein, RAD21; the cellular tumor antigen p53, TP53; the breast cancer type 1 susceptibility protein, BRCA1; the DNA repair protein complementing XP-G cells, ERCC5; the DNA mismatch repair protein, MLH1; and the ras-related protein Rab-10, RB10. Thus, the crosstalk of caspase-6 with these known tumor-associated substrates suggests the potential involvement of caspase-6 in development of cancer.

As mediators of apoptotic cell death, caspases natively play an essential role in preventing the development of cancer. Unregulated cell proliferation and

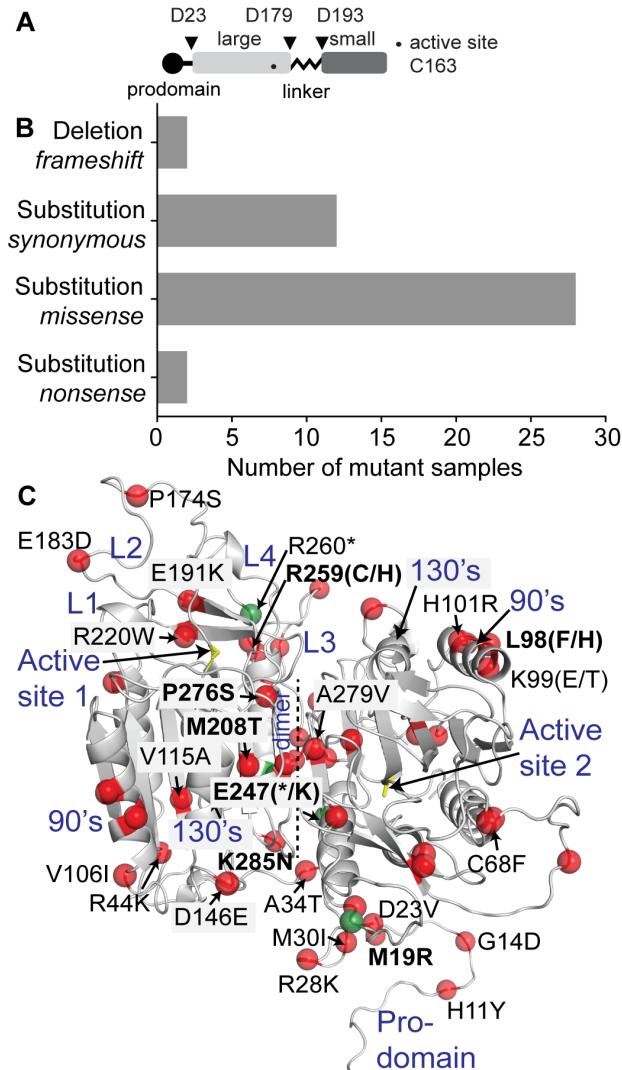


Figure 4.1 Tumor-Associated Mutations are Widely Distributed Across Caspase-6

(A) Linear cartoon of procaspase-6 illustrating the prodomain (*black circle*), large subunit (*light gray box*), intersubunit linker (*black zigzag*) and small subunit (*dark gray box*). The active site Cys–163 is denoted by a dot. Inverse triangles indicate proteolytic cleavage sites. (B) Relative abundance of the types of mutations observed in *CASP6* gene. (C) Observed tumor-associated nonsense (*green sphere*) and missense (*red spheres*) mutations in caspase-6 are mapped onto the model structure of full-length procaspase-6 with the active-site cysteine drawn as yellow sticks. The attachment point for the prodomain is visible only for one of the monomers in this orientation. The model procaspase-6 structure was generated based on zymogen structures 4IYR and 3NR2 with missing regions modeled *de novo*. Substrate-binding loops (L1, L2, L3, L4) along with key regions in caspase-6 (90's, 130's and the active site) are also indicated. Highlighted *bold* are the tumor-associated mutations interrogated in this study. An asterisk (*) indicates a premature appearance of stop codon characteristic of a nonsense mutation.

reduced apoptotic index are hallmarks of cancer, and caspase inhibition can lead to a reduced apoptotic index, thereby promoting tumorigenesis (Hanahan and Weinberg, 2011). Inhibited expression of proapoptotic molecules and the development of inhibitory somatic mutations could downregulate cancer cell apoptosis. Somatic mutations in caspases have been identified in tumor-associated tissues (Frejlich et al., 2013; Hosomi et al., 2003; Kim et al., 2009; Lee et al., 2006; Liu et al., 2002; Soung et al., 2008; Soung et al., 2003; Soung et al., 2004; Yoo et al., 2004). For example, *CASP8* somatic mutations were found in advanced gastric cancer carcinoma that significantly decreased caspase-8 apoptotic activity (Soung et al., 2005a). The well-known MCF-7 breast cancer cell line lacks caspase-3 expression due to a functional deletion mutation in the *CASP3* gene (Devarajan et al., 2002). Importantly, these somatic mutations evidence a decrease in caspase activity when compared to wild type and suggest caspase inhibition contributes to cancer pathogenesis.

Perhaps due to its diminished apoptotic role, caspase-6 has not been as highly scrutinized for its role in cancer pathogenesis as other caspases. Initial work to compile a list of *CASP6* somatic mutations in tumor-associated tissues has been reported more than a decade ago (Lee et al., 2006). Three *CASP6* somatic mutations were detected in gastric and colorectal cancer tissues that were classified to be missense and nonsense mutations, but no studies reporting functional characterization of the proteins resulting from mutant *CASP6* have been reported. To further explore the impact of somatic mutations on the function of caspase-6, in the present study caspase-6 tumor-associated variants were

produced and tested. Selected *CASP6* somatic mutations identified from the Catalogue of Somatic Mutations in Cancer (COSMIC) database (Forbes et al., 2011), a comprehensive resource of occurring somatic mutations in human cancer, and from the initial *CASP6* mutational analysis study (Lee et al., 2006) were selected. *CASP6* mutations from the COSMIC database were chosen based on their confirmed somatic status, their mutation type, and their varied structural location within the enzyme (Table 4.1, Figure 4.1C). Based on these criteria, seven caspase-6 tumor-associated variants were generated with amino acid changes located in the prodomain, large, and small subunit. This panel allowed us to explore the trend of somatic *CASP6* mutations in cancer pathogenesis and associated decreased apoptotic activity.

4.3 Results and Discussion

4.3.1 Mutations in *CASP6* Gene Have Been Identified in Tumor Tissues

One of the hallmarks of cancer is the failure of apoptosis (Hanahan and Weinberg, 2011). Caspase-6 is broadly classified as one of the executioner caspases in the apoptotic cascade; however, the association of caspase-6 in cancer has been largely unexplored. A search of the COSMIC database and other somatic mutations in the human *CASP6* gene (Forbes et al., 2011; Lee et al., 2006) revealed that caspase-6 harbored several mutations in tumor tissues. Of all reported mutations in *CASP6*, 64% resulted from missense mutations encoding a different amino acid after a single nucleotide change in the codon of *CASP6* gene (Figure 4.1B). Caspase-6 also harbored functionally deleterious

mutations including deletions (frameshifts) resulting from a shift in the reading frame and nonsense mutations resulting to a premature appearance of a stop codon within the *CASP6* gene. A significant fraction (27%) also showed synonymous substitution (silent) mutations where a codon change leads to encoding the same amino acid in caspase-6. Interestingly, these tumor-associated mutations, with emphasis on nonsense and missense mutations, are distributed across the structure of caspase-6, impacting regions both within the active site cavity and substrate-binding loops (Figure 4.1C) and outside, suggesting potential of these mutations to modulate caspase-6 function.

In addition, caspase-6 showed a differential gene regulation profiles in various tumor tissues, which have also been tested and catalogued in the COSMIC database (Figure 4.2). Both overexpression and underexpression of caspase-6 have been observed across various tumor and tumor-associated tissues. For a particular tumor tissue, an aberrant gene regulation profile usually correlates with the observation of mutant *CASP6* genotypes in tumors from those tissues (Figure 4.2). There were exceptions to this pattern, particularly in the tumor-associated samples from the adrenal gland, central nervous system (CNS), hematopoietic/lymphoid, lung, and the soft tissues, in which changes in gene regulation patterns did not correlate with enhanced mutational frequency in the *CASP6* gene. Although a number of *CASP6* mutations detected in tumor samples, only 0.13% of the total 29,665 tumor tissue samples showed mutations in *CASP6*.

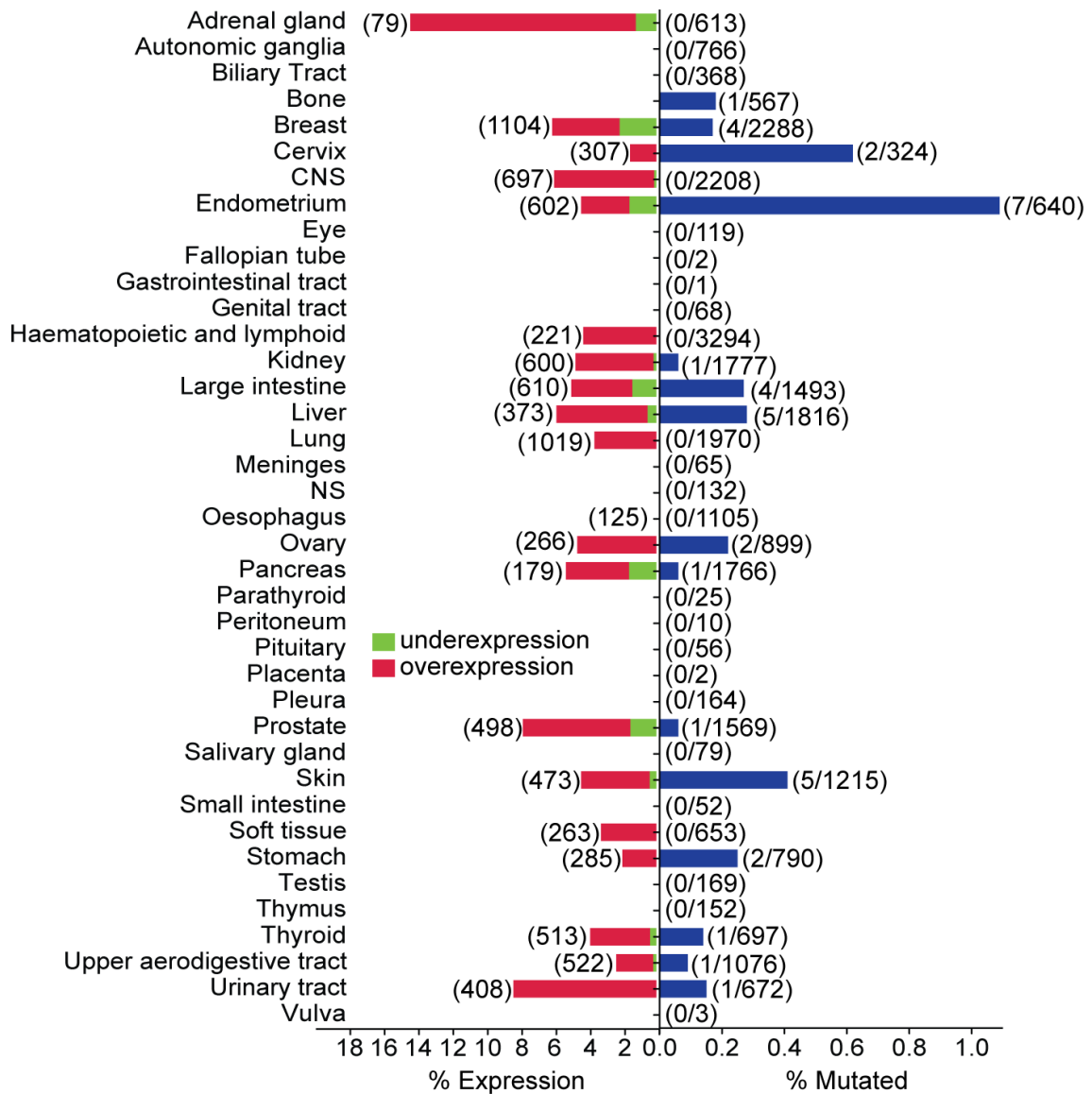


Figure 4.2 Aberrant CASP6 Gene Regulation Correlates with Percent Mutation in Caspase-6 in Tumor-Associated Tissue Types

CASP6 gene expression level in various tumor-associated tissues as catalogued from the COSMIC database. In parenthesis is the total number of samples tested for a given tumor tissue type. Percentage CASP6 gene expression (*left*) is presented as either underexpression (*green*) or overexpression (*red*). Percentage of samples with mutated CASP6 gene in tumor tissue type catalogued from the COSMIC database. In parenthesis is the fraction of the samples with mutations in the CASP6 gene relative the total number of samples (*right*).

While the identities of these mutations in *CASP6* in tumor tissues have been reported, the effect of each mutation on caspase-6 function is completely unstudied. Together, these mutations and atypical gene expression profiles may implicate caspase-6 in tumorigenesis.

Meanwhile, some tumor samples that harbored *CASP6* gene mutations also contain mutations in other caspases (Table 4.1). Particularly interesting is the co-existence of mutations in the initiator *CASP8*, a known oncogene (Stupack, 2013), where 24% of the tumor samples with *CASP6* mutations also harbored *CASP8* mutations. Although the functional consequences of these mutations in other caspases are not known, the co-existence of mutations in other caspases and other apoptotic proteins may be expected. This may suggest the existence of altered regulation of the apoptotic cascade or other nonapoptotic pathways relevant to the evolution of a tumor phenotype.

4.3.2 Caspase-6 Variants from Tumor Tissues Have Decreased Activity

To further investigate the effect of these mutations on caspase-6 function, seven caspase-6 tumor-associated mutations were selected based on their distribution across the caspase-6 structure (highlighted in *bold* in Figure 4.1C). All selected *CASP6* mutations had a confirmed somatic (non-germline) status and we focused our interrogation on less conservative mutations. Representative missense mutations were selected from within the region of the prodomain (M19R), the 90's (L98F), within the dimer interface (M208T and K285N), at the base of the helix adjoining L4 (E247K), and within 8-Å radius of the active site

Table 4.1. Identified Missense and Nonsense Mutations in Caspase-6 from Various Tumor Tissue Types and its Corresponding Tissue Distribution. Data were pooled from the COSMIC database (Forbes et al., 2011) and from a reported *CASP6* mutational study (Lee et al., 2006). Highlighted in **bold** are the specific caspase-6 tumor-associated variants interrogated in this study.

Mutation	Tissue	Histology	Other Caspase Mutations⁺	Reference
H11Y	Prostate	Carcinoma	none	(Robinson et al., 2015)
G14D	Skin	Carcinoma	none	(Pickering et al., 2014)
M19R	Ovary	Carcinoma	none	(CGARN**, 2011)
D23V	Bone	Ewings sarcoma	none	(Crompton et al., 2014)
R28K	Skin	Carcinoma	caspase-8 (S33F, S375F)	(Sharpe et al., 2015)
M30I	Endometrium	Carcinoma	caspase-2 (A259A)	(Forbes et al., 2011)
A34T**	Endometrium, Stomach	Carcinoma	caspase-3 (L118I, D192N); caspase-4 (R55W); caspase-10 (E22D); caspase-14 (E49K)	(Forbes et al., 2011)
R44K	Colon	Carcinoma	caspase-3 (F193L); caspase-8 (R162I)	(Lee et al., 2006)
C68F	Kidney	Carcinoma	none	(Durinck et al., 2015)
L98F	Endometrium	Carcinoma	caspase-1 (frameshift)	(Forbes et al., 2011)
L98H	Thyroid	Carcinoma	none	(Forbes et al., 2011)
K99E** [¶]	Liver	Carcinoma	none	(Forbes et al., 2011)
K99T	Cervix	Carcinoma	caspase-8 (N197T); caspase-14 (Q70K)	(Forbes et al., 2011)
H101R** [¶]	Liver	Carcinoma	none	(Forbes et al., 2011)
V106I	Cervix	Carcinoma	none	(Forbes et al., 2011)
V115A	Stomach	Carcinoma	caspase-5 (frameshift)	(Wang et al., 2014)
D146E	Liver	Carcinoma	none	(Forbes et al., 2011)
P174S	Skin	Carcinoma	none	(Sharpe et al., 2015)
E183D [‡]	Endometrium	Carcinoma	caspase-7 (K109N); caspase-8 (R52I, R111I, T461P, T503P)	(Forbes et al., 2011)
E191K	Urinary tract	Carcinoma	none	(Forbes et al., 2011)
M208T	Large Intestine	Carcinoma	none	(Forbes et al., 2011)
R220W	Endometrium	Carcinoma	caspase-2 (L232R, R417W, L125F); caspase-3 (R207*); casp-4 (V252I); caspase-5 (Y87*, Y116*);	(Forbes et al., 2011)
E247K	Lung	Carcinoma	none	(Forbes et al., 2011)
E247*	Breast	Carcinoma	caspase-4 (E351A); caspase-8 (D73A, D132A, E399*, E441*)	(Forbes et al., 2011)
R259C	Endometrium	Carcinoma	caspase-1 (G85W); caspase-2 (A412V); caspase-4 (K42Q); caspase-7 (T18A); caspase-8 (E36*, E95*)	(Forbes et al., 2011)
R259H	Colon	Carcinoma	none	(Lee et al., 2006)
R260*	Large Intestine	Carcinoma	none	(Forbes et al., 2011)
P276S	Breast	Carcinoma	none	(Forbes et al., 2011)
A279V [‡]	Endometrium	Carcinoma	caspase-7 (K109N); caspase-8 (R52I, R111I, T461P, T503P)	(Forbes et al., 2011)
K285N	Lung	Carcinoma	none	(Forbes et al., 2011)

*Nonsense mutations identified in caspase-6. **Mutation found in two separate samples. [¶]Mutations found in the same sample ID. [‡]Other caspase mutations found in the same sample ID.

Cys-163 (R259H and P276S). These caspase-6 variants were expressed in *E. coli* and purified to homogeneity. The activities of the caspase-6 tumor-associated variants were assessed using a fluorogenic peptide-based substrate, VEID-AMC (Table 4.2). These variants were observed to have 2–457 fold decreases in catalytic efficiency compared to the wild type (WT) caspase-6. Mutations within the substrate-binding groove, P276S and R259H, showed the most negative impact on caspase-6 activity. The decrease in the catalytic efficiency of all the caspase-6 tumor-associated variants suggests that the mutations have caused changes in the structure or dynamics that result in less effective substrate catalysis.

Caspase-6 is the sole caspase for which a mechanism for intramolecular self-cleavage has been observed (Klaiman et al., 2009; Wang et al., 2010) and WT caspase-6 is capable of self-maturation upon bacterial expression (Velazquez-Delgado and Hardy, 2012).

Table 4.2 Kinetic Parameters of Selected Caspase-6 Tumor-Associated Variants Identified from COSMIC Database (Forbes, Bindal et al., 2011) and Other Sources (Lee, Kim et al., 2006).

Caspase-6 mutation	K_M (μM)	k_{cat} (s^{-1})	$10^5 \times k_{cat}/K_M$ ($\text{M}^{-1}\text{s}^{-1}$)	Fold decrease in turnover <i>versus</i> WT
WT	34 ± 3.6	1.1 ± 0.03	32	1
M19R	163 ± 19	0.80 ± 0.04	5.0	6.40
L98F	46 ± 4.2	0.68 ± 0.02	15	2.10
M208T	170 ± 12.0	1.5 ± 0.04	8.8	3.60
E247K	84 ± 10	1.6 ± 0.06	19	1.70
P276S	314 ± 26	0.57 ± 0.02	1.8	18.0
R259H	577 ± 135	0.04 ± 0.01	0.07	457
K285N	50 ± 4.0	0.18 ± 0.01	3.6	8.90

Kinetic parameters of caspase-6 tumor-associated variants were determined using fluorogenic substrate, VEID-AMC using 100-nM enzyme in caspase-6 activity assay buffer. *Error*, represents standard error of the mean (S.E.M.) of two independent experiments.

All of the caspase-6 tumor-associated variants were overexpressed in *E. coli* for 18 h at 20°C and purified in the same manner (described in the Materials and Methods). These expression conditions led to full activation of WT caspase-6. Despite identical conditions of expression and purification, variations in the cleavage patterns of the caspase-6 tumor-associated variants were observed (Figure 4.3A). Typically, caspase-6 is proteolytically cleaved at three sites located in the prodomain and linker regions (Figure 4.1A) that are essential for its full maturation and activation. When caspase-6 tumor-associated variants were allowed to undergo self-proteolysis, L98F and K285N showed nearly full maturation indicated by the presence of only the large and small subunits, suggesting relatively proteolytically active caspases. The rest of the caspase-6 tumor-associated variants were unable to completely remove the linker suggesting a decrease in their proteolytic activity compared to L98F and K285N variants.

The caspase-6 tumor-associated variants were allowed to undergo self-proteolysis *in vitro* by 24-hr incubation in caspase-6 activity assay buffer at 37 °C (Figure 4.3B). As expected, the full-length wild type (FL WT) caspase-6 showed a higher fraction of the fully cleaved large and small subunits, indicating close to full maturation. The caspase-6 phosphomimetic variant, S257D, is a surrogate of a phosphorylated caspase-6 at position 257. The S257D substitution is inactivated due to a misaligned substrate-binding groove of caspase-6 (Velazquez-Delgado and Hardy, 2012) and correspondingly, showed no further cleavage into its large and small subunits (Figure 4.3B). L98F showed similar

cleavage pattern as FL WT. R259H and P276S showed higher fractions of large subunits with attached intersubunit linker, a cleavage pattern different from the FL WT and L98F, which indicates that these variants slowed self-cleavage activity. Thus, the accessibility of the intersubunit linker to caspase-6 appears to

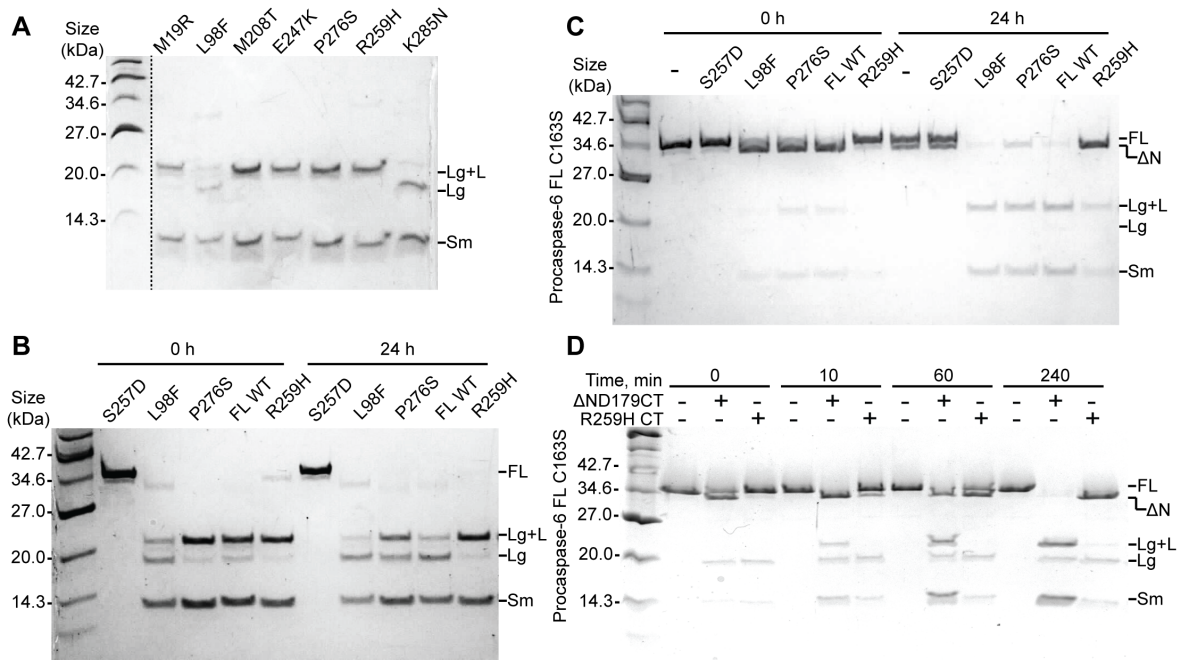


Figure 4.3 Selected Caspase-6 Tumor-Associated Variants Showed Decreased in Proteolytic Activity

(A) Cleavage pattern of caspase-6 tumor-associated variants expressed in *E. coli* and purified to homogeneity. All caspase-6 tumor-associated mutations were introduced into the full-length (FL) caspase-6 wild-type (WT) construct in pET11a bacterial expression vector. (B) Self-cleavage pattern of recombinant caspase-6 tumor-associated variants (3 μ M) before and after 24-h incubation in caspase-6 activity assay buffer at 37 $^{\circ}$ C. (C) Proteolysis of catalytically inactive procaspase-6 C163S (3 μ M) by caspase-6 tumor-associated variants (0.3 μ M) before and after 24-h incubation in caspase-6 activity assay buffer at 37 $^{\circ}$ C. (D) Proteolysis of catalytically inactive procaspase-6 C163S (3 μ M) by caspase-6 tumor-associated variant, R259H CT (0.3 μ M) after incubation in caspase-6 activity assay buffer at 37 $^{\circ}$ C for the indicated times. Two-chain forms of the mature and fully cleaved wild type (Δ N D179CT) and R259H CT caspase-6 variants were generated to allow independent expression of the large and small subunits without the need for proteolytic cleavage for its activation. FL, full-length; Δ N, removal of the N-terminal prodomain (residues 1–23); Lg, large subunit; L, intersubunit linker; Sm, small subunit.

be different in both P276S and R259H suggesting an altered geometry of the substrate-binding cleft leaning towards a less proteolytically active enzyme.

The activities of selected caspase-6 tumor-associated variants in cleaving protein substrate *in trans* (intermolecular cleavage) were tested using procaspase-6 FL C163S, a catalytically inactive variant of caspase-6, as substrate (Figure 4.3C). Consistently, both P276S and R259H showed less proteolytic activity against this protein substrate compared to L98F and WT caspase-6 (Figure 4.3C). R259H emerged as the least active variant in cleaving procaspase-6 FL C163S, underscoring the severity of its impact on the proper assembly of the substrate-binding cavity for efficient proteolysis. As the most inactive among caspase-6 tumor-associated variants in cleaving both peptide-based and protein substrates, we sought to assess whether the R259H impacted function in the fully mature form of caspase-6. To achieve this, the R259H mutation was then introduced into a constitutively two-chain (CT) caspase-6 expression construct (Vaidya et al., 2011) that allows independent expression of the large and small subunits, mimicking a fully cleaved and mature caspase-6. The two-chain R259H CT is dramatically inactivated for cleavage of protein substrate compared to the mature, two-chain (Δ ND179CT) wild-type caspase-6. This result further suggests that the R259H mutation is capable of negatively impacting the activity of the mature (cleaved) caspase-6 in cleaving protein substrates. Together, these data suggest that the majority of inactivating mutations in caspase-6 found in tumor-associated tissues may have acquired

misaligned substrate binding cleft or other defect-introducing structural changes that decrease in caspase-6 catalytic efficiency. Thus, it appears that the impairment of caspase-6 function need only to prevent caspase-6 activity in *trans*, against other substrates, whereas self-cleavage in *cis* poses no significant threat to these cancer cells.

4.3.3 Caspase-6 R259H Disrupts Interaction Necessary for Proper Assembly of Substrate-Binding Groove

R259H is the most inactivating mutation among caspase-6 tumor-associated variants we analyzed. To further understand the impact of the R259H substitution on proper assembly of the substrate-binding groove, the crystal structure of active and mature caspase-6 (PDB code 2WDP) was further inspected. Arg-259, which is located at the base of L4, is part of a network of H-bond and cation- π stacking interactions (Figure 4.4A) that provides a stable foundation for the proper assembly of substrate binding loops, thus essential for the establishment of a catalytically competent caspase-6. The usually positively-charged guanidinium group of arginine exhibits a high propensity to stack against aromatic residues while also capable of H-bonding to neighboring oxygen atoms (Nandi et al., 1993). In caspase-6, Arg-259 forms two H-bonds with Asp-231 and likely interacts with Trp-227 through cation- π stacking. Further, Trp-227 also holds L3 in place through cation- π stacking interaction with His-219. Both residues (His-219 and Trp-227) are part of the S4 substrate-binding pocket in caspase-6. This, cation- π interaction between Arg-259 and Trp-227 is highly

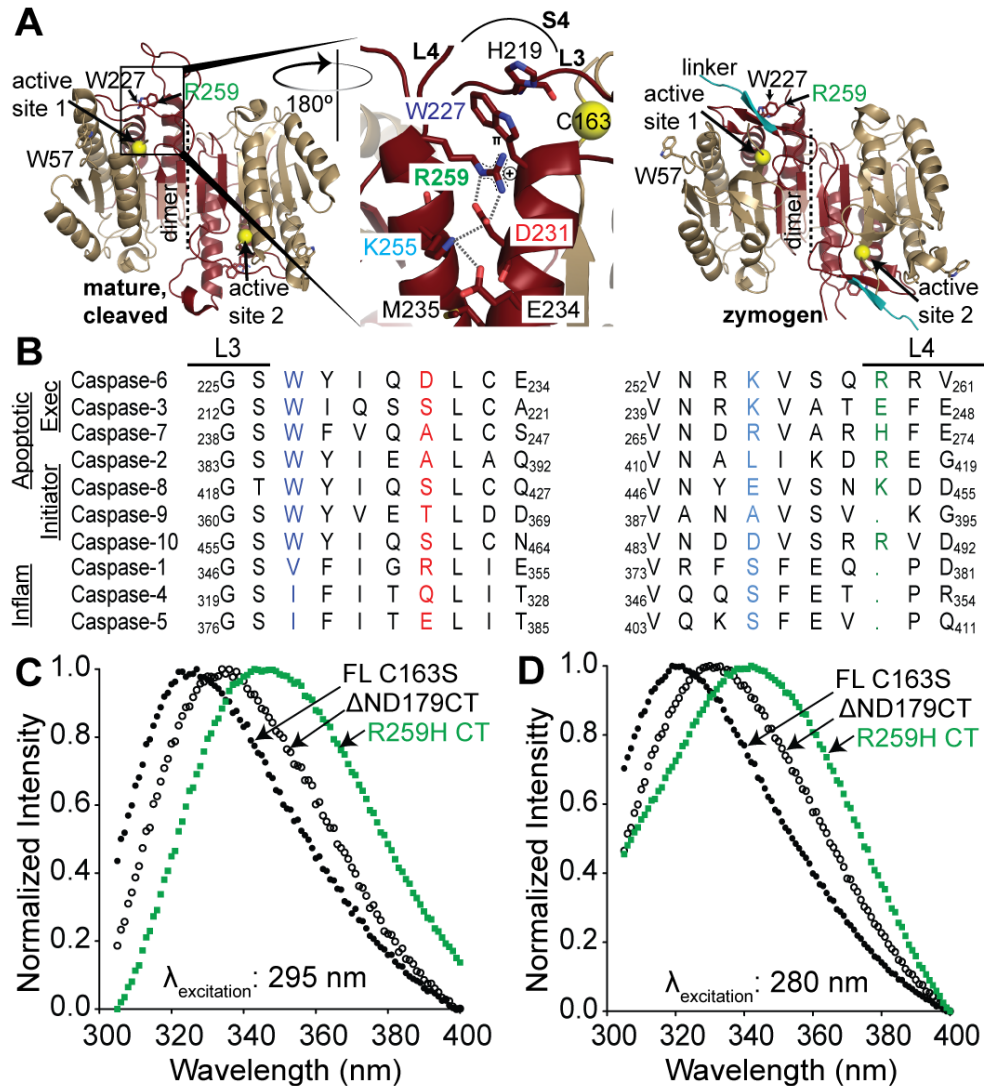


Figure 4.4 R259H Disrupts Interactions Necessary for Proper Assembly of the Substrate-Binding Groove

(A) The crystal structure of the mature, fully cleaved and unliganded caspase-6 (PDB code 2WDP) (*left*). The location of Arg-259, the active site Cys-163, and the two tryptophan residues (Trp-57 and Trp-227) in caspase-6 are indicated. *Inset view* highlights the cation- π stacking and networks of H-bond interactions in which Arg-259 are involved, as well as the substrate binding loops (L3, L4) and substrate-binding pocket (S4) (*middle*). The crystal structure of procaspase-6 zymogen (PDB code 3NR2) and the location of Arg-259, Trp-51, Trp-227, and the intersubunit linker (*cyan*) are indicated (*left*). (B) The amino acid sequence alignment of key residues within the network of interactions of Arg-259 across caspase family including both apoptotic and inflammatory caspases. (C) Intrinsic tryptophan fluorescence profiles of full length procaspase-6 C163S, caspase-6 Δ N D179CT, and caspase-6 Δ N R259H CT. Excitation at 295 nm primarily probes the polarity of the tryptophan microenvironment. (D) Intrinsic fluorescence profiles of caspase-6 variants excited at 280-nm wavelength. Excitation at 280 nm probes the polarity of the microenvironment of all aromatic residues in a protein including tryptophan, tyrosine and phenylalanine.

conserved across caspase family (Figure 4.4B), suggesting that this interaction is widely used among caspases to stabilize the substrate binding groove for efficient substrate binding and catalysis. On the other hand, the Asp-231 position is not conserved across the caspase family, thus the two H-bonds between Arg-259 and Asp-231 is unique to caspase-6. This implies that although common stabilizing interactions exist in caspases, unique interactions are also present for each individual caspase that may be relevant for its specific structure and function. In fact, tumor-associated mutations at this position have not been observed in other caspases. Caspase-7 has a His at the position homologous to caspase-6 Arg-259, however, His is not deleterious in the caspase-7 context because caspase-7 has an Ala at the position homologous to Asp-231. These data suggest that because Arg-259 participates in networks of stabilizing interactions it is a critical residue for caspase function that enabled caspases to properly orient its substrate-binding loops for efficient execution of enzyme catalysis.

The intrinsic fluorescence properties of Trp-227 allows this residue to function as a sensitive probe for the cation- π stacking interaction between Arg-259 and Trp-227 and the other network of interactions that give rise to the proper assembly of the substrate-binding groove. Caspase-6 has only two Trp residues, and they are both located in the substrate binding L1 (Trp-57) and at the base of L4 (Trp-227), which is directly adjacent to Arg-259. Trp-57 in both the zymogen and active forms are constantly solvent-exposed while the microenvironment of the Trp-227 varies between these forms of caspase-6 (Figure 4.4A). Thus, intrinsic tryptophan fluorescence will likely report the relative microenvironment of

Trp-227 between the absence and presence of R25H mutation and in turn, provides structural hints as to the proper assembly of the substrate-binding groove of caspase-6. Intrinsic tryptophan fluorescence is dependent on the polarity of the environment, where shifts in the maximum emission towards longer wavelengths (*red* shift) indicate higher solvent exposure. Intrinsic fluorescence spectra were collected from caspase-6 variants including the catalytically inactive procaspase-6 FL C163S, the mature, fully cleaved caspase-6 (Δ ND179CT), and the two-chain caspase-6 R259H.

As expected, upon specific tryptophan excitation at 295 nm (Figure 4.4C), the procaspase-6 zymogen showed a 10-nm shift in maximum emission towards a shorter wavelength (*blue* shift) compared to the two-chain mature and cleaved caspase-6 wild type (Δ ND179CT) suggesting a less solvent-exposed Trp-227 microenvironment. In the procaspase-6 zymogen structure (Figure 4.4A), the intersubunit linker sits on top of the substrate-binding groove of procaspase-6 zymogen restricting the solvent accessibility of Trp-227, one of the critical residues in the substrate-binding pocket of caspase-6. Meanwhile, the R259H CT variant displayed a significantly extended 12-nm shift in maximum emission towards longer wavelength (*red* shift) compared to caspase-6 Δ ND179CT indicating a highly solvent-exposed Trp-227 microenvironment. A similar trend was observed with 280 nm excitation of all aromatic residues (Trp, Tyr, Phe) (Figure 4.4D). Thus, the change in the polarity of the Trp-227 microenvironment in the presence of the R25H mutation in caspase-6 suggests a disruption of the stabilizing cation- π stacking interaction of Arg-259 with Trp-227 as well as the

disruption of the networks of H-bonding interactions that results in misaligned loops in the substrate binding pocket incapable of efficient catalytic turnover of substrates.

4.4 Conclusions

This study demonstrates that all the selected mutations in caspase-6 found in several tumors resulted to an overall decrease in the catalytic efficiency of caspase-6. The fact that not one of the selected mutations in any of the regions of caspase-6 had not impacted or increased activity strongly suggests that diminishing caspase-6 intrinsic activity via somatic mutation is helpful in establishing a tumorigenic phenotype. In particular, R259H was found to be severely deactivating via a mechanism that disrupts the cation- π stacking and the networks of H-bonding interactions necessary for proper alignment of loops in the substrate-binding groove of caspase-6.

One would anticipate that mutations in caspases would decrease the apoptotic potential of the cells containing mutant caspases. One naturally anticipates that neutralizing/inactivating mutations in caspase-6 should likewise play a role in tumorigenesis. For example, caspase-6 is a direct activator of the initiator caspase-8. Transfection of COS-7 cells with catalytically inactive caspase-6 strongly diminished caspase-8 activation (Cowling and Downward, 2002). Thus, in cellular context, activation through caspase-6 presents one of the regulatory pathways of caspase-8. *CASP8* is a tumor-associated gene and its polymorphisms are correlated with increased risk for various types of cancer (Ji et al., 2014; Mandruzzato et al., 1997; Park et al., 2016; Soung et al., 2005b). In

addition to its central role in apoptosis, caspase-8 has emerging nonapoptotic roles in cells such as potentiating NF- κ B signaling (Su et al., 2005), regulating autophagy (Bell et al., 2008), and cellular adhesion and migration (Barbero et al., 2009; Senft et al., 2007). Thus, regulation of caspase-6 may possibly impact both the apoptotic and the nonapoptotic tumor-associated roles of caspase-8. In addition, natural substrates of caspase-6 in cells has been reported including those involved in cell death, RNA splicing, cytoskeletal organization, regulation of transcription, chromosome organization, and in the cell cycle suggesting the unparalleled importance of the roles of caspase-6 in and outside of the apoptotic cascade (Julien et al., 2016). Several caspase-6 substrates identified from the MS-based approach (Julien et al., 2016) are tumor-associated based on its inclusion in the census of human cancer genes (Futreal et al., 2004) including the cellular tumor antigen p53, TP53 and the breast cancer type 1 susceptibility protein, BRCA1. Thus, the cleavage or miscleavage of these tumor-associated substrates by caspase-6 suggests the possible mechanism for caspase-6 to play a role in tumor development.

Together with the aberrant regulation of caspase-6, there were also mutations in other caspases that have been detected in some tumor-associated tissue samples with caspase-6 mutations. Thus, the co-occurrences of caspase mutations and the mutations in other tumor-associated genes underscore the complexity of each individual event of tumorigenesis. The fact that a number of different mutations in different regions of caspase-6 were observed in different tumors suggests the possibility that unique contributions of various aspects of

caspase-6 function may be at play in different cancers. The roles of each component in the pathway to tumor development will enable a better understanding of the controlling factors that allow the misregulation observed in cancer cells of all varieties. This work demonstrates that in cases when caspase-6 is mutated in tumors significant impacts on catalytic function are observed. What remains to be seen is whether other aspects of caspase-6 regulation, such as post-translational modifications, dynamics and substrate selection are likewise impacted by these tumor-associated mutations.

4.5 Materials and Methods

4.5.1 Database Analysis of *CASP6* Gene Mutations

CASP6 gene mutations in tumor samples were identified from COSMIC database (<http://cancer.sanger.ac.uk/cosmic>) (Forbes et al., 2011) and from a report of *CASP6* gene mutations in colorectal and gastric carcinomas (Lee et al., 2006). Assessment of a total of 29,815 sample tissues across all tumor-associated tissue types was reported for *CASP6* gene mutations. Representative missense mutations were selected based on the location of these mutations in the caspase-6 structure which spans within the region of the prodomain (M19R), the 90's region (L98F), within the dimer interface (M208T and K285N), at the base of the helix adjoining L4 (E247K), and within 8Å radius of the active site Cys-163 (R259H and P276S).

4.5.2 Generation of Caspase-6 Tumor-Associated Variants

The caspase-6 variants full length wild type (FL WT), FL C163S, and Δ N D179CT were derived from the synthetic, *E. coli* codon-optimized (His)₆ C-terminally tagged caspase-6 gene (Celtek Bioscience) that were ligated into the NdeI/BamHI sites of pET11a vector (Vaidya et al., 2011). Selected caspase-6 tumor-associated variants were generated using FL WT as template through Phusion® site-directed mutagenesis (Thermo Scientific™). The caspase-6 R259H CT variant was particularly generated using caspase-6 Δ N D179CT as the template for the site-directed mutagenesis.

4.5.3 Caspase-6 Protein Expression and Purification

Caspase-6 expression constructs were transformed into the BL21(DE3) T7 express strain of *E. coli* (New England Biolabs). Overnight seed cultures were initially grown in 2xYT medium supplemented with 0.1 mg/ml ampicillin (Sigma) at 37 °C. Dense cultures were then diluted 1,000-fold with 2xYT containing 0.1 mg/ml ampicillin and shaken at 37 °C until A_{600} reached 0.6. Protein expression was induced by the addition of 1mM isopropyl 1-thio- β -D-galactopyranoside and cultures were shaken at 20 °C for 18 h. Cells were centrifuged at 4,700 x *g* for 10 min at 4 °C and stored at -20 °C until use. Freeze-thawed cells were lysed using a microfluidizer (Microfluidics, Inc.) in lysis buffer (50 mM Tris, pH 8.5, 300 mM NaCl, 5% glycerol, 50 mM imidazole) and centrifuged at 30,600 x *g* for 1 h at 4 °C. The supernatant was loaded into a 5-ml HiTrap nickel affinity column (GE Healthcare) and washed with lysis buffer until the absorbance returned to baseline levels. These proteins were eluted with

elution buffer (50 mM Tris, pH 8.5, 300 mM NaCl, 5% glycerol, 250 mM imidazole) and diluted 5-fold with buffer A (20 mM Tris, pH 8.5, 2 mM DTT) to reduce the salt concentration. These protein samples were then loaded into a 5-ml HiTrap Q HP column (GE Healthcare). The columns were developed with linear NaCl gradients, and each protein was eluted in 20mM Tris, pH 8.5, 200mM NaCl, 2mM DTT. These eluted proteins were stored at -80°C until use. Purified caspases were analyzed by SDS-PAGE to confirm identity and purity.

4.5.4 Caspase-6 Activity Assays

To measure caspase-6 activity, the activity of 100 nM purified caspase-6 (WT and tumor-associated variants) was assayed over 7 min at 37°C in caspase-6 activity assay buffer (100 mM HEPES, 120 mM NaCl, 0.1% CHAPS, 10% sucrose, 5 mM DTT). For substrate titration, a range of 0-500 μM fluorogenic substrate VEID-AMC [*N*-acetyl-Val-Glu-Ile-Asp-(7-amino-4-methylcoumarin)], Enzo Life Sciences Inc was used. Fluorescence kinetic measurements ($\lambda_{\text{ex}}/\lambda_{\text{em}}$: 365nm/495nm) were performed in two independent trials in 100- μL reactions in a 96-well format using a microplate reader (SpectraMax M5, Molecular Devices). Initial velocities versus substrate concentration were fit to a rectangular hyperbola using GraphPad Prism (GraphPad Software, San Diego, USA) to determine the kinetic parameters K_M and k_{cat} . Enzyme concentrations were determined by active-site titration with the quantitative covalent inhibitor VEID-CHO (*N*-Acetyl-Val-Glu-Ile-Asp-aldehyde; Enzo Life Sciences Inc.). Caspase-6 was added to inhibitor solvated in DMSO in 96-wells V-bottom plates at room temperature for 1.5 hours in caspase-6 activity assay buffer. Aliquots (90

μL) were transferred in duplicate to black-well plates and assayed with 50-fold molar excess of substrate. The protein concentration was determined to be the lowest concentration at which full inhibition was observed and was thus used to calculate k_{cat} .

4.5.5 Self-Proteolysis Assay of Caspase-6 Tumor-Associated Variants

Caspase-6 variants (3 μM) were allowed to self-cleave in caspase-6 activity assay buffer (100 mM HEPES pH 7.5, 10% sucrose, 0.1% CHAPS, 120 mM NaCl, and 5 mM DTT) at 37 °C for 24 h. SDS loading buffer was added to the samples and boiled for 10 mins prior to analysis by 16% SDS-PAGE. The gels were imaged using a ChemiDoc™ MP imaging system (Bio-Rad).

4.5.6 Proteolysis of Procaspase-6 FL C163S Protein by Caspase-6 Tumor-Associated Variants

Catalytically inactive procaspase-6 FL C163S (3 μM) was incubated with each of caspase-6 tumor-associated variants (0.3 μM) in caspase-6 assay buffer (100 mM HEPES pH 7.5, 10% sucrose, 0.1% CHAPS, 120 mM NaCl, and 5 mM DTT) at 37 °C for a predetermined time interval. SDS loading buffer was added to the samples and boiled for 10 mins prior to analysis by 16% SDS-PAGE. The gels were imaged using ChemiDoc™ MP imaging system (Bio-Rad).

4.5.7 Intrinsic Fluorescence Spectroscopy

Caspase-6 tumor-associated variants (3 μM) in 20 mM phosphate buffer, pH 7.5, 120 mM NaCl, and 2 mM DTT were prepared. Fluorescence emission scans (305–400 nm) were collected after excitation at 280 nm or 295 nm using a

J-1500 spectrometer (Jasco) equipped with fluorescence emission monochromator (FMO-522) and detector (FDT-538). The signal was acquired by setting the emission detector at high-tension voltage value of 700 V, the data integration time (D.I.T) to 1 s and data pitch to 1 nm. The bandwidths used for excitation and emission was 2 nm and 10 nm, respectively.

4.5.8 Caspase-6 Full-length Structural Model Generation

The full-length caspase-6 zymogen model (residues 1–293) shown in Figure 4.1B was built from crystal structures of the caspase-6 zymogen. In our model, chain A was derived from PDB code 4iyf (chain A); chain B of this model was derived from PDB code 3NR2 (chain A) as templates. The missing residues ([1–30, 174–186, and 292–293] in PDB code 4iyf (chain A); [1–30, 167–186, 261–271, and 292–293] in PDB code 3NR2 (chain A)) were built by *de novo* modeling using Chimera/Modeller platforms (Pettersen et al., 2004; Webb and Sali, 2014). All illustrations with molecular visualization were generated using the PyMOL Molecular Graphics System (Schrödinger, LLC).

4.6 References

- Barbero, S., A. Mielgo, V. Torres, T. Teitz, D. J. Shields, D. Mikolon, M. Bogoy, D. Barila, J. M. Lahti, D. Schlaepfer, and D. G. Stupack. 2009. Caspase-8 association with the focal adhesion complex promotes tumor cell migration and metastasis. *Cancer Research*, 69:3755-63.
- Bell, B. D., S. Leverrier, B. M. Weist, R. H. Newton, A. F. Arechiga, K. A. Luhrs, N. S. Morrissette, and C. M. Walsh. 2008. FADD and caspase-8 control the outcome of autophagic signaling in proliferating T cells. *Proceedings of the National Academy of Sciences of the United States of America*, 105:16677-82.
- Boatright, K. M., and G. S. Salvesen. 2003. Mechanisms of caspase activation. *Current Opinion in Cell Biology*, 15:725-731.

- Cowling, V., and J. Downward. 2002. Caspase-6 is the direct activator of caspase-8 in the cytochrome c-induced apoptosis pathway- absolute requirement for removal of caspase-6 prodomain. *Cell Death and Differentiation*, 9:1046-1056.
- Devarajan, E., A. A. Sahin, J. S. Chen, R. R. Krishnamurthy, N. Aggarwal, A. M. Brun, A. Sapino, F. Zhang, D. Sharma, X. H. Yang, A. D. Tora, and K. Mehta. 2002. Down-regulation of caspase 3 in breast cancer: a possible mechanism for chemoresistance. *Oncogene*, 21:8843-51.
- Earnshaw, W. C., L. M. Martins, and S. H. Kaufmann. 1999. Mammalian caspases: structure, activation, substrates, and functions during apoptosis. *Annual Review of Biochemistry*, 68:383-424.
- Forbes, S. A., N. Bindal, S. Bamford, C. Cole, C. Y. Kok, D. Beare, M. Jia, R. Shepherd, K. Leung, A. Menzies, J. W. Teague, P. J. Campbell, M. R. Stratton, and P. A. Futreal. 2011. COSMIC: mining complete cancer genomes in the Catalogue of Somatic Mutations in Cancer. *Nucleic Acids Res*, 39:D945-50.
- Frejlich, E., J. Rudno-Rudzinska, K. Janiszewski, L. Salomon, K. Kotulski, O. Pelzer, Z. Grzebieniak, R. Tarnawa, and W. Kielan. 2013. Caspases and their role in gastric cancer. *Adv Clin Exp Med*, 22:593-602.
- Fuentes-Prior, P., and G. S. Salvesen. 2004. The protein structures that shape caspase activity, specificity, activation and inhibition. *Biochem J*, 384:201-32.
- Futreal, P. A., L. Coin, M. Marshall, T. Down, T. Hubbard, R. Wooster, N. Rahman, and M. R. Stratton. 2004. A census of human cancer genes. *Nat Rev Cancer*, 4:177-183.
- Grutter, M. G. 2000. Caspases: key players in programmed cell death. *Current Opinion in Structural Biology*, 10:649-55.
- Hanahan, D., and R. A. Weinberg. 2011. Hallmarks of cancer: the next generation. *Cell*, 144:646-74.
- Hosomi, Y., A. Gemma, Y. Hosoya, M. Nara, T. Okano, K. Takenaka, A. Yoshimura, K. Koizumi, K. Shimizu, and S. Kudoh. 2003. Somatic mutation of the Caspase-5 gene in human lung cancer. *Int J Mol Med*, 12:443-6.
- Inoue, S., G. Browne, G. Melino, and G. M. Cohen. 2009. Ordering of caspases in cells undergoing apoptosis by the intrinsic pathway. *Cell Death Differ*, 16:1053-61.
- Ji, G. H., M. Li, Y. Cui, and J. F. Wang. 2014. The relationship of CASP 8 polymorphism and cancer susceptibility: a meta-analysis. *Cell Mol Biol (Noisy-le-grand)*, 60:20-8.
- Julien, O., M. Zhuang, A. P. Wiita, A. J. O'Donoghue, G. M. Knudsen, C. S. Craik, and J. A. Wells. 2016. Quantitative MS-based enzymology of caspases reveals distinct protein substrate specificities, hierarchies, and cellular roles. *Proceedings of the National Academy of Sciences of the United States of America*, 113:E2001-10.
- Kim, Y. R., K. M. Kim, N. J. Yoo, and S. H. Lee. 2009. Mutational analysis of CASP1, 2, 3, 4, 5, 6, 7, 8, 9, 10, and 14 genes in gastrointestinal stromal tumors. *Hum Pathol*, 40:868-71.

- Klaiman, G., N. Champagne, and A. C. LeBlanc. 2009. Self-activation of Caspase-6 in vitro and in vivo: Caspase-6 activation does not induce cell death in HEK293T cells. *Biochim Biophys Acta*, 1793:592-601.
- Lee, J. W., M. R. Kim, Y. H. Soung, S. W. Nam, S. H. Kim, J. Y. Lee, N. J. Yoo, and S. H. Lee. 2006. Mutational analysis of the CASP6 gene in colorectal and gastric carcinomas. *APMIS*, 114:646-50.
- Liu, B., D. Peng, Y. Lu, W. Jin, and Z. Fan. 2002. A novel single amino acid deletion caspase-8 mutant in cancer cells that lost proapoptotic activity. *J Biol Chem*, 277:30159-64.
- Mandrizzato, S., F. Brasseur, G. Andry, T. Boon, and P. van der Bruggen. 1997. A CASP-8 mutation recognized by cytolytic T lymphocytes on a human head and neck carcinoma. *Journal of Experimental Medicine*, 186:785-93.
- McIlwain, D. R., T. Berger, and T. W. Mak. 2013. Caspase functions in cell death and disease. *Cold Spring Harb Perspect Biol*, 5.
- Nandi, C. L., J. Singh, and J. M. Thornton. 1993. Atomic environments of arginine side chains in proteins. *Protein Engineering*, 6:247-59.
- Park, H. L., A. Ziogas, J. Chang, B. Desai, L. Bessonova, C. Garner, E. Lee, S. L. Neuhausen, S. S. Wang, H. Ma, J. Clague, P. Reynolds, J. V. Lacey, Jr., L. Bernstein, and H. Anton-Culver. 2016. Novel polymorphisms in caspase-8 are associated with breast cancer risk in the California Teachers Study. *BMC Cancer*, 16:14.
- Pettersen, E. F., T. D. Goddard, C. C. Huang, G. S. Couch, D. M. Greenblatt, E. C. Meng, and T. E. Ferrin. 2004. UCSF Chimera--a visualization system for exploratory research and analysis. *J Comput Chem*, 25:1605-12.
- Pop, C., and G. S. Salvesen. 2009. Human caspases: activation, specificity, and regulation. *Journal of Biological Chemistry*, 284:21777-81.
- Ruchaud, S., N. Korfali, P. Villa, T. J. Kottke, C. Dingwall, S. H. Kaufmann, and W. C. Earnshaw. 2002. Caspase-6 gene disruption reveals a requirement for lamin A cleavage in apoptotic chromatin condensation. *EMBO J*, 21:1967-77.
- Senft, J., B. Helfer, and S. M. Frisch. 2007. Caspase-8 interacts with the p85 subunit of phosphatidylinositol 3-kinase to regulate cell adhesion and motility. *Cancer Research*, 67:11505-9.
- Slee, E. A., M. T. Harte, R. M. Kluck, B. B. Wolf, C. A. Casiano, D. D. Newmeyer, H. G. Wang, J. C. Reed, D. W. Nicholson, E. S. Alnemri, D. R. Green, and S. J. Martin. 1999. Ordering the cytochrome c-initiated caspase cascade: hierarchical activation of caspases-2, -3, -6, -7, -8, and -10 in a caspase-9-dependent manner. *J Cell Biol*, 144:281-92.
- Soung, Y. H., E. G. Jeong, C. H. Ahn, S. S. Kim, S. Y. Song, N. J. Yoo, and S. H. Lee. 2008. Mutational analysis of caspase 1, 4, and 5 genes in common human cancers. *Hum Pathol*, 39:895-900.
- Soung, Y. H., J. W. Lee, H. S. Kim, W. S. Park, S. Y. Kim, J. H. Lee, J. Y. Park, Y. G. Cho, C. J. Kim, Y. G. Park, S. W. Nam, S. W. Jeong, S. H. Kim, J. Y. Lee, N. J. Yoo, and S. H. Lee. 2003. Inactivating mutations of CASPASE-7 gene in human cancers. *Oncogene*, 22:8048-52.

- Soung, Y. H., J. W. Lee, S. Y. Kim, J. Jang, Y. G. Park, W. S. Park, S. W. Nam, J. Y. Lee, N. J. Yoo, and S. H. Lee. 2005a. CASPASE-8 gene is inactivated by somatic mutations in gastric carcinomas. *Cancer Res*, 65:815-21.
- . 2005b. CASPASE-8 gene is inactivated by somatic mutations in gastric carcinomas. *Cancer Research*, 65:815-21.
- Soung, Y. H., J. W. Lee, S. Y. Kim, W. S. Park, S. W. Nam, J. Y. Lee, N. J. Yoo, and S. H. Lee. 2004. Somatic mutations of CASP3 gene in human cancers. *Hum Genet*, 115:112-5.
- Srinivasula, S. M., T. Fernandes-Alnemri, J. Zangrilli, N. Robertson, R. C. Armstrong, L. Wang, J. A. Trapani, K. J. Tomaselli, G. Litwack, and E. S. Alnemri. 1996. The Ced-3:Interleukin 1b Converting Enzyme-like Homolog Mch6 and the Lamin-cleaving Enzyme Mch2a Are Substrates for the Apoptotic Mediator CPP32. *The Journal of Biological Chemistry*, 271:27099-27106.
- Stupack, D. G. 2013. Caspase-8 as a Therapeutic Target in Cancer. *Cancer Letters*, 332:133-140.
- Su, H., N. Bidere, L. Zheng, A. Cubre, K. Sakai, J. Dale, L. Salmena, R. Hakem, S. Straus, and M. Lenardo. 2005. Requirement for caspase-8 in NF-kappaB activation by antigen receptor. *Science*, 307:1465-8.
- Suzuki, A., G. Kusakai, A. Kishimoto, Y. Shimojo, S. Miyamoto, T. Ogura, A. Ochiai, and H. Esumi. 2004. Regulation of caspase-6 and FLIP by the AMPK family member ARK5. *Oncogene*, 23:7067-75.
- Talanian, R. V., C. Quinlan, S. Trautz, M. C. Hackett, J. A. Mankovich, D. Banach, T. Ghayur, K. D. Brady, and W. W. Wong. 1997. Substrate specificities of caspase family proteases. *J Biol Chem*, 272:9677-82.
- Vaidya, S., E. M. Velazquez-Delgado, G. Abbruzzese, and J. A. Hardy. 2011. Substrate-induced conformational changes occur in all cleaved forms of caspase-6. *J Mol Biol*, 406:75-91.
- Velazquez-Delgado, E. M., and J. A. Hardy. 2012. Phosphorylation regulates assembly of the caspase-6 substrate-binding groove. *Structure*, 20:742-51.
- Wang, X. J., Q. Cao, X. Liu, K. T. Wang, W. Mi, Y. Zhang, L. F. Li, A. C. LeBlanc, and X. D. Su. 2010. Crystal structures of human caspase 6 reveal a new mechanism for intramolecular cleavage self-activation. *EMBO Rep*, 11:841-7.
- Webb, B., and A. Sali. 2014. Protein structure modeling with MODELLER. *Methods in Molecular Biology*, 1137:1-15.
- Yan, N., and Y. Shi. 2005. Mechanisms of apoptosis through structural biology. *Annu Rev Cell Dev Biol*, 21:35-56.
- Yoo, N. J., J. W. Lee, Y. J. Kim, Y. H. Soung, S. Y. Kim, S. W. Nam, W. S. Park, J. Y. Lee, and S. H. Lee. 2004. Loss of caspase-2, -6 and -7 expression in gastric cancers. *APMIS*, 112:330-5.

CHAPTER 5

PROCASPASE-6 IS INHIBITED BY NUCLEOTIDES AT THE DIMER INTERFACE

This chapter is being prepared for submission as: Eric Okerberg[§], Kevin B. Dagbay[‡], Jennie Green[§], Ishankumar Soni[‡], Tyzoon Nomanbhoy[§], Jeanne A. Hardy[‡] and John Kozarich[§]. Procaspase-6 is inhibited by nucleotides at the dimer interface. KBD performed protein purifications, biochemical assays including mutagenesis, wrote parts of the manuscript and prepared final figures. IS performed protein purification and biochemical assays and prepared final figures. JH directed, edited, and wrote parts of the manuscript. ActivX Biosciences Inc. collaborators performed all mass spectrometry analyses.

Affiliations: [§]ActivX Biosciences, Inc., San Deigo, CA

[‡]Hardy Lab, University of Massachusetts Amherst

5.1 Introduction

Caspases are cysteine aspartate proteases that are associated with diverse cellular functions including apoptosis, inflammation and more recently in neurodegeneration (for reviews see (Friedlander 2003; Wang et al., 2014; Wellington and Hayden, 2000)). In terms of function and length of the prodomain, caspases are grouped into initiators (caspase-2, -8, and -9) and executioners (caspase-3, -6, and -7) of programmed cell death (Nicholson, 1999). Caspases are expressed as inactive zymogens (procaspases) that comprise prodomain, large and small subunits connected by an intersubunit linker region. Canonical procaspase activation requires a series of proteolytic cleavages at conserved aspartate residues between the prodomain and large subunit and in the intersubunit linker region. During procaspase-6 activation, cleavage at the intersubunit linker (Asp-D193) is the critical step in transformation of procaspase-6 to active caspase-6. Subsequent cleavages in the prodomain (Asp-23) and at the Asp-179 site in the linker region generate a fully cleaved and mature

caspase-6. While procaspase-6 is unable to cleave other cellular targets, it appears to be able to cleave the prodomain, even in the zymogen state (Velazquez-Delgado and Hardy, 2012). Procaspase-6 is also the only caspase for which a mechanism for self-activation, a noncanonical route for caspase activation, has been elucidated (Klaiman et al., 2009; Wang et al., 2010). Because procaspase-6 has longer loop 2 (L2) compared with the other caspases, the scissile peptide bond between the Asp-193 and Ala-194 within the intersubunit linker—a contiguous part of L2—sits close to the active site Cys-163 and can then be primed for hydrolysis by intramolecular self-cleavage. In fact, shortening the length of L2 has been shown to abolish the capability of procaspase-6 to auto activate, underscoring the critical role of the longer L2 in procaspase-6 self-activation (Wang et al., 2010).

Notable functions of caspase-6 are highlighted in its role in axonal degeneration in amyloid precursor protein-mediated death receptor 6 signaling (Nikolaev et al., 2009), disruption of neuronal cytoskeleton (Klaiman et al., 2008), and its abundance in neuropathological lesions in the brains of patients with Alzheimer's disease (AD) (Albrecht et al., 2007; Guo et al., 2004). In addition, caspase-6 has also been shown to cleave polyglutamine expanded Huntingtin protein, one of the contributing factors in the onset of Huntington's disease (Graham et al., 2010; Riechers et al., 2016; Warby et al., 2008). Thus, understanding the intricate mechanisms of how caspases are activated and regulated are essential to unraveling strategies to control its multifaceted disease-related functions.

A number of years ago, a cavity was discovered at the dimer interface of caspase-3 and -7 that can be allosterically inhibited by non-native small molecules (Figure 5.1) (Hardy et al., 2004; Hardy and Wells, 2009) This cavity is also present and can be inhibited in caspase-1 (Scheer et al., 2006) and caspase-6 (Dagbay et al., 2014). While the volume, depth and ratio of hydrophobic and polar residues suggests that this cavity is a small molecule-binding site; no natural, native ligand(s) for this cavity have previously been reported. In this work, we identify a class of ligands, specifically, naturally occurring nucleotides that bind to and inhibit procaspase-6 in this region of the procaspase-6, at the dimer interface.

5.2 Results

5.2.1 Procaspase-6 is Robustly Labeled by the ActivX ATP Acyl Phosphate Probe

ActivX Pharmaceuticals has developed a series of nucleotide-based, biotinylated, acyl phosphate probes that have been used to identify several nucleotide-binding proteins (Patricelli et al., 2011; Patricelli et al., 2007). These probes function by binding to nucleotide binding sites and allowing proximity-induced nucleophilic attack at the highly reactive acyl phosphate group, thus forming a covalent bond between the protein and the biotinylated portion of the probe, which can then be enriched using a streptavidin-coated solid support or digested with a protease and identify the labeled peptides using LC-MS/MS. The ATP-based acyl phosphate probe (Figure 5.2A) has been particularly useful for identifying kinases

(Patricelli et al., 2007; Rosenblum et al., 2013). We undertook an unbiased screen for ATP binding proteins. Procaspase-6 was identified as a robust ATP-probe binder, with levels of isolated procaspase-6 being roughly equivalent to levels of many confirmed ATP-binding proteins, including kinases. Using MS/MS we identified Lys-133 as the probe-labeled residue (Figure 5.2B). Lys-133 is in the 130's region of procaspase-6. To confirm that procaspase-6 was indeed bound by the ATP acyl phosphate probe, apoptosis was induced in Jurkat cells with the α -FAS antibody. In lysates from resting cells procaspase-6 predominated, whereas in apoptotic cells, predominantly cleaved (active) caspase-6 was observed by caspase-6 immunoblotting (Figure 5.2B). These same lysates were also treated with the biotinylated ATP acyl phosphate probes. Whereas high levels of procaspase-6 were isolated from resting cells, far less procaspase-6 was isolated from apoptotic cells (Figure 5.2B), further indicating that procaspase-6 was the main caspase-6 cleavage state identified by the ATP probe, and suggesting that ATP may be a *bona fide* binder of procaspase-6. To examine the relative preference of procaspase-6 for ATP, relative to other nucleotides, we undertook a competition strategy. Jurkat cell lysates were treated with the ATP probe and then challenged with 1 mM of various nucleotides (Figure 5.2D). The amount of procaspase-6 labeled by the ATP probe was then quantified using LC-MS/MS. ATP, ADP and NADP⁺ were most effective competitors with the ATP probe labeling. CTP and GTP also showed significant inhibition of probe labeling. Together these data suggest that several nucleotides may be able to bind procaspase-6, and potentially implicating the

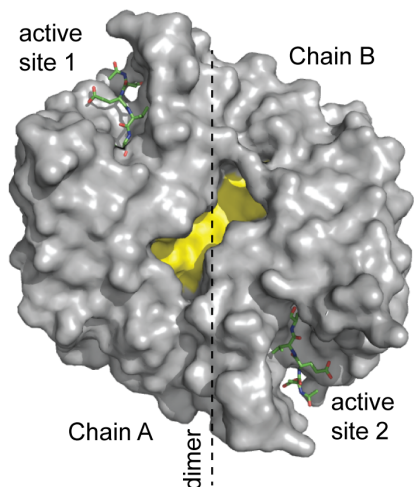
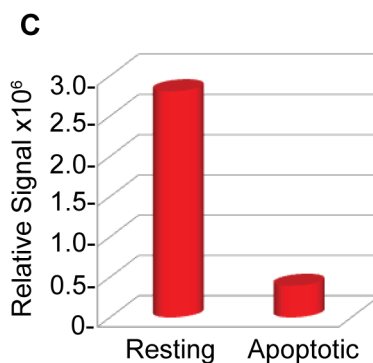
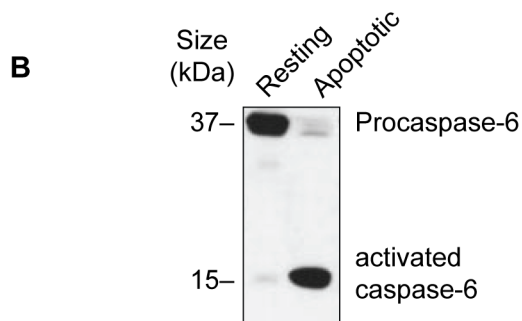
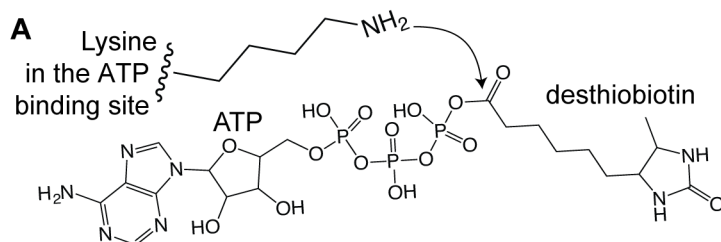


Figure 5.1 An Allosteric Site Exists at the Dimer Interface of Caspases

The cavity at the dimer interface of caspase-3 and -7 can be allosterically inhibited by non-native small molecules (Hardy et al., 2004; Hardy and Wells, 2009). The natural ligand for this cavity has not previously been reported.

Figure 5.2 The ActivX ATP Acyl Phosphate Probe Binds Lys-133 in Procaspase-6

(A) The acyl phosphate in the ActivX desthiobiotin-ATP probe is reactive toward nucleophilic attack by lysine. Using biotin labeling, procaspase-6 was isolated. By mass-spectrometry Lys-133 was identified as being covalently modified by the ATP-probe. (B) Apoptosis was induced in Jurkat cells by addition of the α -FAS antibody. Samples were examined with the α -caspase 6 antibody by immunoblot. Resting cells expressed predominantly procaspase-6, whereas cells induced to undergo apoptosis showed pool of active caspase-6. (C) Resting Jurkat cells, or cells



D

Competitor	% Inhibition
ATP	95
ADP	95
AMP	57
CTP	83
GTP	72
UTP	37
NADH	24
NAD ⁺	56
NADPH	58
NAD ⁺	99

induced to apoptosis by addition of α -FAS antibody were treated with the ActivX desthiobiotin ATP probe. Biotinylated proteins were isolated by streptavidin capture and analyzed by mass spectrometry. The relative signal for procaspase-6 was significantly greater in resting cells than in apoptotic cells. (D) A panel of naturally occurring nucleotides was used to compete with the ActivX ATP probe for binding and labeling of procaspase-6 in Jurkat cell lysates. Percentage inhibition refers to the level of inhibition of probe labeling of procaspase-6.

phosphate or deoxyribose moieties as playing a significant role in procaspase-6 binding.

5.2.2 Procaspase-6 Self-Processing is Inhibited by ATP

Given that ATP-based probes robustly label procaspase-6 it seems plausible that ATP would impact some step in procaspase-6 function. A main function of procaspase-6 is self-processing. We routinely use a C-terminal His₆ tag for isolating active caspase-6. This construct was not appropriate for isolating procaspase-6 because it repeatedly resulted in predominantly active (cleaved) caspase-6. Using a new *N*-terminally His₆ construct, we were able to isolate a nearly homogeneous preparation of procaspase-6 (Figure 5.3A). Procaspase-6 was incubated from 0–8 hours in the presence or absence of 20 mM ATP. At this concentration of ATP, cleavage of procaspase-6 was significantly impeded. Similarly, when procaspase-6 was incubated with increasing concentrations of ATP, it became clear that ATP inhibits procaspase-6 processing in a concentration-dependent manner (Figure 5.3B) with an IC₅₀ of 19 ± 0.8 mM (Figure 5.3C). Conversely, the activity of mature caspase-6 is not affected by increasing concentrations of ATP (Figure 5.3D). From these analyses, procaspase-6 is sensitive to the presence of ATP, which inhibits self-processing, but that the activity of mature caspase-6 is not ATP-sensitive.

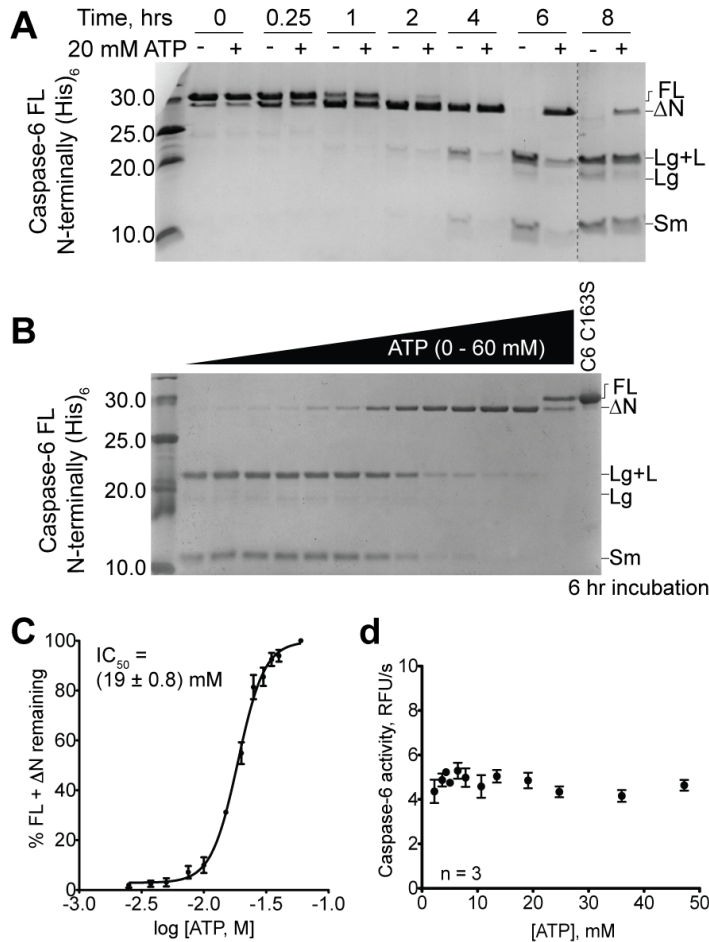


Figure 5.3 ATP Attenuates the Procaspase-6 Activity But Not Caspase-6 Activity

(A) Self-proteolysis of procaspase-6 analog (caspase-6 FL N-terminally (His)₆) in the absence and presence of 20 mM ATP at 37 °C at different time intervals (hr: 0, 0.25, 1, 2, 4, 6, and 8). Increasing incubation time promotes self-activation of procaspase-6 resulting into large and small subunits appearance. The abbreviations (FL: full-length, ΔN: without pro-domain, Lg+L: large subunit attached to linker, Lg: large subunit, and Sm: small subunit) are shown in the figure. After 6 hr of incubation, the pro-domain is fully cleaved in the

presence of ATP while intact in the absence of ATP. (B) Self-proteolysis of caspase-6 FL N-terminally (His)₆ at 6 hr incubation at 37 °C in the presence of various ATP concentrations (mM: 0, 2.5, 3.75, 5, 7.5, 10, 15, 20, 25, 30, 35, 40, 60). (C) The percent remaining band intensities of (FL+ΔN) with respect to Lg+L, Lg, and Sm band intensities were plotted against various Log [ATP, M] to determine the IC₅₀ value. ATP inhibits procaspase-6 activity with an IC₅₀ value of (19 ± 0.8) mM. (D) Caspase-6 activity (RFU/s) vs [ATP, mM].

(A) Self-proteolysis of procaspase-6 analog (caspase-6 FL N-terminally (His)₆) in the absence and presence of 20 mM ATP at 37 °C at different time intervals (hr: 0, 0.25, 1, 2, 4, 6, and 8). Increasing incubation time promotes self-activation of procaspase-6 resulting into large and small subunits appearance. The abbreviations (FL: full-length, ΔN: without pro-domain, Lg+L: large subunit attached to linker, Lg: large subunit, and Sm: small subunit) are shown in the figure. After 6 hr of incubation, the pro-domain is fully cleaved in the presence of ATP while intact in the absence of ATP. (B) Self-proteolysis of caspase-6 FL N-terminally (His)₆ at 6 hr incubation at 37 °C in the presence of various ATP concentrations (mM: 0, 2.5, 3.75, 5, 7.5, 10, 15, 20, 25, 30, 35, 40, 60). (C) The percent remaining band intensities of (FL+ΔN) with respect to Lg+L, Lg, and Sm band intensities were plotted against various Log [ATP, M] to determine the IC₅₀ value. ATP inhibits procaspase-6 activity with an IC₅₀ value of (19 ± 0.8) mM. (D) Caspase-6 activity (RFU/s) vs [ATP, mM].

5.2.3 ATP Binds Procaspase-6 at Y198

The cavity at the dimer interface of procaspase-6 (Figure 5.4A) is like that observed in other caspases (Figure 5.1). In addition to FICA and DICA which bind to the dimer interfaces of caspase-3, -7 (Hardy et al., 2004; Hardy and

Wells, 2009) and -6 (Dagbay et al., 2014), compound 3, an amino-substituted isoquinolinone also binds in this region (Figure 5.5) and is a nanomolar affinity binder of procaspase-6 (Murray et al., 2014). Compound 3 engages Y198 to bind to this cavity. Given that both ATP and compound 3 share similarity in the arrangements of their rings, we reasoned that ATP might bind at the same location as compound 3 (Figure 5.4B). To test this hypothesis, we prepared the Y198A version of caspase-6. This substitution had no impact on catalytic activity of the mature form of the enzyme (Figure 5.4D) suggesting that this mutation does not negatively impact either the structure or the function of the enzyme. In contrast, Y198A had dramatic impacts on the ability of the ATP probe to label procaspase-6. Caspase-6 variants were overexpressed in *E. coli* and lysates were exposed to the ATP probe. WT caspase-6 is fully processed and mature under the expression conditions tested. Mature caspase-6 show very little probe labeling (0.9%, Figure 5.4C). C163S variant, which allows expression of full-length but inactive procaspase-6 zymogen, was fully labeled. When Y198A is introduced in the presence of C163S, full-length zymogen was observed, but this protein was no longer competent to be labeled by the ATP probe. The Y198A variant could also not be labeled by the ATP probe, however this is likely because Y198A is fully processed to the mature form (Figure 5.5). Likewise, for the S257D variant in which approximately half of the enzyme is in the uncleaved zymogen state and half is in the mature cleaved state, only 42% of the sample is competent for

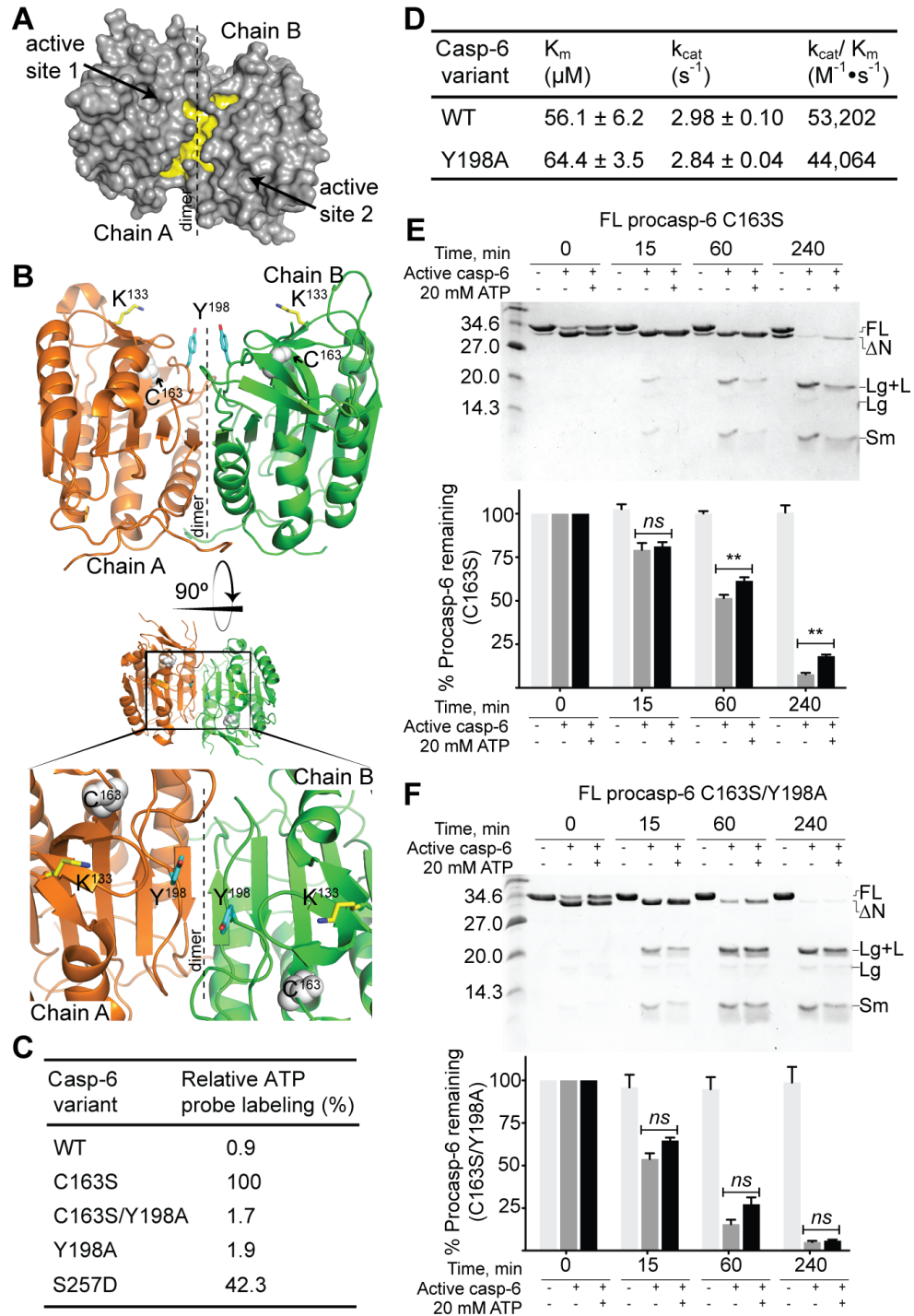


Figure 5.4 Tyr-198 of Procaspase-6 is a Putative Binding Site for ATP Acyl Phosphate Probe and ATP

(A) The surface representation of procaspase-6 (PBD code 3NR2) highlights the cavity (yellow) within the dimer interface, a putative nucleotide-binding site. (B) The dimer interface of procaspase-6 shows the ATP acyl phosphate probe-labeling site (Lys-133) near the active site Cys-163. The two Tyr-198 residues

from each monomer of procaspase-6 form a pi stack within the dimer interface that is essential for ATP acyl phosphate probe binding. (C) Percent relative ATP acyl phosphate probe labeling of cleaved and active caspase-6 (WT and Y198A), catalytically inactive FL caspase-6 S257D, and FL procaspase-6 variants (C163S, C163S/Y198A) in bacterial cell lysate. (D) The kinetic parameters of cleaved and active caspase-6 Y198A is similar to the WT suggest that Tyr-198 site is orthogonal to the active site. The values are reported as mean \pm s.e.m of two independent trials performed on two separate days. (E) FL procaspase-6 C163S and (F) FL procaspase-6 C163S/Y198A were incubated with 10% active caspase-6 in the presence or absence of 20 mM ATP at 37 °C at different time intervals (min: 0, 15, 60, 240). The band intensities of FL procaspase-6 C163S and FL procaspase-6 C163S/Y198A were quantified and set at 100%. The extent of cleavage with or without ATP was reported as percent procaspase-6 remaining at each time point. Error bars represent mean \pm s.e.m of five independent experiments. Statistical analysis was performed using Mann-Whitney t-test (two-tailed): ns, not significant ($P > 0.05$), ** $P < 0.05$.

To date, it has been impossible to express and purify uncleaved Y198A with the active site cysteine intact. We hypothesize that Y198A is more active for self-processing because critical π stacking interactions between Y198 and residues in the intersubunit linker are lost. Loss of these interactions increases flexibility in the procaspase-6 substrate binding groove and active site loop bundle easing self-activation. Due to this hyperactivity in Y198A procaspase-6 toward intra bacterial cell processing upon overexpression, even with 10-minute low temperature inductions, it has been impossible to test the impact of ATP on self-processing of Y198A procaspase-6. Nevertheless, we have observed that ATP significantly slows the processing of FL procaspase-6 C163S catalytically inactive variant by WT caspase-6 (Figure 5.4E). On the other hand, ATP does not impact caspase-6 mediated cleavage of FL procaspase-6 C163S/Y198A (Figure 5.5.4F), suggesting that Y198 is a critical residue for mediating ATP-binding and inhibition.

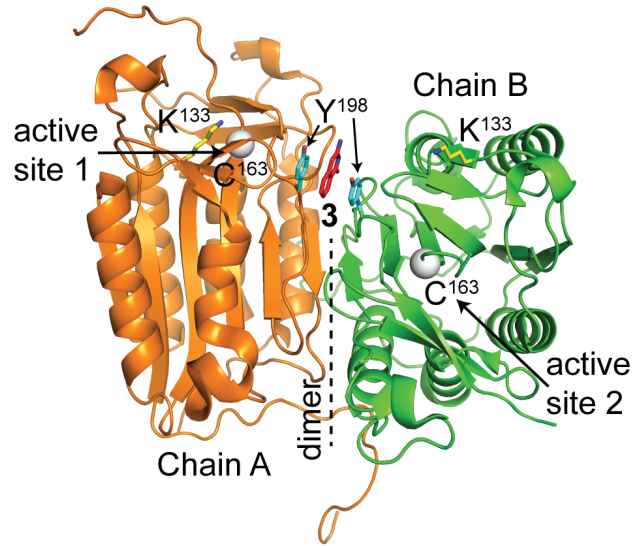


Figure 5.5 The Crystal Structure of Procaspase-6 Bound to Compound 3

Allosteric caspase-6 binder compound 3 (red) is sandwiched at the dimer interface between Lys-198 (cyan) from each monomer of a dimeric procaspase-6 (PDB code 4N6G). Fragment 3 was identified from a fragment-merging strategy that generated nanomolar-affinity ligands of procaspase-6 (Murray et al., 2014).

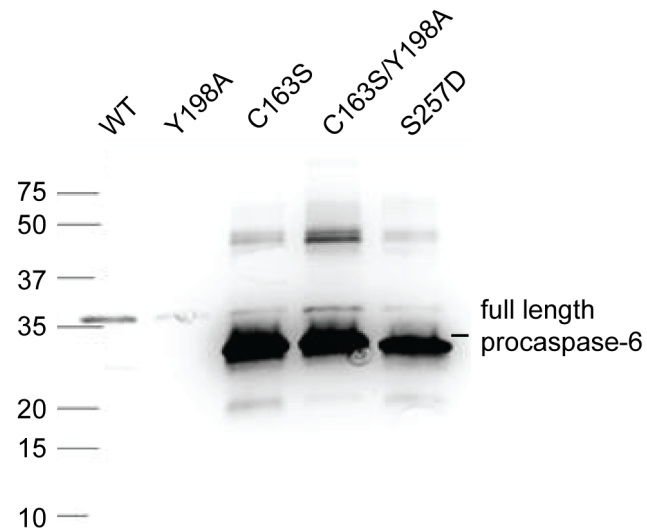


Figure 5.6 Caspase-6 Variants Showed Variation in Cleavage Patterns Dependent on its Activation State

Caspase-6 variants were expressed in *E. coli* and lysed and analyzed by immunoblotting using anti- α -caspase-6 antibody. WT and Y198A are active caspase-6 variants while C163S and C163S/Y198A are catalytically inactive variants of procaspase-6. S257D is an inactivating mutation that mimics a phosphorylated form of caspase-6 at position 257.

5.2.4 Multiple Nucleotides Inhibit Procaspase-6

While it is clear that ATP inhibits procaspase-6 self-processing by a mechanism that involves Y198, it is not clear that *a priori* that ATP is the most significant nucleotide regulator of procaspase-6 activity intracellularly. We reasoned that the nucleotides that exhibit the strongest IC₅₀ relative to their intracellular concentration are likely to serve as the most important small molecule regulators of procaspase-6. Based on their ability to prevent ATP probe binding (Figure 5.4C), we assessed the ability of ATP, dATP, GTP and the dinucleotide, Ap4A. Ap4A is synthesized in cells in response to various cellular stresses including DNA damage (Marriott et al., 2015) and apoptosis (Vartanian et al., 1999; Vartanian et al., 2003) and is recognized as a pleiotropically-acting alarmone in cells (Bochner et al., 1984; Varshavsky, 1983). These nucleotides inhibit procaspase-6 (Figure 5.7) at levels approximately two-fold (for ATP and GTP), 50-fold (for dATP), and 10-fold (for Ap4A) above the reported intracellular concentrations (Chandra et al., 2006; Mesner et al., 1999; Rapaport and Zamecnik, 1976). Although it is clear that ATP binds at the procaspase-6 dimer interface and impacts function, it is not yet clear which nucleotides are most critical for regulating caspase-6 function at what intracellular location and at what stage(s) of the caspase-6 lifecycle.

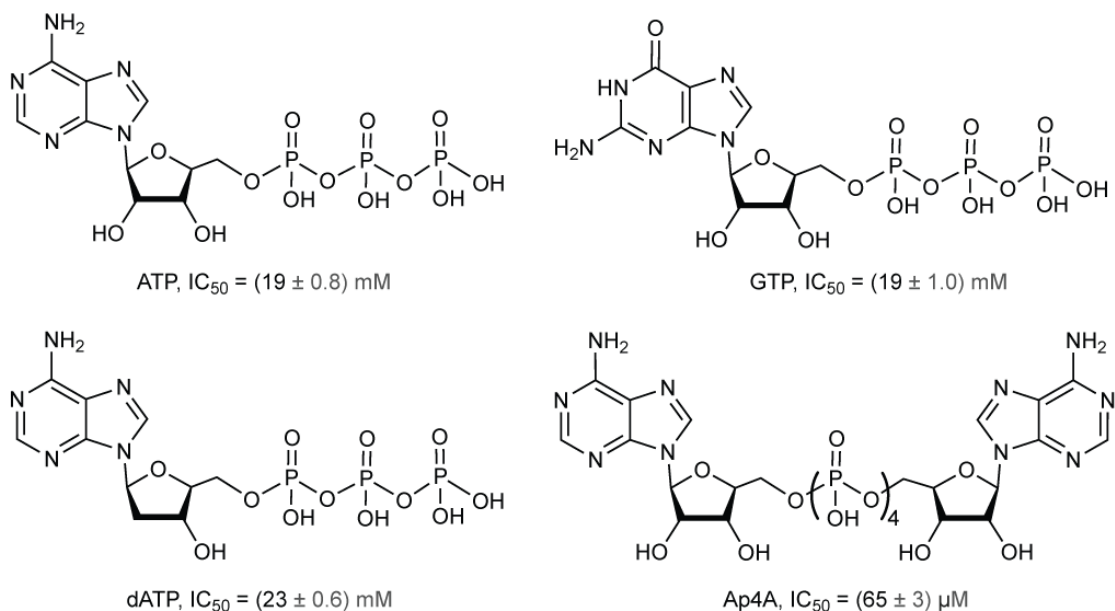


Figure 5.7 Structures of Small-Molecule Metabolites.

The structures of small-molecule metabolites (ATP, dATP, GTP, and Ap4A) are given along with their IC₅₀ values with respect to the self-proteolysis of procaspase-6 *in vitro*.

ATP probe labeling.

5.3 Discussion

Caspases are important mediators of key cellular process including apoptosis, inflammation and in several disease-related pathways. Thus, dissecting the molecular details of each caspase function and regulation is crucial to the understanding of caspase-associated signaling that is relevant in maintaining cellular homeostasis as well as in the molecular evolution of a disease phenotype. Here we show that a set of nucleotides can bind and inhibit procaspase-6 self-activation. Specifically, the dimer interface residue Lys-198 is found to be critical in ATP binding in procaspase-6. The binding of cellular

nucleotide ligands to procaspase-6 represents one direct regulatory route of caspase-6 activation of which cellular consequences are yet to be determined.

Nanomolar-affinity binders of procaspase-6 identified from fragment-merging strategy have recently been reported (Murray et al., 2014). The crystal structures of procaspase-6 with several nanomolar binders, including compound 3, revealed the same binding site as the identified ATP binding site in procaspase-6 reported in this work. Moreover, small molecule thiol-containing inhibitors of caspase-3 and caspase-7 discovered through tethering approach (Hardy et al., 2004; Hardy and Wells, 2009) bind to the homologous dimer interface region in procaspase-6. Thus, the propensity of the dimer interface of caspases to bind to native and non-native small molecules and negatively impacts its activity indicates that this site is regulatory and possibly utilized by caspases in cells.

The Tyr-198 nucleotide-binding site in procaspase-6 is moderately conserved; only caspase-4 and caspase-7 to have tyrosine in the homologous position. Together with the possible electrostatic interactions due to the presence of the phosphate groups, the proposed interaction of nucleotides to Tyr-198 sites in procaspase-6 is predominantly through pi-pi stacking as adenine in ATP showed molecular resemblance to compound 3 (Figure 5.5). In the absence of co-crystal structures of procaspase-6/nucleotide complex, we can only propose a possible regulatory mechanism. Nucleotide binders, like compound 3, may regulate procaspase-6 activity by locking L2 in the inactive helical conformation, thus stabilizing the less active procaspase-6 conformation (Murray et al., 2014).

Although the dimer interface may be utilized by some caspases as a regulatory allosteric site, the type of interaction networks may significantly be divergent. The binding of FICA and DICA to caspase-7 (Hardy et al., 2004) showed a different type of interaction networks where two FICA molecules fill the central cavity in a planar, edge-to-edge network with Tyr-223. On the other hand, DICA interacts with Tyr-223 in *cis*-type network packing its aromatic ring against the wall of the dimer cavity. Both regulatory interaction networks in FICA and DICA trapped mature caspase-6 in the zymogen-like conformation. Together, the accessibility of the caspase dimer interface by small molecules along with its unique regulatory network of interactions suggest that various types of cellular activators or inhibitors could bind to this region and may associate caspases to its diverse and some are yet unknown apoptotic and nonapoptotic functions.

The Tyr-198 pi-pi stacking interaction is only found in the procaspase-6 form. While the Tyr-198 is buried in the dimer interface of procaspase-6 (Wang et al., 2010), this same Tyr-198 residue is exposed to the solvent upon proteolytic activation of caspase-6 (Baumgartner et al., 2009; Vaidya et al., 2011). Evidently, ATP binds procaspase-6 but not mature caspase-6 suggesting that nucleotide binding to procaspase-6 is conformation-specific. Thus, the impact of nucleotide binding is less pronounced for already activated caspase-6 and may insinuate that the regulatory roles of nucleotides are less effective in the signaling cascade where the proteolytic activity of caspase-6 is already in effect.

Several open questions about nucleotide-mediated inhibition of procaspase-6 beg to be addressed: First, under what cellular conditions

procaspase-6 binding to nucleotides is occurring. Second, what concentrations of which specific nucleotides modulate which specific cellular responses. Generally, an increase in the concentration of endogenous nucleotides is thought to be a prosurvival mechanism in cells (Chandra et al., 2006). This idea is supported by other cellular systems where an increased in the endogenous nucleotide levels up to 17-fold above normal promotes survival in response to DNA damage in yeast (Chabes et al., 2003) as well as it promotes proliferation and survival in T lymphocytes (Quemeneur et al., 2003). Likewise, increasing the pool of nucleotides by overexpression of thymidine kinases involved in the *de novo* synthesis of nucleotides (Grusch et al., 2001; Oliver et al., 1997) or exogenous addition of nucleotide precursors (Kelly et al., 2001), promotes resistance to apoptosis. This prosurvival mechanism stems from the direct interference of the cytochrome c binding to Apaf-1 at high nucleotide concentrations, thus prevents apoptosome formation (Chandra et al., 2006), an upstream event in the apoptotic cascade. Moreover, at an ATP concentration greater than 1 mM, caspase-9 function is negatively regulated via direct binding (Chereau et al., 2005). Thus, the high nucleotide concentrations exceeding that of the normal levels during specific cellular response presents a recurring cellular condition that results in the shutdown of the general apoptotic machineries, including caspases. In this work, the inhibition of procaspase-6 at 2-fold higher than normal concentration of nucleotides (GTP and ATP) may suggests an inhibitory effect of these nucleotides in the apoptotic function of caspase-6. While it is clear that

metabolism and apoptosis are highly interconnected, this an example of a class of small-molecule metabolites directly impacting the function of a procaspase.

5.4 Materials and Methods

5.4.1 Generation of Caspase Variants

The full-length wild-type (FL WT) caspase-6 used in this study was derived from a synthetic, *E. coli* codon-optimized (His)₆ C-terminally tagged caspase-6 gene (Celtek Bioscience) that was ligated into the NdeI/BamHI sites of pET11a vector. Caspase-6 variants (C163S, S257D, Y198A, C163S/Y198A) as well as the N-terminally (His)₆ tagged FL casp-6 were generated using Phusion® site-directed mutagenesis (Thermo Scientific™) in the FL WT caspase-6 construct. Fully cleaved and active caspase-6 was also used in a form of a constitutive two-chain (CT) (Vaidya et al., 2011), which was designed to independently express the large and the small subunits of caspase-6 with the prodomain (residues 1-23) and linker (residues 180-193) removed.

5.4.2 Caspase Protein Expression and Purification

All caspase-6 constructs used in this study were transformed into the BL21(DE3) T7 express strain of *E. coli* (NEB). Overnight seed cultures were initially grown in 2×YT media supplemented with 0.1 mg/mL ampicillin (Sigma) at 37°C. Dense cultures were then diluted 1000-fold with 2×YT media containing 0.1 mg/mL ampicillin at 37 °C until A₆₀₀ reached 0.6. For the following caspase-6

variants: FL procaspase-6 C163S (active-site knockout), FL procaspase-6 C163S/Y198A, FL S257D, FL Y198A, protein expression was induced by addition of 1 mM IPTG (Anatrace) at 20°C for 18 h. Cells were centrifuged at 4,700 x g for 10 min at 4°C and stored at -20°C until use. Freeze-thawed cells were lysed using a microfluidizer (Microfluidics, Inc.) in ice-cold lysis buffer (50 mM Tris, pH 8.5, 300 mM NaCl, 5% glycerol, 50 mM imidazole) and centrifuged at 30,600 x g for 1 hour at 4 °C. The supernatant was loaded into a 5-mL HiTrap nickel-affinity column (GE Healthcare) and washed with lysis buffer until the absorbance returned to baseline. The protein was eluted with elution buffer (50 mM Tris, pH 8.5, 300 mM NaCl, 5% glycerol, 250 mM imidazole) and diluted 5-fold with buffer A (20 mM Tris, pH 8.5, 2 mM DTT) to reduce the salt concentration. This protein sample was then loaded into a 5-mL HiTrap Q HP column (GE Healthcare). The column was developed with a linear NaCl gradient and the protein was eluted in 20 mM Tris, pH 8.5, 200 mM NaCl, 2 mM DTT. This eluted protein was stored at -80 °C until use. The purified caspases were analyzed by SDS-PAGE to confirm identity and purity.

The expression and purification of the catalytically competent, N-terminally (His)₆ tagged procaspase-6 was similar to the expression and purification of other caspase-6 variants described above except that the induction with 1 mM IPTG was at 25°C for 30 min. The buffer systems for protein purification have been slightly modified to optimize the production of the zymogen form of the enzyme. The lysis and elution buffer components were similar except that the pH of both buffer solutions was adjusted to pH 9 and DTT was excluded.

5.4.3 ATP Probe Labeling and Mass Spectrometry

Caspase-6 variants (WT, Y198A, C163S, C163S/Y198A, S257D) were expressed in *E. coli* BL21(DE3) cells (NEB). The samples were lysed and prepared for ATP acyl phosphate probe labeling and mass spectrometric analyses as described elsewhere (Patricelli et al., 2011; Patricelli et al., 2007).

5.4.4 Caspase Activity Assays

To measure caspase activity, 100 nM purified caspase was assayed over 7 min at 37°C in casp-6 activity assay buffer (100 mM HEPES, 120 mM NaCl, 0.1% CHAPS, 10% sucrose, 5 mM DTT). For substrate titration, a range of 0-500 μ M fluorogenic substrate VEID-AMC [*N*-acetyl-Val-Glu-Ile-Asp-(7-amino-4-methyl-coumarin), Enzo Life Sciences Inc.] was used. Fluorescence kinetic measurements ($\lambda_{\text{ex}}/\lambda_{\text{em}}$: 365nm/495nm) were performed in three independent trials on three different days in 100- μ L reactions in a 96-well format using a microplate reader (SpectraMax M5, Molecular Devices). Initial velocities versus substrate concentration were fit to a rectangular hyperbola using GraphPad Prism (GraphPad Software, San Diego, USA) to determine the kinetic parameters K_M and k_{cat} . Enzyme concentrations were determined by active-site titration with the quantitative covalent inhibitor VEID-CHO (N-Acetyl-Val-Glu-Ile-Asp-aldehyde; Enzo Life Sciences Inc.). Protein was added to inhibitor solvated in DMSO in 96-wells V-bottom plates at room temperature for 1.5 hours in caspase activity assay buffer. Aliquots (90 μ L) were transferred in duplicate to black-well plates and assayed with 50-fold molar excess of substrate. The protein

concentration was determined to be the lowest concentration at which full inhibition was observed and was thus used to calculate k_{cat} .

5.4.5 Effect of ATP on the Activity of Cleaved and Active Caspase-6

Cleaved and active caspase-6 Δ N D179CT (20 nM) was incubated with increasing concentration of ATP (Fisher Scientific, S25123) (0–40 mM, 1.5-fold dilution) in caspase-6 activity assay buffer (100 mM HEPES pH 7.5, 10% sucrose, 0.1% CHAPS, 120 mM NaCl, and 5 mM DTT) at 37 °C for 1.5 h. VEID-AMC fluorescent substrate (Enzo Life Sciences Inc.) was then added to a final concentration of 60 μ M. The final volume was 30 μ L in a 384-well black flat bottom plate (BD Falcon™). Fluorescent kinetic measurements ($\lambda_{ex}/\lambda_{em}$: 365nm/495nm) were performed over 7-min and the initial velocities were calculated. The data was presented as percent activity of caspase-6 setting the buffer-only control as 100%. The data represent an average of two independent experiments (each run in duplicate) and the reported errors represent S.E.M.

5.4.6 Effect of ATP on the Proteolytic Cleavage of Procaspase-6 by Active Caspase-6

To assess the susceptibility of full-length (FL) inactive procaspase-6 C163S and procaspase-6 C163S/Y198A to cleavage by fully cleaved and active caspase-6 (Δ N D179CT) in the presence or absence of 20 mM ATP, 3 μ M of each procaspase-6 variant was incubated with 0.3 μ M of active caspase-6 in caspase-6 assay buffer (100 mM HEPES pH 7.5, 10% sucrose, 0.1% CHAPS,

120 mM NaCl, and 5 mM DTT) with or without 20 mM ATP at 37°C for a specified time interval (hrs: 0, 0.25, 1, 4). At each time point, SDS loading buffer were added to the sample and boiled for 10 mins, then analyzed by 16% SDS-PAGE to determine effect of ATP on the extent of cleavage of procaspase-6 variants by active caspase-6. The gels were imaged using ChemiDoc™ MP imaging system (Bio-rad) and band intensities were quantified using Image Lab software (Bio-rad). The intensities of full-length procaspase-6 C163S and full-length procaspase-6 C163S/Y198A were set at 100% and extent of cleavage with or without ATP were reported as percent procaspase-6 remaining at each time point. The average of 5 independent trials was reported. Statistical analysis was performed using Mann-Whitney t-test (two-tailed) to determine if ATP has significant effect on the proteolytic cleavage of procaspase-6 variants by active caspase-6.

5.4.7 Effect of Nucleotides on the Self-Activation of Caspase-6

Catalytically competent procaspase-6 (3 μM) was incubated with varying concentrations of ATP (0–60 mM), dATP (0–60 mM, Alfa Aesar™, J64045), GTP (0–60 mM, Sigma-Aldrich, 10106399001), and Ap4A (0–10 mM), Sigma-Aldrich, D1262) in caspase-6 assay buffer (100 mM HEPES pH 7.5, 10% sucrose, 0.1% CHAPS, 120 mM NaCl, and 5 mM DTT) at 37°C for 6 h. SDS loading buffer were added to the sample and boiled for 10 mins and analyzed by 16% SDS-PAGE. The gels were imaged using ChemiDoc™ MP imaging system (Bio-rad) and band intensities were quantified using Image Lab software (Bio-rad). The

intensities of full-length procaspase-6 was set at 100% and extent of cleavage with varying nucleotides concentration was reported as percent procaspase-6 remaining. The IC₅₀ values were determined using nonlinear curve-fitting algorithm (four-parameter equation) in GraphPad Prism (GraphPad Software, San Diego, USA).

A time-point experiment (hrs: 0, 0.25, 1, 2, 4, 6, 8) was also performed to assess the extent of procaspase-6 activation in the presence or absence of 20 mM ATP.

5.5 References

- Albrecht, S., M. Bourdeau, D. Bennett, E. J. Mufson, M. Bhattacharjee, and A. C. LeBlanc. 2007. Activation of caspase-6 in aging and mild cognitive impairment. *Am J Pathol*, 170:1200-9.
- Baumgartner, R., G. Meder, C. Briand, A. Decock, A. D'Arcy, U. Hassiepen, R. Morse, and M. Renatus. 2009. The crystal structure of caspase-6, a selective effector of axonal degeneration. *Biochem J*, 423:429-39.
- Bochner, B. R., P. C. Lee, S. W. Wilson, C. W. Cutler, and B. N. Ames. 1984. AppppA and related adenylylated nucleotides are synthesized as a consequence of oxidation stress. *Cell*, 37:225-32.
- Chabes, A., B. Georgieva, V. Domkin, X. Zhao, R. Rothstein, and L. Thelander. 2003. Survival of DNA damage in yeast directly depends on increased dNTP levels allowed by relaxed feedback inhibition of ribonucleotide reductase. *Cell*, 112:391-401.
- Chandra, D., S. B. Bratton, M. D. Person, Y. Tian, A. G. Martin, M. Ayres, H. O. Fearnhead, V. Gandhi, and D. G. Tang. 2006. Intracellular nucleotides act as critical prosurvival factors by binding to cytochrome C and inhibiting apoptosome. *Cell*, 125:1333-46.
- Chereau, D., H. Zou, A. P. Spada, and J. C. Wu. 2005. A nucleotide binding site in caspase-9 regulates apoptosome activation. *Biochemistry*, 44:4971-6.
- Dagbay, K., S. J. Eron, B. P. Serrano, E. M. Velazquez-Delgado, Y. Zhao, D. Lin, S. Vaidya, and J. A. Hardy. 2014. A multipronged approach for compiling a global map of allosteric regulation in the apoptotic caspases. *Methods Enzymol*, 544:215-49.
- Friedlander, R. M. 2003. Apoptosis and Caspases in Neurodegenerative Diseases. *New England Journal of Medicine*, 348:1365-1375.

- Graham, R. K., Y. Deng, J. Carroll, K. Vaid, C. Cowan, M. A. Pouladi, M. Metzler, N. Bissada, L. Wang, R. L. Faull, M. Gray, X. W. Yang, L. A. Raymond, and M. R. Hayden. 2010. Cleavage at the 586 amino acid caspase-6 site in mutant huntingtin influences caspase-6 activation in vivo. *J Neurosci*, 30:15019-29.
- Grusch, M., M. Fritzer-Szekeres, G. Fuhrmann, G. Rosenberger, C. Luxbacher, H. L. Elford, K. Smid, G. J. Peters, T. Szekeres, and G. Krupitza. 2001. Activation of caspases and induction of apoptosis by novel ribonucleotide reductase inhibitors amidox and didox. *Experimental Hematology*, 29:623-32.
- Guo, H., S. Albrecht, M. Bourdeau, T. Petzke, C. Bergeron, and A. C. LeBlanc. 2004. Active caspase-6 and caspase-6-cleaved tau in neuropil threads, neuritic plaques, and neurofibrillary tangles of Alzheimer's disease. *Am J Pathol*, 165:523-31.
- Hardy, J. A., J. Lam, J. T. Nguyen, T. O'Brien, and J. A. Wells. 2004. Discovery of an allosteric site in the caspases. *Proc Natl Acad Sci U S A*, 101:12461-6.
- Hardy, J. A., and J. A. Wells. 2009. Dissecting an allosteric switch in caspase-7 using chemical and mutational probes. *Journal of Biological Chemistry*, 284:26063-9.
- Kelly, K. J., Z. Plotkin, and P. C. Dagher. 2001. Guanosine supplementation reduces apoptosis and protects renal function in the setting of ischemic injury. *Journal of Clinical Investigation*, 108:1291-8.
- Klaiman, G., N. Champagne, and A. C. LeBlanc. 2009. Self-activation of Caspase-6 in vitro and in vivo: Caspase-6 activation does not induce cell death in HEK293T cells. *Biochim Biophys Acta*, 1793:592-601.
- Klaiman, G., T. L. Petzke, J. Hammond, and A. C. Leblanc. 2008. Targets of caspase-6 activity in human neurons and Alzheimer disease. *Mol Cell Proteomics*, 7:1541-55.
- Marriott, A. S., N. A. Copeland, R. Cunningham, M. C. Wilkinson, A. G. McLennan, and N. J. Jones. 2015. Diadenosine 5', 5'''-P(1),P(4)-tetrphosphate (Ap4A) is synthesized in response to DNA damage and inhibits the initiation of DNA replication. *DNA Repair (Amst)*, 33:90-100.
- Mesner, P. W., Jr., K. C. Bible, L. M. Martins, T. J. Kottke, S. M. Srinivasula, P. A. Svingen, T. J. Chilcote, G. S. Basi, J. S. Tung, S. Krajewski, J. C. Reed, E. S. Alnemri, W. C. Earnshaw, and S. H. Kaufmann. 1999. Characterization of caspase processing and activation in HL-60 cell cytosol under cell-free conditions. Nucleotide requirement and inhibitor profile. *Journal of Biological Chemistry*, 274:22635-45.
- Murray, J., A. M. Giannetti, M. Steffek, P. Gibbons, B. R. Hearn, F. Cohen, C. Tam, C. Pozniak, B. Bravo, J. Lewcock, P. Jaishankar, C. Q. Ly, X. Zhao, Y. Tang, P. Chugha, M. R. Arkin, J. Flygare, and A. R. Renslo. 2014. Tailoring small molecules for an allosteric site on procaspase-6. *ChemMedChem*, 9:73-7, 2.
- Nicholson, D. W. 1999. Caspase structure, proteolytic substrates, and function during apoptotic cell death. *Cell Death Differ*, 6:1028-42.

- Nikolaev, A., T. McLaughlin, D. D. O'Leary, and M. Tessier-Lavigne. 2009. APP binds DR6 to trigger axon pruning and neuron death via distinct caspases. *Nature*, 457:981-9.
- Oliver, F. J., M. K. Collins, and A. Lopez-Rivas. 1997. Overexpression of a heterologous thymidine kinase delays apoptosis induced by factor deprivation and inhibitors of deoxynucleotide metabolism. *Journal of Biological Chemistry*, 272:10624-30.
- Patricelli, M. P., T. K. Nomanbhoy, J. Wu, H. Brown, D. Zhou, J. Zhang, S. Jagannathan, A. Aban, E. Okerberg, C. Herring, B. Nordin, H. Weissig, Q. Yang, J. D. Lee, N. S. Gray, and J. W. Kozarich. 2011. In situ kinase profiling reveals functionally relevant properties of native kinases. *Chemistry and Biology*, 18:699-710.
- Patricelli, M. P., A. K. Szardenings, M. Liyanage, T. K. Nomanbhoy, M. Wu, H. Weissig, A. Aban, D. Chun, S. Tanner, and J. W. Kozarich. 2007. Functional interrogation of the kinome using nucleotide acyl phosphates. *Biochemistry*, 46:350-8.
- Quemeneur, L., L. M. Gerland, M. Flacher, M. Ffrench, J. P. Revillard, and L. Genestier. 2003. Differential control of cell cycle, proliferation, and survival of primary T lymphocytes by purine and pyrimidine nucleotides. *Journal of Immunology*, 170:4986-95.
- Rapaport, E., and P. C. Zamecnik. 1976. Presence of diadenosine 5',5'''-P1, P4-tetraphosphate (Ap4A) in mammalian cells in levels varying widely with proliferative activity of the tissue: a possible positive "pleiotypic activator". *Proceedings of the National Academy of Sciences of the United States of America*, 73:3984-8.
- Riechers, S. P., S. Butland, Y. Deng, N. Skotte, D. E. Ehrnhoefer, J. Russ, J. Laine, M. Laroche, M. A. Pouladi, E. E. Wanker, M. R. Hayden, and R. K. Graham. 2016. Interactome network analysis identifies multiple caspase-6 interactors involved in the pathogenesis of HD. *Hum Mol Genet*, 25:1600-18.
- Rosenblum, J. S., T. K. Nomanbhoy, and J. W. Kozarich. 2013. Functional interrogation of kinases and other nucleotide-binding proteins. *FEBS Letters*, 587:1870-7.
- Scheer, J. M., M. J. Romanowski, and J. A. Wells. 2006. A common allosteric site and mechanism in caspases. *Proceedings of the National Academy of Sciences of the United States of America*, 103:7595-600.
- Vaidya, S., E. M. Velazquez-Delgado, G. Abbruzzese, and J. A. Hardy. 2011. Substrate-induced conformational changes occur in all cleaved forms of caspase-6. *J Mol Biol*, 406:75-91.
- Varshavsky, A. 1983. Diadenosine 5', 5'''-P1, P4-tetraphosphate: a pleiotropically acting alarmone? *Cell*, 34:711-2.
- Vartanian, A., I. Alexandrov, I. Prudowski, A. McLennan, and L. Kisselev. 1999. Ap4A induces apoptosis in human cultured cells. *FEBS Letters*, 456:175-80.

- Vartanian, A. A., H. Suzuki, and A. I. Poletaev. 2003. The involvement of diadenosine 5',5'''-P1,P4-tetraphosphate in cell cycle arrest and regulation of apoptosis. *Biochemical Pharmacology*, 65:227-35.
- Velazquez-Delgado, E. M., and J. A. Hardy. 2012. Phosphorylation regulates assembly of the caspase-6 substrate-binding groove. *Structure*, 20:742-51.
- Wang, X. J., Q. Cao, X. Liu, K. T. Wang, W. Mi, Y. Zhang, L. F. Li, A. C. LeBlanc, and X. D. Su. 2010. Crystal structures of human caspase 6 reveal a new mechanism for intramolecular cleavage self-activation. *EMBO Rep*, 11:841-7.
- Wang, X. J., Q. Cao, Y. Zhang, and X. D. Su. 2014. Activation and Regulation of Caspase-6 and Its Role in Neurodegenerative Diseases. *Annu Rev Pharmacol Toxicol*.
- Warby, S. C., C. N. Doty, R. K. Graham, J. B. Carroll, Y. Z. Yang, R. R. Singaraja, C. M. Overall, and M. R. Hayden. 2008. Activated caspase-6 and caspase-6-cleaved fragments of huntingtin specifically colocalize in the nucleus. *Hum Mol Genet*, 17:2390-404.
- Wellington, C. L., and M. R. Hayden. 2000. Caspases and neurodegeneration: on the cutting edge of new therapeutic approaches. *Clin Genet*, 57:1-10.

CHAPTER 6

DISCOVERY OF POTENT AND SELECTIVE INHIBITORS OF CASPASE-6

This chapter is being prepared for submission as: Narasimha Rao, Kevin B. Dagbay, Yifei Pei, Elih M. Velazquez-Delgado and Jeanne A. Hardy. *Discovery of Potent and Selective Inhibitors of Caspase-6*. KBD performed protein purifications, biochemical assays including inhibition assay, mutagenesis, cell-based assay and mass spectrometry, wrote parts of the manuscript and prepared all final figures. NR performed all synthetic works. YP performed biochemical assay. EV performed initial screen and biochemical assays. JH initiated the work, secured funding, directed the research project and was the principal author for the manuscript.

6.1 Abstract

Caspase-6 is a cysteine aspartate protease that plays causative roles in Alzheimer's and Huntington's Diseases. Although some industrial drug discovery has focused on caspase-6, no caspase-6 inhibitors have progressed due to issues of potency and most critically, lack of selectivity over the other twelve human caspases, which are essential for normal development and homeostasis. To date the most selective reported caspase-6 inhibitors are only 10-fold selective over the most closely related caspases. We have discovered unique caspase-6 inhibitors that are 500- and 10,000-fold selective over the two most closely related caspases. These bis-*N*-oxide-based inhibitors are extremely selective because they bind covalently to Cys-264, a non-conserved residue found only in caspase-6. This cysteine-targeted mechanism of selectivity is one that has been exploited recently by drugs such as ibrutinib, an irreversible, covalent inhibitor of Btk. Our lead bis-*N*-oxide has an IC_{50} against caspase-6 of ~300 nM and also inhibits caspase-6 in neuronal cell lines with an IC_{50} of 20 μ M. The size of these bis-*N*-oxides (305 MW) and the other molecular properties are

generally compatible with accepted guidelines for blood-brain barrier penetrance. Thus, the chemical properties of these compounds are promising as therapeutic leads for neurodegeneration.

6.2 Introduction

Caspases, a family of highly conserved cysteine aspartate proteases, have been found to have critical roles in apoptosis and inflammation as well as in development and neurodegeneration (for a review see (Lamkanfi et al., 2007)). Caspases are produced as inactive procaspase zymogens comprising of a connected prodomain, large subunit, intersubunit linker region, and small subunit. Caspases are classified as either initiators (-2, -8, -9) or executioners (-3, -6, -7) based on their function within the apoptotic cascade. Initiator caspases are expressed as monomers and become active upon dimerization facilitated by formation of molecular platforms, e.g. apoptosome (Bao and Shi, 2007; Chu et al., 2001; Muzio et al., 1996; Oberst et al., 2010; Pop et al., 2006).. In contrast, executioner caspases are expressed as dimeric zymogens and become activated by proteolytic cleavage by initiator caspases. The precise control of activation of these caspases is essential to prevent unwanted apoptotic events and detrimental cellular outcomes.

In the caspase family, caspase-6 is particularly highlighted for its involvement in the critical pathways leading to neurodegeneration. Caspase-6 cleaves microtubule-associated protein Tau, which forms the neurofibrillary tangles that are hallmarks of Alzheimer's disease (AD). In postmortem AD brains,

Tau cleaved by caspase-6 at Asp420 is the dominant form of Tau observed in neurofibrillary (Albrecht et al., 2009; Albrecht et al., 2007; Guo et al., 2004). Caspase-6 has also been reported to cleave polyglutamine expanded Huntingtin (Htt) protein and be causative in the onset and progression of Huntington's disease (HD) (Graham et al., 2010; Riechers et al., 2016; Warby et al., 2008). Because inhibition of caspase-6 can block cleavage of Tau and Htt, caspase-6 has become a drug target of significant interest for treatment of neurodegeneration. One of the major stumbling blocks to exploiting caspase-6 therapeutically is that all 12 human caspases share similar active site chemistry. Inhibition of apoptotic or inflammatory caspases will have a devastating effect on homeostasis, so specific inhibition of caspase-6 is of the utmost importance.

Caspase-6 null mice are grossly normal and breed in the expected Mendelian ratios without considerable apoptotic defects (Zheng et al., 2000), Thus physiologically, caspase-6-associated cellular signaling is likely dispensable to normal growth and development. As a promising therapeutic target for neurodegeneration, several small-molecule (Chu et al., 2009; Leyva et al., 2010; Pakavathkumar et al., 2017; Pakavathkumar et al., 2015) or peptide-based (Ekici et al., 2006; James et al., 2004; Nyormoi et al., 2003) competitive inhibitors of caspase-6 have been reported. These covalent inhibitors possess remarkable potency and neuroprotective effects in cells and in animal models of neurodegenerative diseases. However, due to overlapping substrates specificities in caspases (McStay et al., 2008), inhibitors directed at the active site are quite promiscuous, inhibiting other caspases as well. Inhibition of other

caspases, particularly caspase-3, -7, -8 and -9, are developmentally lethal as reported in the knockout studies of these caspases in mice (Hakem et al., 1998; Kuida et al., 1998; Kuida et al., 1996; Varfolomeev et al., 1998; Woo et al., 1998; Zheng et al., 1999), suggesting the essential role of these caspases in normal growth and development in mammals. Thus, efforts on the discovery and development of an allosteric inhibitor are encouraging to come up with a specific inhibitor of caspase-6.

To date, only three reports of allosteric or uncompetitive inhibitors of caspase-6, either small molecules (Heise et al., 2012; Murray et al., 2014) or peptide-based (Stanger et al., 2012), have surfaced in the literature. The first of its class of uncompetitive inhibitor among caspase family and thus far the most potent (11 nM IC₅₀) caspase-6-specific inhibitor has been reported (Heise et al., 2012). Unfortunately, this inhibitor has binding to the caspase-6-substrate complex only when the substrate is a synthetic peptide substrate. This inhibitor does not inhibit caspase-6 cleavage of natural protein substrates, including lamin A/C because its activity is dependent on the type of P1' residue within the synthetic substrate used for in vitro activity assays. Thus, this compound has absolutely no potential as a therapeutic lead. A phage display approach at Genentech has been successful in identifying a peptide-based inhibitor (Pep419), which is capable of binding and promoting procaspase-6 zymogen tetramerization, thus preventing further proteolytic activation of procaspase-6. Despite its activity in neuronal cells and procaspase-6 isoform selectivity, pep419 has poor cell penetration properties. Pep419 requires electroporation for efficient

cell uptake suggesting a clear threshold for its applications in cellular, animal and human applications. Finally, a fragment-merging strategy was used to identify nanomolar-affinity ligands that bind in the dimer interface and stabilize procaspase-6 and thus prevents procaspase-6 activation (Murray et al., 2014). These compounds have been shown to lock loop 2 (L2) in the inactive conformation making L2 structural rearrangement impossible as part of the loop assembly for a substrate-binding competent active site cavity. However, the selectivity profiles of these inhibitors are unknown, thus the potential of these inhibitors to progress as therapeutic leads are still uncertain. In addition, these allosteric inhibitors that stabilize the procaspase-6 zymogen have less impact on the activity of already activated caspase-6. Because active caspase-6 accrues before the onset, particularly, of AD symptoms, allosteric inhibitors targeting procaspase-6 form present a less effective treatment for neurodegeneration.

In this study, we employed a high-throughput screening strategy to identify potent and selective inhibitors of active caspase-6. We have discovered a unique class of potent and exquisitely selective inhibitors of active caspase-6 that covalently modify Cys-264, a non-conserved residue only found in caspase-6. More importantly, these compounds inhibit caspase-6 function in neuronal cells and are amenable to structure-activity relationship (SAR) studies for further improvement of its biochemical and cell-based potency. Notably, the molecular properties of the identified lead bis-*N*-oxide compound are matched to the accepted guidelines for blood-brain barrier penetrance, suggesting favorable

chemical properties with a potential for use as caspase-6-specific inhibitor for treatment of neurodegeneration.

6.3 Results and Discussion

6.3.1 Compound A is the Most Selective Caspase-6 Inhibitor to Date

Under the NIH molecular libraries program, we were performed a screen of 359,786 compounds at the Broad Institute MLPCN site to identify caspase-6 specific and selective inhibitors (Figure 6.1A). All caspases share similar active-site chemistry so we expected that active site-binders would be eliminated based on counter screening against related caspases. From this screen we identified 3 candidate lead compounds that showed the request selectivity over other caspases: a bis-*N*-oxide, a piperazine and a sugar-like compound. We ultimately selected compound A (Figure 6.1B) as our lead, due to it having the strongest potency and its unparalleled selectivity. To date, the best selectivity of any reported caspase-6 inhibitor is 10-fold selectivity for caspase-6 over the most closely related caspases, caspase-3 and caspase-7 (Aharony et al., 2015; Chu et al., 2009; Ekici et al., 2006; Heise et al., 2012; James et al., 2004; Murray et al., 2014; Nyormoi et al., 2003; Pakavathkumar et al., 2017; Pakavathkumar et al., 2015; Stanger et al., 2012). In contrast, compound exhibits 500-fold selectivity for casp-6 over casp-7 and 10,000-fold selective for casp-6 over casp-3 (Figure 6.2).

A Primary Screen		B
Z' > 0.9	359,786	
Hit rate 0.55% (35% inhibition)	970 MLPCN 135 DOS	
Cherry Pick	1105	
IC ₅₀ Caspase-6	101	
Counterscreen IC ₅₀	3	
Caspase-1, -3, -7, -8, -9		

Figure 6.1 High Throughput Screen Identified Potent and Selective Inhibitors of Caspase-6

(A) Results of caspase-6 screening. (B) Structure of Compound A, a bis-N-oxide, the most selective inhibitor identified from the screen.

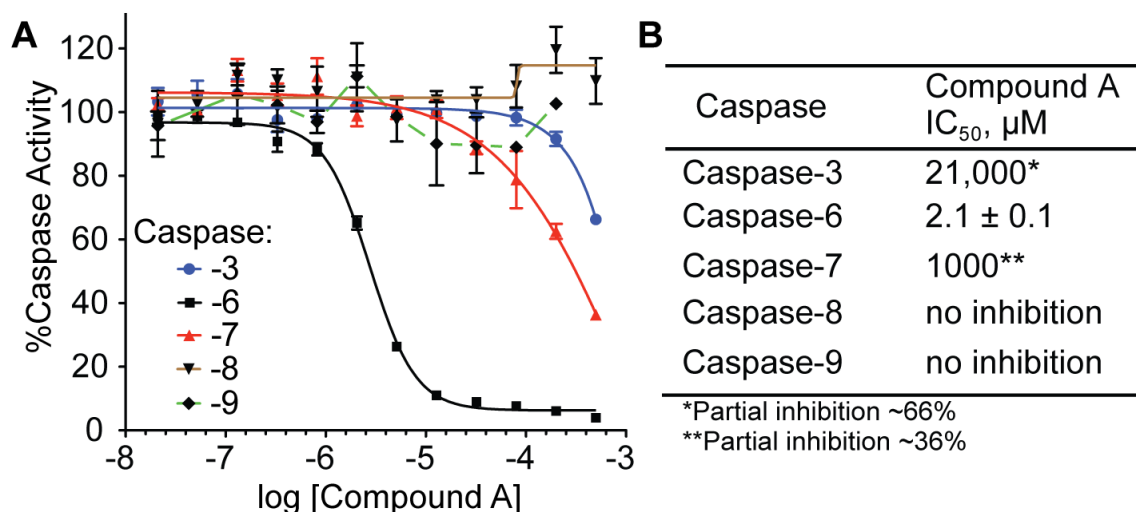


Figure 6.2 Compound A Shows Exquisite Selectivity for Caspase-6

(A) Compound A inhibits caspase-6 selectively over other initiator and executioner caspases. Caspases were incubated with increasing dose of compound A and activity assays were performed using peptide-based fluorogenic substrates appropriate for each caspase. (B). The 500-fold or greater selectivity is greater than of any reported casp-6 inhibitor.

6.3.2 Compound A Stabilizes Caspase-6

Compounds that bind with sufficient affinity typically stabilize proteins toward thermal and chemical denaturation. Active site inhibitors of caspase-6 such as the peptide-based inhibitor VEID-aldehyde (VEID-cho) stabilize it toward thermal denaturation by 8°C (Figure 6.3). Compound A also stabilizes caspase-6 toward thermal denaturation, by 3°C suggesting that compound A binds to caspase-6, and further suggesting that the inhibition is via a direct, binding-mediated mechanism, rather than via some not specific (e.g. denaturation-mediated) mechanism. Notably 3°C is the same amount of stabilization that is observed when caspase-6 adopts the canonical conformation relative to the inactive helical conformation in which it rests prior to substrate binding (Vaidya et al., 2011).

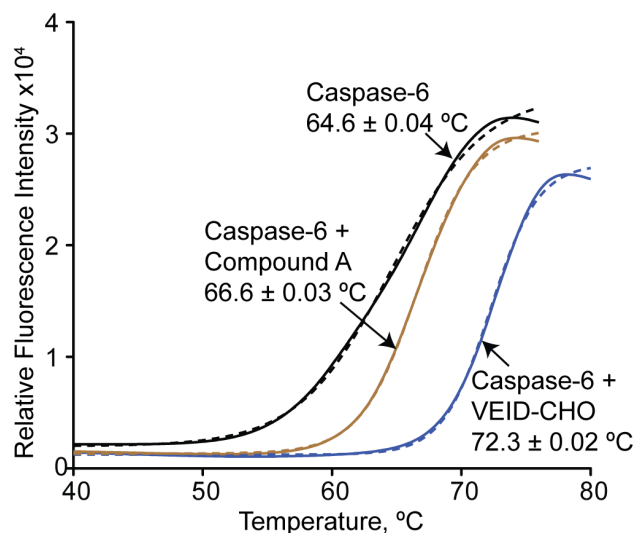


Figure 6.3 Compound A Binds and Stabilizes Caspase-6

Apparent thermal stability of caspase-6 (black solid line) in the presence of compound A (brown solid line) and known active site inhibitor, VEID-CHO (blue solid line) was determined using differential scanning fluorimetry. The dashed lines represent the Boltzmann sigmoidal fit of the thermal shift data, where the apparent melting point is determined as the midpoint of the melting curve.

6.3.3 Compound A Inhibits Caspase-6 in Neuronal Cells

One of the most critical considerations in moving compound A forward is its cell-based activity. To measure cell-based efficacy, we treated SK-N-AS (ATCC[®] CRL-2137[™]) human neuroblastoma cells with increasing concentrations of compound A and monitored cleavage of a well-known caspase-6-specific substrate, lamin A/C, after staurosporine-induced apoptosis. We observed that increasing concentrations of compound A inhibited cleavage of lamin A/C by caspase-6 with an IC₅₀ of 20 μM (Figure 6.4). The fact that inhibition in cells was observed suggests that compound A is somewhat cell penetrant, but the increase in the cell-based IC₅₀ relative to the enzyme-based inhibition, suggest that cell permeability should be improved in future analogs of this compound.

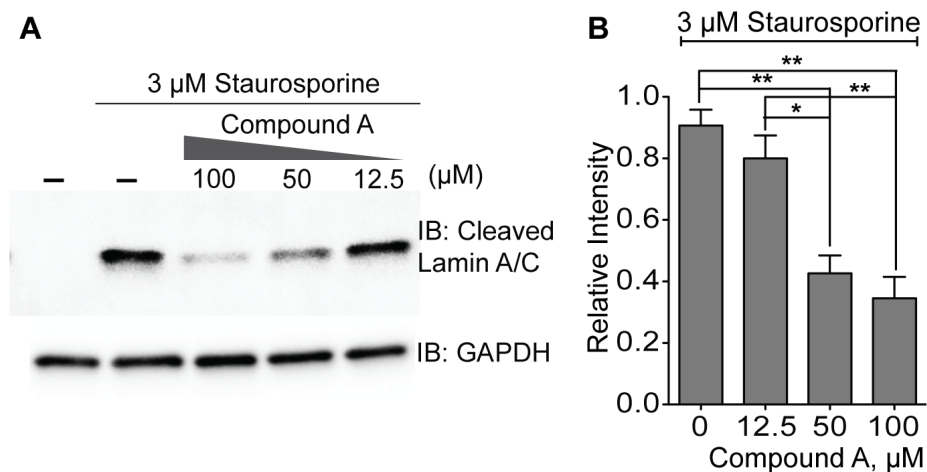


Figure 6.4 Compound A Inhibits Caspase-6 Function in Neuronal Cells

(A) Compound A dose dependent inhibition of staurosporine-induced cleavage of lamin A/C by caspase-6 in SK-N-AS neuroblastoma cells. Western blots were performed for cleaved lamin A/C and GAPDH as protein loading control. (B) Changes in lamin A/C cleavage are significant to the *95th and **99th confidence intervals. One-way analysis of variance (ANOVA) with Bonferroni post hoc (*p<0.05, **p<0.001) was performed. *Error*, represents the mean ± s.e.m of three independent trials. Band quantification of cleaved lamin A/C was normalized to GAPDH protein loading control.

6.3.4 Intrinsic Chemical Reactivity Underlies Selectivity of Compound A

One of the notable features of compound A is that it contains two potentially reactive *N*-oxide moieties, which could react with nucleophiles such as thiols and amines. We found that these *N*-oxides are not intrinsically reactive with typical cysteines or lysines. Caspase-6 is active as a dimer where each monomer is cleaved one large and one small subunit. Caspase-6 has 10 cysteines (6 exposed) and 20 exposed lysine residues on each caspase monomer but our denaturing mass spectrometry analysis of caspase-6 indicated that Compound A reacts with only one cysteine on the small subunit of caspase-6 (Figure 6.5A) as evidenced in the mass difference of the small subunit with or without compound A equal to that of the molecular weight of the compound A (MW 305 g/mol). This is striking because the active site cysteine Cys-163, which is on the large subunit, has a substantially suppressed pKa due to the adjacent His-121. If the activity of compound A was driven by its intrinsic electrophilicity, then Cys-163 on the small subunit would be the natural site of reaction. The fact that Cys-163 is not modified strongly suggests that other features of the compound such as shape complementarity drive its binding and selectivity.

To determine where on the small subunit compound A binds, we performed peptide mapping by tandem mass spectrometry. This analysis showed a modified tryptic peptide that contained Cys-264 and Lys-265, both of which could be the site of compound A reaction (Figure 6.5B). Sequence alignment analysis of all caspases (Figure 6.5C) revealed that the putative binding sites, Cys-264 or Lys-265, are located in the most diversified loop 4 (L4) of caspases

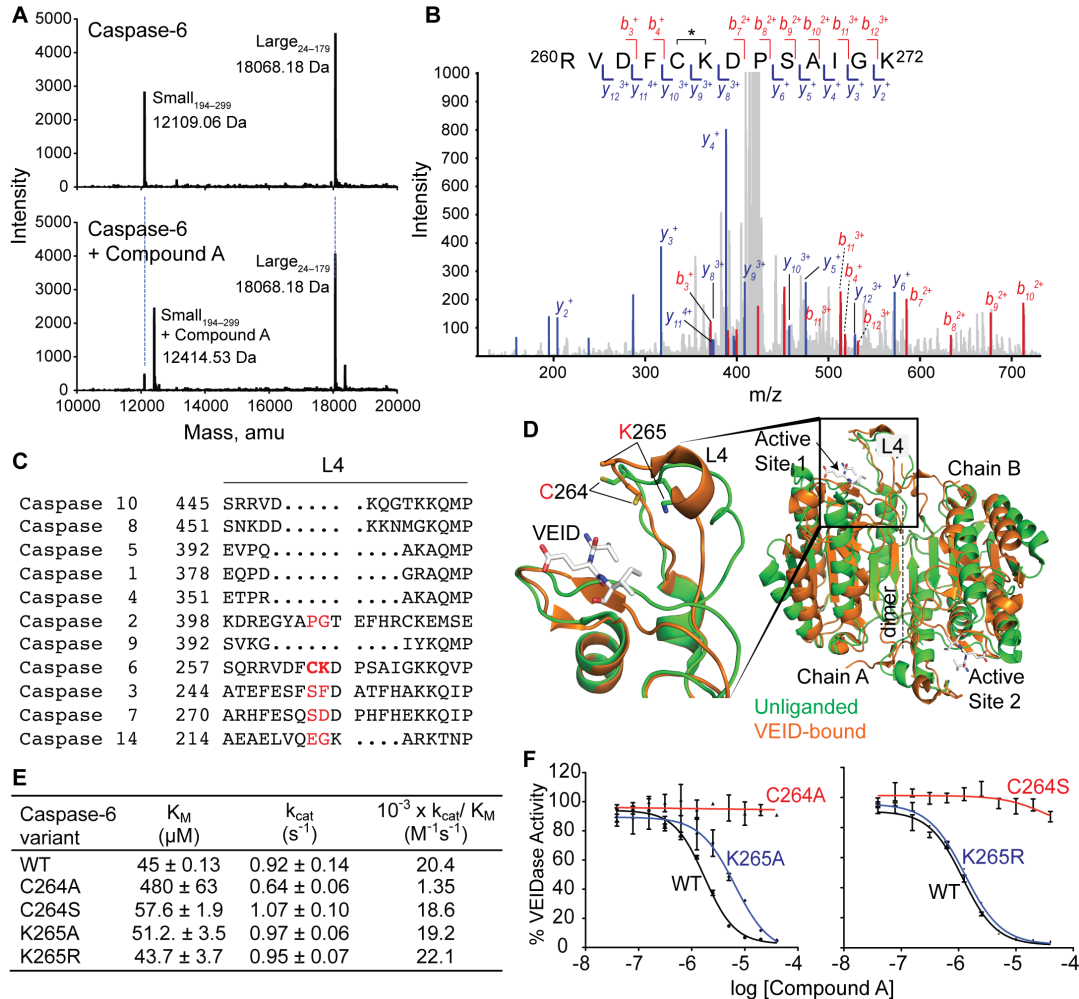


Figure 6.5. Compound A Covalently Binds to a Unique and Non-Active Site Cys–264

(A) The total ion chromatogram from the denaturing mass spectrometry of caspase-6 bound to compound A suggests covalent modification of compound A in the small subunit of caspase-6. Compared with unbound caspase-6, an obvious mass shift could be detected in the caspase-6 + compound A, which has a mass difference similar to the molecular weight of compound A (MW 305 g/mol). (B) MS/MS annotation of compound A-modified tryptic peptide (L4 residues 260–272). The *b* and *y* ions are colored red and blue, respectively. (C) Sequence alignment of L4 residues in caspases. No cysteines are present in the L4 loops region of any other caspases. The absence of cysteine in other caspases underlies the compound A selectivity for caspase-6. (D) The superimposition of unliganded (PDB code 2WDP, green) and VEID-bound (PDB code 3OD5, orange) structures of caspase-6 highlighting the regions of the active site, dimer interface and L4. Inset view shows the putative compound A binding sites, Cys–264 and Lys–264, sit above the substrate-binding groove. (E) Kinetic parameters of the substitution variants of the putative compound A binding sites, Cys–264 and Lys-265. (F) Cys-264 is the site of covalent modification of compound A in caspase-6.

(Figure 6.5D). Importantly, Cys-264 and Lys-265 are unique to caspase-6, which could explain the exquisite selectivity of compound A for caspase-6.

To confirm the specific modification site of compound A, we generated substitutions of Cys-264 to alanine or serine and Lys-265 to alanine or arginine. The kinetic parameters of caspase-6 compound A binding site variants (C264A/S, K265A) showed similar activity to wild type (WT), with the exception of C264A that showed a 15-fold decrease in catalytic efficiency (Figure 6.5E). Mutagenesis of K265R or K265A had no impact on compound A function, but mutagenesis of C264S or C264A dramatically desensitized caspase-6 to the inhibitory effects of compound A (Figure 6.5F), indicating that compound A binds covalently to caspase-6 at a unique Cys-264. In order for caspases to be active, it is critical that all of the loops forming the substrate-binding groove are properly ordered. Thus compound A is likely to bind in a way that prevents substrate binding and may induce an alternate conformation of L4 and the substrate-binding groove.

6.3.5 The Furoxan Moiety is Required for Compound A Reactivity

Compound A has two *N*-oxides, one on the triazole ring and one that is a component of the furoxan of the central ring system. *A priori* it is not clear whether the covalent modification of caspase-6 by compound A requires both *N*-oxides, which would contribute to a large aromatic system spanning the entire core of the compound, or whether a single *N*-oxide could convey the caspase-6 reactivity. We tested four compound A analogs that lack one of the *N*-oxides

(Figure 6.6). Whereas compounds CASP-RT11-9 and CASP-6-III-18, which maintain the furazan *N*-oxide in the furoxan ring, are still reactive, compounds that maintain only the triazole *N*-oxide (compounds 4 and 5) are completely inactive toward caspase-6 (Figure 6.6). This demonstrates that only one *N*-oxide, the one in the furoxan, is required for compound A reactivity and selectivity. In addition to providing a more in depth understanding of the reactivity of compound A, these data also clear the path for development of new classes of compounds. Future analogs of CASP6-III-18, which have only the furazan *N*-oxide represent a departure from the bis-*N*-oxide core and are therefore representative of new chemical entities.

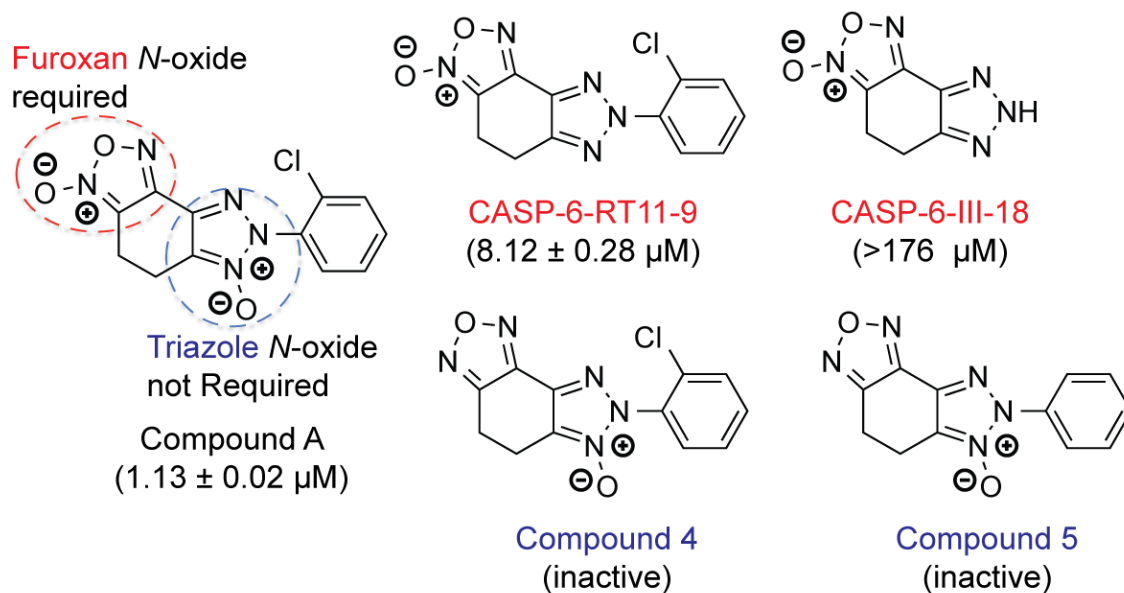


Figure 6.6 The Furozan *N*-Oxide in the Furoxan Moiety is Required for Reactivity, But the Triazole *N*-Oxide is Not Required for Function

6.3.6 The Phenyl Ring Composition Is Important for Affinity

Prior to this work no synthetic scheme for compound A had been published. We developed a 7-step synthetic scheme to achieve compound A and its derivatives. We synthesized compound A analogs with various substitutions at the N2 position in the triazole ring (Table 6.1). We found that this position is very sensitive to substitution and that many substitutions have a dramatic and negative impact on the potency of compound A. From the pool of compound A analogs we have made, 12 compounds exhibit an IC_{50} significantly more potent than compound A. And further suggests that an SAR around the phenyl moiety is a sensitive region that may enable synthesis of analogs of compound A highly potent in both *in vitro* and in cell-based assays. The most potent analogue, CASP-6-III-38, contains a diphenyl substituted amide moiety at the ortho position (Table 6.1D) with an IC_{50} of 290 nM. We also tested one of the more potent compounds (CASP-6-III-20, IC_{50} ~610 nM) and showed the same outstanding selectivity profile as original compound A (Figure 6.7), further suggesting that modifications around the phenyl ring retain the desired reactivity and selectivity. The selectivity assay of other potent compound A analogs is an on-going work in the Hardy Lab. Taken together, the dependence of the reactivity on the various types of substituents around the phenyl ring suggests that there may be very unique packing between compound A and caspase-6 L4 or an adjacent region.

Table 6.1A Compound A Analogs With Substitutions at the Phenyl Ring on the Triazole Moiety.

Code	Structure	IC ₅₀ , μM	Code	Structure	IC ₅₀ , μM
CASP-6-III-1		51.13 ± 0.02	CASP-6-III-10		50.0 ± 0.02
CASP-6-III-2		12.7 ± 0.85	CASP-6-III-11		2.26 ± 0.01
CASP-6-III-4		2.92 ± 0.28	CASP-6-III-12		5.28 ± 0.02
CASP-6-III-5		3.60 ± 0.39	CASP-6-III-13		0.97 ± 0.23
CASP-6-III-6		3.68 ± 0.31	CASP-6-III-14		3.68 ± 0.31
CASP-6-III-7		1.19 ± 0.21	CASP-6-III-15		1.71 ± 0.21
CASP-6-III-8		3.02 ± 0.02	CASP-6-III-16		32.2 ± 0.02
CASP-6-III-9		3.54 ± 0.21	CASP-6-III-17		3.61 ± 0.02

Table 6.1B Compound A Analogs With Substitutions at the Phenyl Ring on the Triazole Moiety.

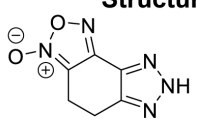
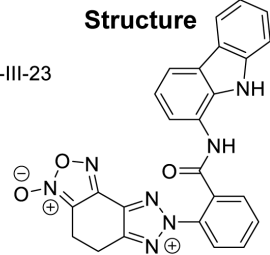
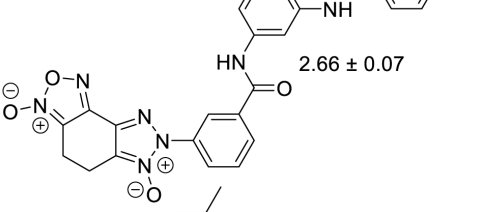
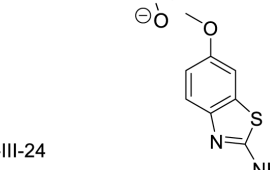
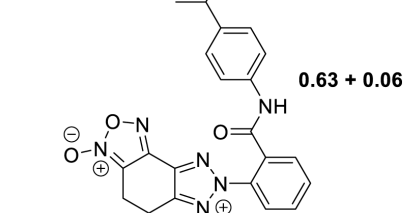
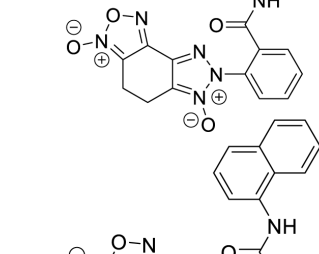
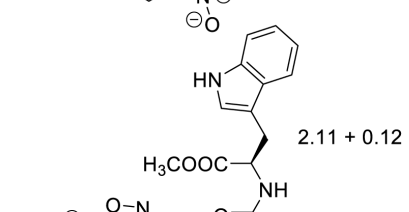
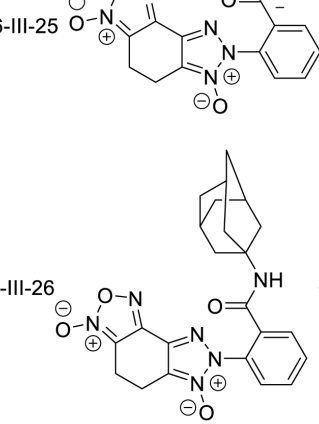
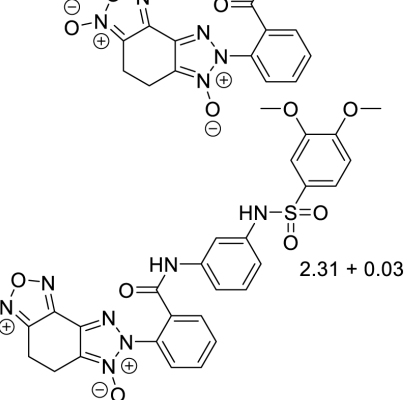
Code	Structure	IC ₅₀ , μM	Code	Structure	IC ₅₀ , μM
CASP-6-III-18		>176 ± 0.02	CASP-6-III-23		0.81 ± 0.058
CASP-6-III-19		2.66 ± 0.07	CASP-6-III-24		6.741 ± 0.175
CASP-6-III-20		0.63 ± 0.06	CASP-6-III-25		0.39 ± 0.03
CASP-6-III-21		2.11 ± 0.12	CASP-6-III-26		1.67 ± 0.01
CASP-6-III-22		2.31 ± 0.03			

Table 6.1C Compound A Analogs With Substitutions at the Phenyl Ring on the Triazole Moiety.

Code	Structure	IC ₅₀ , μM	Code	Structure	IC ₅₀ , μM
CASP-6-III-27		4.64 ± 0.05	CASP-6-III-31		7.15 ± 0.11
CASP-6-III-28		5.98 ± 0.04	CASP-6-III-32		35.99 ± 9.29
CASP-6-III-29		1.94 ± 0.06	CASP-6-III-33		0.71 ± 0.05
CASP-6-III-30		2.06 ± 0.04	CASP-6-III-34		0.44 ± 0.002

Table 6.1D Compound A Analogs With Substitutions at the Phenyl Ring on the Triazole Moiety.

Code	Structure	IC ₅₀ , μM	Code	Structure	IC ₅₀ , μM
CASP-6-III-35		0.36 ± 0.02	CASP-6-III-39		18.43 ± 1.35
CASP-6-III-36		1.01 ± 0.05	CASP-6-III-40		1.47 ± 0.007
CASP-6-III-37		1.81 ± 0.33	CASP-6-III-41		0.34 ± 0.09
CASP-6-III-38		0.29 ± 0.07	CASP-6-III-42		TBD

Table 6.1E Compound A Analogs With Substitutions at the Phenyl Ring on the Triazole Moiety.

Code	Structure	IC ₅₀ , μM	Code	Structure	IC ₅₀ , μM
CASP-6-III-43		0.32 ± 0.04	CASP-6-III-45		0.56 ± 0.06
CASP-6-III-44		TBD	CASP-6-III-46		0.65 ± 0.04
<i>Compound from the MLPCN Library</i>			<i>Commercially Available Analogs</i>		
Compound 1		5.0 ± 1.1	Compound 2		20 ± 1.5* *partial inhibition ~16%
			Compound 3		48 ± 2.5* *partial inhibition ~35%

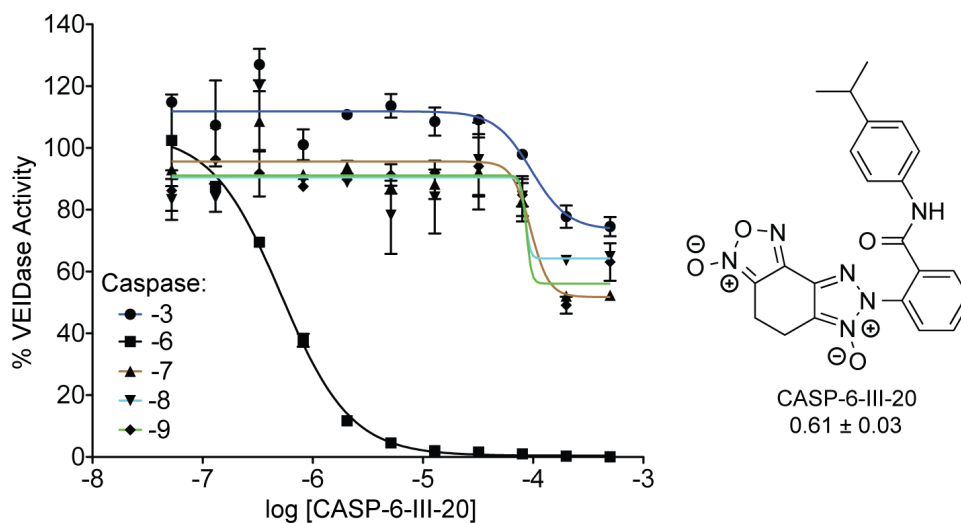
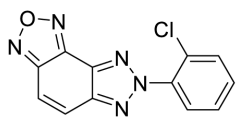
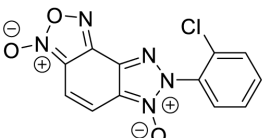
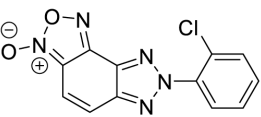
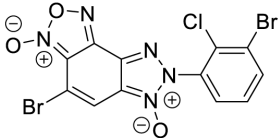
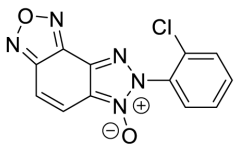
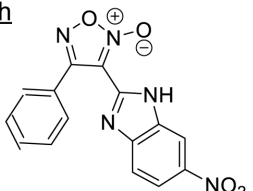


Figure 6.7. The Selectivity Profile of a Representative Compound A Analog (CASP-6-III-20) Shows Potency Higher Than Compound A

6.3.7 The Central Ring in Compound A Can Be Modified

We have developed a 6-step synthetic route that allowed us to install a double bond in the central cyclohexane ring in compound A. Loss of saturation at this position (CASP-6-RT-II-5) decreases affinity of the compound by ~30-fold (Table 6.2). Nevertheless, we have observed that bromination of the double bond (CASP-6-II-1) does not substantially further weaken the derivative's ability to inhibit casp-6 activity. Thus we hypothesize that substitution at this position on the central ring may lead to new compounds that may have improved properties for potency and cell penetrance.

Table 6.2 Compound A Analogs With Double Bond at the Central Cyclohexane Ring.

Code	Structure	IC ₅₀ , μM	Code	Structure	IC ₅₀ , μM
CAS-6-3		> 100	CASP-6-RTII-5		33.6 ± 1.50
CAS-6-III		> 100	CASP-6-II-1		37.4 ± 2.16
CASP-6-RTII-5B		> 100	<u>Compound with Furoxan Only</u> CASP-6-IV-1		155 ± 0.13

6.3.8 The Bis-*N*-Oxides are Predicted to Have Good Blood-Brain Barrier Penetration

For casp-6 inhibitors to have clinical relevance in neurodegeneration, they will need blood brain-barrier penetrance. Investigators at Pfizer have developed a 7-fold multi parameter optimization (MPO) scoring function for predicting blood brain barrier penetrance (Wager et al., 2010) that has been highly successful. Factors in the MPO calculation include: molecular weights between 250-350 Da, LogD of less than 3, no more than two hydrogen bond donors, no more than 4 hydrogen bond acceptors, polar surface area between 25-75 Å², fewer than 4 total rings, fewer than 2 aromatic rings, and fewer than 7 rotatable bonds. We have assessed compound A for these properties. Compound A matches these identified criteria and thus has an overall MPO score consistent with blood brain barrier penetrance. Based on this analysis, we expect that compound A and its derivatives to have blood brain penetrance.

6.4 Summary and Conclusion

We have discovered a series of bis-*N*-oxide compounds that offer the greatest specificity of any caspase-6 inhibitors to date. This remarkable specificity derives from the ability of these compounds to target a cysteine in the most diverse loop, L4, in caspase-6. Cys-264 and the adjacent Lys-265 are not present in L4 of any other caspases. The fact that the bis-*N*-oxides target this cysteine is one of the key features that differentiate this series from all other known caspase-6 inhibitors. Traditionally, covalent compounds have viewed

skeptically by some within the pharmaceutical industry, but recently this view has changed notably (Guterman, 2011; Singh et al., 2011), as the use of covalency has been recognized to provide exquisite specificity for targets of interest. In addition, market successes of compounds like ibrutinib, a covalent Bruton's tyrosine kinase (Btk) inhibitor described as having "outstanding clinical activity and tolerability in B-cell malignancies" (Dubovsky et al., 2013) are changing the covalent drug development paradigm. A Michael's acceptor in Ibrutinib reacts with a non-catalytic cysteine, providing both potency and specificity. The success of ibrutinib led to the \$21B acquisition of Pharmacyclics by AbbVie. Like Ibrutinib, compound A forms a covalent bond to a unique, non-catalytic cysteine providing unparalleled selectivity for caspase-6 inhibition. In conclusion, small covalent inhibitor of caspase activation, such the ones presented here, might be advanced into therapeutic leads for relevant human diseases including Alzheimer's and Huntington's diseases as well as its use as molecular probes to investigate mechanisms and functions of caspase activation and regulation.

6.5 Materials and Methods

6.5.1 Sources of Compound A and its Analogs

Prior to our synthesis of compound A, it was purchased from ChemDiv, Inc., USA (compound ID: 3454-1844) or obtained from a screen library at the Broad Institute of Harvard and MIT (compound ID: BRD-K32954333-001-11-0). Compound 1 (compound ID: BRD-K55066264-001-01-9), compound 4 (compound ID: BRD-K68959369-001-01-4), and compound 5 (compound ID:

BRD-K64914368-001-08-9) were obtained from a screen library at the Broad Institute of Harvard and MIT. Compound 2 (compound ID: 3454-1837) and compound 3 (compound ID: 3473-3473) were purchased from ChemDiv, Inc., USA. All other compounds reported here were synthesized in the Hardy Lab by Narasimha Rao.

6.5.2 Site-Directed Mutagenesis of Caspase-6

The caspase-6 variants were derived from the synthetic, *E. coli* codon-optimized (His)₆ C-terminally tagged caspase-6 gene (Celtek Bioscience), which was ligated into the NdeI/BamHI sites of pET11a vector (Vaidya et al., 2011). All caspase-6 variants used in this study were generated using caspase-6 Δ N D179CT as template through Phusion® site-directed mutagenesis (Thermo Scientific™).

6.5.3 Caspase-3 Protein Expression and Purification

The gene for full-length wild-type caspase-3 in pET23b was transformed into BL21(DE3) *E. coli*. Cultures were grown in 2xYT media with 100 μ g/mL Ampicillin at 37°C with shaking until OD₆₀₀=0.8. Protein expression was induced by addition of 1 mM IPTG at 30°C for 3 h and cells were harvested by centrifugation at 4700 x g for 10 min at 4°C. Cells were freeze-thawed, lysed in a microfluidizer in a buffer containing 50 mM sodium phosphate pH 8.0, 300 mM NaCl and 2 mM imidazole, and centrifuged at 30,600 x g for 50 min at 4°C to remove cellular debris. The supernatant was loaded onto a 5-mL HiTrap Ni-

affinity column (GE Healthcare), washed with 50 mM imidazole and proteins were eluted with 250 mM imidazole in lysis buffer. The eluted protein fraction was diluted six-fold with 20 mM Tris pH 8.0 with 2 mM DTT (buffer A) and loaded onto a HiTrap Q-column (GE Healthcare). Proteins were eluted by a linear gradient from 0-500 mM of NaCl in buffer A. Casp-3 eluted in buffer A with 250 mM NaCl. Peak fractions were analyzed by SDS PAGE for purity and were stored in -80°C until use.

6.5.4 Caspase-6 Protein Expression and Purification

The caspase-6 constructs were transformed into the BL21(DE3) T7 express strain of *E. coli* (New England Biolabs). Overnight seed cultures were initially grown in 2xYT medium supplemented with 0.1 mg/ml ampicillin (Sigma) at 37 °C. Dense cultures were then diluted 1,000-fold with 2xYT containing 0.1 mg/ml ampicillin and shaken at 37 °C until A_{600} reached 0.6. Protein expression was induced by the addition of 1mM isopropyl 1-thio- β -D-galactopyranoside and cultures were shaken at 20 °C for 18 h. Cells were centrifuged at 4,700 x *g* for 10 min at 4 °C and stored at -20 °C until use. Freeze-thawed cells were lysed using a microfluidizer (Microfluidics, Inc.) in lysis buffer (50 mM Tris, pH 8.5, 300 mM NaCl, 5% glycerol, 50 mM imidazole) and centrifuged at 30,600 x *g* for 1 h at 4 °C. The supernatant was loaded into a 5-ml HiTrap nickel affinity column (GE Healthcare) and washed with lysis buffer until the absorbance returned to baseline. The protein was eluted with elution buffer (50 mM Tris, pH 8.5, 300 mM NaCl, 5% glycerol, 250 mM imidazole) and diluted 5-fold with buffer A (20 mM

Tris, pH 8.5, 2 mM DTT) to reduce the salt concentration. This protein sample was then loaded into a 5-ml HiTrap Q HP column (GE Healthcare). The column was developed with a linear NaCl gradient, and the protein was eluted in 20mM Tris, pH 8.5, 200mM NaCl, 2mM DTT. This eluted protein was stored at -80°C until use. The purified caspases were analyzed by SDS-PAGE to confirm identity and purity.

6.5.5 Caspase-7 Protein Expression and Purification

Plasmids encoding human casp-7 and all variants were transformed into BL21(DE3) *E. coli* cells. Cultures were grown in 2xYT media with ampicillin (100 $\mu\text{g}/\text{mL}$, ThermoFisher) at 37°C until they reached an OD_{600} of 0.6. The temperature was reduced to 18°C and cells were induced with 1 mM Isopropyl β -D-1-thiogalactopyranoside (IPTG) for 18 hours. Cell pellets were stored at -80°C , freeze-thawed and lysed in a microfluidizer (Microfluidics, Inc.) in a buffer containing 50 mM sodium phosphate pH 8.0, 300 mM NaCl, and 2 mM imidazole. Lysed cells were centrifuged at 27,000 rcf to remove cellular debris. The supernatant was loaded onto a 5 mL HiTrap Ni-affinity column (GE Healthcare). The column was washed with a buffer of 50 mM sodium phosphate pH 8.0, 300 mM NaCl, and 50 mM imidazole. Casp-7 was eluted with a step gradient to 300 mM imidazole. The eluted fraction was diluted 6-fold into a buffer containing 20 mM Tris pH 8.5 and 2 mM DTT to reduce the salt concentration. This protein was loaded onto a 5 mL Macro-Prep High Q column (Bio-Rad Laboratories, Inc.). The column was developed with a linear NaCl gradient.

Protein eluted in 120 mM NaCl and was assessed for purity by SDS-PAGE and stored at -80°C in elution buffer.

6.5.6 Caspase-8 Protein Expression and Purification

The expression construct encoding human caspase-8 was transformed into BL21(DE3) *E. coli* cells. Cultures were grown in 2xYT media with ampicillin (100µg/mL, ThermoFisher) at 37°C until they reached an OD₆₀₀ of 0.6. The temperature was reduced to 25°C and cells were induced with 1 mM Isopropyl β-D-1-thiogalactopyranoside (IPTG) for 3 hours. Cell pellets were stored at -80°C, freeze-thawed and lysed in a microfluidizer (Microfluidics, Inc.) in a buffer containing 50 mM sodium phosphate pH 8.0, 500 mM NaCl, and 2 mM imidazole. Lysed cells were centrifuged at 27,000 rcf to remove cellular debris. The supernatant was loaded onto a 5 mL HiTrap Ni-affinity column (GE Healthcare). The column was washed with a buffer of 50 mM sodium phosphate pH 8.0, 500 mM NaCl, and 8 mM imidazole. Casp-8 was eluted with a step gradient to 300 mM imidazole. The eluted fraction was diluted 6-fold into a buffer containing 20 mM Tris pH 8.5 and 2 mM DTT to reduce the salt concentration. This sample was loaded onto a 5 mL Macro-Prep High Q column (Bio-Rad Laboratories, Inc.). The column was developed with a linear NaCl gradient. Casp-8 eluted in 100 mM NaCl and was assessed for purity by SDS-PAGE and stored at -80°C in elution buffer.

6.5.7 Caspase-9 Protein Expression and Purification

The caspase-9 wild-type construct was transformed into BL21(DE3) strain of *E. coli*. The cultures were grown in 2xYT media supplemented with 100 µg/mL of ampicillin at 37°C with vigorous shaking until they reached an optical density (OD₆₀₀) between 1-1.2. The temperature was lowered to 15°C and protein expression was induced by adding 1 mM of IPTG (Anatrace). Protein expression was allowed to proceed for 3 h (except for C9 FL WT zymogen which was expressed for only 30 min, C9FL S183A, C9FL S99A/S183A and C9FL S195A/S183A which were expressed for 16 h) and cells were harvested by centrifugation at 4700 x g for 10 min at 4°C. Cell pellets were stored at -80°C, freeze-thawed and lysed in a microfluidizer (Microfluidics, Inc.) in lysis buffer (50 mM sodium phosphate pH 7.0, 300 mM NaCl and 2 mM imidazole). Cell lysates were centrifuged at 30,600 x g for 50 min at 4°C to remove cellular debris. The supernatant was filtered through 0.45 µm PVDF (Millipore) filter and loaded onto a 5-mL HiTrap Ni-affinity column (GE Healthcare). Proteins were eluted using a linear gradient of 2-100 mM imidazole in lysis buffer. Protein fractions were analyzed by SDS PAGE and fractions containing casp-9 were pooled and diluted 8x with a buffer containing 20 mM Tris pH 8.5 and 5 mM DTT (buffer A). The protein solution was filtered through 0.45 µm PVDF filter to remove precipitates and loaded onto a HiTrap Q-column (GE Healthcare). Proteins were eluted by a linear gradient from 0-275 mM of NaCl in buffer A. Casp-9 eluted in buffer A at 180 mM NaCl. Peak fractions were analyzed by SDS PAGE for purity and were stored in -80°C until use.

6.5.8 Caspase-6 Activity Assays

To measure caspase-6 activity, 100 nM purified caspase was assayed over 7 min at 37°C in caspase-6 activity assay buffer (100 mM HEPES, 120 mM NaCl, 0.1% CHAPS, 10% sucrose, 5 mM DTT). For substrate titration, a range of 0-500 μ M fluorogenic substrate VEID-AMC [*N*-acetyl-Val-Glu-Ile-Asp-(7-amino-4-methyl-coumarin), Enzo Life Sciences Inc.] was used. Fluorescence kinetic measurements ($\lambda_{\text{ex}}/\lambda_{\text{em}}$: 365nm/495nm) were performed in two independent trials in 100- μ L reactions in a 96-well format using a microplate reader (SpectraMax M5, Molecular Devices). Initial velocities versus substrate concentration were fit to a rectangular hyperbola using GraphPad Prism (GraphPad Software, San Diego, USA) to determine the kinetic parameters K_M and k_{cat} . Enzyme concentrations were determined by active-site titration with the quantitative covalent inhibitor VEID-CHO (*N*-Acetyl-Val-Glu-Ile-Asp-aldehyde; Enzo Life Sciences Inc.). Caspase-6 was added to inhibitor solvated in DMSO in 96-wells V-bottom plates at room temperature for 1.5 hours in caspase-6 activity assay buffer. Aliquots (90 μ L) were transferred in duplicate to black-well plates and assayed with 50-fold molar excess of substrate. The protein concentration was determined to be the lowest concentration at which full inhibition was observed and was thus used to calculate k_{cat} .

6.5.9 Caspase-6 Inhibition Assay

Active caspase-6 (20 nM final concentration) was incubated with increasing concentration of compound A and its analogs (0–500 μ M, 2.5-fold

dilutions) in caspase-6 activity assay buffer (100 mM HEPES pH 7.5, 10% sucrose, 0.1% CHAPS, 120 mM NaCl, and 5 mM DTT) for 1.5 h at room temperature. VEID-AMC fluorescent substrate (Enzo Life Sciences Inc.) was then added to 60 μ M final concentration. Each inhibition reaction was set up in duplicate with the final reaction volume of 30 μ L in a 384-well plate. Fluorescence kinetic measurements ($\lambda_{\text{ex}}/\lambda_{\text{em}}$: 365nm/495nm) were performed using a microplate reader (SpectraMax M5, Molecular Devices) over 7-min period. Initial velocities were generated from a rectangular hyperbola fit of the fluorescence intensity *versus* time using the built-in equation in the SpectraMax analysis software. The percentage VEIDase activity of caspase-6 was determined by dividing the initial velocities of caspase-6 with inhibitor over the buffer-only-containing caspase-6 control. A plot of percentage VEIDase activity against the log of the inhibitor concentration (in M) was generated and fitted into a non-linear curve-fitting algorithm (4-parameter equation) using GraphPad Prism (GraphPad Software, San Diego, USA) to determine the IC₅₀ values. The data represent an average of three independent experiments and the reported errors represent the standard error of the mean (S.E.M).

6.5.10 Caspase Selectivity Assays

The inhibitory effect of compound A and its analogs were tested against a panel of caspases (3, 6, 7, 8, 9). All enzymes used for the selectivity assay were purified as described in the other parts of this Materials and Methods section. The following enzyme and substrate concentrations were used: Caspase-3 (1

nM), DEVD-AMC (3 μ M); caspase-6 (10 nM), VEID-AMC (10 μ M); caspase-7 (2 nM), DEVD-AMC (10 μ M); caspase-8 (50 nM), IETD-AFC (10 nM); and caspase-9 (800 nM), LEHD-AMC (100 μ M). All fluorogenic substrates were purchased from Enzo Life Sciences Inc. The following caspase activity assay buffers were used: caspase-3 (25mM HEPES pH 7.5, 0.1% CHAPS and 50mM KCl, 10mM DTT); caspase-6 (100 mM HEPES pH 7.5, 10% sucrose, 0.1% CHAPS, 120 mM NaCl, and 5 mM DTT); caspase-7 (100 mM HEPES pH 7.5, 5 mM CaCl₂, 10% PEG 400, 0.1% CHAPS, 5 mM DTT); caspase-8 (10mM PIPES pH 7.2, 0.1 M NaCl, 1mM EDTA, 10% sucrose, 0.05% CHAPS, 5 mM DTT); and caspase-9 (100 mM MES pH 6.5, 10% PEG 8000, 5 mM DTT). All caspases were incubated with increasing concentrations of the inhibitor (0–500 μ M or, 2.5-fold dilutions) in each corresponding caspase activity assay buffer for 1.5 h at room temperature. Fluorescent substrate (Enzo Life Sciences Inc.) was then added to the caspase/inhibitor solution. Each inhibition reaction was set up in duplicate with the final reaction volume of 30 μ L in a 384-well plate. Fluorescence kinetic measurements ($\lambda_{\text{ex}}/\lambda_{\text{em}}$: 365nm/495nm) were performed using a microplate reader (SpectraMax M5, Molecular Devices). Initial velocities were generated from a rectangular hyperbola fit of the fluorescence intensity *versus* time using the built-in equation in the SpectraMax analysis software. The percentage activity of each caspase was determined by dividing the initial velocities of caspase with inhibitor over the buffer-only-containing caspase control. A plot of percentage caspase activity against the log of the inhibitor concentration (in M) was generated and fitted into a non-linear curve-fitting algorithm (4-parameter

equation) using GraphPad Prism (GraphPad Software, San Diego, USA) to determine the IC₅₀ values. The data represent an average of three independent experiments and the reported errors represent the standard error of the mean (S.E.M).

6.5.11 Denaturing Mass Spectrometry of Caspase-6:Compound A Complex

Caspase-6 wild-type (Δ ND179CT) (5 μ M) was incubated with 5-fold molar excess of compound A for 1.5 h at room temperature in a buffer containing 20 mM Tris, pH 8.5, 120 mM NaCl, and 2 mM DTT. Mass spectra were acquired on a QStar-XL (MDS Sciex, Toronto, Canada) hybrid quadrupole/time-of-flight with reverse phase liquid chromatography (Agilent 1100 LC) using a PROTO 300 C4 column (Higgins Analytical, Inc.) to desalt the protein. The eluted protein was injected into the ESI source at a rate of 0.5 mL/min using N₂ as an ion source gas. Protein was eluted from the column using a 30-minute gradient from 0–100% acetonitrile and monitored using UV and TIC. A single peak containing caspase-6 eluted between 10–15 minutes of chromatographic separation. Data was analyzed using Analyst QS (Applied Biosystems) with BioAnalyst extensions. Scanning was carried out between 700 - 1400 m/z and the final spectra obtained were an average of 10 individual spectra. All spectra deconvolutions were analyzed between 10 kD and 40 kD.

6.5.12 Tandem Mass Spectrometry of Caspase-6:Compound A Complex

To identify the residues in caspase-6 covalently modified by compound A, tandem MS was performed on the caspase-6/compound A complex. Caspase-6 wild-type (Δ ND179CT) (28 μ M) was incubated with 10-fold molar excess compound A in 20 mM Tris, pH 8.5, 120 mM NaCl, and 2 mM DTT for 2 h at room temperature. The sample was then pretreated with 10% acetonitrile for 45 min at 40 °C. The pretreated sample was digested with trypsin (sequencing grade, Roche, Cat. #11418025001) in a 1:20 (w/w) trypsin:caspase-6 ratio for 18 h at 37 °C. The digestion reaction was quenched after addition of trifluoroacetic acid to a final concentration of 0.2% (v/v). Trypsin (~23.3 kDa) was removed by centrifugation using a microcon-10kDa centrifugal filter (EMD Millipore). One microliter of ~25 μ M tryptic peptides was subjected to tandem MS using an Orbitrap Fusion Tribrid mass spectrometer (Thermo Scientific, MA) equipped with ultra high pressure liquid chromatography (UHPLC), nano-LC systems, quadruple mass filter, and CID with ion trap detection for MS/MS fragmentation. MS spectra were analyzed using Proteome Discoverer™ (Thermo Scientific, MA) software to identify the peptides modified with compound A.

6.5.13 Thermal Stability by Differential Scanning Fluorimetry

Caspase-6 wild-type (Δ ND179CT) (10 μ M) was incubated with either 5-fold molar excess compound A or 5-fold molar excess of VEID-CHO in 20 mM Tris, pH 8.5, 200 mM NaCl, and 5 mM DTT for 1.5 h at room temperature. Fluorescence-based thermal shift assay was determined using 0.5x SYPRO®

Orange dye (ThermoFisher) in a CFX Connect Real-Time PCR detection system (BioRad). Measurements were performed in a 96-well plate in 50- μ L reactions. Thermal-based fluorescence intensity was monitored from 25–95 °C at a heating rate of 0.5 °C/min. The apparent thermal melting points ($T_{m, \text{ apparent}}$) were determined by curve fitting analysis using GraphPad Prism (GraphPad Software, San Diego, USA).

6.5.14 Cell-Based Caspase-6 Inhibition Assay

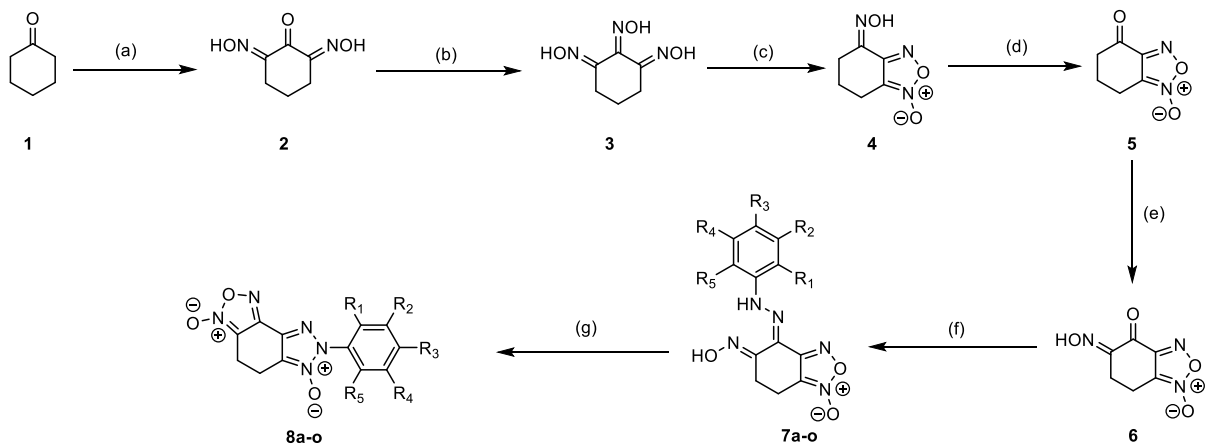
Cell Culture. SKNAS human neuroblastoma cells (ATCC[®] CRL-2137[™]) were grown in high glucose Dulbecco's Modified Eagles Medium (DMEM) (GIBCO[™], Cat. No. 11960044) containing 1% penicillin-streptomycin (MP Biomedicals, Cat. No. 1670049), 1% glutamax (GIBCO[™], Cat. No. 3505006), 0.1 mM non-essential amino acid (NEAA) (ATCC 30-2116), and 10% fetal bovine serum (Hyclone[™], Cat. No. SH30910.03). About 50,000 cells were seeded into a 6-well plate and allowed to attach overnight. Cells were treated with increasing dose of inhibitor for 3 h. After incubation with inhibitor, apoptosis was induced by adding 3 μ M staurosporine for 4 h at 37 °C. Staurosporine-treated cells were collected in cold phosphate-buffered saline PBS using a cell scraper (Falcon), pelleted by centrifugation and lysed in RIPA lysis buffer at for 30 min at 4 °C on a rotating platform. Supernatants were cleared by centrifugation (14,000 rpm at 4 °C for 20 min) and protein concentrations were determined using BCA (Thermo Scientific) assay.

Western Blotting. About 4 μ g of protein was loaded per lane into a 12% SDS-

PAGE gel and ran at 180 V for 55 min. Protein bands were transferred into a PVDF membrane at 100 V for 2 hours. Membrane was then washed with 25 mL of 1x Tris-buffered saline (TBS) (10 mM Tris pH8.0, 150 mM NaCl) for 5 mins and blocked with 5% BSA in TBST (TBS with 0.1% Tween-20) for 1 h at room temperature in a rotating platform. Blots were incubated with primary antibodies to detect the expression of cleaved lamin A (1:1000, Cell Signaling Technologies Cat. No. 2035) or GAPDH (1:1000, GAPDH, ThermoFisher Scientific, Cat. No. MA5-15738) for overnight at 4 °C. Blots were washed three times with 1X TBST and incubated on a rocking platform for 1 h at room temperature with rabbit or mouse horseradish peroxidase-conjugated secondary antibodies (1:50000, Jackson Immuno Research). After washing three times with TBST, protein bands were detected using SuperSignal West Dura Extended Duration Substrate for HRP (ThermoFisher Scientific, Cat. No. 34075) and imaged using ChemiDoc™ MP imaging system (Bio-rad). Band intensities were quantified using Image Lab (Bio-rad) software and normalized to GAPDH control to determine the relative level of cleaved lamin A in presence of increasing concentrations of the inhibitor. One-way analysis of variance (ANOVA) with Bonferroni *post hoc* was applied to three independent trials to determine the statistical significance between samples.

6.5.15 Synthetic Schemes

Scheme-1. Synthesis of Compound-A Analogs (8a-o).



8a R₁ = H; R₂ = OCH₃; R₃ = OCH₃; R₄ = OCH₃; R₅ = H.

8b R₁ = H; R₂ = *N*-methane sulfonamide; R₃ = H; R₄ = H; R₅ = H.

8c R₁ = H; R₂ = *N*-acetamide; R₃ = H; R₄ = H; R₅ = H.

8d R₁ = H; R₂ = F; R₃ = H; R₄ = H; R₅ = H.

8e R₁ = H; R₂ = *N*-methanamide; R₃ = H; R₄ = H; R₅ = H.

8f R₁ = F; R₂ = H; R₃ = H; R₄ = H; R₅ = H.

8g R₁ = COOH; R₂ = H; R₃ = H; R₄ = H; R₅ = H.

8h R₁ = *N*-methanamide; R₂ = H; R₃ = H; R₄ = H; R₅ = H.

8i R₁ = NO₂; R₂ = H; R₃ = H; R₄ = H; R₅ = H.

8j R₁ = CF₃; R₂ = H; R₃ = H; R₄ = H; R₅ = H.

8k R₁ = CH₃; R₂ = H; R₃ = H; R₄ = H; R₅ = H.

8l R₁ = F; R₂ = H; R₃ = H; R₄ = H; R₅ = F.

8m R₁ = H; R₂ = NO₂; R₃ = H; R₄ = H; R₅ = H.

8n R₁ R₂ = Phenyl; R₃ = H; R₄ = H; R₅ = H.

8o R₁ = H; R₂ = COOH; R₃ = H; R₄ = H; R₅ = H.

7a R₁ = H; R₂ = OCH₃; R₃ = OCH₃; R₄ = OCH₃; R₅ = H.

7b R₁ = H; R₂ = *N*-methane sulfonamide; R₃ = H; R₄ = H; R₅ = H.

7c R₁ = H; R₂ = *N*-acetamide; R₃ = H; R₄ = H; R₅ = H.

7d R₁ = H; R₂ = F; R₃ = H; R₄ = H; R₅ = H.

7e R₁ = H; R₂ = *N*-methanamide; R₃ = H; R₄ = H; R₅ = H.

7f R₁ = F; R₂ = H; R₃ = H; R₄ = H; R₅ = H.

7g R₁ = COOH; R₂ = H; R₃ = H; R₄ = H; R₅ = H.

7h R₁ = *N*-methanamide; R₂ = H; R₃ = H; R₄ = H; R₅ = H.

7i R₁ = NO₂; R₂ = H; R₃ = H; R₄ = H; R₅ = H.

7j R₁ = CF₃; R₂ = H; R₃ = H; R₄ = H; R₅ = H.

7k R₁ = CH₃; R₂ = H; R₃ = H; R₄ = H; R₅ = H.

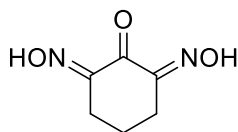
7l R₁ = F; R₂ = H; R₃ = H; R₄ = H; R₅ = F.

7m R₁ = H; R₂ = NO₂; R₃ = H; R₄ = H; R₅ = H.

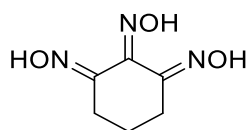
7n R₁ R₂ = Phenyl; R₃ = H; R₄ = H; R₅ = H.

7o R₁ = H; R₂ = COOH; R₃ = H; R₄ = H; R₅ = H.

Reagents and conditions: (a) Diethyl ether, methyl nitrite, 0°- 25 °C, 4h (90%); (b) Na₂CO₃, NH₂OH.HCl, EtOH: H₂O (1:1), 6h (85%); (c) NaOBr aq Sol, H₂O, 30 min (85%); (d) HCHO, Con. HCl, 25 °C, 20 min (90%); (e) NaNO₂, EtOH, AcOH, 25 °C, 12h (90%); (f) Corresponding Hydrazines, EtOH, Cat. AcOH, 25 °C, 20-40 min (90%); (g) activated MnO₂, Acetonitrile, 85 °C, 20-40 min (90%).

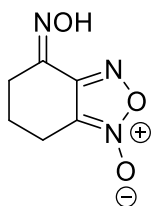


Preparation of 2,6-Dioximinocyclohexanone (2): To a solution of 50 g. (0.509 moles) of cyclohexanone on 200 ml. of ether was added 11 ml. of con. HCl. The reaction mixture was cooled to 10 °C, and nitrogen gas was passed slowly through it for 15-20 min. Then methyl nitrite was passed slowly from an external generator. The methyl nitrite gas was generated by adding a solution of 32 ml. of con. H₂SO₄ in 58 ml. of H₂O dropwise to a mixture of 86 g. of sodium nitrite, 41 g. of methanol, and 76 ml. of H₂O. The temperature was maintained at 5- 10 °C, while the methyl nitrite was passed in over about 2 h until the methyl nitrite gas was seized. A pale Yellow solid was precipitated as the reaction proceeded. Then the reaction mixture was stirred at 25 °C for about 2h, the solid was filtered on Buckner funnel and washed with (100 ml x 2) diethyl ether and dried thoroughly to obtain pure product **2** as a pale yellow solid (70.8 g, 89% yield). ¹H NMR (400 MHz, DMSO-d₆): δ (ppm): 2.69-2.65 (t, *J* = 6.5 Hz, 4H), 1.76-1.69 (m, 2H); ¹³C NMR (100 MHz, DMSO-d₆): δ (ppm): 181.6, 154.6, 24.3, 17.9; MS (EI, m/z): 156 [M]⁺.

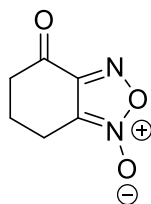


Preparation of 1, 2, 3-Cyclohexane trioxime (3): To a solution of compound-2, 31.3 g. (0.2 moles) in 300 ml. of 50% aq Ethanol was added 12.9g. of Na₂CO₃, followed by 17.4 g of Hydroxylamine hydrochloride at stirring. The stirring was continued at 25 °C for about overnight. The precipitate obtained was filtered on Buckner funnel and washed with (50 ml x 2) of H₂O. The solid was dried thoroughly to obtain compound-3 as a pale brown solid (27 g, 80% yield). ¹H

NMR (400 MHz, DMSO-d₆): δ (ppm): 12.59 (s, 1H), 11.83 (s, 1H), 11.33 (s, 1H), 2.58-2.49 (m, 4H), 1.65-1.56 (m, 2H); ¹³C NMR (100 MHz, DMSO-d₆): δ (ppm): 154.6, 153.1, 144.2, 25.2, 24.9, 18.1; MS (EI, m/z): 171 [M]⁺.

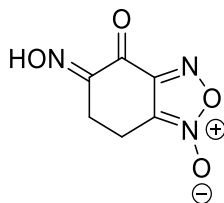


Preparation of 4-Hydroxyimino-4,5,6,7-tetrahydrobenzo[c][1,2,5]oxadiazole 1-oxide (4): To a solution of 10 g. (0.058 moles) of trioxime **3** in 35 ml. of 10% NaOH was added at reaction temperature 5-10 °C a solution of sodium hypobromite prepared from 4.67 g. of NaOH in 44 ml. of water and 1.5 ml. of bromine. The reaction mixture was stirred 1h at 25 °C and 8 ml. of con .HCl was added drop wise over a period of 10 min. The precipitate obtained was filtered on Buckner funnel and washed with (20 ml. x 2) H₂O and dried to obtain compound-**4** as a pale yellow solid (8.1 g. 82% yield). ¹H NMR (400 MHz, DMSO-d₆): δ (ppm): 12.26 (s, 1H), 2.71-2.61 (m, 4H), 1.89-1.81 (m, 2H); ¹³C NMR (100 MHz, DMSO-d₆): δ (ppm): 152.0, 145.3, 114.3, 22.6, 19.5, 19.2; MS (EI, m/z): 169 [M]⁺.



Preparation of 4-oxo-4,5,6,7-tetrahydrobenzo[c][1,2,5]oxadiazole 1-oxide (5): To a stirred solution of 8g (0.04 moles) compound-**4** in 70 ml. of 30% formaldehyde was added 53 ml. of con HCl, slowly dropwise over a period of 20 min. Continued the stirring at 25 °C for about 20 min and extracted with

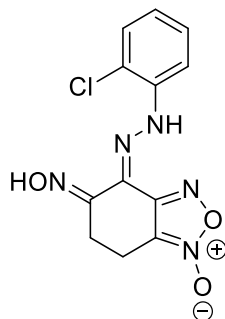
chloroform (2 x 100 ml). The organic layer was separated and washed with water (2 x 100 ml) and dried over anhydrous Na₂SO₄ and concentrated on rota vapour under reduced vacuum to give the product **5** as pale yellow solid (6.5g 90% yield). ¹H NMR (400 MHz, DMSO-d₆): δ (ppm): 2.91-2.85 (t, *J* = 6.25 Hz, 2H), 2.78-2.73 (m, 2H), 2.30-2.21 (m, 2H); ¹³C NMR (100 MHz, DMSO-d₆): δ (ppm): 183.9, 145.9, 108.7, 35.2, 16.2, 14.5; MS (EI, m/z): 154 [M]⁺.



Preparation of 5-(hydroxyimino)-4-oxo-4,5,6,7-tetrahydrobenzo[c][1,2,5]oxadiazole 1-oxide (6): To a stirred solution of 6g (0.038 moles) compound **5** in 46 ml. of ethanol was added 46 ml. of acetic acid and 2.95 g (0.042 moles) of sodium nitrite at 0 °C. The stirring was continues at 0 °C for 4 h and at 25 °C for about overnight. The precipitate was filtered on Buckner funnel and washed with (2 x 10 ml) water and dried thoroughly to obtain product **6** as pale yellow solid. Evaporation of the filtrate gave a further amount of product. (5g, 70% yield). ¹H NMR (400 MHz, DMSO-d₆): δ (ppm): 13.12 (s, 1H), 3.08-3.02 (t, *J* = 6.8 Hz, 2H), 2.88-2.83 (t, *J* = 7.0 Hz, 2H); ¹³C NMR (100 MHz, DMSO-d₆): δ (ppm): 175.2, 153.6, 152.3, 115.1, 20.4, 16.2; MS (EI, m/z): 183 [M]⁺.

General procedure for the preparation of (4)-4-(Substituted aromatic hydrazono)-5-(hydroxyimino)-4,5,6,7-tetrahydrobenzo[c][1,2,5]oxadiazole 1-oxides (7a-z): To a stirred solution of 500 mg (2.73 mmoles, 1equi) of compound

6 in 10 ml. of ethanol was added corresponding hydrazine compounds (2.73 mmoles, 1 equi) and catalytic amount of acetic acid. The stirring was continued at 25 °C for 30 min. The precipitate was filtered on Buckner funnel and washed with (5 ml) of ethanol and dried thoroughly to obtain products (**7a-z**) as solids. (70-85% yield).

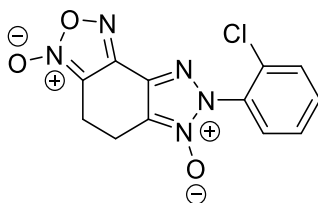


(4Z)-4-(2-(2-chlorophenyl)hydrazono)-5-(hydroxyimino)-4,5,6,7

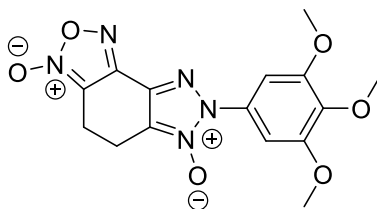
tetrahydrobenzo[c][1,2,5]oxadiazole 1-oxide (CMPD-A): To a stirred solution of 500 mg (2.73 mmoles) compound **6** in 10 ml. of ethanol was added 387 mg (2.73 mmoles) of 2-chlorophenyl hydrazine and catalytic amount of acetic acid. The stirring was continues at 25 °C for 30 min. The precipitate was filtered on Buckner funnel and washed with (5 ml) of ethanol and dried thoroughly to obtain product **7** as yellow solid. (710 mg, 85% yield). ¹H NMR (400 MHz, DMSO-d₆): δ (ppm): 13.33 (s, 1H), 12.4 (s, 1H), 7.71 (d, J = 9.1 Hz, 3.08-3.02 (t, J = 6.8 Hz, 2H), 2.88-2.83 (t, J = 7.0 Hz, 2H); ¹³C NMR (100 MHz, DMSO-d₆): δ (ppm): 153.8, 153.6, 139.9, 129.9, 129.04, 123.9, 122.1, 119.1, 114.9, 113.3, 20.2, 15.9; MS (EI, m/z): 307 [M]⁺.

General procedure for Preparation of 7-(substituted aromatic)-5,7-dihydro-4H-[1,2,3]triazolo[4',5':3,4]benzo[1,2-c][1,2,5]oxadiazole 3,6-dioxide (8a-o):

To a solution of corresponding hydrazones (1 equi) in acetonitrile (100 times), activated MnO₂ (7 equi) was added. The reaction mixture was stirred at 85 °C for 2-3 h. (until all the starting compound has disappeared, TLC monitoring). After completion of the reaction the reaction mixture was cooled to 25 °C and filtered on Buckner funnel over celite and washed with acetonitrile (2x 50 ml). The filtrate was evaporated on rota vapour at reduced vacuum and the crude product was purified by column chromatography (silica gel 120-200 mesh) using Ethylacetate/n-Hexane as eluents to afford the compounds with high purity (**8a-o**).



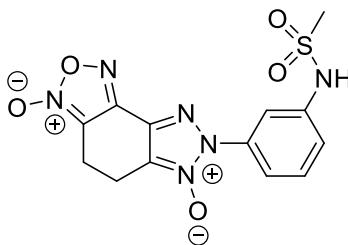
7-(2-Chlorophenyl)-5,7-dihydro-4H-[1,2,3]triazolo[4',5':3,4]benzo[1,2-c][1,2,5]oxadiazole 3,6-dioxide (CMPD-A): Compound **A** was prepared according to the method described in general procedure. Employing compound **7A** (500 mg, 1.62 mmol) in 50 ml. of acetonitrile and MnO₂ (990 mg, 11.4 mmol) to obtain compound-**A** as pale yellow solid (440 mg, 90% yield). ¹H NMR (400 MHz, CDCl₃): δ (ppm): 7.68-7.49 (m, 5H), 3.28-3.21 (m, 2H), 3.19-3.13 (m, 2H); ¹³C NMR (100 MHz, CDCl₃): δ (ppm): 147.9, 134.3, 133.4, 132.6, 131.4, 131.1, 129.1, 125.7, 17.1, 16.5; MS (EI, m/z): 305 [M]⁺.



7-(3,4,5-Trimethoxyphenyl)-5,7-dihydro-4H-

[1,2,3]triazolo[4',5':3,4]benzo[1,2-c][1,2,5]oxadiazole 3,6-dioxide (8a):

Compound **8a** was prepared according to the method described in general procedure. Employing compound **7a** (500 mg, 1.37 mmol) in 50 ml. of acetonitrile and MnO₂ (838 mg, 9.59 mmol) to obtain **8a** as brown solid (460 mg, 95% yield). ¹H NMR (400 MHz, DMSO-d₆): δ (ppm): 7.30 (s, 2H), 3.94(s, 6H), 3.93 (s, 3H), 3.24-3.20 (m, 2H), 3.17-3.13 (m, 2H); ¹³C NMR (100 MHz, DMSO-d₆): δ (ppm): 147.9, 134.3, 133.4, 132.6, 131.4, 131.1, 129.1, 125.7, 17.1, 16.5; MS (EI, m/z): 363 [M]⁺.

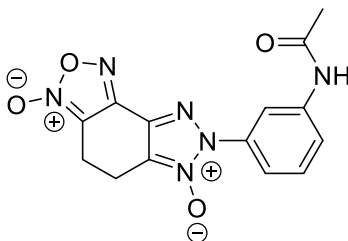


7-(3-(methylsulfonamido)phenyl)-5,7-dihydro-4H-

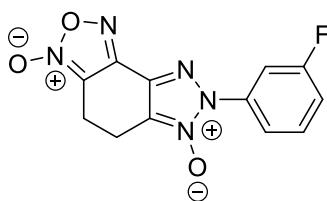
[1,2,3]triazolo[4',5':3,4]benzo[1,2-c][1,2,5]oxadiazole 3,6-dioxide (8b):

Compound **8b** was prepared according to the method described in general procedure. Employing compound **7b** (500 mg, 1.366 mmol) in 50 ml. of acetonitrile and MnO₂ (831 mg, 9.56 mmol) to obtain **8b** as pale yellow solid (440

mg, 90% yield). ^1H NMR (400 MHz, DMSO- d_6): δ (ppm): 10.21 (bs, 1H), 7.79 (s, 1H), 7.67 (d, $J = 8.2$ Hz, 1H), 7.60 (t, $J = 8.1$ Hz, 1H), 7.39 (d, $J = 8.1$ Hz, 1H), 3.32 (s, 3H), 3.01 (s, 4H); ^{13}C NMR (100 MHz, DMSO- d_6): δ (ppm): 147.8, 139.8, 135.2, 132.5, 130.9, 127.2, 120.7, 118.6, 113.9, 112.9, 17.1, 16.6; MS (EI, m/z): 366 $[\text{M}]^+$.

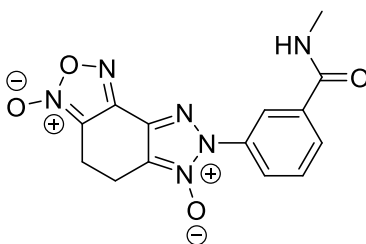


7-(3-acetamidophenyl)-5,7-dihydro-4H-[1,2,3]triazolo[4',5':3,4]benzo[1,2-c][1,2,5]oxadiazole 3,6-dioxide (8c): Compound **8c** was prepared according to the method described in general procedure. Employing compound **7c** (500 mg, 1.5 mmol) in 50 ml. of acetonitrile and MnO_2 (921 mg, 10.6 mmol) to obtain **8c** as pale yellow solid (457 mg, 92% yield). ^1H NMR (400 MHz, DMSO- d_6): δ (ppm): 10.31 (bs, 1H), 8.28 (s, 1H), 7.69 (d, $J = 8.0$ Hz, 1H), 7.61 (d, $J = 8.5$ Hz, 1H), 7.55 (t, $J = 8.1$ Hz, 1H), 3.08 (s, 4H), 2.09 (s, 3H); ^{13}C NMR (100 MHz, DMSO- d_6): δ (ppm): 169.2, 147.8, 140.6, 134.8, 132.4, 130.1, 127.2, 120.3, 118.2, 114.0, 112.9, 24.5, 17.1, 16.6; MS (EI, m/z): 330 $[\text{M}]^+$.



7-(3-fluorophenyl)-5,7-dihydro-4H-[1,2,3]triazolo[4',5':3,4]benzo[1,2-

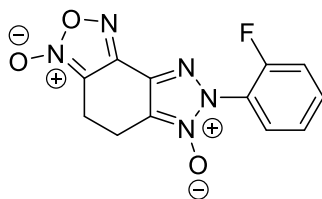
c][1,2,5]oxadiazole 3,6-dioxide (8d): Compound **8d** was prepared according to the method described in general procedure. Employing compound **7d** (500 mg, 1.36 mmol) in 50 ml. of acetonitrile and MnO₂ (1.04 g, 11.97mmol) to obtain **8d** as pale yellow solid (450 mg, 92% yield). ¹H NMR (400 MHz, DMSO-d₆): δ (ppm): 7.91-7.87 (m, 1H), 7.82-7.80 (m, 1H), 7.51-7.46 (m, 1H), 3.09 (s, 4H); ¹³C NMR (100 MHz, DMSO-d₆): δ (ppm):163.3, 160.8, 147.7, 135.6, 132.8, 131.9, 127.3, 119.9, 117.4, 112.9, 111.0, 17.0, 16.6; MS (EI, m/z): 289 [M]⁺.



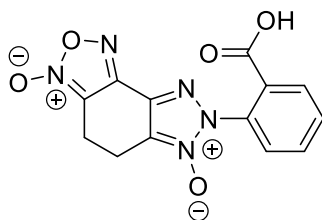
7-(3-(methylcarbamoyl)phenyl)-5,7-dihydro-4H-

[1,2,3]triazolo[4',5':3,4]benzo[1,2-c][1,2,5]oxadiazole 3,6-dioxide (8e):

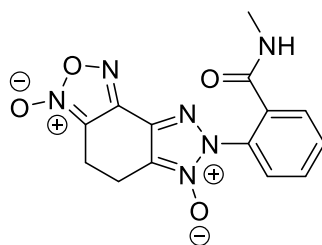
Compound **8e** was prepared according to the method described in general procedure. Employing compound **7e** (500 mg, 1.5mmol) in 50 ml. of acetonitrile and MnO₂ (921 mg, 10.6 mmol) to obtain **8a** as pale yellow solid (457 mg, 92% yield). ¹H NMR (400 MHz, DMSO-d₆): δ (ppm): 8.70 (bs, 1H), 8.35 (t, J = 1.84 Hz, 1H), 8.12-8.03 (m, 2H), 7.75 (t, J = 7.9 Hz, 1H), 3.09 (s, 4H), 2.82 (d, J = 4.5 Hz, 3H); ¹³C NMR (100 MHz, DMSO-d₆): δ (ppm):; MS (EI, m/z): 328 [M]⁺.



7-(2-fluorophenyl)-5,7-dihydro-4H-[1,2,3]triazolo[4',5':3,4]benzo[1,2-c][1,2,5]oxadiazole 3,6-dioxide (8f): Compound **8f** was prepared according to the method described in general procedure. Employing compound **7f** (500 mg, 1.71 mmol) in 50 ml. of acetonitrile and MnO₂ (1.04g, 11.97 mmol) to obtain **8f** as pale yellow solid (450 mg, 92% yield). ¹H NMR (400 MHz, CDCl₃): δ (ppm): 7.68-7.59 (m, 2H), 7.42-7.35 (m, 2H), 3.26-3.22 (m, 2H), 3.17-3.13 (m, 2H); ¹³C NMR (100 MHz, CDCl₃): δ (ppm):158.5, 156.0, 147.8, 134.6, 133.7, 130.3, 126.0, 125.9, 121.4, 117.6, 112.9, 17.1, 16.6; MS (EI, m/z): 289 [M]⁺.



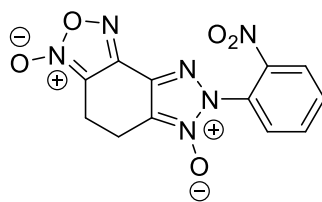
7-(2-carboxyphenyl)-5,7-dihydro-4H-[1,2,3]triazolo[4',5':3,4]benzo[1,2-c][1,2,5]oxadiazole 3,6-dioxide (8g): Compound **8g** was prepared according to the method described in general procedure. Employing compound **7g** (500 mg, 1.57 mmol) in 50 ml. of acetonitrile and MnO₂ (960 mg, 11.04 mmol) to obtain **8g** as pale yellow solid (450 mg, 91% yield). ¹H NMR (400 MHz, DMSO-d₆): δ (ppm): 13.42 (bs, 1H), 8.06 (d, J = 8.2 Hz, 1H), 7.87-7.76 (m, 2H), 3.07 (s, 4H); ¹³C NMR (100 MHz, DMSO-d₆): δ (ppm); MS (EI, m/z): 315 [M]⁺.



7-(2-(methylcarbamoyl)phenyl)-5,7-dihydro-4H-

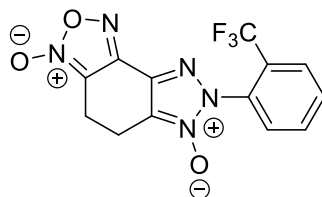
[1,2,3]triazolo[4',5':3,4]benzo[1,2-c][1,2,5]oxadiazole 3,6-dioxide (8h):

Compound **8h** was prepared according to the method described in general procedure. Employing compound **7h** (500 mg, 1.5 mmol) in 50 ml. of acetonitrile and MnO₂ (921 mg, 10.6 mmol) to obtain **8h** as pale yellow solid (450 mg, 92% yield). ¹H NMR (400 MHz, DMSO-d₆): δ (ppm): 8.57 (bs, 1H), 7.80-7.69 (m, 4H), 3.12-3.02 (m, 4H), 2.69-2.65 (m, 3H); ¹³C NMR (100 MHz, DMSO-d₆): δ (ppm): 165.8, 147.9, 134.1, 132.0, 131.7, 131.6, 129.0, 128.9, 125.6, 112.9, 26.6, 17.1, 16.4; MS (EI, m/z): 328 [M]⁺.



7-(2-nitrophenyl)-5,7-dihydro-4H-[1,2,3]triazolo[4',5':3,4]benzo[1,2-

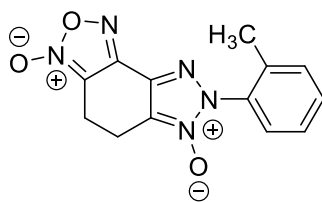
c][1,2,5]oxadiazole 3,6-dioxide (8i): Compound **8i** was prepared according to the method described in general procedure. Employing compound **7i** (500 mg, 1.57 mmol) in 50 ml. of acetonitrile and MnO₂ (956 mg, 11.0 mmol) to obtain **8i** as pale yellow solid (457 mg, 92% yield). ¹H NMR (400 MHz, DMSO-d₆): δ (ppm): 7.68-7.49 (m, 5H), 3.28-3.21 (m, 2H), 3.19-3.13 (m, 2H); ¹³C NMR (100 MHz, DMSO-d₆): δ (ppm):; MS (EI, m/z): 316 [M]⁺.



7-(2-(trifluoromethyl)phenyl)-5,7-dihydro-4H-

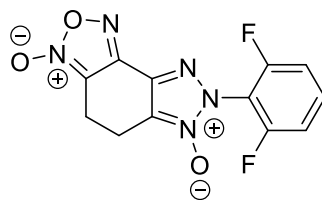
[1,2,3]triazolo[4',5':3,4]benzo[1,2-c][1,2,5]oxadiazole 3,6-dioxide (8j):

Compound **8j** was prepared according to the method described in general procedure. Employing compound **7j** (500 mg, 1.46 mmol) in 50 ml. of acetonitrile and MnO₂ (892 mg, 10.26 mmol) to obtain **8j** as pale yellow solid (462 mg, 93% yield). ¹H NMR (400 MHz, DMSO-d₆): δ (ppm): 8.12 (d, J = 8.7 Hz, 1H), 8.01 (q, J = 7.6, 7.1 Hz, 2H), 7.88 (d, J = 7.2 Hz, 1H), 3.10 (s, 4H); ¹³C NMR (100 MHz, DMSO-d₆): δ (ppm):156.6, 147.7, 134.1, 133.6, 132.1, 130.0, 128.2, 125.1, 112.9, 17.1, 16.5; MS (EI, m/z): 339 [M]⁺.

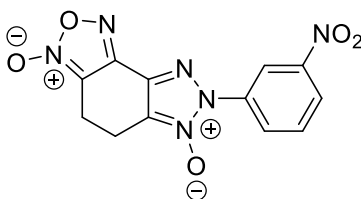


7-(o-tolyl)-5,7-dihydro-4H-[1,2,3]triazolo[4',5':3,4]benzo[1,2-

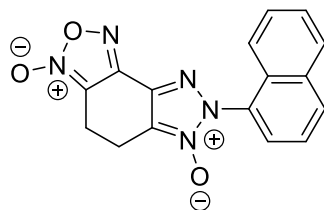
c][1,2,5]oxadiazole 3,6-dioxide (8k): Compound **8k** was prepared according to the method described in general procedure. Employing compound **7k** (500 mg, 1.74 mmol) in 50 ml. of acetonitrile and MnO₂ (1.06 g, 12.19 mmol) to obtain **8k** as pale yellow solid (460 mg, 92% yield). ¹H NMR (400 MHz, CDCl₃): δ (ppm): 7.55-7.51 (m, 1H), 7.45-7.37 (m, 3H), 3.28-3.21 (m, 4H), 2.28 (s, 3H); ¹³C NMR (100 MHz, CDCl₃): δ (ppm):146.3, 137.0, 132.8, 131.9, 131.8, 131.4, 127.9, 127.0, 124.4, 110.4, 17.8, 17.0, 16.5; MS (EI, m/z): 285 [M]⁺.



7-(2,6-difluorophenyl)-5,7-dihydro-4H-[1,2,3]triazolo[4',5':3,4]benzo[1,2-c][1,2,5]oxadiazole 3,6-dioxide (8l): Compound **8l** was prepared according to the method described in general procedure. Employing compound **7l** (500 mg, 1.61 mmol) in 50 ml. of acetonitrile and MnO₂ (892 mg, 10.26 mmol) to obtain **8l** as pale yellow solid (463 mg, 93% yield). ¹H NMR (400 MHz, DMSO-d₆): δ (ppm): 7.95-7.86 (m, 1H), 7.59-7.51 (m, 3H), 3.10 (s, 4H); ¹³C NMR (100 MHz, DMSO-d₆): δ (ppm):159.8, 157.2, 136.1, 133.2, 125.9, 113.7, 13.6, 110.8, 17.0, 16.6; MS (EI, m/z): 307 [M]⁺.

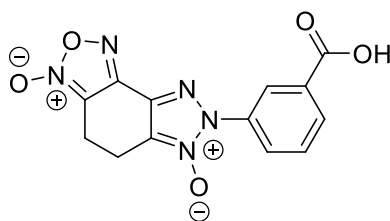


7-(3-nitrophenyl)-5,7-dihydro-4H-[1,2,3]triazolo[4',5':3,4]benzo[1,2-c][1,2,5]oxadiazole 3,6-dioxide (8m): Compound **8m** was prepared according to the method described in general procedure. Employing compound **7m** (500 mg, 1.57 mmol) in 50 ml. of acetonitrile and MnO₂ (950 mg, 11.0 mmol) to obtain **8m** as pale yellow solid (467 mg, 94% yield). ¹H NMR (400 MHz, DMSO-d₆): δ (ppm): 8.85 (s, 1H), 8.44-8.39 (m, 2H), 7.95 (t, J = 8.2 Hz, 1H), 3.11 (s, 4H); ¹³C NMR (100 MHz, DMSO-d₆): δ (ppm):148.3, 147.6, 135.0, 133.2, 131.6, 129.5, 127.5, 124.7, 118.7, 112.9, 17.1, 16.6; MS (EI, m/z): 367 [M]⁺.



7-(naphthalen-1-yl)-5,7-dihydro-4H-[1,2,3]triazolo[4',5':3,4]benzo[1,2-

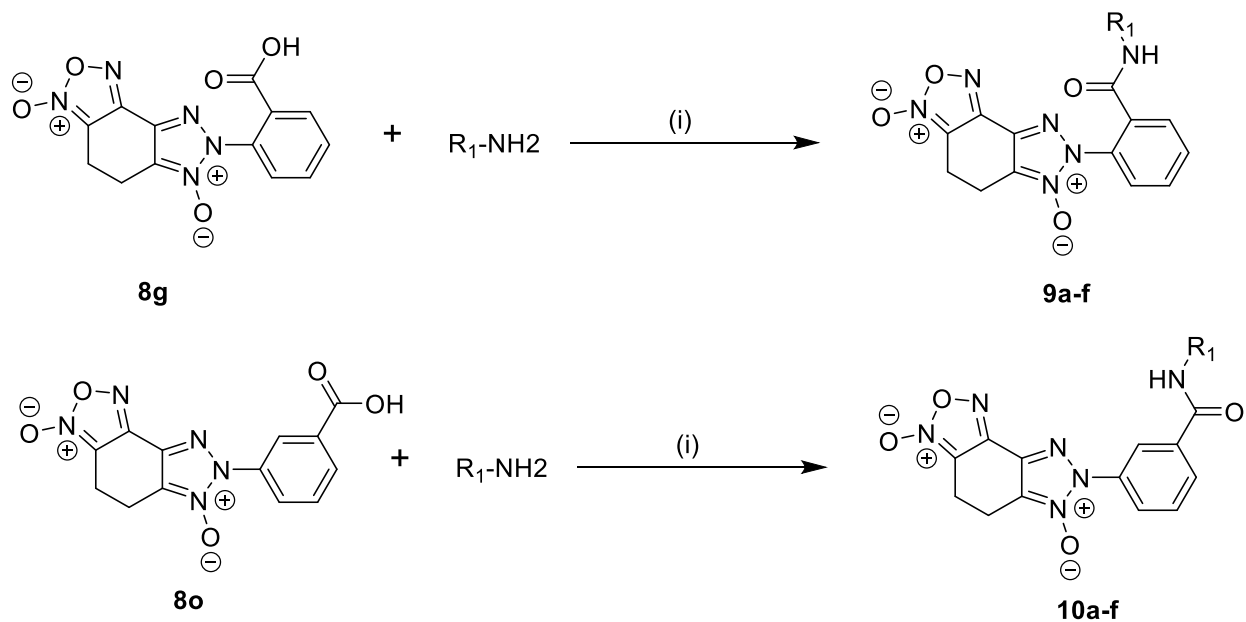
c][1,2,5]oxadiazole 3,6-dioxide (8n): Compound **8n** was prepared according to the method described in general procedure. Employing compound **7n** (500 mg, 1.54 mmol) in 50 ml. of acetonitrile and MnO₂ (940 mg, 10.83 mmol) to obtain **8n** as pale yellow solid (450 mg, 91% yield). ¹H NMR (400 MHz, DMSO-d₆): δ (ppm): 8.32 (d, J = 8.2 Hz, 1H), 8.15 (d, J = 8.6 Hz, 1H), 7.89 (d, J = 7.3 Hz, 1H), 7.77 (t, J = 7.9 Hz, 1H), 7.72-7.69 (m, 2H), 7.48 (d, J = 7.1 Hz, 1H), 3.14 (s, 4H); ¹³C NMR (100 MHz, DMSO-d₆): δ (ppm): 147.9, 134.3, 133.4, 132.6, 131.4, 131.1, 129.1, 125.7, 17.1, 16.5; MS (EI, m/z): 321 [M]⁺.



7-(3-carboxyphenyl)-5,7-dihydro-4H-[1,2,3]triazolo[4',5':3,4]benzo[1,2-

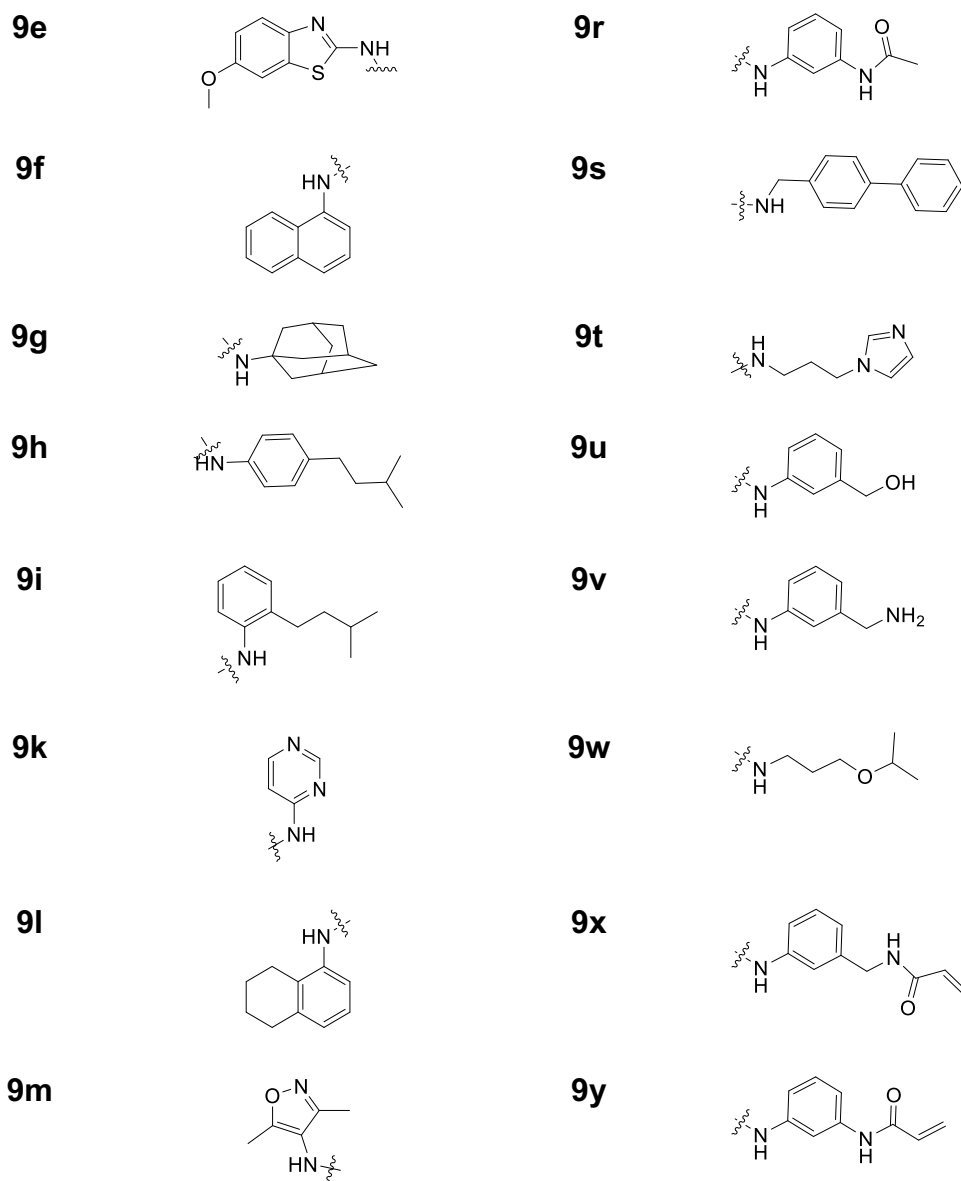
c][1,2,5]oxadiazole 3,6-dioxide (8o): Compound **8o** was prepared according to the method described in general procedure. Employing compound **7o** (500 mg, 1.57 mmol) in 50 ml. of acetonitrile and MnO₂ (960 mg, 11.04 mmol) to obtain **8o** as pale yellow solid (462 mg, 95% yield). ¹H NMR (400 MHz, DMSO-d₆): δ (ppm): 13.21(bs, 1H), 8.46 (s, 1H), 8.12 (d, J = 7.9 Hz, 2H), 7.75 (t, J = 7.9 Hz, 1H), 3.09 (s, 4H); ¹³C NMR (100 MHz, DMSO-d₆): δ (ppm): 147.9, 134.3, 133.4, 132.6, 131.4, 131.1, 129.1, 125.7, 17.1, 16.5; MS (EI, m/z): 315 [M]⁺.

Scheme-II Synthesis of amides (9a-z):



Reagents and conditions: 8g/8o and Corresponding Amines (i) HATU, DIPEA and Dry DMF 25 °C, 4h (90%).

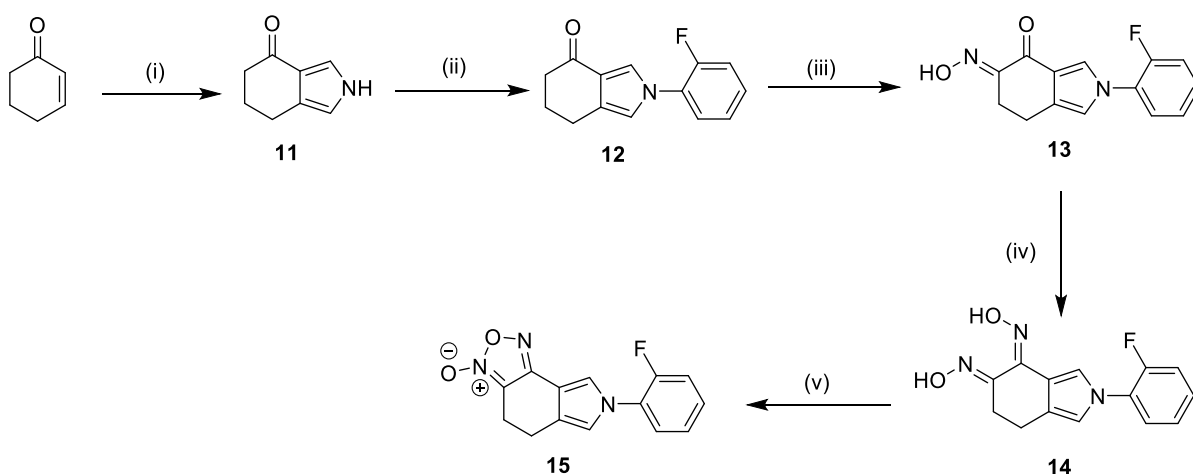
Compound	R ₁	Compound	R ₁
9a		9n	
9b		9o	
9c		9p	
9d		9q	



General procedure for synthesis of compounds (9a-z): To a solution of compounds **8a/8o** (1 equi) in Dry DMF (100 times), HATU (1 equi) and DIPEA (3 equi) was added. The reaction mixture was stirred at 25 °C for 2-3 h. (until all the starting compound has disappeared, TLC monitoring). After completion of the reaction, ethyl acetate (100 mL) was added and washed with sat. NaCl sol. (100 mL x 2) and water (100 mL) separated the organic layer and dried over

anhydrous Na₂SO₄. The solvent was evaporated on rota vapour at reduced vacuum and the crude product was purified by column chromatography (silica gel 120-200 mesh) using Ethylacetate/n-Hexane as eluents to afford the compounds with high purity (**9a-z**).

Scheme-III Synthesis of compound **15**:



Reagents and conditions: (i) *p*-toluenesulfonylmethyl isocyanide (TOSMIC), *t*-BuOK and Dry THF, 25 °C, 1h (85%); (ii) N-methyl-2-pyrrolidone (NMP), K₂CO₃, 2-Fluoroiodobenzene and Copper (I) bromide, 205 °C, 24h (40%); (iii) Isoamyl nitrite, *t*-BuOK *t*-butanol 25 °C for 30 min (60%); (iv) NH₂OH.HCl, MeOH, 70 °C 1h (80%); (v) NaOBr aq Sol, H₂O, 30 min (85%).

6.6 References

Aharony, I., D. E. Ehrnhoefer, A. Shruster, X. Qiu, S. Franciosi, M. R. Hayden, and D. Offen. 2015. A Huntingtin-based peptide inhibitor of caspase-6 provides protection from mutant Huntingtin-induced motor and behavioral deficits. *Hum Mol Genet*, 24:2604-14.

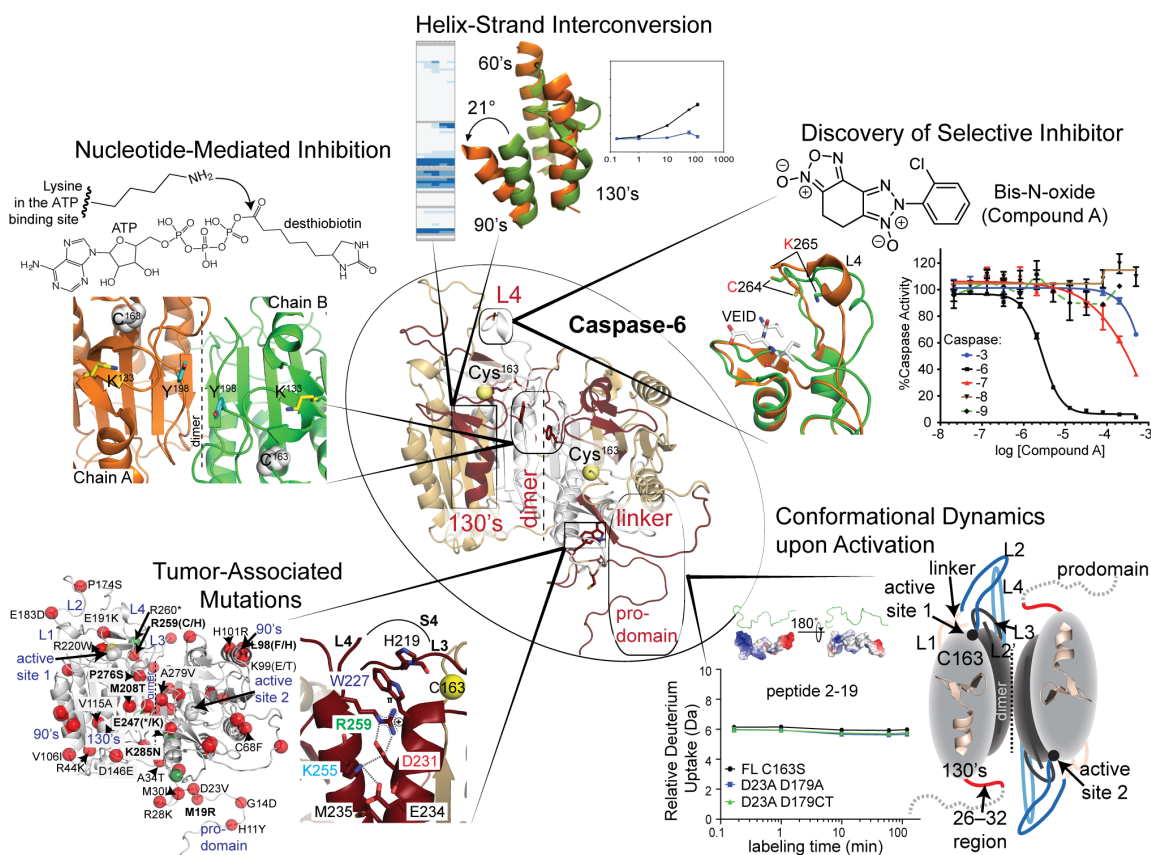
- Albrecht, S., N. Bogdanovic, B. Ghetti, B. Winblad, and A. C. LeBlanc. 2009. Caspase-6 activation in familial alzheimer disease brains carrying amyloid precursor protein or presenilin I or presenilin II mutations. *J Neuropathol Exp Neurol*, 68:1282-93.
- Albrecht, S., M. Bourdeau, D. Bennett, E. J. Mufson, M. Bhattacharjee, and A. C. LeBlanc. 2007. Activation of caspase-6 in aging and mild cognitive impairment. *Am J Pathol*, 170:1200-9.
- Bao, Q., and Y. Shi. 2007. Apoptosome: a platform for the activation of initiator caspases. *Cell Death and Differentiation*, 14:56-65.
- Chu, W., J. Rothfuss, Y. Chu, D. Zhou, and R. H. Mach. 2009. Synthesis and in vitro evaluation of sulfonamide isatin Michael acceptors as small molecule inhibitors of caspase-6. *J Med Chem*, 52:2188-91.
- Chu, Z. L., F. Pio, Z. Xie, K. Welsh, M. Krajewska, S. Krajewski, A. Godzik, and J. C. Reed. 2001. A novel enhancer of the Apaf1 apoptosome involved in cytochrome c-dependent caspase activation and apoptosis. *Journal of Biological Chemistry*, 276:9239-45.
- Dubovsky, J. A., K. A. Beckwith, G. Natarajan, J. A. Woyach, S. Jaglowski, Y. Zhong, J. D. Hessler, T. M. Liu, B. Y. Chang, K. M. Larkin, M. R. Stefanovski, D. L. Chappell, F. W. Frizzera, L. L. Smith, K. A. Smucker, J. M. Flynn, J. A. Jones, L. A. Andritsos, K. Maddocks, A. M. Lehman, R. Furman, J. Sharman, A. Mishra, M. A. Caligiuri, A. R. Satoskar, J. J. Buggy, N. Muthusamy, A. J. Johnson, and J. C. Byrd. 2013. Ibrutinib is an irreversible molecular inhibitor of ITK driving a Th1-selective pressure in T lymphocytes. *Blood*, 122:2539-49.
- Ekici, O. D., Z. Z. Li, A. J. Campbell, K. E. James, J. L. Asgian, J. Mikolajczyk, G. S. Salvesen, R. Ganesan, S. Jelakovic, M. G. Grutter, and J. C. Powers. 2006. Design, synthesis, and evaluation of aza-peptide Michael acceptors as selective and potent inhibitors of caspases-2, -3, -6, -7, -8, -9, and -10. *J Med Chem*, 49:5728-49.
- Graham, R. K., Y. Deng, J. Carroll, K. Vaid, C. Cowan, M. A. Pouladi, M. Metzler, N. Bissada, L. Wang, R. L. Faull, M. Gray, X. W. Yang, L. A. Raymond, and M. R. Hayden. 2010. Cleavage at the 586 amino acid caspase-6 site in mutant huntingtin influences caspase-6 activation in vivo. *J Neurosci*, 30:15019-29.
- Guo, H., S. Albrecht, M. Bourdeau, T. Petzke, C. Bergeron, and A. C. LeBlanc. 2004. Active caspase-6 and caspase-6-cleaved tau in neuropil threads, neuritic plaques, and neurofibrillary tangles of Alzheimer's disease. *Am J Pathol*, 165:523-31.
- Guterman, L. 2011. COVALENT DRUGS FORM LONG-LIVED TIES. *Chemical & Engineering News Archive*, 89:19-26.
- Hakem, R., A. Hakem, G. S. Duncan, J. T. Henderson, M. Woo, M. S. Soengas, A. Elia, J. L. de la Pompa, D. Kagi, W. Khoo, J. Potter, R. Yoshida, S. A. Kaufman, S. W. Lowe, J. M. Penninger, and T. W. Mak. 1998. Differential requirement for caspase 9 in apoptotic pathways in vivo. *Cell*, 94:339-52.

- Heise, C. E., J. Murray, K. E. Augustyn, B. Bravo, P. Chugha, F. Cohen, A. M. Giannetti, P. Gibbons, R. N. Hannoush, B. R. Hearn, P. Jaishankar, C. Q. Ly, K. Shah, K. Stanger, M. Steffek, Y. Tang, X. Zhao, J. W. Lewcock, A. R. Renslo, J. Flygare, and M. R. Arkin. 2012. Mechanistic and structural understanding of uncompetitive inhibitors of caspase-6. *PLoS One*, 7:e50864.
- James, K. E., J. L. Asgian, Z. Z. Li, O. D. Ekici, J. R. Rubin, J. Mikolajczyk, G. S. Salvesen, and J. C. Powers. 2004. Design, synthesis, and evaluation of aza-peptide epoxides as selective and potent inhibitors of caspases-1, -3, -6, and -8. *J Med Chem*, 47:1553-74.
- Kuida, K., T. F. Haydar, C. Y. Kuan, Y. Gu, C. Taya, H. Karasuyama, M. S. Su, P. Rakic, and R. A. Flavell. 1998. Reduced apoptosis and cytochrome c-mediated caspase activation in mice lacking caspase 9. *Cell*, 94:325-37.
- Kuida, K., T. S. Zheng, S. Na, C. Kuan, D. Yang, H. Karasuyama, P. Rakic, and R. A. Flavell. 1996. Decreased apoptosis in the brain and premature lethality in CPP32-deficient mice. *Nature*, 384:368-72.
- Lamkanfi, M., N. Festjens, W. Declercq, T. Vanden Berghe, and P. Vandenabeele. 2007. Caspases in cell survival, proliferation and differentiation. *Cell Death Differ*, 14:44-55.
- Leyva, M. J., F. Degiacomo, L. S. Kaltenbach, J. Holcomb, N. Zhang, J. Gafni, H. Park, D. C. Lo, G. S. Salvesen, L. M. Ellerby, and J. A. Ellman. 2010. Identification and evaluation of small molecule pan-caspase inhibitors in Huntington's disease models. *Chem Biol*, 17:1189-200.
- McStay, G. P., G. S. Salvesen, and D. R. Green. 2008. Overlapping cleavage motif selectivity of caspases: implications for analysis of apoptotic pathways. *Cell Death Differ*, 15:322-31.
- Murray, J., A. M. Giannetti, M. Steffek, P. Gibbons, B. R. Hearn, F. Cohen, C. Tam, C. Pozniak, B. Bravo, J. Lewcock, P. Jaishankar, C. Q. Ly, X. Zhao, Y. Tang, P. Chugha, M. R. Arkin, J. Flygare, and A. R. Renslo. 2014. Tailoring small molecules for an allosteric site on procaspase-6. *ChemMedChem*, 9:73-7, 2.
- Muzio, M., A. M. Chinnaiyan, F. C. Kischkel, K. O'Rourke, A. Shevchenko, J. Ni, C. Scaffidi, J. D. Bretz, M. Zhang, R. Gentz, M. Mann, P. H. Krammer, M. E. Peter, and V. M. Dixit. 1996. FLICE, a novel FADD-homologous ICE/CED-3-like protease, is recruited to the CD95 (Fas/APO-1) death-inducing signaling complex. *Cell*, 85:817-27.
- Nyormoi, O., Z. Wang, and M. Bar-Eli. 2003. Sequence-based discovery of a synthetic peptide inhibitor of caspase 6. *Apoptosis*, 8:371-6.
- Oberst, A., C. Pop, A. G. Tremblay, V. Blais, J. B. Denault, G. S. Salvesen, and D. R. Green. 2010. Inducible dimerization and inducible cleavage reveal a requirement for both processes in caspase-8 activation. *Journal of Biological Chemistry*, 285:16632-42.
- Pakavathkumar, P., A. Noel, C. Lecrux, A. Tubeleviciute-Aydin, E. Hamel, J. E. Ahlfors, and A. C. LeBlanc. 2017. Caspase vinyl sulfone small molecule inhibitors prevent axonal degeneration in human neurons and reverse cognitive impairment in Caspase-6-overexpressing mice. *Mol Neurodegener*, 12:22.

- Pakavathkumar, P., G. Sharma, V. Kaushal, B. Foveau, and A. C. LeBlanc. 2015. Methylene Blue Inhibits Caspases by Oxidation of the Catalytic Cysteine. *Sci Rep*, 5:13730.
- Pop, C., J. Timmer, S. Sperandio, and G. S. Salvesen. 2006. The apoptosome activates caspase-9 by dimerization. *Molecular Cell*, 22:269-75.
- Riechers, S. P., S. Butland, Y. Deng, N. Skotte, D. E. Ehrnhoefer, J. Russ, J. Laine, M. Laroche, M. A. Pouladi, E. E. Wanker, M. R. Hayden, and R. K. Graham. 2016. Interactome network analysis identifies multiple caspase-6 interactors involved in the pathogenesis of HD. *Hum Mol Genet*, 25:1600-18.
- Singh, J., R. C. Petter, T. A. Baillie, and A. Whitty. 2011. The resurgence of covalent drugs. *Nat Rev Drug Discov*, 10:307-17.
- Stanger, K., M. Steffek, L. Zhou, C. D. Pozniak, C. Quan, Y. Franke, J. Tom, C. Tam, J. M. Elliott, J. W. Lewcock, Y. Zhang, J. Murray, and R. N. Hannoush. 2012. Allosteric peptides bind a caspase zymogen and mediate caspase tetramerization. *Nat Chem Biol*, 8:655-60.
- Vaidya, S., E. M. Velazquez-Delgado, G. Abbruzzese, and J. A. Hardy. 2011. Substrate-induced conformational changes occur in all cleaved forms of caspase-6. *J Mol Biol*, 406:75-91.
- Varfolomeev, E. E., M. Schuchmann, V. Luria, N. Chiannikulchai, J. S. Beckmann, I. L. Mett, D. Rebrikov, V. M. Brodianski, O. C. Kemper, O. Kollet, T. Lapidot, D. Soffer, T. Sobe, K. B. Avraham, T. Goncharov, H. Holtmann, P. Lonai, and D. Wallach. 1998. Targeted disruption of the mouse Caspase 8 gene ablates cell death induction by the TNF receptors, Fas/Apo1, and DR3 and is lethal prenatally. *Immunity*, 9:267-76.
- Wager, T. T., R. Y. Chandrasekaran, X. Hou, M. D. Troutman, P. R. Verhoest, A. Villalobos, and Y. Will. 2010. Defining desirable central nervous system drug space through the alignment of molecular properties, in vitro ADME, and safety attributes. *ACS Chem Neurosci*, 1:420-34.
- Warby, S. C., C. N. Doty, R. K. Graham, J. B. Carroll, Y. Z. Yang, R. R. Singaraja, C. M. Overall, and M. R. Hayden. 2008. Activated caspase-6 and caspase-6-cleaved fragments of huntingtin specifically colocalize in the nucleus. *Hum Mol Genet*, 17:2390-404.
- Woo, M., R. Hakem, M. S. Soengas, G. S. Duncan, A. Shahinian, D. Kagi, A. Hakem, M. McCurrach, W. Khoo, S. A. Kaufman, G. Senaldi, T. Howard, S. W. Lowe, and T. W. Mak. 1998. Essential contribution of caspase 3/CPP32 to apoptosis and its associated nuclear changes. *Genes and Development*, 12:806-19.
- Zheng, T. S., S. Hunot, K. Kuida, and R. A. Flavell. 1999. Caspase knockouts: matters of life and death. *Cell Death and Differentiation*, 6:1043-53.
- Zheng, T. S., S. Hunot, K. Kuida, T. Momoi, A. Srinivasan, D. W. Nicholson, Y. Lazebnik, and R. A. Flavell. 2000. Deficiency in caspase-9 or caspase-3 induces compensatory caspase activation. *Nature Medicine*, 6:1241-7.

CHAPTER 7

UNIQUELY CASPASE-6: PROPOSITIONS OF THE DISTINCT STRUCTURAL ARCHITECTURES ON FUNCTION AND TARGETED REGULATION OF CASPASE-6



A human being is a conglomerate of intricately woven cells packed into tissues and organs with specific vital functions. Individual cells within tissues are composed of biomolecules that associate in myriads of combinations within a molecularly crowded environment, to come up with an organized molecular ensemble that is poised to accomplish a specific cellular function. It takes a

village of ingenious minds to comprehend the governing molecular machineries within this tiny single cell. But this shared scientific knowledge amassed by the collective efforts of scientific experts around the world over the years has built the very foundation of the science behind the therapeutics that combat a range of diseases—from cancer to neurodegeneration—that surfaced from the molecular errors made by this tiny single cell along various cellular process.

Caspases are one class of molecular machines that direct programmed cell death in multicellular organisms. Their function must be stringently regulated to avoid the unwanted cellular consequences that result in mostly debilitating or even fatal diseases. The dissertation presents series of careful investigations into the structural dynamics and regulation of caspase-6, the function of which is associated with neurodegenerative diseases. Thus, it is essential to understand the fine and unique structural details of caspase-6, of which are often coupled to its function and regulation. Only then we can precisely control its specific function for therapeutic purposes.

Because of its association with neurodegeneration, caspase-6 has become an increasingly popular molecular target for drug development that is being pursued by both academic and pharmaceutical research laboratories. Nevertheless, existing limitations regarding its structure, function, and specific regulation need to be addressed. The visual summary of the body of work narrated throughout this dissertation is presented in Figure 7.1. In the attempt to relate structure-function relationships in caspase-6, Chapter II of this dissertation presents the structural dynamic studies of caspase-6 that revealed the unique

molecular switch at a potentially regulatory 130's region. Chapter III narrates further structural studies that uncovered the discrete and local dynamic conformational changes in key regions of caspase-6 that can be exploited as a complimentary scaffold for improved design of therapeutics. Meanwhile, the studies on mutations in the *CASP6* gene in several tumors (Chapter IV) took a naturally provided tour of the functionally sensitive regions in caspase-6. This study enabled the identification of stabilizing cation- π stacking interaction that broadly being utilized by caspases to support the proper assembly of its active site loops for substrate binding and catalysis. We have also uncovered another level of regulation through nucleotide binding at the dimer interface that appears to be procaspase-6 (zymogen) specific (Chapter V). The moderately conserved dimer interface emerged as an exploitable region for targeted regulation of caspase-6 as it can bind ligands from both natural and synthetic sources. Finally, an activity-based high throughput screen of specific binders of caspase-6 enabled the discovery of the most potent and selective inhibitors of caspase-6 to date. A series of careful experiments disclosed the specific covalent modification of Cys-264 within the most diversified loop region in caspases that explains the exquisite selectivity of bis-*N*-oxide inhibitors. Along with its favorable cell-based and medicinal chemical properties, the exquisitely selective bis-*N*-oxide inhibitors can potentially offer a targeted regulation of caspase-6 aimed to afford treatment of neurodegeneration as well as molecular tools to discover mechanisms and functions of caspase-6 activation in cells.

7.1 Proposed Functional and Regulatory Roles of the Structural Switch

The mobile loops of caspases are crucial for the assembly of the substrate-binding groove of binding and catalysis. Caspase-6 exists distinctly from other caspases because it has additional mobile regions. Crystallography (Vaidya, 2011; Wang et al., 2010) and the HDX-MS work (Dagbay et al., 2017) presented in Chapter II have identified the two distinct conformational states of the 130's region in caspase-6. Detailed MD simulations, mutagenesis, and thermal stability assays pinpointed Asp-135 within the 130's region to be critical in the helix-strand interconversion where the protonation of this residue contributes to the favoring of the extended helical state of caspase-6. Only upon substrate recruitment does this 130's region exist exclusively in the canonical strand conformation. Careful inspection of the residues on top of the 130's region shows patches of hydrophobic amino acids, e.i. tryptophan, tyrosine, and phenylalanine, that might engage in substrate recognition as a possible exosite. One can imagine the productive coupling of the protonation state of Asp-135 and the hydrophobic patch to be taken advantage by caspase-6 in cellular scenarios where a change in substrate preference is required, for example, under oxidative stress conditions (Majdi et al., 2016) and global brain ischemia (Ding et al., 2012), which both result in slight acidification. Probing the set of unique substrates that employ these hydrophobic patch and extended helix tandem for binding with caspase-6 is crucial in dissecting the specific protein-protein interactions involved in caspase-6 signaling given the association of caspase-6 in the multiple pathways to neurodegeneration (Wang et al., 2014). Recently, an

MS-based approach to identify unique natural substrates of caspases in cellular lysates was reported (Julien et al., 2016). Most substrates identified are novel with significant variations in their rate of cleavage, by up to 500-fold. Using this elegant approach, one can test the hypothesis that changes in substrate preferences by the exosite couple helical caspase-6 (mimicked by E135Q mutation) and the hydrophobic patch in relevant normal and disease neuronal cell lysates. One can specifically aim to make substitution mutations of the exposed hydrophobic patch residues and consider the changes on the substrate specificity and protein-protein interaction of caspase-6 using a panel of known protein substrates, i.e. microtubule-associated protein Tau, lamin A/C, by proteolytic cleavage and pull-down assays, respectively. A broader approach will be subjecting these hydrophobic patch mutation variants to the MS-based approach as described by Julien et al. (2016) using relevant neuronal lysates and determine the overall changes in the pattern of substrate recognition. One would expect that if the hydrophobic patch on top of the 130's helix plays a role in molecular recognition, there would be observed changes in the proteolytic cleavage pattern, protein-protein interaction, and substrate specificity profiles of these hydrophobic patch mutation variants compared with the wild type caspase-6. These approaches will ultimately reveal the relevance of the helix-strand transition along with the possible uncovering of novel neuronal factors within the caspase-6 signaling that may afford strategies for targeted regulation of caspase-6.

Moreover, the implication of the extended helical conformation in the specific regulation of caspase-6 for therapeutic ventures is exceptional. When

locked in the helical conformation, the Cys–His dyad is oriented in such a way that renders caspase-6 catalytically inefficient to turnover substrates. As it has been suggested before (Vaidya and Hardy, 2011; Vaidya et al., 2011), locking caspase-6 in the helical state using small molecules may provide a means for achieving caspase-6-specific inhibition. A continuing effort on the search for caspase-6 helical state binders is an important yet challenging stride. But once the proposed research goal of identifying the substrates that depend on the helical/hydrophobic patch tandem on binding is satisfied, one can strategically identify the caspase-6 binding epitope within the identified substrate through HDX-MS, and use it as a scaffold to develop peptide-based inhibitors directed to bind and lock the inactive helical state of caspase-6.

7.2 Implications of the Local Dynamic Changes and the Disordered

Prodomain

Uncovering the dynamic conformational changes in caspases upon proteolytic activation and substrate binding (Chapter III) provides lasting implications in structure-function studies and regulation of caspases. Over 226 structures of caspases have been reported to date, yet the complete depiction of the underlying mechanisms of caspase activation remain inadequate due to the missing information on conformational dynamics that is not quite satisfied by protein crystallography. Our report on the accompanying dynamic conformational changes along the proteolytic activation path of caspase-6 is the first of its kind within the caspase family. One example of a seemingly global approach to

determining the pattern of structural dynamics within protein family is that of Ras superfamily where distinguishing and shared signatures of dynamic conformational changes were revealed among eight members of Ras and Rho subfamilies (Harrison et al., 2016). Interestingly, the Ras superfamily members, despite varied functions, have similar tertiary structures irrespective of its diverse primary amino acid sequence. But the conformational dynamic profiles of Ras superfamily suggest that tertiary structure conservation does not necessarily result in the conservation of protein structural dynamics. This finding served as an inspiration to use HDX-MS to assess the hypothesis that caspases, despite their similarity in the overall protein fold, have diverse set of conformational dynamics that can contribute to the distinct substrate specificity and unique activation mechanism of each caspase. This will likely benefit future efforts on the design of a caspase-specific regulator to be used in drug discovery or as molecular probes to decipher additional caspase function in cells.

Along with the expected pattern of dynamic conformational changes in the substrate binding loops of caspase-6, these studies revealed several striking dynamic conformational changes in the regions of the prodomain, the directly adjoining 26–32 region, and the linker region (Chapter III). The conformational changes in the 26–32 region are dependent on the activation state of caspase-6. Moreover, the 26–32 region happens to be in the same loop as the exosite for substrate binding in caspase-7 (Boucher et al., 2012), the zinc ligands (Lys–36) identified in caspase-6 (Velazquez-Delgado and Hardy, 2012), and the regulatory phosphorylation site (Ser–30) in caspase-7, which modulates caspase-9 binding.

It is very tempting to speculate that a possible role of this region is in substrate recruitment or binding of key regulators of caspase-6, since this region shows variable conformational dynamics between its zymogen and active forms of the enzyme. One plausible future direction is directly mutating this region and then assess the propensity of this caspase-6 variant to bind a panel of protein substrates or consider its effect on the overall structure of caspase-6. Moreover, sequence alignment of all caspases suggests that the 26–32 is not conserved across caspases, thus opening the possibility that it is a regulatory site that binds to a select group of substrates in one caspase but not in any other caspases.

Finally, this work uncovered the intrinsically disordered nature of the prodomain and a region in the linker, both of which are also computationally predicted to be involved in protein binding. Moreover, a region in the linker is predicted to be involved in protein binding only in caspase-6 but not in other executioner caspases. One cannot avoid speculating that these regions are important protein-binding regions that regulate caspase-6 function. Given the reported roles of the prodomain in other caspases in protein–protein interactions (see Chapter III Discussion Section) and armed with an MS-based approach previously mentioned in a prior section 7.1 of this chapter, one can set out to test the hypothesis that the prodomain and linker are involved in regulatory protein–protein interactions by facilitating binding of caspase-6 to different cellular substrates under certain cellular conditions. The substrate preference of caspase-6 may vary depending on the presence of the prodomain or linker or both. Moreover, the inhibitory effect of the prodomain is observed in cells but not

under *in vitro* conditions (Klaiman et al., 2009) further suggesting that the presumed regulatory protein–protein interaction can only occur in the permissive environment of the cell. In addition, the fact that the prodomain in caspases is one of the most distinctive regions highlights the plethora of unique possible combinations of protein–protein interactions one caspase can make through its prodomain region, thus suggesting a route to targeted regulation in caspases. In fact, with the advent of the advanced antibody engineering technology, one could develop an antibody against each caspase prodomain, in a targeted way that would cater to a particular basic research or therapeutic ventures. This concept has been imagined in the past and now has recently been realized in a recent report on designing antibodies directed towards a specific epitope within intrinsically disordered region using disordered proteins and peptides associated with neurodegenerative and systematic misfolding diseases (Gao et al., 2009; Sormanni et al., 2015).

7.3. Consequences of the Mutagenic Pressure in Caspases-6

The Catalogue of Somatic Mutations in Cancer (COSMIC) database (Forbes et al., 2011) is a comprehensive resource of somatic mutations observed in human cancer. In Chapter IV of this work, we have selected mutations in *CASP6* gene from the COSMIC database as well as from a mutational study in *CASP6* gene in colorectal and gastric carcinoma (Lee et al., 2006) to assess the effect of these mutations in caspase-6 activity. Our results showed that these tumor-associated mutations are deactivating, effectively slowing the ability of

caspase-6 to process its substrates. One interesting observation that surfaced from this work is the recognition that cation- π stacking interaction may be widely used across the family of caspases to stabilize the mobile loops for proper assembly of the substrate binding groove, thus productive enzyme catalysis. This observation is suggested by the inactivating R259H mutation from a malignant tumor in the colon. Although the inhibitory effect of the R259H mutation *in vitro* is clear, its precise oncogenic contribution in cells is still unmasked. The cell-based assay on the determination of the effect of R259H on the apoptotic index of the normal and tumor-associated cells might be relevant to explore as well as those of other observed mutations in caspase-6. The rationale for this exploration is the fact that caspase-6 expression profiling through immunohistochemistry showed 60–90% of the tumors tested showed expression of caspase-6 (Lee et al., 2006). Likewise, aberrant regulation indicated by the presence of underexpressed or overexpressed *CASP6* gene across various tumor-associated tissue types has been annotated in the COSMIC database (Chapter IV). Moreover, the hypothesis that caspase-6 may be operational in select chemotherapeutic anti-cancer mechanisms merits further investigation as it has been shown in several reports that certain type of cancers can undergo caspase-6-mediated apoptotic cell death (Martin et al., 2016; Shahzidi et al., 2013; Suboj et al., 2012; Yang et al., 2014). In fact, a report has shown that the resistance of neoplastic cells to chemotherapeutic insults is through inhibition of caspase-6 activation by survivin-3B (Vegran and Boidot, 2013). And thus, downregulation of caspase-6 may promote apoptotic resistance in some tumor cells. The association of caspase-6

with cancer is another yet unexplored area with the potential to contribute cancer therapeutics.

7.4 Caspase Dimer Interface, a Structural Hideout for Natural Ligands

Chapter V of this dissertation describes a collaborative project between the Hardy Lab and ActivX Biosciences, Inc. to explore the regulatory role of nucleotides on caspases. It was a surprise finding on the part of our ActivX collaborators to observe that one of the peptides modified by their ATP acyl phosphate probe was derived from procaspase-6. We then further explored the ATP acyl phosphate probe binding characteristics and found that it binds to the dimer interface in procaspase-6 requiring the critical Lys-198 residue possibly binding through π - π stacking interactions. Moreover, other nucleotide probes can bind to this dimer interface in procaspase-6. We also showed that inhibition of procaspase-6 activation is a consequence of nucleotide binding to the dimer interface. Thus, these data suggest that the dimer interface in procaspase-6 is a regulatory nucleotide-binding site.

The question of why nucleotides bind procaspase-6 and possibly to other caspases is remained unaddressed. I have provided some discussions to address this question in Chapter V of this dissertation. One key realization from this work and others is that nucleotides bind procaspase-6 to inhibit its apoptotic function under cellular conditions that required nucleotides concentrations greater than normal levels, presumably to promote cell survival in response to various stress conditions, e.g. DNA damage. However, in the absence of a

crystal structure, we can only propose a possible mechanism of action of nucleotide binding to procaspase-6. Ishankumar Soni, a graduate student in the Hardy Lab, is pursuing the co-crystal structures of procaspase-6 bound to nucleotides with the goal of unraveling a possibly broad mechanism of nucleotide binding to the dimer interface of procaspase-6.

Moreover, detailed cellular studies on the effect of varying endogenous levels of nucleotides on procaspase-6 activation in cells through various reported chemical and genetic tools may help further assess the functional role of nucleotide binding to procaspase-6. Substitutions at the critical nucleotide-binding residue Lys-198 would be essential for assessing changes in the cellular apoptotic index in the background of varying nucleotide concentrations in order to further implicate the role of nucleotide binding to the apoptotic function of caspase-6.

Meanwhile, the dimer interface residues of caspases are moderately conserved thus provides a possible strategy to find caspase-specific binders that take advantage of this cavity. The findings of the series of nanomolar affinity binders of procaspase-6 identified through fragment-merging technology (Murray et al., 2014) and the nucleotide binders of procaspase-6 provide the necessary scaffolds for the future synthesis of a class of binders and activators specific to bind to procaspase-6 dimer interface.

7.5 Cys-264, a Perfect Anchor for the Specific Regulation of Caspase-6

With the discovery of the seemingly perfect inhibitor of caspase-6 that covalently modifies Cys-264 in the most diversified loop of caspases, we now have the capacity to interrogate the specific inhibition of caspase-6 and its impact on the treatment strategies for neurodegeneration. Moreover, this inhibitor can be developed as a powerful molecular probe to discover novel functions of caspase-6 in both normal and disease state conditions.

However, there are still a lot of exciting strides to overcome including the ongoing search for the most promising lead compound with improved potency in both *in vitro* and in cell-based assays. The unwavering contributions of Narasimha Rao, a postdoctoral fellow in the Hardy Lab, for all the synthetic efforts for this work have seen unprecedented progress toward this goal with the constant support of Yifei Pei, a graduate student in the Hardy Lab, who provides expertise in both *in vitro* and in cell-based assays of the synthesized compounds. In addition, despite several attempts to solve the co-crystal structure of caspase-6 with compound A, there is still no available structure of caspase-6;compound A complex that will definitely provide unparalleled contribution to the future design of more potent analogs of compound A.

The current derivative of the bis-*N*-oxide lead compound with attached biotin moiety can be a powerful chemical tool to facilitate the identification of cellular off-targets of compound A through pull-down assays and mass spectrometric analyses. Looking forward, this same technique can be applied to identify protein and natural small molecule binders as well as other not yet

identified post-translational modifications (PTM) of caspase-6. It would be relevant to treat several types of cells from normal to diseased neuronal cells with compound A–biotin to uncover some cell-specific interactors and novel PTMs of caspase-6 between these cell types. One can also imagine the synthesis of a compound A derivative with a fluorescent moiety to assess cellular functions of caspase-6 in cells in terms of localization and distribution of caspase-6 at various cellular conditions, e.g. inflammation and axonal degeneration.

Meanwhile, the assessment of the efficacy of the most potent compound A derivatives in Alzheimer's or Huntington's mouse model will greatly impact the potential of these caspase-6-specific inhibitors to be tested in humans with neurodegenerative conditions.

In conclusion, the body of work presented in this dissertation is a commencement of a thrilling future basic and applied research endeavors that may impact the fields of apoptosis, cancer, and drug discovery efforts in neurodegeneration.

7.6 References

- Boucher, D., V. Blais, and J. B. Denault. 2012. Caspase-7 uses an exosite to promote poly(ADP ribose) polymerase 1 proteolysis. *Proc Natl Acad Sci U S A*, 109:5669-74.
- Dagbay, K. B., N. Bolik-Coulon, S. N. Savinov, and J. A. Hardy. 2017. Caspase-6 Undergoes a Distinct Helix-Strand Interconversion Upon Substrate Binding. *Journal of Biological Chemistry*.
- Ding, Z. M., B. Wu, W. Q. Zhang, X. J. Lu, Y. C. Lin, Y. J. Geng, and Y. F. Miao. 2012. Neuroprotective effects of ischemic preconditioning and postconditioning on global brain ischemia in rats through the same effect on inhibition of apoptosis. *Int J Mol Sci*, 13:6089-101.

- Forbes, S. A., N. Bindal, S. Bamford, C. Cole, C. Y. Kok, D. Beare, M. Jia, R. Shepherd, K. Leung, A. Menzies, J. W. Teague, P. J. Campbell, M. R. Stratton, and P. A. Futreal. 2011. COSMIC: mining complete cancer genomes in the Catalogue of Somatic Mutations in Cancer. *Nucleic Acids Res*, 39:D945-50.
- Gao, J., S. S. Sidhu, and J. A. Wells. 2009. Two-state selection of conformation-specific antibodies. *Proceedings of the National Academy of Sciences of the United States of America*, 106:3071-6.
- Harrison, R. A., J. Lu, M. Carrasco, J. Hunter, A. Manandhar, S. Gondi, K. D. Westover, and J. R. Engen. 2016. Structural Dynamics in Ras and Related Proteins upon Nucleotide Switching. *Journal of Molecular Biology*, 428:4723-4735.
- Julien, O., M. Zhuang, A. P. Wiita, A. J. O'Donoghue, G. M. Knudsen, C. S. Craik, and J. A. Wells. 2016. Quantitative MS-based enzymology of caspases reveals distinct protein substrate specificities, hierarchies, and cellular roles. *Proceedings of the National Academy of Sciences of the United States of America*, 113:E2001-10.
- Klaiman, G., N. Champagne, and A. C. LeBlanc. 2009. Self-activation of Caspase-6 in vitro and in vivo: Caspase-6 activation does not induce cell death in HEK293T cells. *Biochim Biophys Acta*, 1793:592-601.
- Lee, J. W., M. R. Kim, Y. H. Soung, S. W. Nam, S. H. Kim, J. Y. Lee, N. J. Yoo, and S. H. Lee. 2006. Mutational analysis of the CASP6 gene in colorectal and gastric carcinomas. *APMIS*, 114:646-50.
- Majdi, A., J. Mahmoudi, S. Sadigh-Eteghad, S. E. Golzari, B. Sabermarouf, and S. Reyhani-Rad. 2016. Permissive role of cytosolic pH acidification in neurodegeneration: A closer look at its causes and consequences. *Journal of Neuroscience Research*, 94:879-87.
- Martin, R., C. Desponds, R. O. Eren, M. Quadroni, M. Thome, and N. Fasel. 2016. Caspase-mediated cleavage of raptor participates in the inactivation of mTORC1 during cell death. *Cell Death Discov*, 2:16024.
- Murray, J., A. M. Giannetti, M. Steffek, P. Gibbons, B. R. Hearn, F. Cohen, C. Tam, C. Pozniak, B. Bravo, J. Lewcock, P. Jaishankar, C. Q. Ly, X. Zhao, Y. Tang, P. Chugha, M. R. Arkin, J. Flygare, and A. R. Renslo. 2014. Tailoring small molecules for an allosteric site on procaspase-6. *ChemMedChem*, 9:73-7, 2.
- Shahzidi, S., A. Brech, M. Sioud, X. Li, Z. Suo, J. M. Nesland, and Q. Peng. 2013. Lamin A/C cleavage by caspase-6 activation is crucial for apoptotic induction by photodynamic therapy with hexaminolevulinate in human B-cell lymphoma cells. *Cancer Letters*, 339:25-32.
- Sormanni, P., F. A. Aprile, and M. Vendruscolo. 2015. Rational design of antibodies targeting specific epitopes within intrinsically disordered proteins. *Proceedings of the National Academy of Sciences of the United States of America*, 112:9902-9907.
- Suboj, P., S. Babykutty, P. Srinivas, and S. Gopala. 2012. Aloe emodin induces G2/M cell cycle arrest and apoptosis via activation of caspase-6 in human colon cancer cells. *Pharmacology*, 89:91-8.

- Vaidya, S. 2011. Structure and Function of Caspase-6, University of Massachusetts.
- Vaidya, S., and J. A. Hardy. 2011. Caspase-6 latent state stability relies on helical propensity. *Biochemistry*, 50:3282-7.
- Vaidya, S., E. M. Velazquez-Delgado, G. Abbruzzese, and J. A. Hardy. 2011. Substrate-induced conformational changes occur in all cleaved forms of caspase-6. *J Mol Biol*, 406:75-91.
- Vegran, F., and R. Boidot. 2013. Survivin-3B promotes chemoresistance and immune escape by inhibiting caspase-8 and -6 in cancer cells. *Oncoimmunology*, 2:e26328.
- Velazquez-Delgado, E. M., and J. A. Hardy. 2012. Zinc-mediated allosteric inhibition of caspase-6. *J Biol Chem*, 287:36000-11.
- Wang, X. J., Q. Cao, X. Liu, K. T. Wang, W. Mi, Y. Zhang, L. F. Li, A. C. LeBlanc, and X. D. Su. 2010. Crystal structures of human caspase 6 reveal a new mechanism for intramolecular cleavage self-activation. *EMBO Rep*, 11:841-7.
- Wang, X. J., Q. Cao, Y. Zhang, and X. D. Su. 2014. Activation and Regulation of Caspase-6 and Its Role in Neurodegenerative Diseases. *Annu Rev Pharmacol Toxicol*.
- Yang, K. M., B. M. Kim, and J. B. Park. 2014. omega-Hydroxyundec-9-enoic acid induces apoptosis through ROS-mediated endoplasmic reticulum stress in non-small cell lung cancer cells. *Biochemical and Biophysical Research Communications*, 448:267-73.

BIBLIOGRAPHY

- Abel, K., M. D. Yoder, R. Hilgenfeld, and F. Journak. 1996. An alpha to beta conformational switch in EF-Tu. *Structure*, 4:1153-9.
- Aharony, I., D. E. Ehrnhoefer, A. Shruster, X. Qiu, S. Franciosi, M. R. Hayden, and D. Offen. 2015. A Huntingtin-based peptide inhibitor of caspase-6 provides protection from mutant Huntingtin-induced motor and behavioral deficits. *Hum Mol Genet*, 24:2604-14.
- Akpan, N., E. Serrano-Saiz, B. E. Zacharia, M. L. Otten, A. F. Ducruet, S. J. Snipas, W. Liu, J. Velloza, G. Cohen, S. A. Sosunov, W. H. Frey, 2nd, G. S. Salvesen, E. S. Connolly, Jr., and C. M. Troy. 2011. Intranasal delivery of caspase-9 inhibitor reduces caspase-6-dependent axon/neuron loss and improves neurological function after stroke. *J Neurosci*, 31:8894-904.
- Albrecht, S., N. Bogdanovic, B. Ghetti, B. Winblad, and A. C. LeBlanc. 2009. Caspase-6 activation in familial Alzheimer disease brains carrying amyloid precursor protein or presenilin 1 or presenilin 2 mutations. *J Neuropathol Exp Neurol*, 68:1282-93.
- Albrecht, S., M. Bourdeau, D. Bennett, E. J. Mufson, M. Bhattacharjee, and A. C. LeBlanc. 2007. Activation of caspase-6 in aging and mild cognitive impairment. *Am J Pathol*, 170:1200-9.
- Allsopp, T. E., J. McLuckie, L. E. Kerr, M. Macleod, J. Sharkey, and J. S. Kelly. 2000. Caspase 6 activity initiates caspase 3 activation in cerebellar granule cell apoptosis. *Cell Death Differ*, 7:984-93.
- Alnemri, E. S., D. J. Livingston, D. W. Nicholson, G. Salvesen, N. A. Thornberry, W. W. Wong, and J. Yuan. 1996. Human ICE/CED-3 protease nomenclature. *Cell*, 87:171.
- Bao, Q., and Y. Shi. 2007. Apoptosome: a platform for the activation of initiator caspases. *Cell Death and Differentiation*, 14:56-65.
- Barbero, S., A. Mielgo, V. Torres, T. Teitz, D. J. Shields, D. Mikolon, M. Bogoy, D. Barila, J. M. Lahti, D. Schlaepfer, and D. G. Stupack. 2009. Caspase-8 association with the focal adhesion complex promotes tumor cell migration and metastasis. *Cancer Research*, 69:3755-63.
- Baumgartner, R., G. Meder, C. Briand, A. Decock, A. D'Arcy, U. Hassiepen, R. Morse, and M. Ratus. 2009. The crystal structure of caspase-6, a selective effector of axonal degeneration. *Biochem J*, 423:429-39.
- Bell, B. D., S. Leverrier, B. M. Weist, R. H. Newton, A. F. Arechiga, K. A. Luhrs, N. S. Morrissette, and C. M. Walsh. 2008. FADD and caspase-8 control the outcome of autophagic signaling in proliferating T cells. *Proceedings of the National Academy of Sciences of the United States of America*, 105:16677-82.
- Black, R. A., S. R. Kronheim, and P. R. Sleath. 1989. Activation of interleukin-1 beta by a co-induced protease. *FEBS Letters*, 247:386-90.

- Boatright, K. M., M. Renatus, F. L. Scott, S. Sperandio, H. Shin, I. M. Pedersen, J. E. Ricci, W. A. Edris, D. P. Sutherlin, D. R. Green, and G. S. Salvesen. 2003. A unified model for apical caspase activation. *Molecular Cell*, 11:529-41.
- Boatright, K. M., and G. S. Salvesen. 2003. Mechanisms of caspase activation. *Current Opinion in Cell Biology*, 15:725-731.
- Bochner, B. R., P. C. Lee, S. W. Wilson, C. W. Cutler, and B. N. Ames. 1984. AppppA and related adenylated nucleotides are synthesized as a consequence of oxidation stress. *Cell*, 37:225-32.
- Burke, J. E., O. Perisic, G. R. Masson, O. Vadas, and R. L. Williams. 2012. Oncogenic mutations mimic and enhance dynamic events in the natural activation of phosphoinositide 3-kinase p110alpha (PIK3CA). *Proceedings of the National Academy of Sciences of the United States of America*, 109:15259-64.
- Cain, K., S. B. Bratton, C. Langlais, G. Walker, D. G. Brown, X. M. Sun, and G. M. Cohen. 2000. Apaf-1 oligomerizes into biologically active approximately 700-kDa and inactive approximately 1.4-MDa apoptosome complexes. *Journal of Biological Chemistry*, 275:6067-70.
- Cao, Q., X. J. Wang, L. F. Li, and X. D. Su. 2014. The regulatory mechanism of the caspase 6 pro-domain revealed by crystal structure and biochemical assays. *Acta Crystallogr D Biol Crystallogr*, 70:58-67.
- Cao, Q., X. J. Wang, C. W. Liu, D. F. Liu, L. F. Li, Y. Q. Gao, and X. D. Su. 2012. Inhibitory mechanism of caspase-6 phosphorylation revealed by crystal structures, molecular dynamics simulations, and biochemical assays. *J Biol Chem*, 287:15371-9.
- Cerretti, D. P., C. J. Kozlosky, B. Mosley, N. Nelson, K. Van Ness, T. A. Greenstreet, C. J. March, S. R. Kronheim, T. Druck, L. A. Cannizzaro, and et al. 1992. Molecular cloning of the interleukin-1 beta converting enzyme. *Science*, 256:97-100.
- Chabes, A., B. Georgieva, V. Domkin, X. Zhao, R. Rothstein, and L. Thelander. 2003. Survival of DNA damage in yeast directly depends on increased dNTP levels allowed by relaxed feedback inhibition of ribonucleotide reductase. *Cell*, 112:391-401.
- Chai, J., Q. Wu, E. Shiozaki, S. M. Srinivasula, E. S. Alnemri, and Y. Shi. 2001. Crystal structure of a procaspase-7 zymogen: mechanisms of activation and substrate binding. *Cell*, 107:399-407.
- Chalmers, M. J., S. A. Busby, B. D. Pascal, Y. He, C. L. Hendrickson, A. G. Marshall, and P. R. Griffin. 2006. Probing protein ligand interactions by automated hydrogen/deuterium exchange mass spectrometry. *Analytical Chemistry*, 78:1005-14.
- Chandra, D., S. B. Bratton, M. D. Person, Y. Tian, A. G. Martin, M. Ayres, H. O. Fearnhead, V. Gandhi, and D. G. Tang. 2006. Intracellular nucleotides act as critical prosurvival factors by binding to cytochrome C and inhibiting apoptosome. *Cell*, 125:1333-46.
- Chereau, D., H. Zou, A. P. Spada, and J. C. Wu. 2005. A nucleotide binding site in caspase-9 regulates apoptosome activation. *Biochemistry*, 44:4971-6.

- Choi, Y. E., M. Butterworth, S. Malladi, C. S. Duckett, G. M. Cohen, and S. B. Bratton. 2009. The E3 ubiquitin ligase cIAP1 binds and ubiquitinates caspase-3 and -7 via unique mechanisms at distinct steps in their processing. *Journal of Biological Chemistry*, 284:12772-82.
- Chu, W., J. Rothfuss, Y. Chu, D. Zhou, and R. H. Mach. 2009. Synthesis and in vitro evaluation of sulfonamide isatin Michael acceptors as small molecule inhibitors of caspase-6. *J Med Chem*, 52:2188-91.
- Chu, Z. L., F. Pio, Z. Xie, K. Welsh, M. Krajewska, S. Krajewski, A. Godzik, and J. C. Reed. 2001. A novel enhancer of the Apaf1 apoptosome involved in cytochrome c-dependent caspase activation and apoptosis. *Journal of Biological Chemistry*, 276:9239-45.
- Clark, A. C. 2016. Caspase Allostery and Conformational Selection. *Chem Rev*.
- Cowling, V., and J. Downward. 2002. Caspase-6 is the direct activator of caspase-8 in the cytochrome c-induced apoptosis pathway- absolute requirement for removal of caspase-6 prodomain. *Cell Death and Differentiation*, 9:1046-1056.
- Dagbay, K., S. J. Eron, B. P. Serrano, E. M. Velazquez-Delgado, Y. Zhao, D. Lin, S. Vaidya, and J. A. Hardy. 2014. A multipronged approach for compiling a global map of allosteric regulation in the apoptotic caspases. *Methods Enzymol*, 544:215-49.
- Dagbay, K. B., N. Bolik-Coulon, S. N. Savinov, and J. A. Hardy. 2017. Caspase-6 Undergoes a Distinct Helix-Strand Interconversion upon Substrate Binding. *Journal of Biological Chemistry*, 292:4885-4897.
- Denecker, G., P. Ovaere, P. Vandenameele, and W. Declercq. 2008. Caspase-14 reveals its secrets. *Journal of Cell Biology*, 180:451-8.
- Devarajan, E., A. A. Sahin, J. S. Chen, R. R. Krishnamurthy, N. Aggarwal, A. M. Brun, A. Sapino, F. Zhang, D. Sharma, X. H. Yang, A. D. Tora, and K. Mehta. 2002. Down-regulation of caspase 3 in breast cancer: a possible mechanism for chemoresistance. *Oncogene*, 21:8843-51.
- Di Russo, N. V., D. A. Estrin, M. A. Marti, and A. E. Roitberg. 2012. pH-Dependent conformational changes in proteins and their effect on experimental pK(a)s: the case of Nitrophorin 4. *PLoS Comput Biol*, 8:e1002761.
- Ding, Z. M., B. Wu, W. Q. Zhang, X. J. Lu, Y. C. Lin, Y. J. Geng, and Y. F. Miao. 2012. Neuroprotective effects of ischemic preconditioning and postconditioning on global brain ischemia in rats through the same effect on inhibition of apoptosis. *Int J Mol Sci*, 13:6089-101.
- Doostzadeh-Cizeron, J., S. Yin, and D. W. Goodrich. 2000. Apoptosis induced by the nuclear death domain protein p84N5 is associated with caspase-6 and NF-kappa B activation. *J Biol Chem*, 275:25336-41.
- Dubovsky, J. A., K. A. Beckwith, G. Natarajan, J. A. Woyach, S. Jaglowski, Y. Zhong, J. D. Hessler, T. M. Liu, B. Y. Chang, K. M. Larkin, M. R. Stefanovski, D. L. Chappell, F. W. Frizzera, L. L. Smith, K. A. Smucker, J. M. Flynn, J. A. Jones, L. A. Andritsos, K. Maddocks, A. M. Lehman, R. Furman, J. Sharman, A. Mishra, M. A. Caligiuri, A. R. Satoskar, J. J. Buggy, N. Muthusamy, A. J. Johnson, and J. C. Byrd. 2013. Ibrutinib is an irreversible molecular inhibitor of ITK driving a Th1-selective pressure in T lymphocytes. *Blood*, 122:2539-49.

- Earnshaw, W. C., L. M. Martins, and S. H. Kaufmann. 1999. Mammalian caspases: structure, activation, substrates, and functions during apoptosis. *Annual Review of Biochemistry*, 68:383-424.
- Eichhold, T. H., E. B. Hookfin, Y. O. Taiwo, B. De, and K. R. Wehmeyer. 1997. Isolation and quantification of fluoroacetate in rat tissues, following dosing of Z-Phe-Ala-CH₂-F, a peptidyl fluoromethyl ketone protease inhibitor. *Journal of Pharmaceutical and Biomedical Analysis*, 16:459-467.
- Ekici, O. D., Z. Z. Li, A. J. Campbell, K. E. James, J. L. Asgian, J. Mikolajczyk, G. S. Salvesen, R. Ganesan, S. Jelakovic, M. G. Grutter, and J. C. Powers. 2006. Design, synthesis, and evaluation of aza-peptide Michael acceptors as selective and potent inhibitors of caspases-2, -3, -6, -7, -8, -9, and -10. *J Med Chem*, 49:5728-49.
- Englander, S. W. 2006. Hydrogen exchange and mass spectrometry: A historical perspective. *Journal of the American Society for Mass Spectrometry*, 17:1481-9.
- Englander, S. W., and N. R. Kallenbach. 1983. Hydrogen exchange and structural dynamics of proteins and nucleic acids. *Q Rev Biophys*, 16:521-655.
- Eron, S. J., K. Raghupathi, and J. A. Hardy. 2017. Dual Site Phosphorylation of Caspase-7 by PAK2 Blocks Apoptotic Activity by Two Distinct Mechanisms. *Structure*, 25:27-39.
- Feeney, B., and A. C. Clark. 2005. Reassembly of active caspase-3 is facilitated by the propeptide. *J Biol Chem*, 280:39772-85.
- Fernandes-Alnemri, T., G. Litwack, and E. S. Alnemri. 1994. CPP32, a novel human apoptotic protein with homology to *Caenorhabditis elegans* cell death protein Ced-3 and mammalian interleukin-1 beta-converting enzyme. *Journal of Biological Chemistry*, 269:30761-4.
- Forbes, S. A., N. Bindal, S. Bamford, C. Cole, C. Y. Kok, D. Beare, M. Jia, R. Shepherd, K. Leung, A. Menzies, J. W. Teague, P. J. Campbell, M. R. Stratton, and P. A. Futreal. 2011. COSMIC: mining complete cancer genomes in the Catalogue of Somatic Mutations in Cancer. *Nucleic Acids Res*, 39:D945-50.
- Foveau, B., L. Van Der Kraak, N. Beauchemin, S. Albrecht, and A. C. LeBlanc. 2014. Inflammation-induced tumorigenesis in mouse colon is caspase-6 independent. *PLoS One*, 9:e114270.
- Frejlich, E., J. Rudno-Rudzinska, K. Janiszewski, L. Salomon, K. Kotulski, O. Pelzer, Z. Grzebieniak, R. Tarnawa, and W. Kielan. 2013. Caspases and their role in gastric cancer. *Adv Clin Exp Med*, 22:593-602.
- Friedlander, R. M. 2003. Apoptosis and Caspases in Neurodegenerative Diseases. *New England Journal of Medicine*, 348:1365-1375.
- Fuentes-Prior, P., and G. S. Salvesen. 2004. The protein structures that shape caspase activity, specificity, activation and inhibition. *Biochem J*, 384:201-32.
- Futreal, P. A., L. Coin, M. Marshall, T. Down, T. Hubbard, R. Wooster, N. Rahman, and M. R. Stratton. 2004. A census of human cancer genes. *Nat Rev Cancer*, 4:177-183.

- Galvan, V., S. Chen, D. Lu, A. Logvinova, P. Goldsmith, E. H. Koo, and D. E. Bredesen. 2002. Caspase cleavage of members of the amyloid precursor family of proteins. *J Neurochem*, 82:283-94.
- Galvan, V., O. F. Gorostiza, S. Banwait, M. Ataie, A. V. Logvinova, S. Sitaraman, E. Carlson, S. A. Sagi, N. Chevallier, K. Jin, D. A. Greenberg, and D. E. Bredesen. 2006. Reversal of Alzheimer's-like pathology and behavior in human APP transgenic mice by mutation of Asp664. *Proc Natl Acad Sci U S A*, 103:7130-5.
- Gao, J., S. S. Sidhu, and J. A. Wells. 2009. Two-state selection of conformation-specific antibodies. *Proceedings of the National Academy of Sciences of the United States of America*, 106:3071-6.
- Geromanos, S. J., J. P. Vissers, J. C. Silva, C. A. Dorschel, G. Z. Li, M. V. Gorenstein, R. H. Bateman, and J. I. Langridge. 2009. The detection, correlation, and comparison of peptide precursor and product ions from data independent LC-MS with data dependant LC-MS/MS. *Proteomics*, 9:1683-95.
- Gervais, F. G., D. Xu, G. S. Robertson, J. P. Vaillancourt, Y. Zhu, J. Huang, A. LeBlanc, D. Smith, M. Rigby, M. S. Shearman, E. E. Clarke, H. Zheng, L. H. T. Van Der Ploeg, S. C. Ruffolo, N. A. Thornberry, S. Xanthoudakis, R. J. Zamboni, S. Roy, and D. W. Nicholson. 1999. Involvement of Caspases in Proteolytic Cleavage of Alzheimer's Amyloid- β Precursor Protein and Amyloidogenic A β Peptide Formation. *Cell*, 97:395-406.
- Giaime, E., C. Sunyach, C. Druon, S. Scarzello, G. Robert, S. Grosso, P. Auberger, M. S. Goldberg, J. Shen, P. Heutink, J. Pouyssegur, G. Pages, F. Checler, and C. Alves da Costa. 2010. Loss of function of DJ-1 triggered by Parkinson's disease-associated mutation is due to proteolytic resistance to caspase-6. *Cell Death Differ*, 17:158-69.
- Graham, R. K., Y. Deng, J. Carroll, K. Vaid, C. Cowan, M. A. Pouladi, M. Metzler, N. Bissada, L. Wang, R. L. Faull, M. Gray, X. W. Yang, L. A. Raymond, and M. R. Hayden. 2010. Cleavage at the 586 amino acid caspase-6 site in mutant huntingtin influences caspase-6 activation in vivo. *J Neurosci*, 30:15019-29.
- Graham, R. K., Y. Deng, E. J. Slow, B. Haigh, N. Bissada, G. Lu, J. Pearson, J. Shehadeh, L. Bertram, Z. Murphy, S. C. Warby, C. N. Doty, S. Roy, C. L. Wellington, B. R. Leavitt, L. A. Raymond, D. W. Nicholson, and M. R. Hayden. 2006. Cleavage at the caspase-6 site is required for neuronal dysfunction and degeneration due to mutant huntingtin. *Cell*, 125:1179-91.
- Grusch, M., M. Fritzer-Szekeres, G. Fuhrmann, G. Rosenberger, C. Luxbacher, H. L. Elford, K. Smid, G. J. Peters, T. Szekeres, and G. Krupitza. 2001. Activation of caspases and induction of apoptosis by novel ribonucleotide reductase inhibitors amidox and didox. *Experimental Hematology*, 29:623-32.
- Grutter, M. G. 2000. Caspases: key players in programmed cell death. *Current Opinion in Structural Biology*, 10:649-55.

- Guo, H., S. Albrecht, M. Bourdeau, T. Petzke, C. Bergeron, and A. C. LeBlanc. 2004. Active caspase-6 and caspase-6-cleaved tau in neuropil threads, neuritic plaques, and neurofibrillary tangles of Alzheimer's disease. *Am J Pathol*, 165:523-31.
- Guo, H., D. Petrin, Y. Zhang, C. Bergeron, C. G. Goodyer, and A. C. LeBlanc. 2006. Caspase-1 activation of caspase-6 in human apoptotic neurons. *Cell Death Differ*, 13:285-92.
- Guterman, L. 2011. COVALENT DRUGS FORM LONG-LIVED TIES. *Chemical & Engineering News Archive*, 89:19-26.
- Hakem, R., A. Hakem, G. S. Duncan, J. T. Henderson, M. Woo, M. S. Soengas, A. Elia, J. L. de la Pompa, D. Kagi, W. Khoo, J. Potter, R. Yoshida, S. A. Kaufman, S. W. Lowe, J. M. Penninger, and T. W. Mak. 1998. Differential requirement for caspase 9 in apoptotic pathways in vivo. *Cell*, 94:339-52.
- Hanahan, D., and R. A. Weinberg. 2011. Hallmarks of cancer: the next generation. *Cell*, 144:646-74.
- Hardy, J. A., J. Lam, J. T. Nguyen, T. O'Brien, and J. A. Wells. 2004. Discovery of an allosteric site in the caspases. *Proc Natl Acad Sci U S A*, 101:12461-6.
- Hardy, J. A., and J. A. Wells. 2004. Searching for new allosteric sites in enzymes. *Current Opinion in Structural Biology*, 14:706-15.
- Harrington, E. P., C. Zhao, S. P. Fancy, S. Kaing, R. J. Franklin, and D. H. Rowitch. 2010. Oligodendrocyte PTEN is required for myelin and axonal integrity, not remyelination. *Annals of Neurology*, 68:703-16.
- Harrison, R. A., J. Lu, M. Carrasco, J. Hunter, A. Manandhar, S. Gondy, K. D. Westover, and J. R. Engen. 2016. Structural Dynamics in Ras and Related Proteins upon Nucleotide Switching. *Journal of Molecular Biology*, 428:4723-4735.
- Heise, C. E., J. Murray, K. E. Augustyn, B. Bravo, P. Chugha, F. Cohen, A. M. Giannetti, P. Gibbons, R. N. Hannoush, B. R. Hearn, P. Jaishankar, C. Q. Ly, K. Shah, K. Stanger, M. Steffek, Y. Tang, X. Zhao, J. W. Lewcock, A. R. Renslo, J. Flygare, and M. R. Arkin. 2012. Mechanistic and structural understanding of uncompetitive inhibitors of caspase-6. *PLoS One*, 7:e50864.
- Hermel, E., J. Gafni, S. S. Propp, B. R. Leavitt, C. L. Wellington, J. E. Young, A. S. Hackam, A. V. Logvinova, A. L. Peel, S. F. Chen, V. Hook, R. Singaraja, S. Krajewski, P. C. Goldsmith, H. M. Ellerby, M. R. Hayden, D. E. Bredesen, and L. M. Ellerby. 2004. Specific caspase interactions and amplification are involved in selective neuronal vulnerability in Huntington's disease. *Cell Death and Differentiation*, 11:424-438.
- Hill, M. E., D. J. MacPherson, P. Wu, O. Julien, J. A. Wells, and J. A. Hardy. 2016. Reprogramming Caspase-7 Specificity by Regio-Specific Mutations and Selection Provides Alternate Solutions for Substrate Recognition. *ACS Chem Biol*, 11:1603-12.
- Hodkinson, J. P., S. E. Radford, and A. E. Ashcroft. 2012. The role of conformational flexibility in beta2-microglobulin amyloid fibril formation at neutral pH. *Rapid Communications in Mass Spectrometry*, 26:1783-92.

- Horowitz, P. M., K. R. Patterson, A. L. Guillozet-Bongaarts, M. R. Reynolds, C. A. Carroll, S. T. Weintraub, D. A. Bennett, V. L. Cryns, R. W. Berry, and L. I. Binder. 2004. Early N-terminal changes and caspase-6 cleavage of tau in Alzheimer's disease. *J Neurosci*, 24:7895-902.
- Hosomi, Y., A. Gemma, Y. Hosoya, M. Nara, T. Okano, K. Takenaka, A. Yoshimura, K. Koizumi, K. Shimizu, and S. Kudoh. 2003. Somatic mutation of the Caspase-5 gene in human lung cancer. *Int J Mol Med*, 12:443-6.
- Houde, D., S. A. Berkowitz, and J. R. Engen. 2011. The utility of hydrogen/deuterium exchange mass spectrometry in biopharmaceutical comparability studies. *J Pharm Sci*, 100:2071-86.
- Hsu, Y. H., D. A. Johnson, and J. A. Traugh. 2008. Analysis of conformational changes during activation of protein kinase Pak2 by amide hydrogen/deuterium exchange. *J Biol Chem*, 283:36397-405.
- Inoue, S., G. Browne, G. Melino, and G. M. Cohen. 2009. Ordering of caspases in cells undergoing apoptosis by the intrinsic pathway. *Cell Death Differ*, 16:1053-61.
- James, K. E., J. L. Asgian, Z. Z. Li, O. D. Ekici, J. R. Rubin, J. Mikolajczyk, G. S. Salvesen, and J. C. Powers. 2004. Design, synthesis, and evaluation of aza-peptide epoxides as selective and potent inhibitors of caspases-1, -3, -6, and -8. *J Med Chem*, 47:1553-74.
- Ji, G. H., M. Li, Y. Cui, and J. F. Wang. 2014. The relationship of CASP 8 polymorphism and cancer susceptibility: a meta-analysis. *Cell Mol Biol (Noisy-le-grand)*, 60:20-8.
- Julien, O., M. Zhuang, A. P. Wiita, A. J. O'Donoghue, G. M. Knudsen, C. S. Craik, and J. A. Wells. 2016. Quantitative MS-based enzymology of caspases reveals distinct protein substrate specificities, hierarchies, and cellular roles. *Proceedings of the National Academy of Sciences of the United States of America*, 113:E2001-10.
- Jung, J. Y., S. R. Lee, S. Kim, S. W. Chi, K. H. Bae, B. C. Park, J. H. Kim, and S. G. Park. 2014. Identification of novel binding partners for caspase-6 using a proteomic approach. *J Microbiol Biotechnol*, 24:714-8.
- Kelly, K. J., Z. Plotkin, and P. C. Dagher. 2001. Guanosine supplementation reduces apoptosis and protects renal function in the setting of ischemic injury. *Journal of Clinical Investigation*, 108:1291-8.
- Kerr, J. F., A. H. Wyllie, and A. R. Currie. 1972. Apoptosis: a basic biological phenomenon with wide-ranging implications in tissue kinetics. *British Journal of Cancer*, 26:239-57.
- Kim, Y. R., K. M. Kim, N. J. Yoo, and S. H. Lee. 2009. Mutational analysis of CASP1, 2, 3, 4, 5, 6, 7, 8, 9, 10, and 14 genes in gastrointestinal stromal tumors. *Hum Pathol*, 40:868-71.
- Kirschke, E., D. Goswami, D. Southworth, P. R. Griffin, and D. A. Agard. 2014. Glucocorticoid receptor function regulated by coordinated action of the Hsp90 and Hsp70 chaperone cycles. *Cell*, 157:1685-97.

- Klaiman, G., N. Champagne, and A. C. LeBlanc. 2009. Self-activation of Caspase-6 in vitro and in vivo: Caspase-6 activation does not induce cell death in HEK293T cells. *Biochim Biophys Acta*, 1793:592-601.
- Klaiman, G., T. L. Petzke, J. Hammond, and A. C. Leblanc. 2008. Targets of caspase-6 activity in human neurons and Alzheimer disease. *Mol Cell Proteomics*, 7:1541-55.
- Konermann, L., J. Pan, and Y. H. Liu. 2011. Hydrogen exchange mass spectrometry for studying protein structure and dynamics. *Chem Soc Rev*, 40:1224-34.
- Kostura, M. J., M. J. Tocci, G. Limjuco, J. Chin, P. Cameron, A. G. Hillman, N. A. Chartrain, and J. A. Schmidt. 1989. Identification of a monocyte specific pre-interleukin 1 beta convertase activity. *Proceedings of the National Academy of Sciences of the United States of America*, 86:5227-31.
- Kuida, K., T. F. Haydar, C. Y. Kuan, Y. Gu, C. Taya, H. Karasuyama, M. S. Su, P. Rakic, and R. A. Flavell. 1998. Reduced apoptosis and cytochrome c-mediated caspase activation in mice lacking caspase 9. *Cell*, 94:325-37.
- Kuida, K., T. S. Zheng, S. Na, C. Kuan, D. Yang, H. Karasuyama, P. Rakic, and R. A. Flavell. 1996. Decreased apoptosis in the brain and premature lethality in CPP32-deficient mice. *Nature*, 384:368-72.
- Lamkanfi, M., N. Festjens, W. Declercq, T. Vanden Berghe, and P. Vandenabeele. 2007. Caspases in cell survival, proliferation and differentiation. *Cell Death Differ*, 14:44-55.
- Landgraf, Rachele R., D. Goswami, F. Rajamohan, Melissa S. Harris, M. F. Calabrese, Lise R. Hoth, R. Magyar, Bruce D. Pascal, Michael J. Chalmers, Scott A. Busby, R. G. Kurumbail, and Patrick R. Griffin. Activation of AMP-Activated Protein Kinase Revealed by Hydrogen/Deuterium Exchange Mass Spectrometry. *Structure*, 21:1942-1953.
- LeBlanc, A., H. Liu, C. Goodyer, C. Bergeron, and J. Hammond. 1999. Caspase-6 role in apoptosis of human neurons, amyloidogenesis, and Alzheimer's disease. *J Biol Chem*, 274:23426-36.
- LeBlanc, A. C. 2013. Caspase-6 as a novel early target in the treatment of Alzheimer's disease. *Eur J Neurosci*, 37:2005-18.
- Lee, A. W., N. Champagne, X. Wang, X. D. Su, C. Goodyer, and A. C. Leblanc. 2010. Alternatively spliced caspase-6B isoform inhibits the activation of caspase-6A. *J Biol Chem*, 285:31974-84.
- Lee, J. W., M. R. Kim, Y. H. Soung, S. W. Nam, S. H. Kim, J. Y. Lee, N. J. Yoo, and S. H. Lee. 2006. Mutational analysis of the CASP6 gene in colorectal and gastric carcinomas. *APMIS*, 114:646-50.
- Leuenberger, P., S. Ganscha, A. Kahraman, V. Cappelletti, P. J. Boersema, C. von Mering, M. Claassen, and P. Picotti. 2017. Cell-wide analysis of protein thermal unfolding reveals determinants of thermostability. *Science*, 355.

- Leyva, M. J., F. Degiacomo, L. S. Kaltenbach, J. Holcomb, N. Zhang, J. Gafni, H. Park, D. C. Lo, G. S. Salvesen, L. M. Ellerby, and J. A. Ellman. 2010. Identification and evaluation of small molecule pan-caspase inhibitors in Huntington's disease models. *Chem Biol*, 17:1189-200.
- Liao, S. Y., K. J. Fritzsching, and M. Hong. 2013. Conformational analysis of the full-length M2 protein of the influenza A virus using solid-state NMR. *Protein Science*, 22:1623-38.
- Liu, B., D. Peng, Y. Lu, W. Jin, and Z. Fan. 2002. A novel single amino acid deletion caspase-8 mutant in cancer cells that lost proapoptotic activity. *J Biol Chem*, 277:30159-64.
- Liu, Y., Y. W. Zhang, X. Wang, H. Zhang, X. You, F. F. Liao, and H. Xu. 2009. Intracellular trafficking of presenilin 1 is regulated by beta-amyloid precursor protein and phospholipase D1. *J Biol Chem*, 284:12145-52.
- Lu, D. C., S. Rabizadeh, S. Chandra, R. F. Shayya, L. M. Ellerby, X. Ye, G. S. Salvesen, E. H. Koo, and D. E. Bredesen. 2000. A second cytotoxic proteolytic peptide derived from amyloid β -protein precursor. *Nature Medicine*, 6:397-404.
- MacKenzie, S. H., and A. C. Clark. 2008. Targeting cell death in tumors by activating caspases. *Curr Cancer Drug Targets*, 8:98-109.
- Majdi, A., J. Mahmoudi, S. Sadigh-Eteghad, S. E. Golzari, B. Sabermarouf, and S. Reyhani-Rad. 2016. Permissive role of cytosolic pH acidification in neurodegeneration: A closer look at its causes and consequences. *Journal of Neuroscience Research*, 94:879-87.
- Mandrizzato, S., F. Brasseur, G. Andry, T. Boon, and P. van der Bruggen. 1997. A CASP-8 mutation recognized by cytolytic T lymphocytes on a human head and neck carcinoma. *Journal of Experimental Medicine*, 186:785-93.
- Marriott, A. S., N. A. Copeland, R. Cunningham, M. C. Wilkinson, A. G. McLennan, and N. J. Jones. 2015. Diadenosine 5', 5'''-P(1),P(4)-tetrphosphate (Ap4A) is synthesized in response to DNA damage and inhibits the initiation of DNA replication. *DNA Repair (Amst)*, 33:90-100.
- Martin, M. C., L. A. Allan, E. J. Mancini, and P. R. Clarke. 2008. The docking interaction of caspase-9 with ERK2 provides a mechanism for the selective inhibitory phosphorylation of caspase-9 at threonine 125. *Journal of Biological Chemistry*, 283:3854-65.
- Martin, R., C. Desponds, R. O. Eren, M. Quadroni, M. Thome, and N. Fasel. 2016. Caspase-mediated cleavage of raptor participates in the inactivation of mTORC1 during cell death. *Cell Death Discov*, 2:16024.
- McIlwain, D. R., T. Berger, and T. W. Mak. 2013. Caspase functions in cell death and disease. *Cold Spring Harb Perspect Biol*, 5.
- McStay, G. P., G. S. Salvesen, and D. R. Green. 2008. Overlapping cleavage motif selectivity of caspases: implications for analysis of apoptotic pathways. *Cell Death Differ*, 15:322-31.
- Meergans, T., A. K. Hildebrandt, D. Horak, C. Haenisch, and A. Wendel. 2000. The short prodomain influences caspase-3 activation in HeLa cells. *Biochem J*, 349:135-40.

- Mehmood, S., C. Domene, E. Forest, and J. M. Jault. 2012. Dynamics of a bacterial multidrug ABC transporter in the inward- and outward-facing conformations. *Proceedings of the National Academy of Sciences of the United States of America*, 109:10832-6.
- Mesner, P. W., Jr., K. C. Bible, L. M. Martins, T. J. Kottke, S. M. Srinivasula, P. A. Svingen, T. J. Chilcote, G. S. Basi, J. S. Tung, S. Krajewski, J. C. Reed, E. S. Alnemri, W. C. Earnshaw, and S. H. Kaufmann. 1999. Characterization of caspase processing and activation in HL-60 cell cytosol under cell-free conditions. Nucleotide requirement and inhibitor profile. *Journal of Biological Chemistry*, 274:22635-45.
- Milnerwood, A. J., C. M. Gladding, M. A. Pouladi, A. M. Kaufman, R. M. Hines, J. D. Boyd, R. W. Ko, O. C. Vasuta, R. K. Graham, M. R. Hayden, T. H. Murphy, and L. A. Raymond. 2010. Early increase in extrasynaptic NMDA receptor signaling and expression contributes to phenotype onset in Huntington's disease mice. *Neuron*, 65:178-90.
- Mittag, T., L. E. Kay, and J. D. Forman-Kay. 2010. Protein dynamics and conformational disorder in molecular recognition. *Journal of Molecular Recognition*, 23:105-16.
- Morgan, C. R., and J. R. Engen. 2009. Investigating solution-phase protein structure and dynamics by hydrogen exchange mass spectrometry. *Curr Protoc Protein Sci*, Chapter 17:Unit 17 6 1-17.
- Muller, I., M. B. Lamers, A. J. Ritchie, C. Dominguez, I. Munoz-Sanjuan, and A. Kiselyov. 2011a. Structure of human caspase-6 in complex with Z-VAD-FMK: New peptide binding mode observed for the non-canonical caspase conformation. *Bioorg Med Chem Lett*, 21:5244-7.
- Muller, I., M. B. Lamers, A. J. Ritchie, H. Park, C. Dominguez, I. Munoz-Sanjuan, M. Maillard, and A. Kiselyov. 2011b. A new apo-caspase-6 crystal form reveals the active conformation of the apoenzyme. *Journal of Molecular Biology*, 410:307-15.
- Murakami, S., R. Nakashima, E. Yamashita, T. Matsumoto, and A. Yamaguchi. 2006. Crystal structures of a multidrug transporter reveal a functionally rotating mechanism. *Nature*, 443:173-9.
- Murray, J., A. M. Giannetti, M. Steffek, P. Gibbons, B. R. Hearn, F. Cohen, C. Tam, C. Pozniak, B. Bravo, J. Lewcock, P. Jaishankar, C. Q. Ly, X. Zhao, Y. Tang, P. Chugha, M. R. Arkin, J. Flygare, and A. R. Renslo. 2014. Tailoring small molecules for an allosteric site on procaspase-6. *ChemMedChem*, 9:73-7, 2.
- Muzio, M., A. M. Chinnaiyan, F. C. Kischkel, K. O'Rourke, A. Shevchenko, J. Ni, C. Scaffidi, J. D. Bretz, M. Zhang, R. Gentz, M. Mann, P. H. Krammer, M. E. Peter, and V. M. Dixit. 1996. FLICE, a novel FADD-homologous ICE/CED-3-like protease, is recruited to the CD95 (Fas/APO-1) death--inducing signaling complex. *Cell*, 85:817-27.
- Muzio, M., B. R. Stockwell, H. R. Stennicke, G. S. Salvesen, and V. M. Dixit. 1998. An induced proximity model for caspase-8 activation. *Journal of Biological Chemistry*, 273:2926-30.

- Nandi, C. L., J. Singh, and J. M. Thornton. 1993. Atomic environments of arginine side chains in proteins. *Protein Engineering*, 6:247-59.
- Nedergaard, M., R. P. Kraig, J. Tanabe, and W. A. Pulsinelli. 1991. Dynamics of interstitial and intracellular pH in evolving brain infarct. *American Journal of Physiology*, 260:R581-8.
- Nguyen, T. V., V. Galvan, W. Huang, S. Banwait, H. Tang, J. Zhang, and D. E. Bredesen. 2008. Signal transduction in Alzheimer disease: p21-activated kinase signaling requires C-terminal cleavage of APP at Asp664. *J Neurochem*, 104:1065-80.
- Nicholson, D. W. 1999. Caspase structure, proteolytic substrates, and function during apoptotic cell death. *Cell Death Differ*, 6:1028-42.
- Nikolaev, A., T. McLaughlin, D. D. O'Leary, and M. Tessier-Lavigne. 2009. APP binds DR6 to trigger axon pruning and neuron death via distinct caspases. *Nature*, 457:981-9.
- Nutt, L. K., S. S. Margolis, M. Jensen, C. E. Herman, W. G. Dunphy, J. C. Rathmell, and S. Kornbluth. 2005. Metabolic regulation of oocyte cell death through the CaMKII-mediated phosphorylation of caspase-2. *Cell*, 123:89-103.
- Nyormoi, O., Z. Wang, and M. Bar-Eli. 2003. Sequence-based discovery of a synthetic peptide inhibitor of caspase 6. *Apoptosis*, 8:371-6.
- Oberst, A., C. Pop, A. G. Tremblay, V. Blais, J. B. Denault, G. S. Salvesen, and D. R. Green. 2010. Inducible dimerization and inducible cleavage reveal a requirement for both processes in caspase-8 activation. *Journal of Biological Chemistry*, 285:16632-42.
- Oliver, F. J., M. K. Collins, and A. Lopez-Rivas. 1997. Overexpression of a heterologous thymidine kinase delays apoptosis induced by factor deprivation and inhibitors of deoxynucleotide metabolism. *Journal of Biological Chemistry*, 272:10624-30.
- Orth, K., A. M. Chinnaiyan, M. Garg, C. J. Froelich, and V. M. Dixit. 1996. The CED-3:ICE-like Protease Mch2 Is Activated during Apoptosis and Cleaves the Death Substrate Lamin A. *The Journal of Biological Chemistry*, 271:16443-16446.
- Pakavathkumar, P., A. Noel, C. Lecrux, A. Tubeleviciute-Aydin, E. Hamel, J. E. Ahlfors, and A. C. LeBlanc. 2017. Caspase vinyl sulfone small molecule inhibitors prevent axonal degeneration in human neurons and reverse cognitive impairment in Caspase-6-overexpressing mice. *Mol Neurodegener*, 12:22.
- Pakavathkumar, P., G. Sharma, V. Kaushal, B. Foveau, and A. C. LeBlanc. 2015. Methylene Blue Inhibits Caspases by Oxidation of the Catalytic Cysteine. *Sci Rep*, 5:13730.
- Pan, K. M., M. Baldwin, J. Nguyen, M. Gasset, A. Serban, D. Groth, I. Mehlhorn, Z. Huang, R. J. Fletterick, F. E. Cohen, and et al. 1993. Conversion of alpha-helices into beta-sheets features in the formation of the scrapie prion proteins. *Proceedings of the National Academy of Sciences of the United States of America*, 90:10962-6.

- Pan, L. Y., O. Salas-Solano, and J. F. Valliere-Douglass. 2014. Conformation and dynamics of interchain cysteine-linked antibody-drug conjugates as revealed by hydrogen/deuterium exchange mass spectrometry. *Analytical Chemistry*, 86:2657-64.
- Park, H. L., A. Ziogas, J. Chang, B. Desai, L. Bessonova, C. Garner, E. Lee, S. L. Neuhausen, S. S. Wang, H. Ma, J. Clague, P. Reynolds, J. V. Lacey, Jr., L. Bernstein, and H. Anton-Culver. 2016. Novel polymorphisms in caspase-8 are associated with breast cancer risk in the California Teachers Study. *BMC Cancer*, 16:14.
- Park, K. J., C. A. Grosso, I. Aubert, D. R. Kaplan, and F. D. Miller. 2010. p75NTR-dependent, myelin-mediated axonal degeneration regulates neural connectivity in the adult brain. *Nature Neuroscience*, 13:559-66.
- Patricelli, M. P., T. K. Nomanbhoy, J. Wu, H. Brown, D. Zhou, J. Zhang, S. Jagannathan, A. Aban, E. Okerberg, C. Herring, B. Nordin, H. Weissig, Q. Yang, J. D. Lee, N. S. Gray, and J. W. Kozarich. 2011. In situ kinase profiling reveals functionally relevant properties of native kinases. *Chemistry and Biology*, 18:699-710.
- Patricelli, M. P., A. K. Szardenings, M. Liyanage, T. K. Nomanbhoy, M. Wu, H. Weissig, A. Aban, D. Chun, S. Tanner, and J. W. Kozarich. 2007. Functional interrogation of the kinome using nucleotide acyl phosphates. *Biochemistry*, 46:350-8.
- Pettersen, E. F., T. D. Goddard, C. C. Huang, G. S. Couch, D. M. Greenblatt, E. C. Meng, and T. E. Ferrin. 2004. UCSF Chimera--a visualization system for exploratory research and analysis. *J Comput Chem*, 25:1605-12.
- Pirrone, G. F., R. E. Iacob, and J. R. Engen. 2015. Applications of hydrogen/deuterium exchange MS from 2012 to 2014. *Anal Chem*, 87:99-118.
- Polekhina, G., S. Thirup, M. Kjeldgaard, P. Nissen, C. Lippmann, and J. Nyborg. 1996. Helix unwinding in the effector region of elongation factor EF-Tu-GDP. *Structure*, 4:1141-51.
- Pop, C., and G. S. Salvesen. 2009. Human caspases: activation, specificity, and regulation. *Journal of Biological Chemistry*, 284:21777-81.
- Pop, C., J. Timmer, S. Sperandio, and G. S. Salvesen. 2006. The apoptosome activates caspase-9 by dimerization. *Molecular Cell*, 22:269-75.
- Qin, B. Y., M. C. Bewley, L. K. Creamer, H. M. Baker, E. N. Baker, and G. B. Jameson. 1998. Structural basis of the Tanford transition of bovine beta-lactoglobulin. *Biochemistry*, 37:14014-23.
- Qin, H., S. M. Srinivasula, G. Wu, T. Fernandes-Alnemri, E. S. Alnemri, and Y. Shi. 1999. Structural basis of procaspase-9 recruitment by the apoptotic protease-activating factor 1. *Nature*, 399:549-57.
- Quemeneur, L., L. M. Gerland, M. Flacher, M. Ffrench, J. P. Revillard, and L. Genestier. 2003. Differential control of cell cycle, proliferation, and survival of primary T lymphocytes by purine and pyrimidine nucleotides. *Journal of Immunology*, 170:4986-95.

- Rapaport, E., and P. C. Zamecnik. 1976. Presence of diadenosine 5',5''' -P1, P4-tetraphosphate (Ap4A) in mamalian cells in levels varying widely with proliferative activity of the tissue: a possible positive "pleiotypic activator". *Proceedings of the National Academy of Sciences of the United States of America*, 73:3984-8.
- Riechers, S. P., S. Butland, Y. Deng, N. Skotte, D. E. Ehrnhoefer, J. Russ, J. Laine, M. Laroche, M. A. Pouladi, E. E. Wanker, M. R. Hayden, and R. K. Graham. 2016. Interactome network analysis identifies multiple caspase-6 interactors involved in the pathogenesis of HD. *Hum Mol Genet*, 25:1600-18.
- Riedl, S. J., and Y. Shi. 2004. Molecular mechanisms of caspase regulation during apoptosis. *Nat Rev Mol Cell Biol*, 5:897-907.
- Rosenblum, J. S., T. K. Nomanbhoy, and J. W. Kozarich. 2013. Functional interrogation of kinases and other nucleotide-binding proteins. *FEBS Letters*, 587:1870-7.
- Ruchaud, S., N. Korfali, P. Villa, T. J. Kottke, C. Dingwall, S. H. Kaufmann, and W. C. Earnshaw. 2002. Caspase-6 gene disruption reveals a requirement for lamin A cleavage in apoptotic chromatin condensation. *EMBO J*, 21:1967-77.
- Saganich, M. J., B. E. Schroeder, V. Galvan, D. E. Bredesen, E. H. Koo, and S. F. Heinemann. 2006. Deficits in synaptic transmission and learning in amyloid precursor protein (APP) transgenic mice require C-terminal cleavage of APP. *J Neurosci*, 26:13428-36.
- Scheer, J. M., M. J. Romanowski, and J. A. Wells. 2006. A common allosteric site and mechanism in caspases. *Proceedings of the National Academy of Sciences of the United States of America*, 103:7595-600.
- Schoenmann, Z., E. Assa-Kunik, S. Tiomny, A. Minis, L. Haklai-Topper, E. Arama, and A. Yaron. 2010. Axonal degeneration is regulated by the apoptotic machinery or a NAD⁺-sensitive pathway in insects and mammals. *Journal of Neuroscience*, 30:6375-86.
- Schulman, B. A., D. L. Lindstrom, and E. Harlow. 1998. Substrate recruitment to cyclin-dependent kinase 2 by a multipurpose docking site on cyclin A. *Proceedings of the National Academy of Sciences of the United States of America*, 95:10453-8.
- Senft, J., B. Helfer, and S. M. Frisch. 2007. Caspase-8 interacts with the p85 subunit of phosphatidylinositol 3-kinase to regulate cell adhesion and motility. *Cancer Research*, 67:11505-9.
- Shahzidi, S., A. Brech, M. Sioud, X. Li, Z. Suo, J. M. Nesland, and Q. Peng. 2013. Lamin A/C cleavage by caspase-6 activation is crucial for apoptotic induction by photodynamic therapy with hexaminolevulinate in human B-cell lymphoma cells. *Cancer Lett*, 339:25-32.
- Shepard, L. A., A. P. Heuck, B. D. Hamman, J. Rossjohn, M. W. Parker, K. R. Ryan, A. E. Johnson, and R. K. Tweten. 1998. Identification of a membrane-spanning domain of the thiol-activated pore-forming toxin *Clostridium perfringens* perfringolysin O: an alpha-helical to beta-sheet transition identified by fluorescence spectroscopy. *Biochemistry*, 37:14563-74.

- Simon, D. J., R. M. Weimer, T. McLaughlin, D. Kallop, K. Stanger, J. Yang, D. D. O'Leary, R. N. Hannoush, and M. Tessier-Lavigne. 2012. A caspase cascade regulating developmental axon degeneration. *Journal of Neuroscience*, 32:17540-53.
- Singh, J., R. C. Petter, T. A. Baillie, and A. Whitty. 2011. The resurgence of covalent drugs. *Nat Rev Drug Discov*, 10:307-17.
- Skotte, N. H., S. S. Sanders, R. R. Singaraja, D. E. Ehrnhoefer, K. Vaid, X. Qiu, S. Kannan, C. Verma, and M. R. Hayden. 2016. Palmitoylation of caspase-6 by HIP14 regulates its activation. *Cell Death and Differentiation*.
- Slee, E. A., M. T. Harte, R. M. Kluck, B. B. Wolf, C. A. Casiano, D. D. Newmeyer, H. G. Wang, J. C. Reed, D. W. Nicholson, E. S. Alnemri, D. R. Green, and S. J. Martin. 1999. Ordering the cytochrome c-initiated caspase cascade: hierarchical activation of caspases-2, -3, -6, -7, -8, and -10 in a caspase-9-dependent manner. *J Cell Biol*, 144:281-92.
- Snijder, J., M. Benevento, C. L. Moyer, V. Reddy, G. R. Nemerow, and A. J. Heck. 2014. The cleaved N-terminus of pVI binds peripentonal hexons in mature adenovirus. *Journal of Molecular Biology*, 426:1971-9.
- Sormanni, P., F. A. Aprile, and M. Vendruscolo. 2015. Rational design of antibodies targeting specific epitopes within intrinsically disordered proteins. *Proceedings of the National Academy of Sciences of the United States of America*, 112:9902-9907.
- Soung, Y. H., E. G. Jeong, C. H. Ahn, S. S. Kim, S. Y. Song, N. J. Yoo, and S. H. Lee. 2008. Mutational analysis of caspase 1, 4, and 5 genes in common human cancers. *Hum Pathol*, 39:895-900.
- Soung, Y. H., J. W. Lee, H. S. Kim, W. S. Park, S. Y. Kim, J. H. Lee, J. Y. Park, Y. G. Cho, C. J. Kim, Y. G. Park, S. W. Nam, S. W. Jeong, S. H. Kim, J. Y. Lee, N. J. Yoo, and S. H. Lee. 2003. Inactivating mutations of CASPASE-7 gene in human cancers. *Oncogene*, 22:8048-52.
- Soung, Y. H., J. W. Lee, S. Y. Kim, J. Jang, Y. G. Park, W. S. Park, S. W. Nam, J. Y. Lee, N. J. Yoo, and S. H. Lee. 2005. CASPASE-8 gene is inactivated by somatic mutations in gastric carcinomas. *Cancer Research*, 65:815-21.
- Soung, Y. H., J. W. Lee, S. Y. Kim, W. S. Park, S. W. Nam, J. Y. Lee, N. J. Yoo, and S. H. Lee. 2004. Somatic mutations of CASP3 gene in human cancers. *Hum Genet*, 115:112-5.
- Srinivasula, S. M., M. Ahmad, M. MacFarlanes, Z. Luo, Z. HUang, T. Fernandes-Alnemri, and E. S. Alnemri. 1998. Generation of Constitutively Active Recombinant Caspases-3 and -6 by Rearrangement of Their Subunits. *The Journal of Biological Chemistry*, 273:10107-10111.
- Srinivasula, S. M., T. Fernandes-Alnemri, J. Zangrilli, N. Robertson, R. C. Armstrong, L. Wang, J. A. Trapani, K. J. Tomaselli, G. Litwack, and E. S. Alnemri. 1996. The Ced-3:Interleukin 1b Converting Enzyme-like Homolog Mch6 and the Lamin-cleaving Enzyme Mch2a Are Substrates for the Apoptotic Mediator CPP32. *The Journal of Biological Chemistry*, 271:27099-27106.

- Stanger, K., M. Steffek, L. Zhou, C. D. Pozniak, C. Quan, Y. Franke, J. Tom, C. Tam, J. M. Elliott, J. W. Lewcock, Y. Zhang, J. Murray, and R. N. Hannoush. 2012. Allosteric peptides bind a caspase zymogen and mediate caspase tetramerization. *Nat Chem Biol*, 8:655-60.
- Stupack, D. G. 2013. Caspase-8 as a Therapeutic Target in Cancer. *Cancer Letters*, 332:133-140.
- Su, H., N. Bidere, L. Zheng, A. Cubre, K. Sakai, J. Dale, L. Salmena, R. Hakem, S. Straus, and M. Lenardo. 2005. Requirement for caspase-8 in NF-kappaB activation by antigen receptor. *Science*, 307:1465-8.
- Suboj, P., S. Babykutty, P. Srinivas, and S. Gopala. 2012. Aloe emodin induces G2/M cell cycle arrest and apoptosis via activation of caspase-6 in human colon cancer cells. *Pharmacology*, 89:91-8.
- Suzuki, A., G. Kusakai, A. Kishimoto, Y. Shimojo, S. Miyamoto, T. Ogura, A. Ochiai, and H. Esumi. 2004. Regulation of caspase-6 and FLIP by the AMPK family member ARK5. *Oncogene*, 23:7067-75.
- Suzuki, Y., Y. Nakabayashi, K. Nakata, J. C. Reed, and R. Takahashi. 2001. X-linked inhibitor of apoptosis protein (XIAP) inhibits caspase-3 and -7 in distinct modes. *Journal of Biological Chemistry*, 276:27058-63.
- Takahashi, A., E. S. Alnemri, Y. A. Lazebnik, T. Fernandes-Alnemri, G. Litwack, R. D. Moir, R. D. Goldman, G. G. Poirier, S. H. Kaufmann, and W. C. Earnshaw. 1996. Cleavage of lamin A by Mch2 alpha but not CPP32: multiple interleukin 1 beta-converting enzyme-related proteases with distinct substrate recognition properties are active in apoptosis. *Proc Natl Acad Sci U S A*, 93:8395-400.
- Talanian, R. V., C. Quinlan, S. Trautz, M. C. Hackett, J. A. Mankovich, D. Banach, T. Ghayur, K. D. Brady, and W. W. Wong. 1997. Substrate specificities of caspase family proteases. *J Biol Chem*, 272:9677-82.
- Thornberry, N. A., H. G. Bull, J. R. Calaycay, K. T. Chapman, A. D. Howard, M. J. Kostura, D. K. Miller, S. M. Molineaux, J. R. Weidner, J. Aunins, and et al. 1992. A novel heterodimeric cysteine protease is required for interleukin-1 beta processing in monocytes. *Nature*, 356:768-74.
- Thornberry, N. A., T. A. Rano, E. P. Peterson, D. M. Rasper, T. Timkey, M. Garcia-Calvo, V. M. Houtzager, P. A. Nordstrom, S. Roy, J. P. Vaillancourt, K. T. Chapman, and D. W. Nicholson. 1997. A combinatorial approach defines specificities of members of the caspase family and granzyme B. Functional relationships established for key mediators of apoptosis. *J Biol Chem*, 272:17907-11.
- Tinel, A., and J. Tschopp. 2004. The PIDDosome, a protein complex implicated in activation of caspase-2 in response to genotoxic stress. *Science*, 304:843-6.
- Vaidya, S., and J. A. Hardy. 2011. Caspase-6 latent state stability relies on helical propensity. *Biochemistry*, 50:3282-7.
- Vaidya, S., E. M. Velazquez-Delgado, G. Abbruzzese, and J. A. Hardy. 2011. Substrate-induced conformational changes occur in all cleaved forms of caspase-6. *J Mol Biol*, 406:75-91.

- Varfolomeev, E. E., M. Schuchmann, V. Luria, N. Chiannikulchai, J. S. Beckmann, I. L. Mett, D. Rebrikov, V. M. Brodianski, O. C. Kemper, O. Kollet, T. Lapidot, D. Soffer, T. Sobe, K. B. Avraham, T. Goncharov, H. Holtmann, P. Lonai, and D. Wallach. 1998. Targeted disruption of the mouse Caspase 8 gene ablates cell death induction by the TNF receptors, Fas/Apo1, and DR3 and is lethal prenatally. *Immunity*, 9:267-76.
- Varshavsky, A. 1983. Diadenosine 5', 5'''-P1, P4-tetraphosphate: a pleiotropically acting alarmone? *Cell*, 34:711-2.
- Vartanian, A., I. Alexandrov, I. Prudowski, A. McLennan, and L. Kisselev. 1999. Ap4A induces apoptosis in human cultured cells. *FEBS Letters*, 456:175-80.
- Vartanian, A. A., H. Suzuki, and A. I. Poletaev. 2003. The involvement of diadenosine 5',5'''-P1,P4-tetraphosphate in cell cycle arrest and regulation of apoptosis. *Biochemical Pharmacology*, 65:227-35.
- Vegran, F., and R. Boidot. 2013. Survivin-3B promotes chemoresistance and immune escape by inhibiting caspase-8 and -6 in cancer cells. *Oncoimmunology*, 2:e26328.
- Velazquez-Delgado, E. M., and J. A. Hardy. 2012a. Phosphorylation regulates assembly of the caspase-6 substrate-binding groove. *Structure*, 20:742-51.
- . 2012b. Zinc-mediated allosteric inhibition of caspase-6. *J Biol Chem*, 287:36000-11.
- Venter, P. A., A. Dirksen, D. Thomas, M. Manchester, P. E. Dawson, and A. Schneemann. 2011. Multivalent display of proteins on viral nanoparticles using molecular recognition and chemical ligation strategies. *Biomacromolecules*, 12:2293-301.
- Voss, O. H., S. Batra, S. J. Kolattukudy, M. E. Gonzalez-Mejia, J. B. Smith, and A. I. Doseff. 2007. Binding of caspase-3 prodomain to heat shock protein 27 regulates monocyte apoptosis by inhibiting caspase-3 proteolytic activation. *J Biol Chem*, 282:25088-99.
- Wager, T. T., R. Y. Chandrasekaran, X. Hou, M. D. Troutman, P. R. Verhoest, A. Villalobos, and Y. Will. 2010. Defining desirable central nervous system drug space through the alignment of molecular properties, in vitro ADME, and safety attributes. *ACS Chem Neurosci*, 1:420-34.
- Wales, T. E., and J. R. Engen. 2006. Hydrogen exchange mass spectrometry for the analysis of protein dynamics. *Mass Spectrometry Reviews*, 25:158-70.
- Wales, T. E., K. E. Fadgen, G. C. Gerhardt, and J. R. Engen. 2008. High-speed and high-resolution UPLC separation at zero degrees Celsius. *Anal Chem*, 80:6815-20.
- Wang, L., J. H. Kang, K. H. Kim, and E. K. Lee. 2010a. Expression of intein-tagged fusion protein and its applications in downstream processing. *Journal of Chemical Technology and Biotechnology*, 85:11-18.
- Wang, X. J., Q. Cao, X. Liu, K. T. Wang, W. Mi, Y. Zhang, L. F. Li, A. C. LeBlanc, and X. D. Su. 2010b. Crystal structures of human caspase 6 reveal a new mechanism for intramolecular cleavage self-activation. *EMBO Rep*, 11:841-7.

- Wang, X. J., Q. Cao, Y. Zhang, and X. D. Su. 2014. Activation and Regulation of Caspase-6 and Its Role in Neurodegenerative Diseases. *Annu Rev Pharmacol Toxicol*.
- Warby, S. C., C. N. Doty, R. K. Graham, J. B. Carroll, Y. Z. Yang, R. R. Singaraja, C. M. Overall, and M. R. Hayden. 2008. Activated caspase-6 and caspase-6-cleaved fragments of huntingtin specifically colocalize in the nucleus. *Hum Mol Genet*, 17:2390-404.
- Ward, J. J., L. J. McGuffin, K. Bryson, B. F. Buxton, and D. T. Jones. 2004. The DISOPRED server for the prediction of protein disorder. *Bioinformatics*, 20:2138-9.
- Watanabe, C., G. L. Shu, T. S. Zheng, R. A. Flavell, and E. A. Clark. 2008. Caspase 6 regulates B cell activation and differentiation into plasma cells. *J Immunol*, 181:6810-9.
- Webb, B., and A. Sali. 2014. Protein structure modeling with MODELLER. *Methods in Molecular Biology*, 1137:1-15.
- Wei, Y., T. Fox, S. P. Chambers, J. Sintchak, J. T. Coll, J. M. Golec, L. Swenson, K. P. Wilson, and P. S. Charifson. 2000. The structures of caspases-1, -3, -7 and -8 reveal the basis for substrate and inhibitor selectivity. *Chemistry and Biology*, 7:423-32.
- Wellington, C. L., and M. R. Hayden. 2000. Caspases and neurodegeneration: on the cutting edge of new therapeutic approaches. *Clin Genet*, 57:1-10.
- Witkowski, W. A., and J. A. Hardy. 2011. A designed redox-controlled caspase. *Protein Sci*, 20:1421-31.
- Wong, B. K., D. E. Ehrnhoefer, R. K. Graham, D. D. Martin, S. Ladha, V. Uribe, L. M. Stanek, S. Franciosi, X. Qiu, Y. Deng, V. Kovalik, W. Zhang, M. A. Pouladi, L. S. Shihabuddin, and M. R. Hayden. 2015. Partial rescue of some features of Huntington Disease in the genetic absence of caspase-6 in YAC128 mice. *Neurobiol Dis*, 76:24-36.
- Woo, M., R. Hakem, M. S. Soengas, G. S. Duncan, A. Shahinian, D. Kagi, A. Hakem, M. McCurrach, W. Khoo, S. A. Kaufman, G. Senaldi, T. Howard, S. W. Lowe, and T. W. Mak. 1998. Essential contribution of caspase 3/CPP32 to apoptosis and its associated nuclear changes. *Genes and Development*, 12:806-19.
- Yan, N., and Y. Shi. 2005. Mechanisms of apoptosis through structural biology. *Annu Rev Cell Dev Biol*, 21:35-56.
- Yang, K. M., B. M. Kim, and J. B. Park. 2014. omega-Hydroxyundec-9-enoic acid induces apoptosis through ROS-mediated endoplasmic reticulum stress in non-small cell lung cancer cells. *Biochemical and Biophysical Research Communications*, 448:267-73.
- Yaoita, Y. 2002. Inhibition of nuclear transport of caspase-7 by its prodomain. *Biochem Biophys Res Commun*, 291:79-84.
- Yassine, W., N. Taib, S. Federman, A. Milochau, S. Castano, W. Sbi, C. Manigand, M. Laguerre, B. Desbat, R. Oda, and J. Lang. 2009. Reversible transition between alpha-helix and beta-sheet conformation of a transmembrane domain. *Biochimica et Biophysica Acta*, 1788:1722-30.

- Yoo, N. J., J. W. Lee, Y. J. Kim, Y. H. Soung, S. Y. Kim, S. W. Nam, W. S. Park, J. Y. Lee, and S. H. Lee. 2004. Loss of caspase-2, -6 and -7 expression in gastric cancers. *APMIS*, 112:330-5.
- Yuan, J., S. Shaham, S. Ledoux, H. M. Ellis, and H. R. Horvitz. 1993. The *C. elegans* cell death gene *ced-3* encodes a protein similar to mammalian interleukin-1 beta-converting enzyme. *Cell*, 75:641-52.
- Zhao, H., W. Zhao, K. Lok, Z. Wang, and M. Yin. 2014. A synergic role of caspase-6 and caspase-3 in Tau truncation at D421 induced by H₂O₂. *Cell Mol Neurobiol*, 34:369-78.
- Zhao, M., J. Su, E. Head, and C. W. Cotman. 2003. Accumulation of caspase cleaved amyloid precursor protein represents an early neurodegenerative event in aging and in Alzheimer's disease. *Neurobiol Dis*, 14:391-403.
- Zheng, T. S., S. Hunot, K. Kuida, and R. A. Flavell. 1999. Caspase knockouts: matters of life and death. *Cell Death and Differentiation*, 6:1043-53.
- Zheng, T. S., S. Hunot, K. Kuida, T. Momoi, A. Srinivasan, D. W. Nicholson, Y. Lazebnik, and R. A. Flavell. 2000. Deficiency in caspase-9 or caspase-3 induces compensatory caspase activation. *Nature Medicine*, 6:1241-7.